Experimental Investigations of Nucleation Rates of Ice and Clathrate Hydrates

by

Xin Zhang

A thesis submitted in partial fulfillment of the requirements for the degree of

Doctor of Philosophy

in

Petroleum Engineering

Department of Civil and Environmental Engineering
University of Alberta

ABSTRACT

Clathrate hydrate is a multi-component system in which the "guest" gas molecules are accommodated by the "host" water. It has many potential applications in energy storage, CO_2 capture and sequestration, gas separation and others. We wish to promote the formation of clathrate hydrate in these applications since the formation of clathrate hydrate is desired. However, in oil and gas industry, we wish to prevent the formation of hydrate due to the flow assurance problems.

Nucleation is the first step of clathrate hydrate formation. It is a kinetic effect and occurs stochastically. The nucleation probability increases with time and the system size, which is volume for homogeneous nucleation and interfacial area for heterogeneous nucleation. For either homogeneous nucleation or heterogeneous nucleation, the nucleation rate which is defined as the nucleation probability per unit size in unit time is the most important measure that characterizes the nucleation phenomenon of a given system.

For now, there's relatively few experimental studies focused on the nucleation of clathrate hydrate, especially quantitative studies that reliably quantify the nucleation rates of clathrate hydrate. In addition, it is challenging to understand the mechanism of clathrate hydrate nucleation due to the reasons such as the uncertainties in how to apply classical nucleation theory, experimental difficulties, and the inability of determining the nucleation rate reliably. Therefore, studying a structurally similar and less complex system, such as ice, may provide an indirect method to help understanding the mechanism of clathrate hydrate nucleation.

Compared to clathrate hydrate, ice has more literature data available for comparison and validation. Therefore, the study of ice nucleation might provide an indirect method to help understanding the mechanism of clathrate hydrate nucleation. The nucleation of ice could not only lay the foundation for the study of clathrate hydrate nucleation, but also has application in global

climate change, food engineering, biology, and other fields. Since ice and clathrate hydrate have similar structures, findings in one of ice nucleation and clathrate hydrate nucleation will aid to the understanding of the other. For example, if a material is found to be effective for promoting/inhibiting the nucleation of ice or clathrate hydrate but not for the other, it would shed light for the potential mechanism. Although ice nucleation has been studied over decades, many problems still remain. For example, there's no comprehensive heterogeneous nucleation theory or standard for a baseline to which the effects of additives can be compared. For the study of additives, although many substances were found to promote or inhibit ice nucleation, it is still unclear that (1) what is the most important factor that influences the nucleation, (2) why these substances could promote/inhibit the ice nucleation efficiently, and (3) how to design effective promoters/inhibitors.

In this study, in order to enhance the understanding of mechanisms of both clathrate hydrate nucleation and ice nucleation, we plan to take dual approaches, studying the nucleation of ice and clathrate hydrate and using findings in one of them to help understanding of the other. Firstly, a new experimental setup was established, calibrated, and assessed for the measurement of ice nucleation rate. The nucleation rates of ice were investigated in three microliter-sized water systems: 1) quasi-free water droplet supported by stable wetting films; 2) quasi-free water droplet suspended between two immiscible liquids; and 3) water directly in contact with a hydrophobic Teflon wall. The results showed that the nucleation rates measured in two quasi-free water droplet systems were broadly similar to each other, which suggested the quasi-free droplet systems could provide a reliable baseline for future studies in the presence of additives. The nucleation rates measured in water directly contact with a Teflon wall were somewhat higher than those of two quasi-free droplet systems, but the difference was not big.

After the baseline was set up, the nucleation rates of ice in the presence of seven nucleation promoters (including AgI, kaolinite, Snomax, cholesterol, steroid and two types of celluloses) were investigated in water directly in contact with a Teflon wall. The efficacy of these seven promoters could be ranked as: Snomax $\approx$ AgI $\geq$ kaolinite $>$ steroid $>$ cholesterol $\approx$ celluloses $\geq$ Teflon wall.

Snomax was found to be the most effective promoter among the seven tested promoters and it was postulated that the efficacy of Snomax might be aided by its larger interfacial area for heterogeneous nucleation since it could be dispersed in water. Therefore, the three nucleation promoters that we previously found to be effective- AgI, kaolinite and cholesterol – were attempted to be dispersed in water to increase the interfacial area. It was found that the dispersion of these promoters into water was difficult and required the addition of TBAB (Tetrabutylammonium bromide) to the aqueous phase before they could be dispersed. The nucleation rates measured in the dispersed nucleation promoter suspensions were investigated. And the results showed that dispersing AgI into 1 mM TBAB solution further promoted the ice nucleation while dispersing kaolinite or cholesterol in TBAB solutions did not promote ice nucleation more so than the TBAB solutions without kaolinite or cholesterol.

Other than promoters, the impact of monovalent electrolytes with concentrations lower than 100 mM was investigated in quasi-free droplets suspended between two immiscible liquids. It was found that none of the tested salts inhibited the nucleation of ice, to the contrary, some monovalent salts unexpectedly increased the nucleation rate of ice at low supercoolings.

Finally, the formation of CO_2 hydrate in quasi-free droplets of dilute electrolytes was investigated. The results showed that NaCl (sodium chloride) had no inhibition effect while KI (potassium iodide) had a weak promotion effect at low concentrations. And the impacts of these two salts on the nucleation of CO_2 hydrate were broadly similar to the previous findings of ice.

PREFACE

A version of Chapter 3 has been published as Zhang X., Li, H., and Maeda N. (2021). Nucleation curves of ice in quasi-free water droplets. *Chemical Engineering Science*, 242, 116751. Zhang X. is responsible for the setup assembly, experimental investigation and validation, data collection and analysis, and manuscript composition. Maeda N. is responsible for the conceptualization, methodology, and manuscript revision. Li H. and Maeda N. supervised the study.

A version of Chapter 4 has been published as Zhang X. and Maeda N. (2022). Nucleation curves of ice in the presence of nucleation promoters. *Chemical Engineering Science*, 262, 118017. Zhang X. is responsible for the experimental investigation, data collection and analysis, and manuscript composition. Maeda N. is the supervisor and gets involved in the conceptualization and manuscript revision.

A version of Chapter 5 has been published as Zhang X., Wei Y., and Maeda N. (2024). Ice nucleation in the presence of nucleation promoters dispersed in tetrabutylammonium bromide (TBAB) solutions. *Chemical Engineering Science*, 287, 119746. Zhang X. is responsible for the experimental investigation, data collection and analysis, and manuscript composition. Wei Y. helped with the experiments. Maeda N. is the supervisor and gets involved in the conceptualization and manuscript revision.

A version of Chapter 6 has been published as Zhang X., Li H., and Maeda N. (2023). Nucleation curves of ice in dilute salt solutions. *Energy & Fuels*, 37(18), 13937-13948. Zhang X. is responsible for the experimental investigation, data collection and analysis, and manuscript composition. Maeda N. is responsible for the conceptualization and manuscript revision. Li H. and Maeda N. supervised the study.

A version of Chapter 7 is submitted to *Energy & Fuels* for publication and currently under peer-review as Zhang X., Li H., and Maeda N. (2024). Nucleation of CO_2 hydrate in quasi-free droplets of dilute electrolytes. Zhang X. is responsible for the experimental investigation, data collection and analysis, and manuscript composition. Maeda N. is the supervisor and gets involved in the conceptualization and manuscript revision. Li H. provided the apparatus and supervised this study.

Chapter 1 summarizes the research background, problem statement, research objectives and the structure of this thesis. Chapter 2 summarizes the literature studies on structure of clathrate hydrate and ice, nucleation and nucleation rate, nucleation of clathrate hydrate and ice, and the promoters/inhibitors of clathrate hydrate and ice. Chapter 8 summarizes the conclusions reached in this thesis and the recommendations for the future study. Chapter 1, 2 and 8 are originally written by Zhang, X.

DEDICATION

This dissertation is dedicated to my beloved families, especially to my dearest grandparents: Mr.

Shifeng Pan and Mrs. Guangzhen Xu.

ACKNOWLEDGEMENT

TABLE OF CONTENTS

LIST OF TABLES

LIST OF FIGURES

CHAPTER 1 INTRODUCTION

1.1   Research Background

Clathrate hydrate is a multi-component system that the "guest" gas molecules are accommodated by the "host" water [1]. In oil and gas industry, the formation of clathrate hydrate is undesirable and needs to be inhibited since it could destroy the structural integrity of the pipelines or surface facilities, resulting in lowering the drilling or production efficiency [2]. In addition, the formation of gas hydrates could also cause flow assurance problems since it could result in blockage and lead to serious operation and safety hazards if it is not controlled properly. However, in some applications such as gas separation, CO_2 capture and sequestration, water desalination, and others, we wish to promote the formation of clathrate hydrate since it is desired.

Nucleation is the essential step of the formation of clathrate hydrate. It is the process of surmounting an activation barrier that originates from the interfacial energy between the emerging and the parent phases [3, 4]. The nucleation probability increases with time and the system size, which is volume for homogeneous nucleation and interfacial area for heterogeneous nucleation. In reality, most nucleation is heterogeneous nucleation and homogeneous nucleation can only occur in very limited circumstances [4]. For either homogeneous nucleation or heterogeneous nucleation, the nucleation rate which is defined as the nucleation probability per unit size in unit time is the most important measure that characterizes the nucleation phenomenon of a given system [3].

For now, there are few experimental studies focused on the nucleation of clathrate hydrate, especially quantitative studies that reliably quantify the nucleation rates of clathrate hydrate. Most of the literature failed to draw a holistic understanding of the nucleation of clathrate hydrate [2]. The reason for the lack of literature data might be the experimental difficulties. The non-polar

"guest" gases usually have low solubility in the "host" water, this property would increase the experimental difficulty due to the mass-transfer limitations [5]. Besides, the conventional measurement method is time-consuming and lack repeatability. It is challenging to understand the mechanism of the nucleation of clathrate hydrate due to reasons such as experimental difficulties and the inability of determining the nucleation rate reliably. In this case, studying the nucleation of a system that has similar structure to clathrate hydrate but less complex, such as ice, might be a good indirect method for enhancing the understanding of the nucleation of clathrate hydrate.

Ice is a single-component system, it is less complex and easier to study than clathrate hydrate which is multi-component and requires elevated pressures. Since clathrate hydrate has similar structure with ice, there are some similarities between them in properties such as mechanical properties and thermal properties [6]. Therefore, the study of one of the clathrate hydrate and ice could help to enhance the understanding of the other. The nucleation of ice could not only lay a baseline for the study of the nucleation of clathrate hydrate [7], it also has great impacts on global climate [8] and the water on aircraft wings [9], bridge cables [10], and other engineered and structured surfaces, which could result in dangerous equipment failures or even losses if not controlled properly. In addition, the study of ice nucleation has potential applications in medicine, food engineering, mineralogy [11], biology [12], and other fields. Although ice nucleation was studied by experimental [8] and modeling [13] methods for decades and hence has more literature data available for comparison and validation. However, still several unsolved problems remain. For example, there's no a-priori standard for a baseline to which the effects of additives can be compared. For the study of additives, although many substances have been reported to promote or inhibit the nucleation process of ice, it is still hard to find a reliable standard nucleation promoter/inhibitor since many potential impacts of sample variations such as purity,

grain size, and aging [14] should be considered [4]. Besides, it is unclear (1) what the most important factor is that influence the efficiency of the promoter/inhibitor, (2) why these substances are efficient in promoting/inhibiting the nucleation process, and (3) how to design an efficient nucleation promoter/inhibitor [4].

Nucleation rate is central to nucleation phenomena but yet nucleation rates of ice/clathrate hydrate in the presence of various additives have not been characterized very well. For example, researchers only reported some substances were effective nucleation promoters/inhibitors for the nucleation of ice/clathrate hydrate, but were unable to quantify by how much, compared to other promising additives. Therefore, a probabilistic approach that based on a large number of measurements is required to determine the nucleation rate and describe the efficacy of additives quantitatively.

In this study, we plan to study the nucleation of both ice and clathrate hydrate and use the findings in one of them to help the understanding of the other. Since there are much less literature data in clathrate hydrate and it is also more complex than ice (single component), we started from the measurement of ice nucleation. We aim to establish a new experimental setup that could be used for the investigations of ice nucleation, then calibrate and assess its reliability. After that, the baseline for the investigation of ice nucleation rate in the presence of different additives was set up. Because there are many experimental methods to investigate the ice nucleation rate, which included suspending water droplets in a gas, supporting sessile water droplets on hydrophobic surfaces, and suspending water droplets in oil or between two mutually immiscible oil layers [8], we compared the nucleation rates of ice measured in three water systems, including two quasi-free water droplet systems (water droplet supported by stable wetting films and water droplet suspended between two immiscible liquids) and water directly in contact with a hydrophobic

Teflon wall. After the baseline is set, we investigated the effects of nucleation promoters and/or inhibitors for both ice and clathrate hydrates and ranked their efficacy according to the nucleation rates. The findings would put some insights into finding reliable and effective promoters/inhibitors for controlling the nucleation process of both clathrate hydrate and ice.

1.2　Problem Statement

Although many substances were found to accelerate/delay the nucleation process of ice or clathrate hydrate, some problems still remain. One of the most important problems is that nucleation rate is central to nucleation phenomena and yet nucleation rates of ice and clathrate hydrate in the presence of various additives have not been characterized very well. Therefore, it is difficult to compare the efficacy of a range of promoters/inhibitors quantitatively on the nucleation of ice/clathrate hydrate. For example, researchers reported that cholesterols, steroids [15], some bacteria [16], pollen [17], etc. are effective ice nucleation promoters that can nucleate ice at -1 °C, but it is impossible to tell if these substances are more or less effective than other promising promoters such as AgI. Besides, researchers applied various experimental apparatus, different experimental methods (e.g., constant temperature method and linear cooling method) and samples with a wide range of droplet size, thus it is unable to quantify or compare the efficacy of the reported substances with other promoters/inhibitors if only based on the supercoolings which were usually reported in the literature. In other words, the ranking/quantifying the efficacy of different promoters/inhibitors reported in the literature could only be possible by systematic comparing the nucleation rates. Therefore, a probabilistic approach is needed for experimentally determining the nucleation rates, which could further rank the efficacy of a range of promoters/inhibitors that have been reported in the literature for the nucleation of ice/clathrate hydrate.

1.3   Research Objectives

In order to solve the issues in the Problem Statement section, we aim to characterize the nucleation rates that is central to the nucleation phenomena of both ice and clathrate hydrate in the presence of different promoters/inhibitors. a probabilistic approach based on a large number of measurements is required for the experimental determinations of nucleation rates.

The detailed description of research objectives is listed below:

- Set up a system that can be used for investigations of ice nucleation. Establish a new experimental setup, calibrate and assess its reliability. This experimental setup could also provide a reference point for the studies on clathrate hydrate nucleation.

- Investigate the ice nucleation rate using three different water systems: water droplet supported by stable wetting films of squalane, water droplet suspended between two immiscible liquids and water directly in contact with a hydrophobic Teflon wall. Develop a baseline for the studies of ice nucleation in the presence of nucleation promoters/inhibitors, etc. This also provides a reference point for the studies on the nucleation of clathrate hydrate.

- Investigate the effects of different types of promoters on ice nucleation. Determine the nucleation rates and rank the efficacy of the tested promoters quantitatively.

- Investigate the impact of dispersion and the concomitant increasing interfacial area on the efficacy of ice nucleation promoters.

- Investigate the nucleation rates of both ice and CO_2 hydrate in dilute salt solutions.

1.4   Thesis Structure

There are eight chapters in this dissertation. In Chapter 1, we introduce the research background, problem statement, and research objectives. In Chapter 2, we review the literature related to this research, including the structure of clathrate hydrates and ice, nucleation and nucleation rate, nucleation of clathrate hydrates and ice, and promoters/inhibitors for clathrate hydrates and ice. In Chapter 3, we establish a new experimental setup for the investigations of ice nucleation and measure the nucleation rates in two quasi-free water droplet systems (quasi-free water droplet supported by a stable film and quasi-free water droplet suspended by two immiscible liquids). Chapter 4 presents the investigation of ice nucleation rate in a third water system (water directly in contact with a hydrophobic solid wall) and in the presence of seven different types of nucleation promoters. In Chapter 5, we attempt to disperse the nucleation promoters of ice into water with the aid of TBAB and study on the effect of dispersed promoter suspensions on ice nucleation rate. In Chapter 6, we investigate the ice nucleation rates in quasi-free droplets of dilute monovalent salt solutions. Chapter 7 shows the nucleation rates of CO_2 hydrate in the presence of dilute electrolytes. Finally, Chapter 8 summarizes the conclusions and limitations of the present study and the suggestions for future work.

1.5   References

1.   N. Maeda, *Nucleation of Gas Hydrates*. 2020, Springer: Cham, Switzerland.

2.   M. Khurana, Z. Yin and P. Linga, *A review of clathrate hydrate nucleation.* ACS Sustainable Chemistry & Engineering, 2017. **5**(12): p. 11176-11203.

3.   D. Kashchiev, *Nucleation*. 2000, Elsevier: Oxford, UK.

4.   N. Maeda, *Brief Overview of Ice Nucleation.* Molecules, 2021. **26**(2): p. 392.

5. N. Maeda, *Nucleation curves of methane hydrate from constant cooling ramp methods.* Fuel, 2018. **223**: p. 286-293.

6. E.D. Sloan Jr and C.A. Koh, *Clathrate hydrates of natural gases*. 2007: CRC press.

7. G.A. Kimmel, Y. Xu, A. Brumberg, N.G. Petrik, R.S. Smith and B.D. Kay, *Homogeneous ice nucleation rates and crystallization kinetics in transiently-heated, supercooled water films from 188 K to 230 K.* The Journal of Chemical Physics, 2019. **150**(20): p. 204509.

8. B. Murray, D. O'sullivan, J. Atkinson and M. Webb, *Ice nucleation by particles immersed in supercooled cloud droplets.* Chemical Society Reviews, 2012. **41**(19): p. 6519-6554.

9. F.T. Lynch and A. Khodadoust, *Effects of ice accretions on aircraft aerodynamics.* Progress in Aerospace Sciences, 2001. **37**(8): p. 669-767.

10. C. Demartino, H.H. Koss, C.T. Georgakis and F. Ricciardelli, *Effects of ice accretion on the aerodynamics of bridge cables.* Journal of Wind Engineering and Industrial Aerodynamics, 2015. **138**: p. 98-119.

11. E. Tollefsen, G. Stockmann, A. Skelton, C.-M. Mörth, C. Dupraz and E. Sturkell, *Chemical controls on ikaite formation.* Mineralogical Magazine, 2018. **82**(5): p. 1119-1129.

12. K. Kelton and A.L. Greer, *Nucleation in condensed matter: applications in materials and biology*. 2010: Elsevier.

13. A. Haji-Akbari and P.G. Debenedetti, *Direct calculation of ice homogeneous nucleation rate for a molecular model of water.* Proceedings of the National Academy of Sciences, 2015. **112**(34): p. 10582-10588.

14. M. Polen, E. Lawlis and R.C. Sullivan, *The unstable ice nucleation properties of Snomax® bacterial particles.* Journal of Geophysical Research: Atmospheres, 2016. **121**(19): p. 11,666-11,678.

15. G.C. Sosso, T.F. Whale, M.A. Holden, P. Pedevilla, B.J. Murray and A. Michaelides, *Unravelling the origins of ice nucleation on organic crystals.* Chemical science, 2018. **9**(42): p. 8077-8088.

16. R. Pandey, K. Usui, R.A. Livingstone, S.A. Fischer, J. Pfaendtner, E.H. Backus, Y. Nagata, J. Fröhlich-Nowoisky, L. Schmüser and S. Mauri, *Ice-nucleating bacteria control the order and dynamics of interfacial water.* Science Advances, 2016. **2**(4): p. e1501630.

17. B.G. Pummer, H. Bauer, J. Bernardi, S. Bleicher and H. Grothe, *Suspendable macromolecules are responsible for ice nucleation activity of birch and conifer pollen.* Atmospheric Chemistry and Physics, 2012. **12**(5): p. 2541-2550.

CHAPTER 2 LITERATURE REVIEW

2.1 Structures of Clathrate Hydrate and Ice

Both clathrate hydrate and ice have several different crystal structures. Clathrate hydrate is ice-like solid in which some "guest" molecules are accommodated by the "host" hydrogen-bonded water molecules under proper temperature and pressure conditions [1]. Under relatively low pressure conditions, clathrate hydrate has three most common crystal structures, including cubic structure I (sI), cubic structure II (sII), and hexagonal structure H (sH) [2, 3]. Structure I is composed of two 5^{12} cages and six $5^{12}6^2$ cages, and it usually formed with guest molecules such as methane, ethane, carbon dioxide, etc. [4]. Structure II is composed of 16 5^{12} cages and eight $5^{12}6^4$ cages, and some typical guest gases are propane, cyclopentane, hydrogen, etc. [4]. As for structure H, it is composed of three 5^{12} cages, two $4^35^66^3$ cages and one $5^{12}6^8$ cage, and it generally formed with mixture gas molecules [5]. Other than these three common structures, there are also other less common crystal structures of clathrate hydrate under high pressure conditions or formed by compounds other than natural gas guests, such as Jeffrey's structures III-VII, structure T, etc. [1, 6, 7]. In this thesis, we only concentrated on the CO_2 hydrate (sI hydrate).

Compared to clathrate hydrate, the structure of ice seems to be "simpler" since it only has hollow structure consisted of hydrogen-bonded water molecules. It was known that only ice I could form at the atmospheric pressure [8], and ice I was commonly divided into two distinct forms, including the cubic phase (ice Ic) and the hexagonal phase (ice Ih) [9]. When changing the temperature and pressure conditions, some other phases would appear due to the changes of the water molecule network structure and the increasing distortion of the O-O-O angles [10]. For now,

ice was reported to have 19 different phases under different temperature and pressure conditions [10-12]. In this thesis, we concentrated on the experimental investigations of ice Ih.

On a molecular basis, ice has hollow structures that formed by hydrogen-bonded water molecules and the structures of clathrate hydrate are guest gas molecules "trapped" in the hydrogen-bonded water molecule cages, they thus thought to be structural similar and some properties of clathrate hydrate were similar to that of ice [1]. Sloan and Koh summarized the comparisons of the properties of hydrates and ice, including mechanical properties (mechanical strength and elastic properties) and thermal properties (thermal conductivity and thermal expansion) [1]. Tse et al. applied molecular dynamics methods to study the dynamical behaviour of ice Ic and methane hydrate (sI hydrate) and reported that they had similar phonon densities of states [13]. Schicks et al. reported that the Raman spectra of gas hydrate and ice Ih showed some similarities [14]. In addition, the similarities between clathrate hydrate and ice also provided insights to finding new phases of clathrate hydrates/ice. For example, Falenty et al. experimentally established the ice XVI phase by removing all guest gases from the sII clathrate hydrate structure [15].

2.2   Nucleation and Nucleation Rate

Nucleation is the kinetic process by which new phases begin to form and it is stochastic. During some processes such as crystallization, condensation and evaporation, nucleation is the initial step which plays an important role [16]. To explain it more specifically, nucleation is the process of surmounting an activation barrier that originates from the interfacial energy between the emerging and the parent phases [16, 17]. Traditionally, it could be divided into homogeneous nucleation (nucleation in a homogeneous bulk phase) and heterogeneous nucleation (nucleation at

an interface such as solid wall or impurities). In reality, most nucleation is heterogeneous nucleation and homogeneous nucleation can only occur in very limited circumstances [16].

The most common theoretical framework for nucleation is the Classical Nucleation Theory [17]. Based on the Classical Nucleation Theory, the nucleation rate can be expressed by Eq. 2.1 [16, 17]. It is defined as the nucleation probability density per unit time, and it is usually normalized to a proper system size (either system volume for homogeneous nucleation or surface/interfacial area for heterogeneous nucleation) [16].

$$J = AN_0 \exp(-\Delta g / kT) \qquad \text{Eq. 2.1}$$

where J is the nucleation rate, A is a kinetic constant, N_0 is the concentration of potential nucleation sites, Δg is the height of the activation barrier, k is the Boltzmann constant, T is the temperature.

Although the classical nucleation theory has been applied in many fields, it has some limitations such as assuming that the nucleating phase is a thermodynamically stable phase, assuming the initial cluster is spherical, and assuming the formation of a single critically-sized nucleus in a given system could result in the macroscopic phase transition of the whole system, etc. [9, 16].

Nucleation rate is the most important parameter that characterize the nucleation phenomenon quantitatively. However, few researchers reported the nucleation rates of clathrate hydrates due to reasons such as experimental difficulties and the uncertainties on how to apply the Classical Nucleation Theory. For the nucleation of ice, although there are more literature reporting the nucleation rates than clathrate hydrate, many problems or mechanisms remain unclear. In addition, the nucleation rates of ice/clathrate hydrate in the presence of various additives have not

been characterized very well. To this end, we aimed to investigate the nucleation rates of ice/clathrate hydrate in the presence of different types of promoters/inhibitors in this study.

2.3   Nucleation of Ice

The nucleation of ice has been studied for decades since it plays an important role on global climate, the prevention of icing on engineering and structural surfaces, food cryopreservation and many other fields [9, 18-20]. In oil and gas industry, the nucleation of ice could also lay a foundation for the study of nucleation of clathrate hydrate [21].

Generally, the nucleation of ice could be divided into two categories: nucleation from vapor and nucleation from liquid water. For the nucleation of ice from vapor, it is unclear now whether the supersaturated water vapor in the atmosphere nucleate to ice directly or condense to water droplet firstly and followed by nucleating to ice [16]. As for the nucleation of ice from liquid water, either homogeneous nucleation or surface nucleation in the absence of a solid wall, while contact nucleation or immersion nucleation would occur in the presence of a solid wall [9, 16, 22].

For now, there are many experimental methods applied for the investigations of the nucleation of ice from liquid water. Kramer et al. determined the homogeneous nucleation rates measured in micrometer-sized levitated water droplets in an electrodynamic Paul-trap [23]. Stockel et al. applied similar experimental method to investigate the ice nucleation in electrodynamic levitated charged droplets of water (H_2O) and heavy water (D_2O) and reported the homogeneous ice nucleation rates in the temperature range of 236.37 to 237.91 K [24]. However, it was proposed that the polarization of the levitated droplets in the electrostatic field may affect the water surface tension, which would bring some uncertainties into the experimental process [25]. Some researchers then applied acoustically levitated water droplets for the investigation of ice nucleation [26, 27]. Other

than levitating water droplets electrodynamically or acoustically, suspending the droplets in an airflow/gas flow was also commonly used for the studies on ice nucleation. And some typical apparatuses included the Mainz vertical wind tunnel (M-WT) [28], continuous-flow diffusion chamber [29, 30], Zurich ice nucleation chamber [31], cloud chambers [32], etc.

Other than the techniques mentioned above, water droplets immobilised on water repellent surfaces or suspended in oil/between oil layers were also commonly used for studying the ice nucleation. The water repellent surfaces are usually the hydrophobic solid surfaces or the hydrophobic/superhydrophobic coating surfaces. Jung et al. investigated the freezing of sessile water droplets on different surfaces with a wettability that ranges from hydrophobic to superhydrophobic [33]. Zhang et al. investigated the nucleation of sessile water droplets on a cold hydrophobic plate (with a wetting angle of 85°) and reported the nucleation rates based on the Classical Nucleation Theory [34]. Tobo [35] reported some modifications of the cold-stage-based freezing experiments on millimeter-sized water droplets that deposited on the aluminum plate coated with a thin Vaseline layer. For the experimental methods using suspending water droplets in oil/between oil layers, Bigg firstly applied the suspended water droplets at the interface of two immiscible liquids to study the nucleation of ice [36]. Ning and Liu investigated the ice nucleation in micro-sized water droplets suspended between two oil layers [37]. And they reported the nucleation rates and proposed that the volume had a great impact on the nucleation kinetics at the microscale [37]. Similar experimental method was also applied in the studies of other researchers [38]. Compared to the open experimental droplet systems, the methods of suspending droplets between two layers of immiscible oils could largely minimize the effect of contacting with the container wall and also diminish the potential impacts of water droplet evaporation, droplet contamination by airborne particles, and the influence of neighbouring freezing droplets by frost growth [39].

2.4   Nucleation of Clathrate Hydrate

The nucleation of clathrate hydrate is more difficult to understand since it involves more components than ice [7]. In addition, characterizing the nucleation phenomenon quantitatively is challenging due to the stochastic nature of the hydrate nucleation, the multi-factors (e.g., seed size, driving force, etc.) that may affect the nucleation, as well as the experimental difficulties such as the mass transfer problems and so on [17, 40, 41]. There are two main experimental methods to study the nucleation rate for clathrate hydrate and any other systems, including the constant temperature method and linear cooling ramp method. The former one uses constant supercooling (driving force) during the whole experiment, while the latter gradually increases the system supercooling (driving force) until nucleation is induced, and the linear cooling ramps always take a shorter induction time before the nucleation event occurs compared to the constant temperature [7].

There were several types of experimental apparatuses for the experimental investigations of the nucleation and formation of clathrate hydrate, such as rocking cell, high-pressure cells, autoclaves and high-pressure differential scanning calorimeter (HP-μDSC) [7, 42]. Due to the low solubility of gas molecules in the liquid phase and the complexity of nucleation process in the multi-component system, the nucleation rates of gas hydrates are usually low and difficult to measure [43]. In this case, some traditional high pressure setups were found to be difficult to get enough experimental data efficiently because of the inability to apply shear or fast cooling rates [43, 44]. Some researchers tried to describe the kinetics of clathrate hydrate quantitatively and investigate the nucleation rate by using some improved high-pressure apparatuses [42]. Maeda et al. applied the high pressure automated lag time apparatus (HP-ALTA) to study the nucleation and growth of clathrate hydrate [45], and he also developed a systematic method to determine a nucleation curve

over the whole experimental supercooling [46]. Metaxas et al. investigated the nucleation of mixed gas hydrate that induced at a constant supercooling in an improved high-pressure stirred automated lag time apparatus (HPS-ALTA) [47]. They determined the nucleation and growth rate of mixed gas hydrate and reported that the nucleation rates obtained were broadly consistent with other literature data that using a different apparatus. Barwood et al. presented a method for determining the nucleation rates from the constant cooling experiments in a similar HPS-ALTA apparatus as that used in Metaxas et al.'s study [40]. And their results suggested that both the number of heterogeneous nucleation sites and the average energy barriers would increase with the supercooling.

Complications arose when researchers tried to determine the area-normalised nucleation rates for clathrate hydrate. It is unclear whether the experimental nucleation rates for clathrate hydrate were proportional to the liquid-gas interface or the length of the three-phase-line where the solid wall, liquid and the gas met [45, 48]. In order to diminish the impact of solid wall and make the interfacial area on which the nucleation process occurs quantifiable, some researchers investigated the nucleation of clathrate hydrate on "quasi-free" droplets. Tanaka et al. reported the visual observations of the formation of clathrate hydrate on the water droplets supported by a hydrophobic Polytetrafluoroethylene (Teflon) stage [49]. Maeda investigated the nucleation of 90 mol% methane and 10 mol% propane (C1/C3) mixed gas hydrates on quasi-free water droplets that supported by a perfluorodecalin film [46, 50]. Wei and Maeda reported the nucleation curves of CO_2 hydrate measured on water droplets that supported by a perfluoromethyldecalin film and compared the results with those measured in the presence of solid walls (glass wall and stainless steel wall) [51]. Jeong et al. observed the nucleation and growth of mixed gas hydrates (molar composition: 0.78 methane + 0.12 ethane + 0.06 propane + 0.01 isobutane + 0.03 carbon dioxide) on acoustically levitated water droplets [43, 52].

2.5 Promoters/Inhibitors for Ice

2.5.1 Promoters for Ice

The nucleation promoters for ice have been studied for decades due to their application in cloud seeding [16]. Silver iodide (AgI) was widely used as a promoter for ice nucleation, but the promotion mechanism of it remains questioned/unclear to this day [53]. Researchers firstly attributed the effective nucleation ability to the perfect lattice matching between the AgI surface and ice, but the role of lattice matching in promoting ice nucleation was questioned because of 1) ice was found to grow as discrete hexagonal islands instead of an expected uniform film on the AgI surface; 2) other substances such as cadmium sulfide (CdS) and barium fluoride (BaF_2) also have similar lattice spacing with ice but couldn't act as effective promoters for ice nucleation; 2) some organic materials such as cholesterol were reported to have similar promotion effect to AgI although their crystal lattices have no relationships to that of ice [16, 53-55].

In addition to AgI, soot particles and some clay minerals such as kaolinite and illite were reported to have promotion effect on ice nucleation. Gorbunov et al. reported that the soot particles tested in their study could nucleate ice as high as -10 °C [56]. Mahrt et al. experimentally investigated the ice nucleation abilities of different types of soot particles in a HINC (horizontal ice nucleation chamber) and reported that soot particles were able to nucleate ice via a pore condensation and freezing mechanism [57]. Pinti et al. investigated the ice nucleation efficiency of different types of clay minerals including kaolinites, illites and montmorillonites. And they proposed that the freezing temperature of ice in the presence of clay minerals depended on the amount of clay mineral per droplet and the type of the clay mineral [58].

Other than the materials mentioned above, Snomax, which is a commercial product, was reported to nucleate ice at temperatures of up to -2 °C [59]. Some organic molecules such as steroids and cholesterol were also reported to be effective nucleation promoters [60], and Sosso et al. tried to reveal the origins of the nucleating activity of steroids such as cholesterol [61]. Besides, some bacteria [62], pollen [63], and water-soluble macromolecules such as fungal species [64] were studied for enhancing the ice nucleation process for years.

Although many substances were found to promote ice nucleation and many criteria for what make an effective nucleation promoter were proposed [65, 66], several problems still remain unknown, including the reason these substances accelerate/delay the nucleation process, the most important properties of effective promotor/inhibitor, the way to design an effective promoter/inhibitor, etc. [16]. Besides, few researchers determined the nucleation rate to describe the efficiency of promoters quantitatively.

2.5.2 Inhibitors for Ice

Holt proposed that two main classes substances that could inhibit the nucleation of ice, including the solutes which decrease the freezing point and the materials that have inhibition ability without affecting the freezing significantly [67]. Salts are known as the thermodynamic inhibitors for the nucleation of ice by decreasing the activity of water and depressing the melting point of ice [68]. For example, Espinosa et al. reported that sodium chloride (NaCl) with a concentration of 1.85 M could inhibit the nucleation of ice by increasing the ice-liquid interfacial free energy [69]. Miyata et al. investigated the effects of different monovalent ions on the nucleation temperatures of ice formation and concluded that the cationic effect on nucleation temperature

increased with the decreasing cationic radius while the anionic effect on nucleation temperature increased with the increasing anionic radius [70].

Several types of antifreeze proteins (AFP) were also studied to inhibit the freezing process of ice [66]. Du et al. examined the impact of one type of fish AFP on the formation of ice and proposed that the tested AFP could inhibit the ice nucleation by adsorbing onto the surfaces of ice nuclei and dust particles [71]. Kutschan et al. concluded two effects of AFPs in inhibiting the formation of ice, including 1) AFPs could lower the interfacial energy and 2) ice crystals formed faster in the presence of AFPs but became "locked" at smaller sizes. They proposed that AFPs couldn't prevent the formation of ice crystals but inhibit the further growth of the initial ice nuclei [72]. It is interesting that Eickhoff et al. found the contrasting behavior of the two types AFPs they investigated: inhibit the growth of pre-existing ice crystals but promote the nucleation of new ice crystals from supercooled solution [73]. Other than salts and AFPs, some polymers such as Poly(vinyl alcohol) was also reported to have a significant molecular weight dependent ice nucleation inhibition effect [74].

2.6   Promoters/Inhibitors for Clathrate Hydrate

2.6.1   Promoters for Clathrate Hydrate

The formation of clathrate hydrate has applications in many fields such as gas separation[75, 76], energy storage[77, 78], CO_2 capture and sequestration[79, 80], water desalination[81, 82] and so on. The promoters of clathrate hydrates were found to be essential in those applications where the formation of clathrate hydrate is desired.

Some surfactants that could lower the liquid-gas interfacial tension and increase the mass transfer were studied as kinetic hydrate promoters, including anionic, cationic, and nonionic

surfactants [83]. Fazlali et al. reported the impact of different surfactants including SDS (sodium dodecyl sulfate), HTABr (hexa decyl trimethyl ammonium bromide), Brij-58 (polyoxy ethylene cetyl ether) and their mixtures on the formation of methane hydrate [84]. They found that all the surfactants tested in the study could reduce the induction time and increase the formation rate, and SDS with a concentration of 500 ppm seemed to be the best promoter among all tested surfactants [84]. Pandey et al. investigated the promotion effect of the surfactant SDS on the formation of methane hydrate and reported a trade-off between formation rate and gas uptake for the optimum SDS concentration [85]. Karaaslan and Parlaktuna investigated the impact of different types of surfactants on the hydrate formation rate [86]. They reported that the anionic surfactant with all concentrations could promote the formation process of hydrate, while the non-ionic surfactant was not as effective as anionic surfactant and the cationic surfactant is only effective as a hydrate promoter at low concentrations [86].

Other than surfactants, some organic compounds (e.g., THF (tetrahydrofuran), cyclopentane, TBAB (Tetrabutyl ammonium bromide), etc.) were also used as promoters to accelerate the formation of clathrate hydrate under conditions of higher temperatures and/or lower pressures in some applications such as hydrogen storage and gas separation. These organic compounds are known to form clathrate hydrates with water and could form a mixed hydrate with the guest molecule when added into the system [2]. Ricaurte et al. reported a hydrate based process to separate CO_2 gas from CO_2-CH_4 gas mixture by adding THF (tetrahydrofuran) into the system [87]. And they found that CO_2 and/or CH_4 + THF mixed hydrate formed at a higher temperature in the presence of THF comparing to that of pure water. Trueba et al. reported the phase equilibrium measurements of sII clathrate hydrate of H_2 with several organic promoters including furan, 2,5-dihydrofuran, tetrahydropyran, 1,3-dioxolane and cyclopentane [2]. The results showed that the

mixed organic hydrates had a much higher stability compared to a pure H_2 hydrate, indicating the organic materials acted as promoters for clathrate hydrate [2].

2.6.2 Inhibitors for Clathrate Hydrate

Since clathrate hydrate formed during deep-water well testing could result in blockage and lead to serious operation and safety hazards, methods to prevent and inhibit the formation of hydrates were studied for years. The most common method to inhibit clathrate hydrate formation is applying chemical inhibitors, and there are two main classes of inhibitors including Thermodynamic Hydrate Inhibitors (THI) and Low Dosage Hydrate Inhibitors (LDHIs) [88]. And LDHIs could further divide into Kinetic Hydrate Inhibitors (KHIs) and Anti-agglomerates (AAs) [88].

The role of THIs is to interfere with the hydrogen bonding of water molecules and consequently shift the hydrate phase boundary to a lower temperature and higher pressure condition [89]. Alcohols such as methanol and glycol are commonly used as THIs in oil and gas industry to inhibit the formation of clathrate hydrate. However, the dosage of the THIs used in the deep temperature conditions was 40 wt.% to ensure the effective inhibition, which consequently increase the cost [90]. In addition, the volatility of the THIs could cause environmental problems and also leads to additional costs for hydrocarbon refinery and chemical losses [90, 91]. Other than alcohols, electrolytes (e.g., sodium chloride, calcium chloride, potassium carbonate, etc.) are also known to be thermodynamic inhibitors for the formation of clathrate hydrate [89].

Compared to THIs, KHIs are more environmental-friendly and promising at a low dosage [92]. KHIs are mainly polymers or copolymers such as PVP (polyvinylpyrrolidone), PVCap (poly(vinyl caprolactam)), N-vinylcaprolactam, etc., and it is reported that the effective KHIs

always have amide groups and hydrophobic parts [42]. Ivall et al. investigated the effects of PVP on the formation of methane hydrate [93]. And they reported that PVP could adsorb onto the hydrate surface which further inhibit the formation of hydrate. Yang et al. investigated the inhibition impact of a copolymer on the formation of methane-propane hydrate with different concentrations and within a supercooling range from 5 to 20 °C [92]. They reported a "concentration effect" concept and proposed two internal mechanisms including the "weakened adsorption" hypothesis and the "competition" hypothesis [92].

Other than the materials mentioned above, some biologically organic compounds such as amino acids and antifreeze proteins were also found to be effective in inhibiting the crystallization of clathrate hydrate [94-96]. Different from THIs and KHIs, AAs allow hydrate to form but prevent it from further growth [42].

2.7 References

(1)   Sloan Jr, E. D.; Koh, C. A. Clathrate hydrates of natural gases; CRC press, 2007.

(2)   Trueba, A. T.; Rovetto, L. J.; Florusse, L. J.; Kroon, M. C.; Peters, C. J. Phase equilibrium measurements of structure II clathrate hydrates of hydrogen with various promoters. Fluid Phase Equilibria 2011, 307 (1), 6-10.

(3)   Sum, A. K.; Koh, C. A.; Sloan, E. D. Clathrate hydrates: from laboratory science to engineering practice. Industrial & Engineering Chemistry Research 2009, 48 (16), 7457-7465.

(4)   Sloan, E. D. Clathrate hydrates: the other common solid water phase. Industrial & Engineering Chemistry Research 2000, 39 (9), 3123-3129.

(5)   Takeya, S.; Kida, M.; Minami, H.; Sakagami, H.; Hachikubo, A.; Takahashi, N.; Shoji, H.; Soloviev, V.; Wallmann, K.; Biebow, N. Structure and thermal expansion of natural gas clathrate hydrates. Chemical Engineering Science 2006, 61 (8), 2670-2674.

(6)   Udachin, K. A.; Ratcliffe, C. I.; Ripmeester, J. A. A dense and efficient clathrate hydrate structure with unusual cages. Angewandte Chemie 2001, 113 (7), 1343-1345.

(7)   Maeda, N. Nucleation of Gas Hydrates. Springer, 2020.

(8)   Salzmann, C. G.; Radaelli, P. G.; Slater, B.; Finney, J. L. The polymorphism of ice: five unresolved questions. Physical Chemistry Chemical Physics 2011, 13 (41), 18468-18480.

(9)   Murray, B.; O'sullivan, D.; Atkinson, J.; Webb, M. Ice nucleation by particles immersed in supercooled cloud droplets. Chemical Society Reviews 2012, 41 (19), 6519-6554.

(10)   Bartels-Rausch, T.; Bergeron, V.; Cartwright, J. H.; Escribano, R.; Finney, J. L.; Grothe, H.; Gutiérrez, P. J.; Haapala, J.; Kuhs, W. F.; Pettersson, J. B. Ice structures, patterns, and processes: A view across the icefields. Reviews of Modern Physics 2012, 84 (2), 885.

(11)   Salzmann, C. G.; Loveday, J. S.; Rosu-Finsen, A.; Bull, C. L. Structure and nature of ice XIX. Nature Communications 2021, 12 (1), 3162.

(12)   Millot, M.; Coppari, F.; Rygg, J. R.; Correa Barrios, A.; Hamel, S.; Swift, D. C.; Eggert, J. H. Nanosecond X-ray diffraction of shock-compressed superionic water ice. Nature 2019, 569 (7755), 251-255.

(13)   Tse, J. S.; Klein, M. L.; McDonald, I. R. Molecular dynamics studies of ice Ic and the structure I clathrate hydrate of methane. The Journal of Physical Chemistry 1983, 87 (21), 4198-4203.

(14)   Schicks, J.; Erzinger, J.; Ziemann, M. Raman spectra of gas hydrates—differences and analogies to ice 1h and (gas saturated) water. Spectrochimica acta part A: molecular and biomolecular spectroscopy 2005, 61 (10), 2399-2403.

(15)   Falenty, A.; Hansen, T. C.; Kuhs, W. F. Formation and properties of ice XVI obtained by emptying a type sII clathrate hydrate. Nature 2014, 516 (7530), 231-233.

(16)   Maeda, N. Brief Overview of Ice Nucleation. Molecules 2021, 26 (2), 392.

(17)   Kashchiev, D. Nucleation. Elsevier, 2000.

(18)   Morris, G. J.; Acton, E. Controlled ice nucleation in cryopreservation–a review. Cryobiology 2013, 66 (2), 85-92.

(19)   You, Y.; Kang, T.; Jun, S. Control of ice nucleation for subzero food preservation. Food Engineering Reviews 2021, 13, 15-35.

(20)   Vali, G. Ice nucleation—A review. Nucleation and atmospheric aerosols 1996 1996, 271-279.

(21)   Kimmel, G. A.; Xu, Y.; Brumberg, A.; Petrik, N. G.; Smith, R. S.; Kay, B. D. Homogeneous ice nucleation rates and crystallization kinetics in transiently-heated, supercooled water films from 188 K to 230 K. The Journal of Chemical Physics 2019, 150 (20).

(22)   Djikaev, Y.; Ruckenstein, E. Thermodynamics of heterogeneous crystal nucleation in contact and immersion modes. The Journal of Physical Chemistry A 2008, 112 (46), 11677-11687.

(23)   Krämer, B.; Hübner, O.; Vortisch, H.; Wöste, L.; Leisner, T.; Schwell, M.; Rühl, E.; Baumgärtel, H. Homogeneous nucleation rates of supercooled water measured in single levitated microdroplets. The Journal of Chemical Physics 1999, 111 (14), 6521-6527.

(24)   Stöckel, P.; Weidinger, I. M.; Baumgärtel, H.; Leisner, T. Rates of homogeneous ice nucleation in levitated H2O and D2O droplets. The Journal of Physical Chemistry A 2005, 109 (11), 2540-2546.

(25)   Lü, Y.; Xie, W.; Wei, B. Observation of ice nucleation in acoustically levitated water drops. Applied Physics Letters 2005, 87 (18).

(26)   Diehl, K.; Debertshäuser, M.; Eppers, O.; Schmithüsen, H.; Mitra, S.; Borrmann, S. Particle surface area dependence of mineral dust in immersion freezing mode: investigations with freely suspended drops in an acoustic levitator and a vertical wind tunnel. Atmospheric Chemistry and Physics 2014, 14 (22), 12343-12355.

(27)   Jing, F.; Yixin, L.; Pengjv, M.; Yongkun, G.; Shichao, G.; Bing, C.; Junkun, T.; Yudong, L. Supercooling and heterogeneous nucleation in acoustically levitated deionized water and graphene oxide nanofluids droplets. Experimental Thermal and Fluid Science 2019, 103, 143-148.

(28)   Szakáll, M.; Debertshäuser, M.; Lackner, C. P.; Mayer, A.; Eppers, O.; Diehl, K.; Theis, A.; Mitra, S. K.; Borrmann, S. Comparative study on immersion freezing utilizing single-droplet levitation methods. Atmospheric Chemistry and Physics 2021, 21 (5), 3289-3316.

(29)   Rogers, D. C. Development of a continuous flow thermal gradient diffusion chamber for ice nucleation studies. Atmospheric Research 1988, 22 (2), 149-181.

(30)   Rogers, D. C. Detecting Ice Nuclei with a Continuous—Flow Diffusion Chamber-Some Exploratory Tests of Instrument Response. Journal of Atmospheric and Oceanic Technology 1994, 11 (4), 1042-1047.

(31)   Stetzer, O.; Baschek, B.; Lüönd, F.; Lohmann, U. The Zurich Ice Nucleation Chamber
        (ZINC)-A new instrument to investigate atmospheric ice formation. Aerosol science and
        technology 2008, 42 (1), 64-74.

(32)   DeMott, P. J.; Rogers, D. C. Freezing nucleation rates of dilute solution droplets measured
        between −30 and −40 C in laboratory simulations of natural clouds. Journal of the
        atmospheric sciences 1990, 47 (9), 1056-1064.

(33)   Jung, S.; Tiwari, M. K.; Doan, N. V.; Poulikakos, D. Mechanism of supercooled droplet
        freezing on surfaces. Nature communications 2012, 3 (1), 615.

(34)   Zhang, X.; Liu, X.; Wu, X.; Min, J. Experimental investigation and statistical analysis of
        icing nucleation characteristics of sessile water droplets. Experimental Thermal and Fluid
        Science 2018, 99, 26-34.

(35)   Tobo, Y. An improved approach for measuring immersion freezing in large droplets over
        a wide temperature range. Scientific reports 2016, 6 (1), 1-9.

(36)   Bigg, E. K. The supercooling of water. Proceedings of the Physical Society. Section B
        1953, 66 (8), 688.

(37)   Ning, D.; Liu, X. Controlled ice nucleation in microsized water droplet. Applied physics
        letters 2002, 81 (3), 445-447.

(38)   Zhang, Z.; Liu, X.-Y. Control of ice nucleation: freezing and antifreeze strategies.
        Chemical Society Reviews 2018, 47 (18), 7116-7139.

(39)   Stopelli, E.; Conen, F.; Zimmermann, L.; Alewell, C.; Morris, C. E. Freezing nucleation
        apparatus puts new slant on study of biological ice nucleators in precipitation. Atmospheric
        measurement techniques 2014, 7, 129-134.

(40)   Barwood, M. T.; Metaxas, P. J.; Lim, V. W.; Sampson, C. C.; Johns, M. L.; Aman, Z. M.; May, E. F. Extracting nucleation rates from ramped temperature measurements of gas hydrate formation. Chemical Engineering Journal 2022, 450, 137895.

(41)   Ke, W.; Kelland, M. A. Kinetic hydrate inhibitor studies for gas hydrate systems: a review of experimental equipment and test methods. Energy & Fuels 2016, 30 (12), 10015-10028.

(42)   Khurana, M.; Yin, Z.; Linga, P. A review of clathrate hydrate nucleation. ACS Sustainable Chemistry & Engineering 2017, 5 (12), 11176-11203.

(43)   Jeong, K.; Metaxas, P. J.; Chan, J.; Kuteyi, T. O.; Aman, Z. M.; Stanwix, P. L.; Johns, M. L.; May, E. F. Hydrate nucleation and growth on water droplets acoustically-levitated in high-pressure natural gas. Physical Chemistry Chemical Physics 2019, 21 (39), 21685-21688.

(44)   May, E. F.; Wu, R.; Kelland, M. A.; Aman, Z. M.; Kozielski, K. A.; Hartley, P. G.; Maeda, N. Quantitative kinetic inhibitor comparisons and memory effect measurements from hydrate formation probability distributions. Chemical Engineering Science 2014, 107, 1-12.

(45)   Maeda, N.; Wells, D.; Becker, N. C.; Hartley, P. G.; Wilson, P. W.; Haymet, A. D.; Kozielski, K. A. Development of a high pressure automated lag time apparatus for experimental studies and statistical analyses of nucleation and growth of gas hydrates. Review of Scientific Instruments 2011, 82 (6), 065109.

(46)   Maeda, N. Nucleation curves of model natural gas hydrates on a quasi-free water droplet. AIChE Journal 2015, 61 (8), 2611-2617.

(47)   Metaxas, P. J.; Lim, V. W.; Booth, C.; Zhen, J.; Stanwix, P. L.; Johns, M. L.; Aman, Z. M.; Haandrikman, G.; Crosby, D.; May, E. F. Gas hydrate formation probability distributions: Induction times, rates of nucleation and growth. Fuel 2019, 252, 448-457.

(48)   Wu, R.; Kozielski, K. A.; Hartley, P. G.; May, E. F.; Boxall, J.; Maeda, N. Methane–propane mixed gas hydrate film growth on the surface of water and Luvicap EG solutions. Energy & fuels 2013, 27 (5), 2548-2554.

(49)   Tanaka, R.; Sakemoto, R.; Ohmura, R. Crystal growth of clathrate hydrates formed at the interface of liquid water and gaseous methane, ethane, or propane: variations in crystal morphology. Crystal Growth and Design 2009, 9 (5), 2529-2536.

(50)   Maeda, N. Fuel gas hydrate formation probability distributions on quasi-free water droplets. Energy & Fuels 2015, 29 (1), 137-142.

(51)   Wei, Y.; Nobuo, M. Nucleation Curves of Carbon Dioxide Hydrate in the Absence of a Solid Wall. Energy & Fuels 2023, 37 (5), 3760-3774.

(52)   Jeong, K.; Metaxas, P. J.; Helberg, A.; Johns, M. L.; Aman, Z. M.; May, E. F. Gas hydrate nucleation in acoustically levitated water droplets. Chemical Engineering Journal 2022, 433, 133494.

(53)   Marcolli, C.; Nagare, B.; Welti, A.; Lohmann, U. Ice nucleation efficiency of AgI: review and new insights. Atmospheric Chemistry and Physics 2016, 16 (14), 8915-8937.

(54)   Vonnegut, B. The nucleation of ice formation by silver iodide. Journal of applied physics 1947, 18 (7), 593-595.

(55)   Conrad, P.; Ewing, G. E.; Karlinsey, R. L.; Sadtchenko, V. Ice nucleation on BaF2 (111). The Journal of chemical physics 2005, 122 (6).

(56)   Gorbunov, B.; Baklanov, A.; Kakutkina, N.; Windsor, H.; Toumi, R. Ice nucleation on soot particles. Journal of Aerosol Science 2001, 32 (2), 199-215.

(57)   Mahrt, F.; Marcolli, C.; David, R. O.; Grönquist, P.; Barthazy Meier, E. J.; Lohmann, U.; Kanji, Z. A. Ice nucleation abilities of soot particles determined with the Horizontal Ice Nucleation Chamber. Atmospheric Chemistry and Physics 2018, 18 (18), 13363-13392.

(58)   Pinti, V.; Marcolli, C.; Zobrist, B.; Hoyle, C. R.; Peter, T. Ice nucleation efficiency of clay minerals in the immersion mode. Atmospheric Chemistry and Physics 2012, 12 (13), 5859-5878.

(59)   Polen, M.; Lawlis, E.; Sullivan, R. C. The unstable ice nucleation properties of Snomax® bacterial particles. Journal of Geophysical Research: Atmospheres 2016, 121 (19), 11,666-611,678.

(60)   Head, R. B. Steroids as ice nucleators. Nature 1961, 191 (4793), 1058-1059.

(61)   Sosso, G. C.; Whale, T. F.; Holden, M. A.; Pedevilla, P.; Murray, B. J.; Michaelides, A. Unravelling the origins of ice nucleation on organic crystals. Chemical science 2018, 9 (42), 8077-8088.

(62)   Pandey, R.; Usui, K.; Livingstone, R. A.; Fischer, S. A.; Pfaendtner, J.; Backus, E. H.; Nagata, Y.; Fröhlich-Nowoisky, J.; Schmüser, L.; Mauri, S. Ice-nucleating bacteria control the order and dynamics of interfacial water. Science advances 2016, 2 (4), e1501630.

(63)   Pummer, B. G.; Bauer, H.; Bernardi, J.; Bleicher, S.; Grothe, H. Suspendable macromolecules are responsible for ice nucleation activity of birch and conifer pollen. Atmospheric Chemistry and Physics 2012, 12 (5), 2541-2550.

(64)   Pummer, B.; Budke, C.; Augustin-Bauditz, S.; Niedermeier, D.; Felgitsch, L.; Kampf, C.; Huber, R.; Liedl, K.; Loerting, T.; Moschen, T. Ice nucleation by water-soluble macromolecules. Atmospheric Chemistry and Physics 2015, 15 (8), 4077-4091.

(65)   Pruppacher, H. R.; Klett, J. D. Microphysics of Clouds and Precipitation; 1997.

(66)   Zachariassen, K. E.; Kristiansen, E. Ice nucleation and antinucleation in nature. Cryobiology 2000, 41 (4), 257-279.

(67)   Holt, C. Substances which inhibit ice nucleation: a review. CryoLetters 2003, 24 (5), 269-274.

(68)   Koop, T.; Luo, B.; Tsias, A.; Peter, T. Water activity as the determinant for homogeneous ice nucleation in aqueous solutions. Nature 2000, 406 (6796), 611-614.

(69)   Espinosa, J. R.; Soria, G. D.; Ramirez, J.; Valeriani, C.; Vega, C.; Sanz, E. Role of salt, pressure, and water activity on homogeneous ice nucleation. The Journal of Physical Chemistry Letters 2017, 8 (18), 4486-4491.

(70)   Miyata, K.; Kanno, H.; Niino, T.; Tomizawa, K. Cationic and anionic effects on the homogeneous nucleation of ice in aqueous alkali halide solutions. Chemical physics letters 2002, 354 (1-2), 51-55.

(71)   Du, N.; Liu, X. Y.; Hew, C. L. Ice nucleation inhibition: mechanism of antifreeze by antifreeze protein. Journal of Biological Chemistry 2003, 278 (38), 36000-36004.

(72)   Kutschan, B.; Morawetz, K.; Thoms, S. Dynamical mechanism of antifreeze proteins to prevent ice growth. Physical Review E 2014, 90 (2), 022711.

(73)   Eickhoff, L.; Dreischmeier, K.; Zipori, A.; Sirotinskaya, V.; Adar, C.; Reicher, N.; Braslavsky, I.; Rudich, Y.; Koop, T. Contrasting behavior of antifreeze proteins: Ice

growth inhibitors and ice nucleation promoters. The journal of physical chemistry letters 2019, 10 (5), 966-972.

(74)   Congdon, T.; Dean, B. T.; Kasperczak-Wright, J.; Biggs, C. I.; Notman, R.; Gibson, M. I. Probing the biomimetic ice nucleation inhibition activity of poly (vinyl alcohol) and comparison to synthetic and biological polymers. Biomacromolecules 2015, 16 (9), 2820-2826.

(75)   Ahmadloo, F.; Mali, G.; Chapoy, A.; Tohidi, B. Gas separation and storage using semi-clathrate hydrates. 2008.

(76)   Prasad, P. S.; Sai Kiran, B. Clathrate hydrates of greenhouse gases in the presence of natural amino acids: storage, transportation and separation applications. Scientific reports 2018, 8 (1), 8560.

(77)   Castellani, B.; Morini, E.; Filipponi, M.; Nicolini, A.; Palombo, M.; Cotana, F.; Rossi, F. Clathrate hydrates for thermal energy storage in buildings: overview of proper hydrate-forming compounds. Sustainability 2014, 6 (10), 6815-6829.

(78)   Kumar, A.; Kushwaha, O. S.; Rangsunvigit, P.; Linga, P.; Kumar, R. Effect of additives on formation and decomposition kinetics of methane clathrate hydrates: Application in energy storage and transportation. The Canadian Journal of Chemical Engineering 2016, 94 (11), 2160-2167.

(79)   Hirai, S.; Tabe, Y.; Kuwano, K.; Ogawa, K.; Okazaki, K. MRI measurement of hydrate growth and an application to advanced CO2 sequestration technology. Annals of the New York Academy of Sciences 2000, 912 (1), 246-253.

(80)   Kim, K.; Truong-Lam, H. S.; Lee, J. D.; Sa, J.-H. Facilitating clathrate hydrates with extremely rapid and high gas uptake for chemical-free carbon capture and methane storage. Energy 2023, 270, 126902.

(81)   Babu, P.; Nambiar, A.; Chong, Z. R.; Daraboina, N.; Albeirutty, M.; Bamaga, O. A.; Linga, P. Hydrate-based desalination (HyDesal) process employing a novel prototype design. Chemical Engineering Science 2020, 218, 115563.

(82)   Babu, P.; Bollineni, C.; Daraboina, N. Energy analysis of methane-hydrate-based produced water desalination. Energy & Fuels 2021, 35 (3), 2514-2519.

(83)   Kumar, A.; Bhattacharjee, G.; Kulkarni, B.; Kumar, R. Role of surfactants in promoting gas hydrate formation. Industrial & Engineering Chemistry Research 2015, 54 (49), 12217-12232.

(84)   Fazlali, A.; Kazemi, S. A.; Keshavarz‑Moraveji, M.; Mohammadi, A. H. Impact of different surfactants and their mixtures on methane‑hydrate formation. Energy Technology 2013, 1 (8), 471-477.

(85)   Pandey, J. S.; Daas, Y. J.; Solms, N. v. Insights into kinetics of methane hydrate formation in the presence of surfactants. Processes 2019, 7 (9), 598.

(86)   Karaaslan, U.; Parlaktuna, M. Surfactants as hydrate promoters? Energy & Fuels 2000, 14 (5), 1103-1107.

(87)   Ricaurte, M.; Dicharry, C.; Broseta, D.; Renaud, X.; Torre, J.-P. CO2 removal from a CO2–CH4 gas mixture by clathrate hydrate formation using THF and SDS as water-soluble hydrate promoters. Industrial & Engineering Chemistry Research 2013, 52 (2), 899-910.

(88) Igboanusi, U.; Opara, A. The advancement from thermodynamic inhibitors to kinetic inhibitors and anti-agglomerants in natural gas flow assurance. International Journal of Chemical and Environmental Engineering 2011, 2 (2).

(89) Nasir, Q.; Suleman, H.; Elsheikh, Y. A. A review on the role and impact of various additives as promoters/inhibitors for gas hydrate formation. Journal of Natural Gas Science and Engineering 2020, 76, 103211.

(90) Rossi, F.; Gambelli, A. M. Thermodynamic phase equilibrium of single-guest hydrate and formation data of hydrate in presence of chemical additives: A review. Fluid Phase Equilibria 2021, 536, 112958.

(91) Broni-Bediako, E.; Amorin, R.; Bavoh, C. B. Gas hydrate formation phase boundary behaviour of synthetic natural gas system of the keta basin of Ghana. The Open Petroleum Engineering Journal 2017, 10 (1).

(92) Yang, C.; Zi, M.; Wu, G.; Zou, X.; Liu, K.; Chen, D. Concentration effect of kinetic hydrate inhibitor on hydrate formation and inhibition. Fuel 2022, 323, 124448.

(93) Ivall, J.; Pasieka, J.; Posteraro, D.; Servio, P. Profiling the concentration of the kinetic inhibitor polyvinylpyrrolidone throughout the methane hydrate formation process. Energy & fuels 2015, 29 (4), 2329-2335.

(94) Walker, V. K.; Zeng, H.; Ohno, H.; Daraboina, N.; Sharifi, H.; Bagherzadeh, S. A.; Alavi, S.; Englezos, P. Antifreeze proteins as gas hydrate inhibitors. Canadian Journal of Chemistry 2015, 93 (8), 839-849.

(95) Tang, C.; Liang, D. Inhibitory effects of novel green inhibitors on gas hydrate formation. Chinese Journal of Chemical Engineering 2019, 27 (9), 2107-2117.

(96)   Sa, J.-H.; Lee, B. R.; Park, D.-H.; Han, K.; Chun, H. D.; Lee, K.-H. Amino acids as natural

inhibitors for hydrate formation in CO2 sequestration. Environmental science &

technology 2011, 45 (13), 5885-5891.

CHAPTER 3 NUCLEATION CURVES OF ICE IN QUASI-FREE WATER DROPLETS

A version of this chapter has been accepted for publication in *Chemical Engineering Science*.

Abstract

Ice nucleation is important in global climate change and could also have implications to nucleation of more complex systems like clathrate hydrates. A new setup for experimental investigations of nucleation of ice that uses linear cooling ramps is described. The nucleation rates of ice in (1) microliter–sized quasi–free water droplets suspended at an interface between an inert fluorocarbon oil, perfluoromethyldecalin, and an inert hydrocarbon oil, squalane, and (2) microliter–sized quasi–free water droplets supported by stable wetting films of squalane, were determined from the procedure that was previously developed for clathrate hydrates. The impact of the number of the data points and the experimental cooling rate was investigated in detail. The nucleation curve of a given system was found to remain largely unchanged with the addition of data after about the first 100 data points. Additional 300 to 400 data points confirmed such convergence. The results also showed that the nucleation rate increased with the system supercooling, as expected, and the whole nucleation curve shifted somewhat downward with the use of a slower cooling rate. The nucleation rates of ice in the water droplets supported by stable wetting films of squalane were broadly similar to but slightly greater than those suspended between two immiscible liquids. We then compared our data to the nucleation rate of ice reported in the literature, which showed broad agreements when the differences in the scales were accounted for. The experimental method described was found to be reliable and the setup provides a basis for future studies on ice nucleation that may involve nucleation promoters, inhibitors or more complex entities.

3.1 Introduction

Ice formation has great impacts on the properties of clouds, which affects the global climate substantially [1]. It also strongly affects the water on engineered and structured surfaces such as aircraft wings [2-4], airfoils [5], bridge cables [6] and wind turbines [7], which could result in dangerous equipment failures or even losses if not controlled properly. In the process of ice formation, nucleation is the initial step that precedes the growth of ice crystals [8]. We wish to promote nucleation when the formation of ice is desirable and inhibit nucleation when the formation of ice is undesirable. The study of ice nucleation not only contributes to the global climate, aerospace and aerodynamic science, but also has potential applications in petroleum engineering [9], mineralogy [10], biology [11], and others. In oil and gas area, nucleation of ice could lay a baseline for the study of nucleation of gas hydrate, which is a multi-component process [12].

Ice nucleation in pure water was studied by experimental [1] and modelling [13] methods for decades. There were several experimental methods for studying the immersion mode of ice nucleation, which includes suspending of water droplets in a gas, supporting sessile water droplets on hydrophobic surfaces, and suspending water droplets in an oil or between two mutually immiscible oil layers [1]. The size of the water droplets that has been investigated ranged from sub-micrometers to millimeters. Some researchers studied the ice nucleation in water droplets suspended in a gas using continuous–flow thermal gradient diffusion chambers [14, 15], cloud chambers [16], Zurich ice nucleation chamber [17], laminar flow diffusion chambers [18, 19] and other techniques. Most of these techniques used aerosol particles or cloud–sized droplets as

research objects, and the ice nucleation potency was quantified as a function of the relative humidity and temperature [20].

Other than the techniques mentioned above, water droplets immobilised on a hydrophobic surface or suspended in an oil were also commonly used for studying ice nucleation. For example, Whale et al. [20] investigated ice nucleation in 1 µL water droplets supported on a hydrophobic surface. Tobo [21] reported a few modifications to cold–stage–based freezing experiments of millimeter–sized water droplets. Here the droplets were deposited onto the aluminum plate coated with a thin Vaseline layer and cooled in a clean booth. Zhang et al. [22] measured the nucleation temperatures of sessile water droplets on a cold horizontal plate and calculated the nucleation rate using classical nucleation theory. However, there were concerns like water droplet evaporation, droplet contamination by airborne particles, and the influence of neighbouring freezing droplets by frost growth when measuring in an open experimental droplet system [23]. Compared to the experiments that use water droplets in air, the methods of suspending water droplets into one or two layers of immiscible oils [24, 25] could largely minimize the effect of contacting with the container wall and foreign particles.

Although ice nucleation has been studied for decades, many questions still remain [26]. Here, we set up a system that can be used for future investigations of ice nucleation. We determined the nucleation rate of ice in (1) microliter–sized quasi–free water droplets suspended at an interface between an inert fluorocarbon oil, perfluoromethyldecalin, and an inert hydrocarbon oil, squalane, and (2) microliter–sized quasi–free water droplets supported by stable wetting films of squalane. The millimeter-sized water droplets were used for the study because the large–sized water droplets have bigger surface area per droplet, which is beneficial for determining the nucleation potencies over a broad temperature range [20]. The main purpose of the current study is to establish a new

experimental setup, calibrate it and assess its reliability. The setup described here could provide a reference point for some of the future studies on ice nucleation. For now, there is no a-priori standard for a baseline to which the effects of additives can be compared. It is also difficult to choose a reliable nucleator that can nucleate ice with certainty since many potential impacts of sample variations such as purity, grain size and aging [27] should be considered. After the baseline is set, we may investigate the effects of thermal history, nucleation promoters, nucleation inhibitors or solid walls in future studies.

3.2   Materials and Methods

3.2.1   The Experimental Setup

The experimental setup (shown in **Figure 3.1**) consisted of a custom-made cuboid sample cell, a refrigerated circulator (FPW50-HE, Julabo Company, capable of cooling down to 223 K), an aluminum lab jack (Fisher Scientific Company), two webcams (Model C922 and C270, Logitech), and a computer (DELL). The sample cell was either made of Poly (methyl methacrylate) (PMMA) or Polytetrafluoroethylene (Teflon). The dimensions of both the PMMA and the Teflon sample cells were 63 mm in the length, 63 mm in the width and 15 mm in its height. Each of them had 36 vertical holes and the dimensions of each hole were 5 mm in the inner diameter and 10 mm in the depth. Ethanol (95% purity) was chosen as the coolant and a lab jack was placed inside of the refrigerated circulator. For PMMA sample cell (shown in **Figure 3.1** (a)), it was placed into a slightly larger metal container because the PMMA sample cell could react with the ethanol when in direct contact, and squalane (95% purity, purchased from Sigma-Aldrich and used as received) was added into the gap between the sample cell and the metal container to improve thermal conduction. Then a glass cover was placed on the metal container to prevent the ethanol from

going inside. A chemically inert vacuum grease (Dow Corning, High vacuum grease) was applied between the glass cover and the metal container. Then the metal container with the sample cell inside was placed on the lab jack and its height was adjusted so that the bottom half of the metal container was submerged in the coolant. For Teflon sample cell (shown in **Figure 3.1** (b)), it is directly placed on the lab jack and its height was adjusted so that the bottom half of the Teflon sample cell was submerged in direct contact with the coolant. After that, another large glass cover was placed on the top of the refrigerated circulator bath to prevent the evaporation of the coolant. The webcam C922 and webcam C270 were supported by two laboratory stands and controlled by software on the PC to record the image of the sample cell from above and the digital thermometer reading shown on the panel of the refrigerated circulator, respectively.
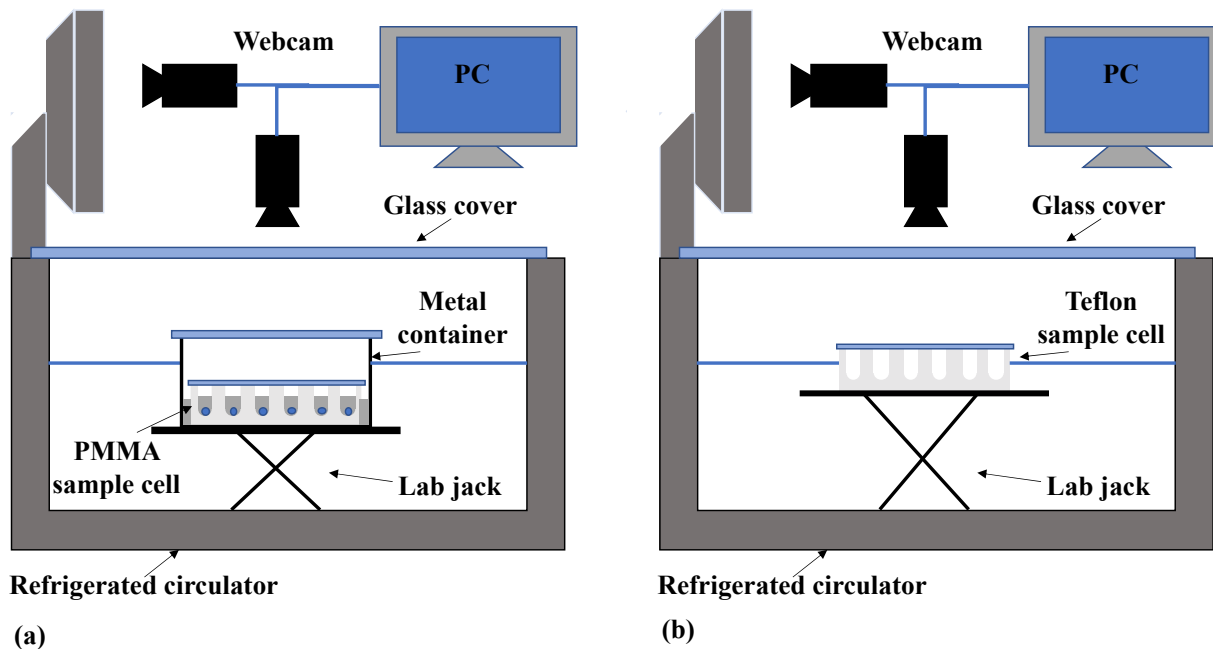
Figure 3.1. Schematic illustration of experimental setup with PMMA sample cell (a) and Teflon sample cell (b). For PMMA sample cell, it was placed into a slightly larger metal container because it would react with ethanol. For the Teflon sample cell, it was directly placed on the lab jack, contacted with ethanol.

3.2.2   Calibration of the Setup

Presence of a thermometer in contact with a sample will most likely impact the heterogeneous nucleation rate of ice. We therefore avoid direct contacts of a thermometer to any part of our samples. Because there usually is a differential between the real temperature of the sample and the temperature measured by a digital thermometer, we carried out a series of temperature calibrations. For the calibration using the PMMA sample cell, about 120 µL of squalane was placed into each hole of the PMMA sample cell using a syringe (Hamilton Company) and a thermometer (BIOS, Model#119) was inserted into a hole of the PMMA sample cell to record the temperature inside the hole, both at a fixed temperature of our selection and during linear cooling ramps. A similar procedure was used for the calibration of the Teflon sample cell. The cooling rates used for the temperature calibration during liner cooling ramps were the same as those used in the real experiments of 0.003 K/s, 0.001 K/s and 0.0003 K/s. The procedure was then repeated for different holes of either PMMA or Teflon sample cell and calibration tables were constructed which will be used to account for (1) potential temperature variation among the 36 holes and (2) potential thermal lags between the temperature of the samples in all holes and that of the reference point at which the experimental temperature was measured.

3.2.3   Cleaning Procedure

The PMMA sample cell was cleaned by Milli-Q water (ultra-pure water of 18.2 MΩ resistivity from a Millipore unit) and dried before use. The Teflon sample cell was cleaned by ethanol and dried before use. In order to avoid cross contamination, we only used a single designated syringe and a vial for each liquid (e.g., perfluoromethyldecalin, squalane, water). The

glassware was cleaned by sodium hydroxide solution, rinsed with large quantities of Milli-Q water and dried before use.

It is noted that the cartridge of the Milli-Q water equipment was regularly changed (every 6 months). In addition, we routinely checked the cleanliness of the water by shaking the glassware with water in it to make sure that bubbles burst immediately and no water droplets form on the glass walls (i.e., complete wetting).

3.2.4   Samples

Our measurements of ice nucleation rates were carried out using quasi-free water droplets supported by stable wetting films of squalane for the PMMA cell (shown in **Figure 3.2** (a)) or suspended at an interface between perfluoromethyldecalin and squalane for the Teflon cell (shown in **Figure 3.2** (b)). The setting is very similar to the one used for the investigations of nucleation rates of natural gas hydrates in quasi-free water droplets suspended in squalane [28]. Squalane is chemically inert, involatile, non-toxic and remain liquid down to at least 235 K. It also has a higher refractive index than that of water which is important in rendering the van der Waals forces of the squalane film between water and PMMA repulsive [28]. For the PMMA sample cell, about 80 µL of squalane was placed into the bottom of each hole by a designated syringe, then a small amount of Milli-Q water (60 mg) was added onto the squalane. Although squalane is less dense than water, and hence the water droplet sank to the bottom of the squalane, a thick and stable squalane film was expected to separate the water droplet from the PMMA wall due to the repulsive van der Waals forces [29, 30] (shown in **Figure 3.2** (a)). For the Teflon sample cell, about 50 µL of squalane and about 50 µL of perfluoromethyldecalin were placed into each hole by designated syringes, then a small amount of Milli-Q water (60 mg) was added into the liquids.

Perfluoromethyldecalin is chemically inert, involatile, non-toxic and remain liquid down to 203 K. Because the perfluoromethyldecalin is denser than water and the squalane is less dense than water, the water droplet was trapped between the two liquids (**Figure 3.2** (b)). Although the shape of the water droplet was non-spherical, we assumed that all the water droplets had the same spherical shape of about 4.86 mm in diameter and the corresponding surface area of about 74 mm^2. It is noted that this approximation is equivalent to ignoring the effect of gravity, and that the real surface area of a given water droplet would have been somewhat larger than 74 mm^2. However, given the typically large variations in nucleation rates, we consider such a factor to be insignificant. Then, the sample cell was sealed using a glass lid (66mm × 66mm) with the vacuum grease.
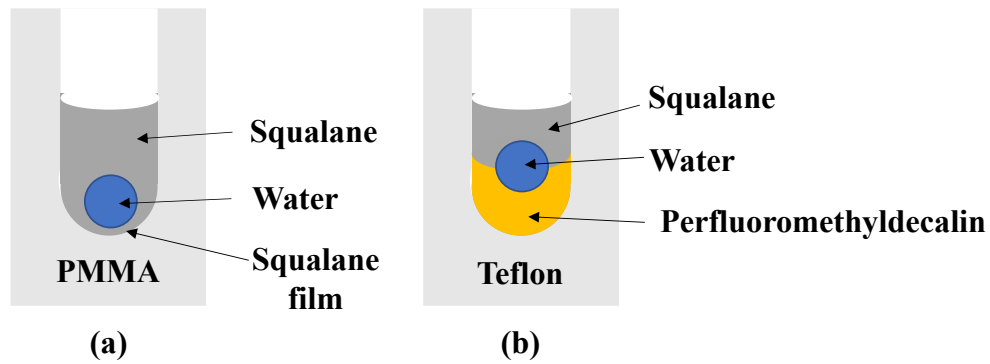
Figure 3.2. Schematic illustration of sample water droplets in PMMA and Teflon sample cell: quasi-free water droplet supported by stable wetting films of squalane (a), quasi-free water droplet suspended between two immiscible liquids (b).

3.2.5   Experimental Runs

A linear cooling ramp gradually increases the system supercooling (the driving force for nucleation) until nucleation is induced. A linear cooling ramp measurement thus takes a shorter time before the nucleation event occurs compared to an induction time measurement at a constant temperature [31]. Therefore, we use the linear cooling ramp method here for the experimental runs of ice formation. The cooling rates used in this study were 0.003 K/s, 0.001 K/s and 0.0003 K/s.

Before each cooling ramp, the sample cell was rapidly cooled from room temperature (about 20 °C) to 5 °C and held at that temperature for 15 min. The sample cell was then cooled linearly (at a constant cooling rate) from 5 °C to – 40 °C. At the end of each cooling ramp, the sample cell was warmed back to the room temperature again.

Typical photos of the top view of the Teflon sample cell with sample water droplets suspended between two immiscible liquids at different stages of a cooling ramp are shown in **Figure 3.3**. For each cooling ramp, all the water droplets were transparent and unfrozen at room temperature (**Figure 3.3** (a)). With cooling, some supercooled water droplets first expanded quickly and then gradually became opaque, which indicated freezing of the droplets (**Figure 3.3** (b)). The lag between the initial expansion and the subsequent change in the opaqueness was less than 2 minutes. Eventually, all the sample water droplets froze (**Figure 3.3** (c)) by the end of the experimental cooling ramp. The two webcams recorded the image of the top view of the sample cell and the temperature reading shown on the panel of the refrigerated circulator every 1 minute during the cooling ramp. The freezing temperature (T_f) of each droplet was obtained after correcting for the temperature differential obtained from the calibration table. The chronological array of T_f is the raw data of the experiments. We can then derive a survival curve and a nucleation curve from the experimental data, following the protocol we will describe in detail in the next section.

Frozen droplets (became opaque)
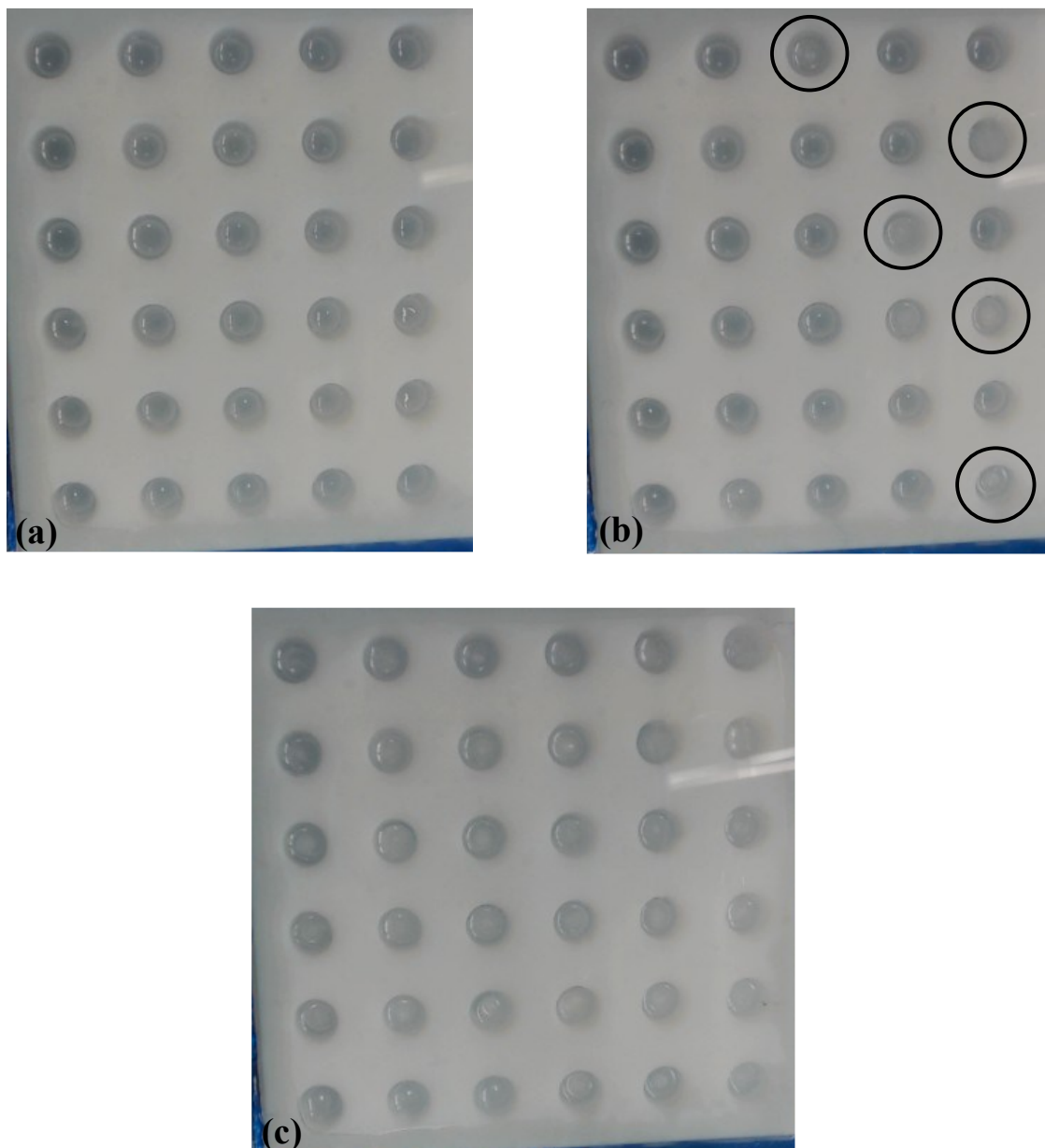
Figure 3.3. Photos of Teflon sample cell with water droplets suspended between two immiscible liquids at different stages during the cooling process. During each cooling ramp, all the water droplets were unfrozen at the beginning (a), after which more and more droplets became frozen (b) and all the water droplets were frozen at the end (c). All the photos were captured by webcam C922.

Since we recorded the images at an interval of 1 min, the corresponding uncertainties in the detection of the system supercoolings were 0.18 K, 0.06 K and 0.018 K, for the experimental cooling rates of 0.003 K/s, 0.001 K/s and 0.0003 K/s, respectively. We note that the computer disk space would overflow quickly if a higher frequency (e.g., 1 s) was used. Here, the recording of an image every minute is deemed to be sufficient given all the other sources of error. As expected, the systematic error increases with the cooling rate. Any thermal lag that could arise from the use of a linear cooling ramp is also expected to worsen with the cooling rate. Thus, an advantage of using a slow cooling rate is to reduce the potential errors in the measured supercooling values. In addition, a sample spends more time, and hence has more chance of nucleation, in a given temperature range. A disadvantage is that the use of a slow cooling rate renders each measurement more time-consuming.

The volume expansion due to freezing was instantaneous (the volume expansion completed in a shorter time than the time resolution of the setup) and hence was an ideal signal of freezing. However, in rare occasions the volume expansion was hard to detect due to poor optics, and in such cases we chose the moment at which the droplets became opaque as the frozen time and the corresponding supercooling was calculated from the temperature at which the droplet became opaque. The delay between the volume expansion and the change in the transparency of a water droplet was less than 2 minutes from a sequence for which a clear volume expansion was recorded, which corresponded to the maximum errors of up to 0.36 K, 0.12 K and 0.036 K for the use of 0.003 K/s, 0.001 K/s and 0.0003 K/s cooling rates, respectively. It is noted that we used visual inspections of the images to detect freezing, as the volume expansion upon freezing was sudden and unmistakable.

3.3 Results

3.3.1 Derivation of Nucleation Curves

A nucleation curve relates the nucleation rate of a system to the driving force for nucleation. We first outline a systematic procedure of determining a nucleation curve over the entire experimentally accessible range of supercooling that has previously been developed for nucleation of gas hydrates [32, 33]. The same procedure can be applied to nucleation of ice. The starting point of the procedure is construction of a survival curve, also known as a survival probability distribution. A survival curve is defined as the survival probability, F, as a function of the driving force for nucleation. The survival probability is the complement of *cumulative* nucleation probability (1 – cumulative nucleation probability), and an experimentally convenient measure of the driving force is system supercooling [32]. In practice, the survival probability at time t is the probability that ice is absent until time t in the water droplet of interest.

We deduced the "true" sample temperature, T_{sample}, by applying the calibration table to the detected system temperature at the time of freezing of each sample droplet, which is $T_{detected}$. Then corresponding "true" supercooling is;

$$\Delta T \equiv 273.15 - T_{sample} \qquad \text{Eq. 3.1}$$

For each individual survival curve, all "true" supercoolings (ΔT) corresponding to each experimental water droplet are arranged in an ascending order. After that, the survival probability, F, was calculated from the number of surviving water droplets at a given temperature divided by the total number of water droplets and plotted as a function of "true" supercooling.

The second step of the nucleation curve derivation is calculating the natural logarithm of the survival probability, $\ln F$, with respect to lag time, t. Since linear cooling ramps were used in this study, the shape of the curve of $\ln F(t)$ is the same as that of the curve of $\ln F(\Delta T)$ as a function

of "true" supercooling ΔT, except that the x–axis is re-scaled by the experimental cooling rate. The lag time can be calculated from the "true" supercooling ΔT divided by the nominal cooling rate $\alpha_{nominal}$. The nominal lag time, t, calculated this way was shorter than the actual recorded lag time (t_{true}) of the freezing event, which was the numerical difference in time from when the system passed 273.15 K to when the freezing of a sample droplet was detected. The application of the temperature calibration table to the detected temperature rendered the "true" sample temperature slightly higher than the nominal temperature and the temperature gap between the nominal and the real temperatures gradually increased with the supercooling, as expected. The difference in the actual recorded lag time and the nominal lag time was found to be 960 sec in the worst case (at the largest supercooling) for the experimental cooling rate of 0.001 K/s, which corresponded to an error in the supercooling of 0.96 K.

Strictly speaking, the actual recorded lag time should be considered as the "true" lag time because the "true" cooling rate would be somewhat slower than the nominal experimental cooling rate due to the thermal lag of the sample. To investigate how the derivation of the nucleation curve may be impacted by the errors in the lag times and the temperature calibration, we reanalyzed the data of quasi-free water droplets supported by stable wetting films of squalane with the cooling rate of 0.001 K/s. For this reanalysis, we compared the nucleation curve (nucleation rate per unit area) that used (1) the nominal (un–calibrated) temperature and the nominal (un–calibrated) lag time (the supercooling was calculated by subtracting the nominal temperature from 273.15 K and the corresponding nominal lag time was calculated from the calculated supercooling divided by the nominal cooling rate), (2) the calibrated temperature and the corresponding nominal (un–calibrated) lag time, which was calculated from the calibrated supercooling divided by the nominal cooling rate, and (3) the calibrated temperature and "true" (recorded) lag time. The comparison is

shown in **Figure 3.4**. As can be seen, the temperature calibration is important in that the use of un–calibrated temperature causes large systematic errors. In contrast, the use of nominal lag times in the place of calibrated lag time causes only negligible errors as long as the calibrated temperatures are used for the calculation of the nominal lag times.
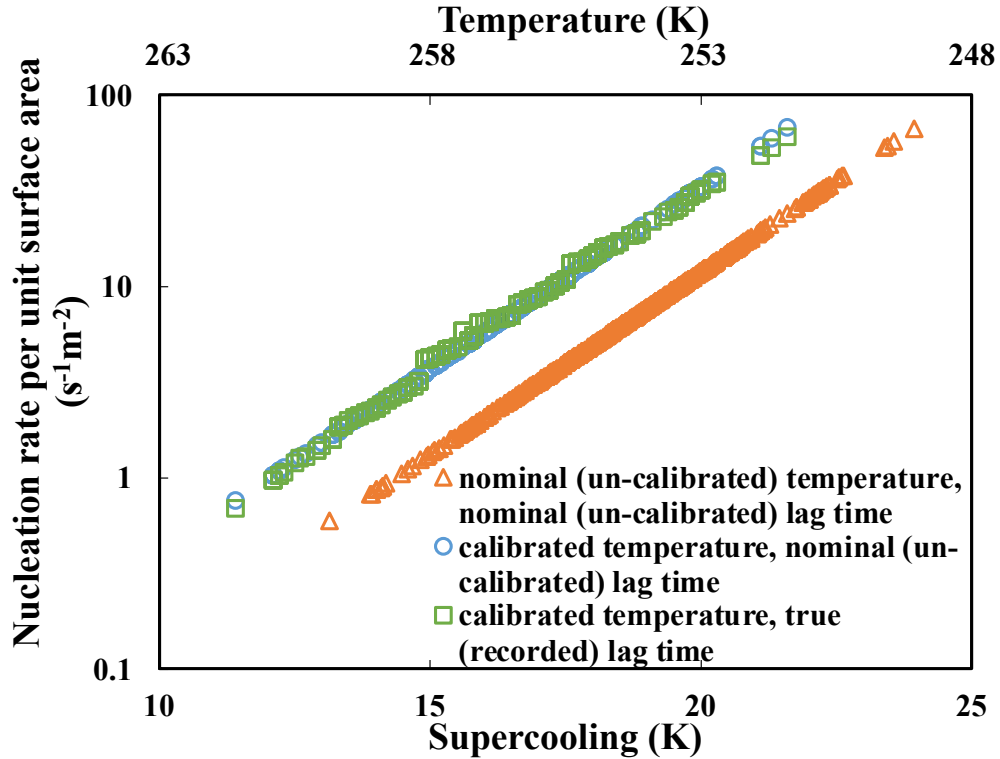
Figure 3.4. Nucleation curve (nucleation rate per unit surface area) of ice formation on water droplets supported by stable wetting films of squalane with a cooling rate of 0.001 K/s and the reanalyzed curves. The nucleation curve derived from calibrated temperature and nominal (un-calibrated) lag time was the same as the nucleation curve at 0.001 K/s cooling rate shown in Fig. 11. The curve derived from the nominal (un-calibrated) temperature and nominal (un-calibrated) lag time was shown by the orange triangle mark. The curve derived from the calibrated temperature and true (recorded) lag time was shown by green square mark. All the data were measured under atmospheric pressure.

After fitting a curve to $\ln F(t)$ and analytically differentiating the fitted curve with respect to t (nominal lag time), the negative of the local slope at each t was obtained. We note that several

choices are possible for the functional form of such fitted curves. Here we used exponential functions of the form $A \cdot \exp(Bt) + C$ for the fitting. Use of simple power laws resulted in similar nucleation curves and the difference in the nucleation rates between them was at most by a factor of 4 over the entire range of supercooling. The choice of a functional form for the fitting thus has a minor impact on the values of the nucleation rates over the range of supercooling for which the data exist, however, such choice could make a substantial difference if the nucleation curve were to be extrapolated beyond the range of existing data. Finally, the most probable nucleation rate at a given supercooling can be obtained by correcting each local slope by a factor of ln2 [32, 33]. Since we used the local slope of $\ln F(t)$ with respect to time for the calculation of the nucleation rate, and the local slope (derivative) is expected to be insensitive to the largely constant (only gradually increasing) temperature shift due to the application of the calibration table, we expect the error that arises from not knowing the "true" cooling rate or what the "true" lag time of the sample is small [34].

Thus obtained experimental nucleation rate of a given system depends on the system size, so it has to be normalized by using an appropriate measure of the system size for which the number of potential nucleation sites is expected to be proportional. Here we show both nucleation rate per unit area (1 m^2) and nucleation rate per unit volume (1 m^3) of our water droplets. The former corresponds to the case that the nucleation in our droplets was due to heterogeneous nucleation and the latter corresponds to the case that the nucleation in our droplets was due to homogeneous nucleation. We first show each type of these data measured in water droplets supported by stable wetting films of squalane in six batches of 100 points each that are in the chronological order. **Figure 3.5** shows each of the six individual survival curves that have 100 data points. The survival curves of ice formation were concentrated at the supercooling range of 12 to 22 K. The

corresponding ln*F* of these survival curves are shown in **Figure 3.6**. Finally, the nucleation curves

are shown in **Figure 3.7** and **Figure 3.8**. **Figure 3.5**-**Figure 3.8** were all for the data measured in

quasi-free droplets supported by stable wetting films of squalane in the PMMA sample cell.

In the current study, we didn't determine the error bars in the measured nucleation curves.

We note that Murray et al. [35] compartmentalized their data to small increments of time Δt over

which changes in the temperature are small, and calculated the standard deviation (error bars)

based on the several cooling ramp experiments that were contained within each compartment.

However, the physical meaning of such error bars is not clear. Not only the size of the error bars

would depend on the choice of the size of each compartment, induction time distributions (which

are the inverse of the nucleation rates) at a constant temperature are known to be very broad to an

extent that cannot be practically measured because an arbitrary cut-off maximum waiting time will

typically have to be introduced [32, 34, 36]. How the statistical errors (standard deviations for

which a Gaussian distribution is often implicitly assumed) in the nucleation rates obtained from

an ensemble of cooling ramp experiments of a selected cooling rate is related to the scatter

(standard deviation) of the nucleation rates obtained from the inverse of the induction times at a

constant temperature is beyond the scope of this work. Nevertheless, we show our data in Figures

5 through 8 as groups of 100 data points which provide some idea about the variability in our data.

We note that, philosophically, one should not expect to obtain error bars for nucleation data as a

conventional measure of the size of the random errors because it is experimentally impossible to

"repeat" or "reproduce" a nucleation event, in a deterministic sense [26].
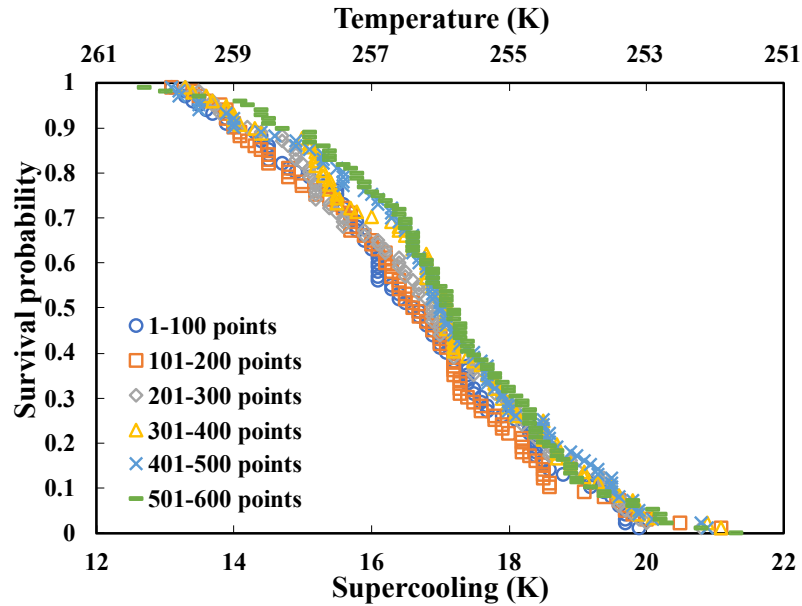
Figure 3.5. The survival curves of ice formation on water droplets supported by stable wetting films of squalane. Different types of markers correspond to different individual groups of data points. All the survival curves were measured at room pressure and using the same cooling rate of 0.003 K/s.
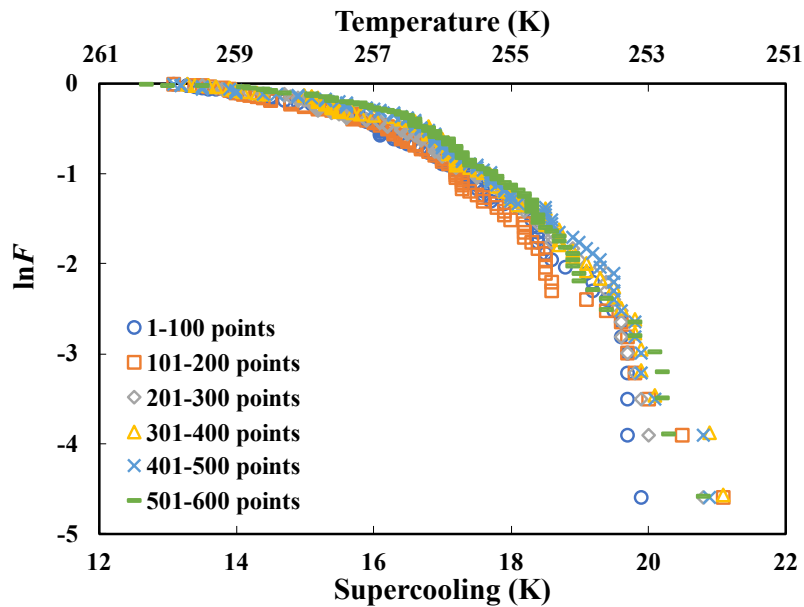
Figure 3.6. Natural logarithm of the survival curves (lnF vs ΔT) of ice formation on water droplets supported by stable wetting films of squalane. Different types of marker were corresponding to different individual groups of data points. All data were measured at room pressure and using the same cooling rate of 0.003 K/s.
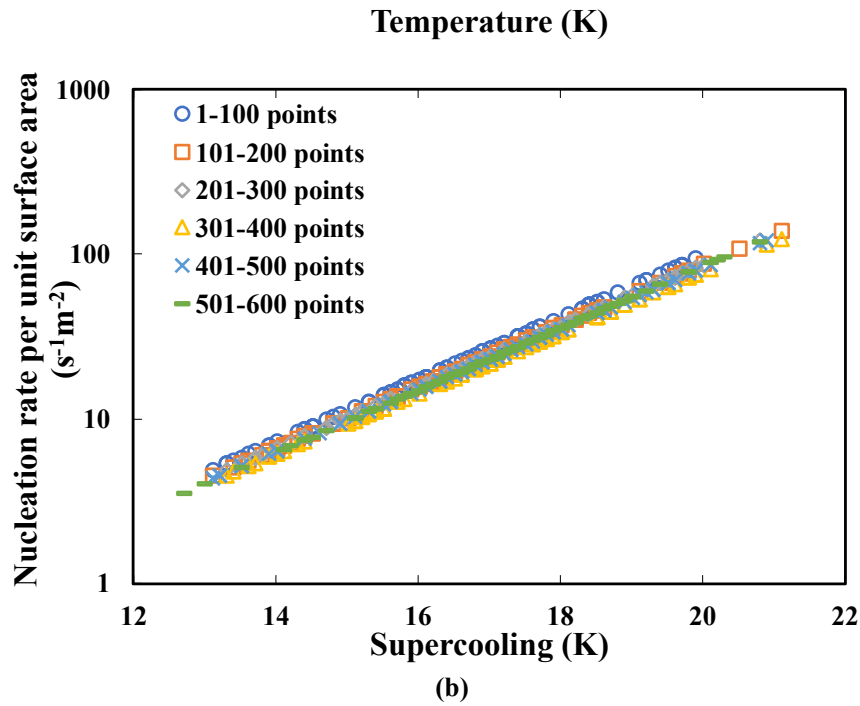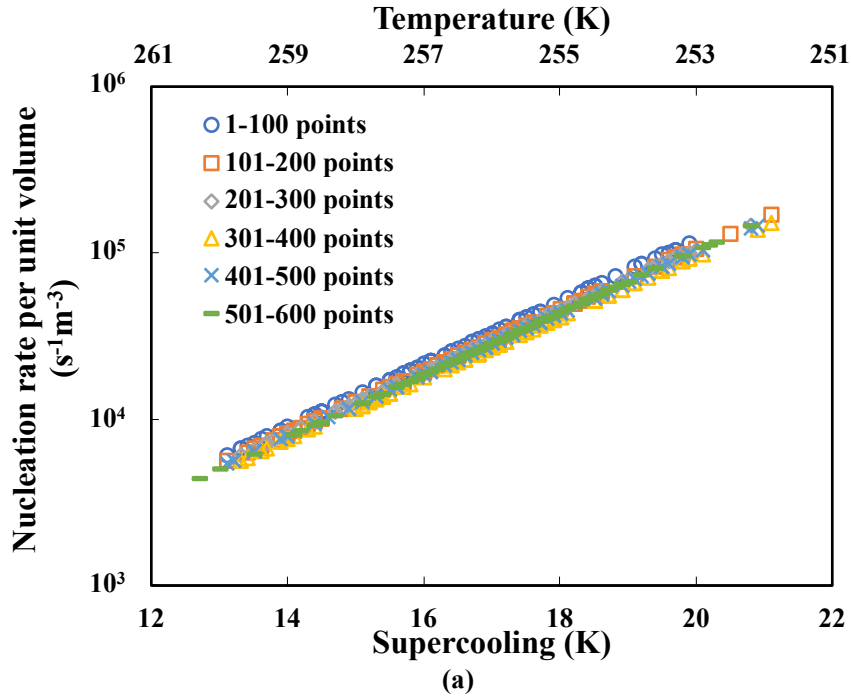
Figure 3.7. Nucleation curves (nucleation rate per unit volume (a) and nucleation rate per unit surface area (b)) of ice formation on water droplets supported by stable wetting films of squalane at room pressure and using 0.003 K/s as cooling rate. Different types of marker were corresponding to different individual groups of data points.
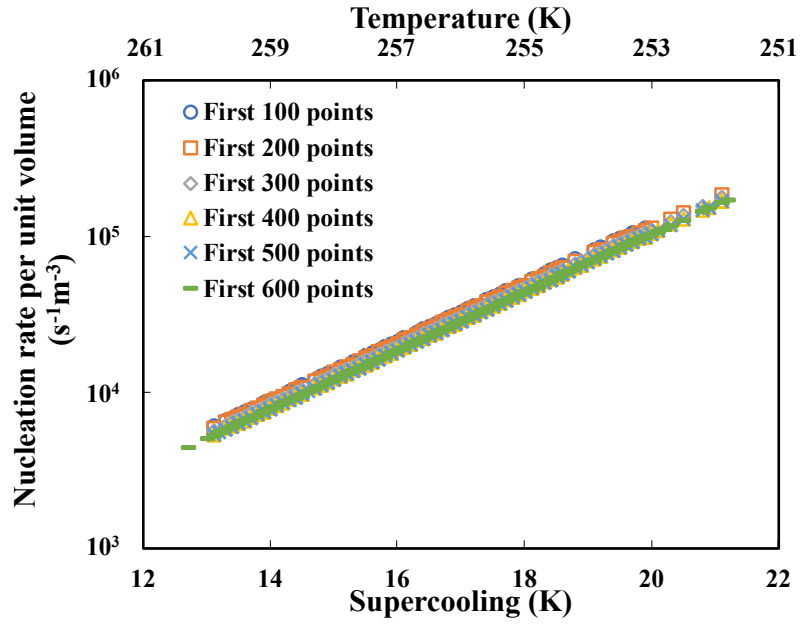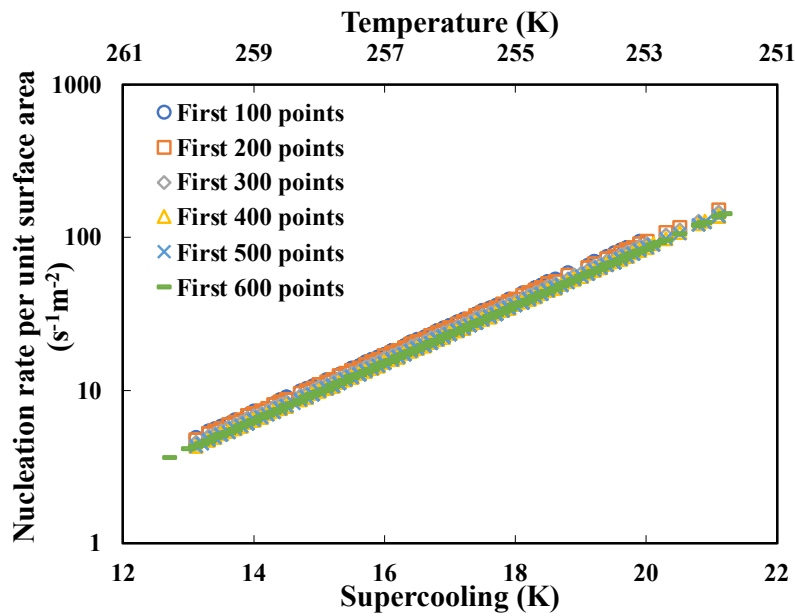
Figure 3.8. Nucleation curves (nucleation rate per unit volume (a) and nucleation rate per unit surface area (b)) of ice formation on water droplets supported by stable wetting films of squalane at room pressure and using 0.003 K/s as cooling rate. Different types of marker were corresponding to different accumulative groups of data points.

3.3.2   Number of Data Points Dependence

One of the primary concerns in the systematic and simultaneous derivation of the entire nucleation curve is: how many data points are sufficient for a reliable derivation? This is one of the most fundamental questions when using linear cooling ramps for the measurement of nucleation curves [33]. In order to study the effect of the number of data points on the nucleation rates of ice, we took two different ways to analyze the 600 data points measured in quasi-free droplet supported by stable wetting films of squalane (in the PMMA sample cell). The first is to analyze each individual group of the 100 data points (the first 100 points, the second 100 points, the third 100 points, etc.). The result is shown in **Figure 3.7**. The other one is to analyze the cumulative groups of the data points (the first 100 points, the first 200 points, the first 300 points, etc.). The result is shown in Figure *3.8*.

Both **Figure 3.7** and **Figure 3.8** show that the nucleation curve hardly changed with the accumulation of data after the first 100 data points. Still, at least 300 or 400 data points are required to confirm such convergence. We thus conclude that 300 or 400 data points are probably sufficient for a reliable derivation of a nucleation curve of ice in water droplets. This finding is somewhat similar to the conversion of the nucleation curves of methane hydrate that required accumulation of 400 data points [33].

3.3.3   Cooling Rate Dependence

Other than the number of data points dependence, another fundamental question related to the linear cooling ramp method is how slow the linear cooling rate needs to be for a reliable derivation of the nucleation curve [33]. In order to study the effect of the cooling rate on the nucleation rate of ice, we repeated the cooling ramps using three different cooling rates over one

order of magnitude of 0.001 K/s, 0.003 K/s and 0.0003 K/s. Here, we used the data measured using quasi-free water droplets supported by stable wetting films of squalane to study the cooling rate dependence. For each cooling rate, 600 data points were collected for the determination of the nucleation curves. The survival curves of ice formation at various cooling rates are shown in **Figure 3.9**, and the natural logarithm of the survival probability for these three cooling rates are shown in **Figure 3.10**. The survival curves of ice formation were found to be concentrated at the supercooling range of 12.7 to 21.2 K, 11.4 to 21.6 K and 11 to 20 K for the cooling rates of 0.003 K/s, 0.001 K/s and 0.0003 K/s, respectively. The water droplets seemed to freeze at a higher temperature (lower supercooling) with the use of a slower cooling rate, as expected, because each sample spent more time and hence would have had more chance of nucleation at higher temperatures. The local slope of $\ln F$ at the same supercooling became somewhat less steep as the cooling rate slowed, as shown in **Figure 3.10**, which resulted in somewhat lower nucleation rates as the cooling rate became slower, as shown in **Figure 3.11**.
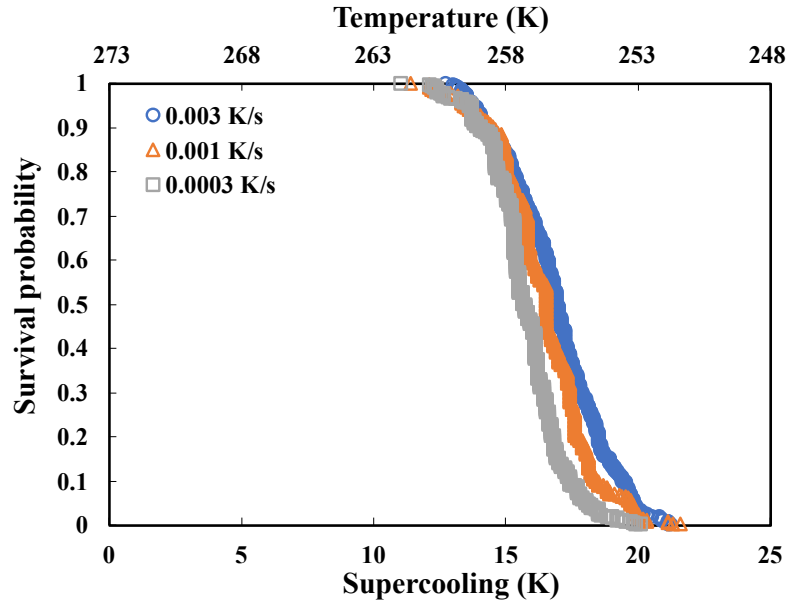
Figure 3.9. The survival curves of ice formation on water droplets supported by stable wetting films of squalane at various cooling rates. The blue circle, orange triangle and grey square corresponds to data points at cooling rates of 0.003 K/s, 0.001 K/s and 0.0003 K/s, respectively. All the data were measured at room pressure.
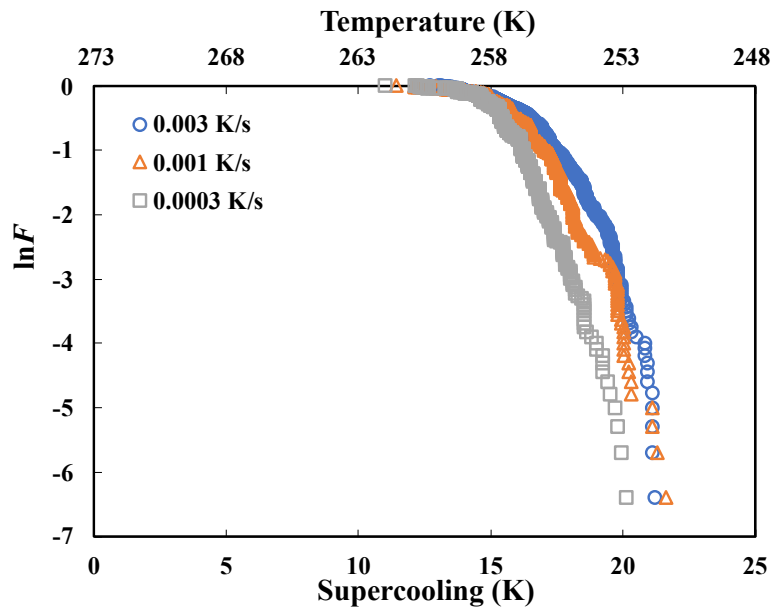
Figure 3.10. Natural logarithm of survival curves ($\ln F$ vs ΔT) of ice formation on water droplets supported by stable wetting films of squalane at various cooling rates. The blue circle, orange triangle and grey square corresponds to data points at cooling rates of 0.003 K/s, 0.001 K/s and 0.0003 K/s, respectively. All the data were measured at room pressure.

56
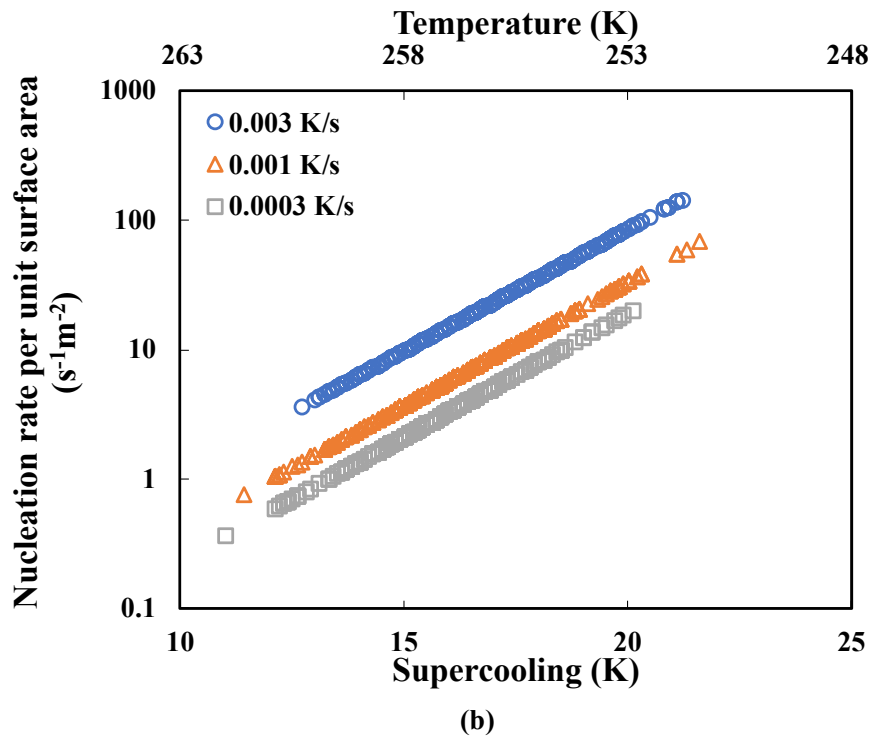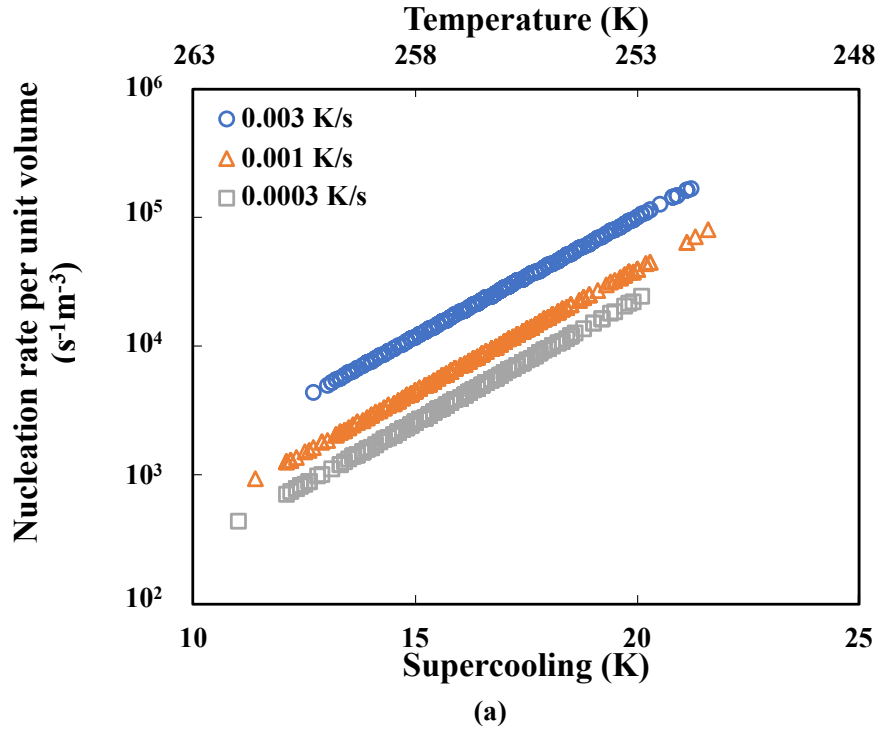
Figure 3.11. Nucleation curves (nucleation rate per unit volume (a) and nucleation rate per unit surface area (b)) of ice formation on water droplets supported by stable wetting films of squalane at room pressure using various cooling rates. The blue circle, orange triangle and grey square corresponds to data points at cooling rates of 0.003 K/s, 0.001 K/s and 0.0003 K/s, respectively.

This trend that the nucleation rate decreased as the experimental cooling rate slowed was observed before for nucleation of clathrate hydrates and remains one of the unresolved issues of the linear cooling ramp method [28, 33]. Because the nucleus could only be detected after it grows to an experimentally detectable size, the true ΔT at which the nucleation happened must be earlier in time and hence at a ΔT that is somewhat smaller than the experimental ΔT. This means that the real nucleation rate should be lower than the experimental nucleation rate at a given ΔT [31].

At the time of this writing, the most plausible explanation is that each experimentally determined nucleation curve by the linear cooling ramp method may be interpreted to represent *the upper bound* of the "true" nucleation rate at each system supercooling [31]. In short, the "true" nucleation rate is likely lower but cannot be higher than the experimentally determined nucleation curve that uses linear cooling ramps. Then we may have a way of explaining the observed trend because the *gap* between the experimentally determined nucleation curve and the "true" (alberit unknown) nucleation curve would progressively narrow as the experimentally determined nucleation curve progressively shifts downward as the slower cooling rate is used [31]. An experimentally determined nucleation curve would then eventually asymptotically approach and match the "true" nucleation curve when an infinitesimal cooling rate is used. We note that the difference referred to above (that arises from the use of different experimental cooling rate) is small in the context of nucleation rate and is well within the much larger scatter of a typical induction time distribution at a constant temperature [32].

3.3.4 Comparison Between the Quasi-Free Water Droplets Suspended Between Two Immiscible Liquids and Those that are Supported by Stable Wetting Films of Squalane

As mentioned above, for now there is no a-priori standard for a baseline to which the effects of additives can be compared. In this study, we compared the ice nucleation rates measured in quasi-free water droplets supported by stable wetting films of squalane and suspended at an interface between perfluoromethyldecalin and squalane.

The nucleation curves, both normalized to unit volume and normalized to unit surface area, were shown in **Figure 3.12**. For the water droplets supported by stable wetting films of squalane, 600 data points were collected for the determination of the nucleation curve with each cooling rate. For the water droplets suspended between the two immiscible liquids, about 500 data points were collected for the determination of the nucleation curve with cooling rate 0.003 K/s and 0.001 K/s, and about 400 data points were collected for the determination of the nucleation curve with cooling rate 0.0003 K/s.
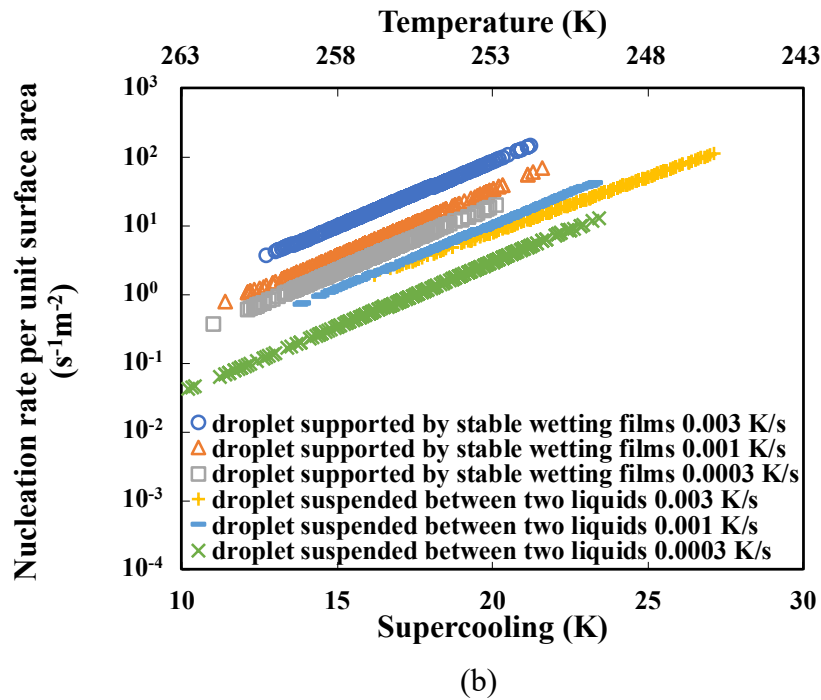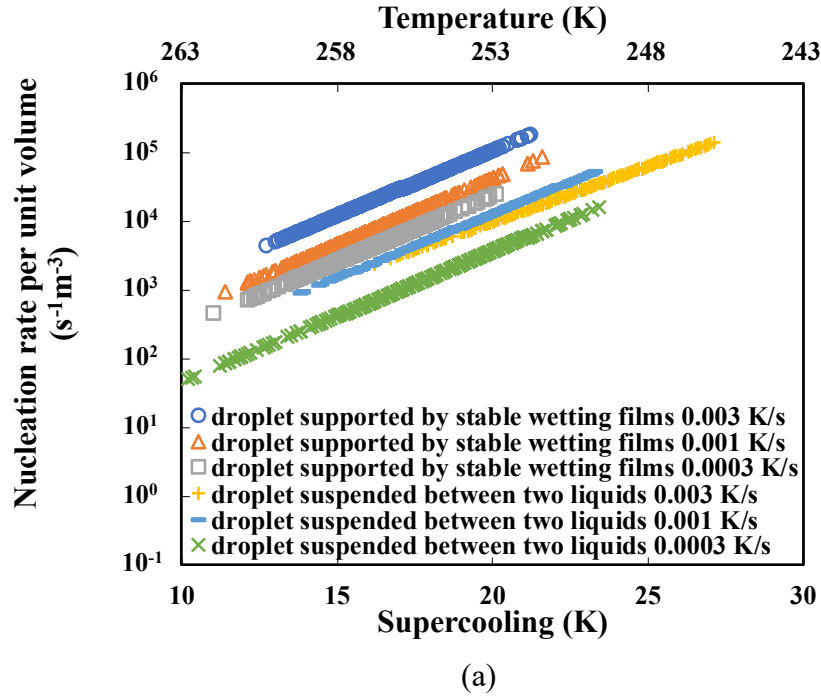
Figure 3.12. Nucleation curves (nucleation rate per unit volume (a) and per unit surface area (b)) measured in quasi-free water droplets supported by stable wetting films of squalane and water droplets suspended at the interface of between perfluoromethyldecalin, with three different cooling rates. When using the same cooling rate, the nucleation curve measured in droplets suspended between two liquids could reach a deeper supercooling than that measured in droplets supported by stable wetting films of squalane, and the nucleation rate measured in droplet suspended between two liquids was lower than that measured in droplet supported by stable wetting films of squalane at the same supercooling.

60

As shown in **Figure 3.12**, the nucleation curves measured in the water droplets supported by stable wetting films of squalane were concentrated in the supercooling range of 12.7 to 21.2 K, 11.4 to 21.6 K and 11 to 20 K for the cooling rates of 0.003 K/s, 0.001 K/s and 0.0003 K/s, respectively. For the water droplets suspended between the two immiscible liquids, the nucleation curves were concentrated in the supercooling range of 16.2 to 27.1 K, 13.8 to 23.3 K and 10.2 to 23.4 K for the cooling rates of 0.003 K/s, 0.001 K/s and 0.0003 K/s, respectively. When using the same cooling rate, the nucleation curve measured in the water droplets suspended between two immiscible liquids (perfluoromethyldecalin and squalane) appeared to reach somewhat deeper supercoolings (lower temperatures) than those supported by stable wetting films of squalane. And for cooling rates of 0.003 K/s and 0.001 K/s, the supercooling range in the water droplets suspended between the two immiscible liquids were also somewhat larger. In addition, the nucleation rates in the water droplets suspended between two liquids were somewhat lower than those supported by stable wetting films of squalane at the same supercooling. However, the difference in the nucleation rates was generally less than 1 and at most 2 orders of magnitude. Even though the van der Waals forces in the stable wetting films of squalane between water and PMMA are expected to be repulsive (the disjoining pressure should be positive), the water droplets are nevertheless within the range of the surface forces exerted by PMMA and that may have influenced the nucleation rate of ice in these water droplets.

3.4   Discussion

3.4.1   The Robustness of the Experimental Method

While analyzing the experimental data measured in the water droplets supported by stable wetting films of squalane, we noticed that a few water droplets in particular holes froze somewhat earlier than the others in some of the 600 linear cooling ramps. Potential presence of impurities that can provide heterogeneous nucleation sites in such droplets or compartments could induce freezing of the water droplet earlier (at a higher temperature) than it would in the absence of such impurities. Thus, if such early freezing repeatedly occurred in the same hole, the nucleation data from that particular hole would be suspect. To investigate how the derivation of the nucleation curve may be impacted by the presence of such a few outlier data points, we reanalyzed the data measured in droplets supported by stable wetting films of squalane of the 0.001 K/s cooling rate after removing some droplets that nucleated early (at high temperatures).

For this reanalysis, we reanalyzed the data by (1) removing all the data points that came from <u>one</u> water droplet in the same hole AND that corresponded to the nucleation events that were earlier than any other nucleation events from the other water droplets (only the data points that corresponded to early nucleation events were removed and the data points that corresponded to later freezing events were not removed even if they came from the same droplets), and (2) removing all the data points that came from <u>three</u> water droplets in the same three holes AND froze earlier than the water droplets that were in any other holes (only the data points that corresponded to early freezing events were removed and the data points that corresponded to later freezing events were left even though they came from the same droplets). The rationale of limiting this exercise to the first three water droplets is that (1) the locations of the holes in which nucleation took place

were totally random by then, and (2) the difference in the lag times between the successive freezing events was very short by then. The re-analyzed curves were shown in **Figure 3.13**-**Figure 3.15**.
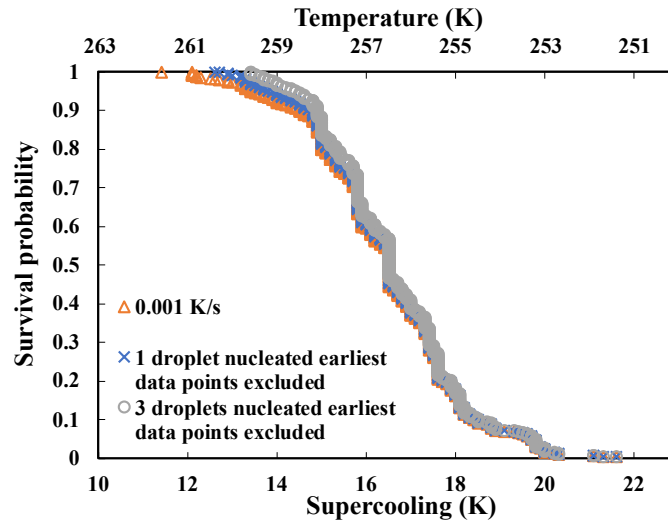
Figure 3.13. The survival curve of ice formation on water droplets supported by stable wetting films of squalane with cooling rate of 0.001 K/s and the reanalyzed curves. The survival curve at 0.001 K/s cooling rate was the same as that in Figure 3.9. The curve derived by excluding the data points coming from 1 droplet in the same hole nucleated earliest was shown by blue cross mark. The curve derived by excluding the data points coming from 3 droplets in the same three holes nucleated earliest was shown in grey circle mark. All the data were measured at room pressure.
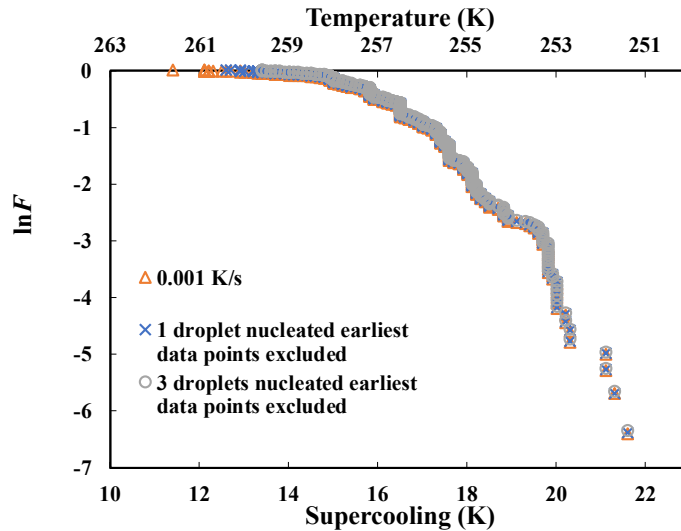
Figure 3.14. Natural logarithm of survival curve (lnF vs ΔT) of ice formation on water droplets supported by stable wetting films of squalane with cooling rate of 0.001 K/s and the reanalyzed

curves. The natural logarithm of survival curve at 0.001 K/s cooling rate was the same as that in Figure 3.10. The curve derived by excluding the data points coming from 1 droplet in the same hole nucleated earliest was shown by blue cross mark. The curve derived by excluding the data points coming from 3 droplets in the same three holes nucleated earliest was shown by grey circle mark. All the data were measured at room pressure.
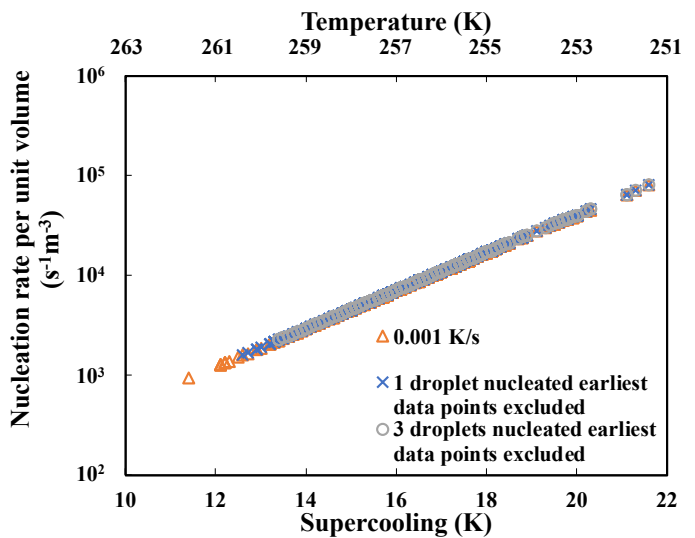
(a)
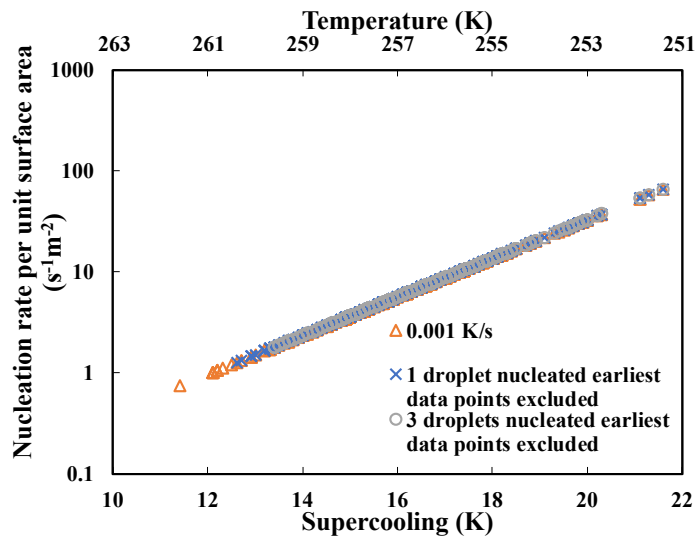
(b)

Figure 3.15. Nucleation curves (nucleation rate per unit volume (a) and nucleation rate per unit surface area (b)) of ice formation on water droplets supported by stable wetting films of squalane with cooling rate of 0.001 K/s and the reanalyzed curves. The nucleation curves at 0.001 K/s cooling rate were the same as those in Figure 3.11. The curve derived by excluding the data points coming from 1 droplet in the same hole nucleated earliest was shown by blue cross mark.

The curve derived by excluding the data points coming from 3 droplets in the same three holes nucleated earliest was shown by grey circle mark. All the data were measured at room pressure.

The removal of the several outlier data points led to the reduction in the denominator that calculated the survival probability in each case. Thus, re–calculation of the survival probability after such removal of the data points is expected to impact the numerical values of the survival probability at each supercooling temperature. However, as can be seen from **Figure 3.15**, although the removal of such outlier data points truncated the nucleation curve at the lower supercooling end (the higher temperature end), its impact to the numerical values of the nucleation rates turned out to be negligibly small. The underlying reason is that the change in the numerical values of the survival probability was largely insensitive to the <u>local slope</u> of $\ln F$ (not the absolute values of $\ln F$) with respect to t and hence to the nucleation rates. Thus, an important conclusion here is that even though several nucleation data might have been impacted by the presence of impurities, *the systematic derivation of the nucleation curve remains robust in that the nucleation rates at deeper supercoolings remain largely unaffected by the presence or absence of such potential nucleation events at low supercoolings*. Of course, if all the droplets in every cooling ramp were uniformly impacted by the presence of impurities then the entire nucleation curve would be impacted, and this method of re-analysis would not provide any new insights.

3.4.2   Normalization Constant of Nucleation Rate

In the following subsection, we will compare our results to those of Bigg [24], Murray et al. [35] and Stockel et al. [37]. In order to make meaningful comparisons, the nucleation rate must be normalized to the unit system size based on the presumed density of the number of the potential nucleation sites. The two leading methods of such normalization is the system volume that

corresponds to homogeneous nucleation and the interfacial area that corresponds to heterogeneous nucleation.

It has been known that homogeneous nucleation of water will not occur at temperatures higher than about – 42°C (231 K) [38]. Indeed, Fig. 10 of Ickes et al. [39] shows that no modern studies on homogeneous nucleation had been done accurately above temperatures of 240 K. In addition, the comparison of our results to the results of Stockel et al. [37] who used an acoustically levitated water droplets shows that it is highly unlikely that homogeneous nucleation has taken place in our system. These results suggest that the nucleation of ice in our system is likely heterogeneous and as such we should use interfacial area as the normalization constant of our droplets.

Other than the possibility of minute amounts of tiny impurities that may act as potential heterogeneous nucleation sites, the so–called surface nucleation suggests that the appropriate measure of the system size should be the interfacial area, not the volume [40]. In surface nucleation, the number of potential nucleation sites, N_0, scales with the square of the droplet radius (N_0 is proportional to the surface area), whereas in homogeneous nucleation, the number of potential nucleation sites scales with the cube of the droplet radius (N_0 is proportional to the system volume). We can envision several mechanisms that may be possible for such surface enhancements of nucleation rates. First, tiny impurities are expected to accumulate at the interface. This phenomenon is because of the virtually irreversible adsorption of nanoparticles to interfaces due to the typically large adsorption energies, the feature that has been extensively used for the stabilization of the Pickering emulsions [41]. In addition, many organic substances have been found to be effective ice nucleators and these substances have lower specific surface free energy values than those of liquid water or ice, which suggests that these substances are more likely to be

present on a surface of liquid water or ice than in the interior of liquid water or ice [26]. Second, even in the absence of such mundane issue of impurities, so-called surface nucleation suggests that the nucleation is more likely and becomes heterogeneous in nature because the system symmetry breaks at an interface [40, 42]. Third, even if the system were free of any contaminants / impurities, there is a possibility that squalane we used to suspend or support our water droplets could potentially act as an ice nucleator, given that many organic compounds have been found to be very effective ice nucleators [26]. We note that Bigg used water droplets trapped between two immiscible oil layers that were away from a solid wall and obtained similar nucleation rates to ours at comparable temperature ranges [24]. To this end, there's still possibility that homogeneous nucleation occurred in our quasi-free water droplet suspended between two liquids if no tiny impurities existed and the organic compounds we used had no impact on ice nucleation. However, it is unclear whether so-called surface nucleation or homogeneous nucleation occurred in this study. In this case, we still applied both volume and surface area as the normalization constants for the comparison with the literature data in the following section.

3.4.3   Comparison of the Nucleation Rate of Ice with the Literature Data

It is not obvious how best we can compare our results (both measured in quasi-free water droplets supported by stable wetting films of squalane and those suspended at the interface between perfluoromethyldecalin and squalane) to the literature data [16, 24, 35, 37, 43-48]. Here we attempted two methods; (1) the range of supercoolings in terms of the range in the droplet diameter (which is shown in **Figure 3.16**) and (2) the range of nucleation rate in terms of the range of supercoolings (which is shown in **Figure 3.17**).
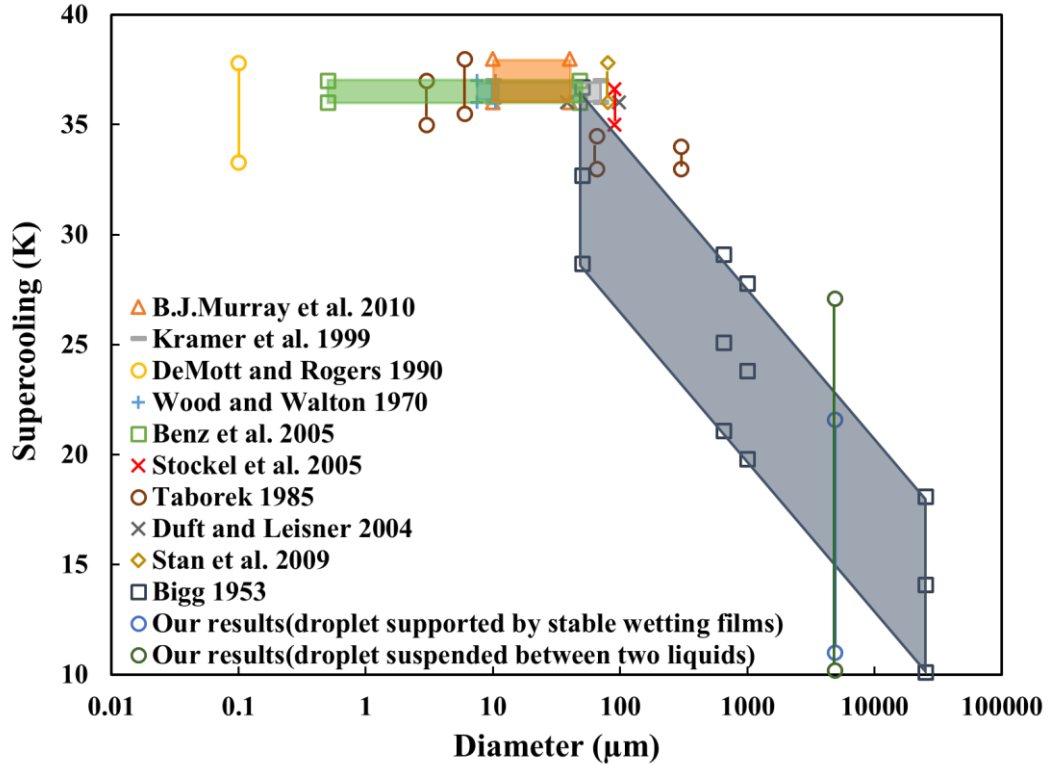
Figure 3.16. Comparison of the supercooling range in the literature data as a function of the droplet diameter. The vertical lines show the range of supercoolings for a fixed droplet size and the parallelogram shows the range of supercoolings over a range of droplet sizes.

In **Figure 3.16**, the vertical lines show the range of supercoolings for a fixed droplet size and the parallelogram shows the range of supercoolings over a range of droplet sizes. It is noted that Bigg only provided the mean freezing temperature as a function of droplet diameter over the range of droplet diameter he studied (50 µm to 2.5 cm). He also noted that the range of the freezing temperature of 1 mm diameter droplets was from around -19 to -28 °C (the mean freezing temperature was -23.8 °C) [24]. In **Figure 3.16** we assumed that the supercooling range for each droplet diameter in his study was (mean supercooling ± 5 K).
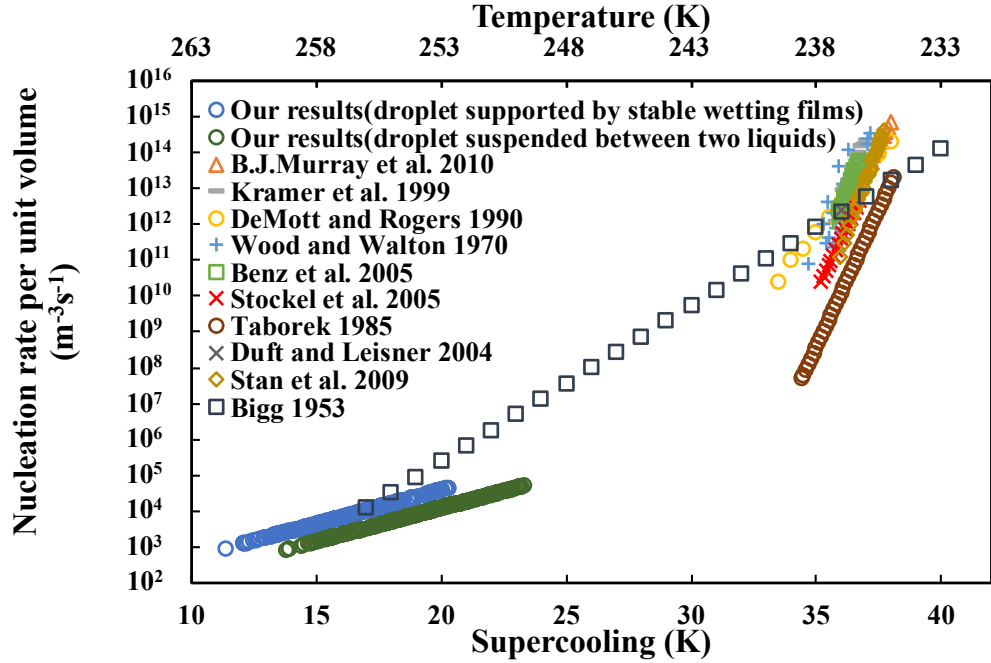
Figure 3.17. Distribution of the nucleation rate per unit volume as a function of the supercooling in the literature. The nucleation curves for our result are for the medium cooling rate of 0.001 K/s shown in Figure 3.12 (a).

In **Figure 3.17**, we compared our results (both data measured in quasi-free water droplet supported by stable wetting films of squalane and suspended at the interface between perfluoromethyldecalin and squalane) for the cooling rate of 0.001 K/s with other literature data. We noted that the Bigg's data was obtained from substituting different values of supercoolings into the un-numbered equation that appears in the middle of the text, $W/\partial V \partial t = 5.2 \times 10^{-10} \exp(T_s - 1)$ he derived in ref. [24] (the correlation between the freezing probability in a unit volume per unit time ($W/\partial V \partial t$) and the supercooling (T_s) from the experimental data that used the cooling rate of 0.0083 K/s). It is also noted that Bigg did not spell out the unit of the nucleation rate in his paper. However, he provided an equation that related the droplet diameter to the mean freezing temperature in another un-numbered equation ($-\ln V = T_s - 16.2$ of ref. [24]). Substitution of the data points in his paper to the equation (the mean freezing temperature of a 1mm diameter droplet

69

is –23.8 °C and a 0.65mm diameter droplet is –25.1 °C) reveals that the unit volume Bigg used was in fact 1 cm^3.

Figure 3.16 shows that the nucleation events in large droplets occur at lower supercoolings (higher temperatures) as expected. A contributing factor might be that the cooling rate we used was substantially slower than that used in the other literature data. As a water droplet spends longer times they have more chances of nucleation at shallow supercoolings (high temperatures) when a slow cooling rate is used. A related matter is that the use of a fast cooling rate or quenching has been known to allow a sample to attain very large supercoolings (low temperatures). The underlying physical reason is simple: the sample does not have sufficient time to respond to the change in its environment. The viscosity of a liquid increases with cooling, so longer times are required for supercooled liquid molecules to rearrange themselves. Practically, this feature of the use of slow cooling rates is advantageous because it allows sampling of nucleation rate data over a wider range of supercooling.

Figure 3.17 shows that the nucleation rates we measured using the cooling rate of 0.001 K/s were quite similar to Bigg's results at the comparable range of supercooling (from about 17 to 20 K). Bigg's results are also similar to those of the other literature data at the other end of his range (the high supercooling (low temperature)). We note that the nucleation rate of Bigg's data in **Figure 3.17** is for the average nucleation rate at each supercooling shown.

Interestingly, in both **Figure 3.16** and **Figure 3.17** Bigg's data appear to bridge the gap between our data and the other data in the literature that were obtained at deep supercoolings using smaller droplets. It is not clear at this stage as to what this connection means. We note that **Figure 3.17** used the droplet volume as the measure of the system size; i.e. (J/N_0) with an assumption that N_0 is proportional to the system volume. Below, we will see if similar conclusions can be drawn if

we use the surface area of the water droplet as the measure of the system size; i.e., (J/N_0) with an assumption that N_0 is proportional to the surface area for heterogeneous nucleation.
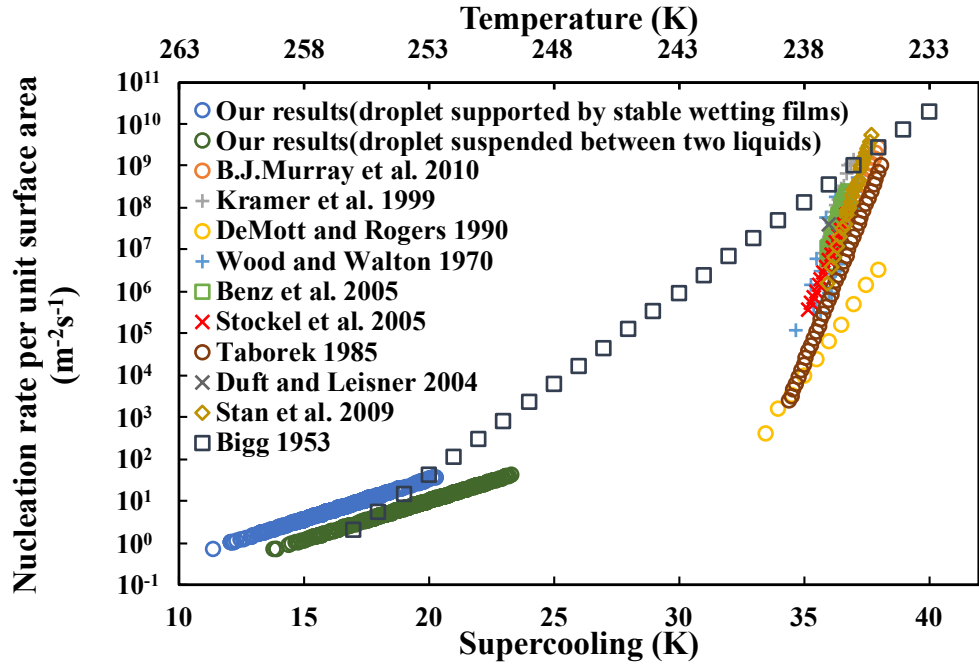
Figure 3.18. Distribution of the nucleation rate per unit surface area as a function of the supercooling in the literature. The nucleation curves for our result are for the medium cooling rate of 0.001 K/s shown in Figure 3.12 (b).

The distribution of the nucleation rate per unit surface area as a function of the supercooling in the literature was shown in **Figure 3.18**. In this figure, we simply assumed that the water droplets in the other literature data are spherical. For the literature which only provided a range of droplet diameter or several values of droplet diameters, we used the average of the droplet diameters or chose the droplet diameters that were used for the calculation of the nucleation rate per unit surface area in the relevant studies. For calculation of Bigg's results, we assumed that the water droplets were spherical and 1mm in diameter.

Compared to **Figure 3.17**, both the overlapping between our data and Bigg's data and the overlapping between Bigg's data and the other data in the literature are less. Our data overlapped with Bigg's data only at the highest supercoolings that corresponded to the largest nucleation rates. Likewise, the other data in the literature also overlapped with Bigg's data only at the highest supercoolings that corresponded to the largest nucleation rates.

What all these comparisons mean, physically, is not clear at this stage. Both **Figure 3.17** and **Figure 3.18** show that the slope of our data is much smaller than the slopes of the data of small droplets in the literature (except for the Bigg's). If both data sets were extrapolated, they would intersect around 240 K. There have been many reports about nucleation of (thermodynamically metastable) cubic ice when the size of the water droplets was small and the temperatures were low [26]. Thus we may speculate that a possibility is that our data might be for the nucleation rate of hexagonal ice and the data of small droplets in the literature (except for the Bigg's) might be for the nucleation rate of cubic ice.

3.5   Conclusions

In this paper, we measured the nucleation curves of ice in supercooled microliter–sized water droplets supported by stable wetting films of squalane and water droplets suspended at the interface between perfluoromethyldecalin and squalane. The freezing temperatures of the water droplets were concentrated in the range of 251 to 262 K for droplet supported by stable wetting films of squalane and 246 to 263 K for droplet suspended at the interface between perfluoromethyldecalin and squalane, when the linear cooling rates between 0.0003 and 0.003 K/s were used. Both the system volume and the interfacial area were used as the normalization constants for the derivation of the nucleation rate of ice. For each nucleation curve, 300 to 400

data points should be collected for a reliable derivation and confirmation of convergence. The nucleation rate increased with the system supercooling, as expected, and the whole nucleation curve shifted downward with the decreasing cooling rate. We note that the cooling rates we used were slower than those in other studies. Although it has the shortcomings of consuming time, the use of slow cooling rates has its own advantages of allowing for the collection of the nucleation rate data over a wider range of system supercooling.

The nucleation rates measured using droplets supported by stable wetting films of squalane and suspended between two immiscible liquids were broadly similar to each other, which indicated that quasi-free droplet systems might provide a baseline for the study of the ice nucleation. The method using droplets suspended at an interface of two immiscible liquids appeared to be slightly better than using droplets supported by stable wetting films of squalane. The nucleation rates thus obtained were similar to those of Bigg's results in the temperature range for which the data overlap. Bigg's results were similar to the other literature data at high supercooling (low temperature).

The experimental method was shown to be robust in that the nucleation curves almost remained unaffected with the number of the data points beyond the first few hundreds points or by the removal of several outlier data points at shallow supercoolings. The setup provides the baseline for future measurements of the nucleation curves of ice in the presence of a range of nucleation promoters or inhibitors.

3.6 References

1.   B. Murray, D. O'sullivan, J. Atkinson and M. Webb, *Ice nucleation by particles immersed in supercooled cloud droplets.* Chemical Society Reviews, 2012. **41**(19): p. 6519-6554.

2.   F.T. Lynch and A. Khodadoust, *Effects of ice accretions on aircraft aerodynamics.* Progress in Aerospace Sciences, 2001. **37**(8): p. 669-767.

3.   T. Cebeci and F. Kafyeke, *Aircraft icing.* Annual review of fluid mechanics, 2003. **35**(1): p. 11-21.

4.   Y. Cao, C. Ma, Q. Zhang and J. Sheridan, *Numerical simulation of ice accretions on an aircraft wing.* Aerospace Science and Technology, 2012. **23**(1): p. 296-304.

5.   S. Özgen and M. Canıbek, *Ice accretion simulation on multi-element airfoils using extended Messinger model.* Heat and Mass Transfer, 2009. **45**(3): p. 305.

6.   C. Demartino, H.H. Koss, C.T. Georgakis and F. Ricciardelli, *Effects of ice accretion on the aerodynamics of bridge cables.* Journal of Wind Engineering and Industrial Aerodynamics, 2015. **138**: p. 98-119.

7.   S. Saleh, R. Ahshan and C. Moloney, *Wavelet-based signal processing method for detecting ice accretion on wind turbines.* IEEE Transactions on Sustainable Energy, 2012. **3**(3): p. 585-597.

8.   Z. Zhang and X.-Y. Liu, *Control of ice nucleation: freezing and antifreeze strategies.* Chemical Society Reviews, 2018. **47**(18): p. 7116-7139.

9.   S. Liang, K.W. Hall, A. Laaksonen, Z. Zhang and P.G. Kusalik, *Characterizing key features in the formation of ice and gas hydrate systems.* Philosophical Transactions of the Royal Society A, 2019. **377**(2146): p. 20180167.

10.   E. Tollefsen, G. Stockmann, A. Skelton, C.-M. Mörth, C. Dupraz and E. Sturkell, *Chemical controls on ikaite formation.* Mineralogical Magazine, 2018. **82**(5): p. 1119-1129.

11.   K. Kelton and A.L. Greer, *Nucleation in condensed matter: applications in materials and biology.* 2010: Elsevier.

12.   G.A. Kimmel, Y. Xu, A. Brumberg, N.G. Petrik, R.S. Smith and B.D. Kay, *Homogeneous ice nucleation rates and crystallization kinetics in transiently-heated, supercooled water films from 188 K to 230 K.* The Journal of Chemical Physics, 2019. **150**(20): p. 204509.

13.   A. Haji-Akbari and P.G. Debenedetti, *Direct calculation of ice homogeneous nucleation rate for a molecular model of water.* Proceedings of the National Academy of Sciences, 2015. **112**(34): p. 10582-10588.

14.   D.C. Rogers, *Development of a continuous flow thermal gradient diffusion chamber for ice nucleation studies.* Atmospheric Research, 1988. **22**(2): p. 149-181.

15.   D.C. Rogers, *Detecting Ice Nuclei with a Continuous—Flow Diffusion Chamber-Some Exploratory Tests of Instrument Response.* Journal of Atmospheric and Oceanic Technology, 1994. **11**(4): p. 1042-1047.

16.   P.J. Demott and D.C. Rogers, *Freezing nucleation rates of dilute solution droplets measured between− 30 and− 40 C in laboratory simulations of natural clouds.* Journal of the atmospheric sciences, 1990. **47**(9): p. 1056-1064.

17.   O. Stetzer, B. Baschek, F. Lüönd and U. Lohmann, *The Zurich Ice Nucleation Chamber (ZINC)-A new instrument to investigate atmospheric ice formation.* Aerosol science and technology, 2008. **42**(1): p. 64-74.

18.   H. Lihavainen and Y. Viisanen, *A laminar flow diffusion chamber for homogeneous nucleation studies.* The Journal of Physical Chemistry B, 2001. **105**(47): p. 11619-11629.

19.   D. Brus, A.-P. Hyvärinen, V. Ždímal and H. Lihavainen, *Homogeneous nucleation rate measurements of 1-butanol in helium: A comparative study of a thermal diffusion cloud chamber and a laminar flow diffusion chamber.* The Journal of chemical physics, 2005. **122**(21): p. 214506.

20. T.F. Whale, B.J. Murray, D. O'sullivan, T.W. Wilson, N. Umo, K.J. Baustian, J.D. Atkinson, D. Workneh and G. Morris, *A technique for quantifying heterogeneous ice nucleation in microlitre supercooled water droplets.* Atmospheric Measurement Techniques Discussions, 2015. **8**.

21. Y. Tobo, *An improved approach for measuring immersion freezing in large droplets over a wide temperature range.* Scientific reports, 2016. **6**(1): p. 1-9.

22. X. Zhang, X. Liu, X. Wu and J. Min, *Experimental investigation and statistical analysis of icing nucleation characteristics of sessile water droplets.* Experimental Thermal and Fluid Science, 2018. **99**: p. 26-34.

23. E. Stopelli, F. Conen, L. Zimmermann, C. Alewell and C.E. Morris, *Freezing nucleation apparatus puts new slant on study of biological ice nucleators in precipitation.* Atmospheric measurement techniques, 2014. **7**: p. 129-134.

24. E.K. Bigg, *The supercooling of water.* Proceedings of the Physical Society. Section B, 1953. **66**(8): p. 688.

25. D. Ning and X. Liu, *Controlled ice nucleation in microsized water droplet.* Applied physics letters, 2002. **81**(3): p. 445-447.

26. N. Maeda, *Brief Overview of Ice Nucleation.* molecules, 2021. **26**(392).

27. M. Polen, E. Lawlis and R.C. Sullivan, *The unstable ice nucleation properties of Snomax® bacterial particles.* Journal of Geophysical Research: Atmospheres, 2016. **121**(19): p. 11,666-11,678.

28. N. Maeda, *Nucleation curves of methane–propane mixed gas hydrates in hydrocarbon oil.* Chemical Engineering Science, 2016. **155**: p. 1-9.

29. J.N. Israelachvili, *Intermolecular and surface forces*. 2011: Academic press.

30.   J. Mahanty and B.W. Ninham, *Dispersion forces*. Vol. 1. 1976: Academic Press.

31.   N. Maeda, *Nucleation Curve of Carbon Dioxide Hydrate from a Linear Cooling Ramp Method.* The Journal of Physical Chemistry A, 2019. **123**(37): p. 7911-7919.

32.   N. Maeda, *Nucleation curves of model natural gas hydrates on a quasi-free water droplet.* AIChE Journal, 2015. **61**(8): p. 2611-2617.

33.   N. Maeda, *Nucleation curves of methane hydrate from constant cooling ramp methods.* Fuel, 2018. **223**: p. 286-293.

34.   N. Maeda, *Nucleation of Gas Hydrates*. 2020, Springer: Cham, Switzerland.

35.   B. Murray, S. Broadley, T. Wilson, S. Bull, R. Wills, H. Christenson and E. Murray, *Kinetics of the homogeneous freezing of water.* Physical Chemistry Chemical Physics, 2010. **12**(35): p. 10380-10387.

36.   T.W. Barlow and A. Haymet, *ALTA: An automated lag-time apparatus for studying the nucleation of supercooled liquids.* Review of scientific instruments, 1995. **66**(4): p. 2996-3007.

37.   P. Stöckel, I.M. Weidinger, H. Baumgärtel and T. Leisner, *Rates of homogeneous ice nucleation in levitated H2O and D2O droplets.* The Journal of Physical Chemistry A, 2005. **109**(11): p. 2540-2546.

38.   P.G. Debenedetti, *Supercooled and glassy water.* Journal of Physics: Condensed Matter, 2003. **15**(45): p. R1669.

39.   L. Ickes, A. Welti, C. Hoose and U. Lohmann, *Classical nucleation theory of homogeneous freezing of water: thermodynamic and kinetic parameters.* Physical Chemistry Chemical Physics, 2015. **17**(8): p. 5514-5537.

40. A. Tabazadeh, Y.S. Djikaev and H. Reiss, *Surface crystallization of supercooled water in clouds.* Proceedings of the National Academy of Sciences, 2002. **99**(25): p. 15873-15878.

41. A. Adamsom and A. Gast, *Physical Chemistry of surfaces*. 1997, Wiley, New York.

42. C. Gurganus, J. Charnawskas, A. Kostinski and R. Shaw, *Nucleation at the contact line observed on nanotextured surfaces.* Physical review letters, 2014. **113**(23): p. 235701.

43. B. Krämer, O. Hübner, H. Vortisch, L. Wöste, T. Leisner, M. Schwell, E. Rühl and H. Baumgärtel, *Homogeneous nucleation rates of supercooled water measured in single levitated microdroplets.* The Journal of Chemical Physics, 1999. **111**(14): p. 6521-6527.

44. G. Wood and A. Walton, *Homogeneous nucleation kinetics of ice from water.* Journal of Applied Physics, 1970. **41**(7): p. 3027-3036.

45. S. Benz, K. Megahed, O. Möhler, H. Saathoff, R. Wagner and U. Schurath, *T-dependent rate measurements of homogeneous ice nucleation in cloud droplets using a large atmospheric simulation chamber.* Journal of Photochemistry and Photobiology A: Chemistry, 2005. **176**(1-3): p. 208-217.

46. P. Taborek, *Nucleation in emulsified supercooled water.* Physical Review B, 1985. **32**(9): p. 5902.

47. D. Duft and T. Leisner, *Laboratory evidence for volume-dominated nucleation of ice in supercooled water microdroplets.* 2004.

48. C.A. Stan, G.F. Schneider, S.S. Shevkoplyas, M. Hashimoto, M. Ibanescu, B.J. Wiley and G.M. Whitesides, *A microfluidic apparatus for the study of ice nucleation in supercooled water drops.* Lab on a Chip, 2009. **9**(16): p. 2293-2305.

Appendix 3-A: Temperature Calibration for PMMA Sample Cell

When proceeding the temperature calibration for PMMA sample cell, about 120 µL squalane was placed into each hole of PMMA sample cell using a syringe (Hamilton Company). After that, thermometers (BIOS, Model#119) were inserted into holes at different positions of the PMMA cell to record the temperature change inside the holes during the linear cooling ramps. The cooling rates were 0.003 K/s, 0.001 K/s and 0.0003 K/s, and the linear cooling ramps were proceeded as we described in the Section 3.2.5 Experimental Runs. It is noted that we divided the 36 holes of PMMA sample cell into 4 categories (shown in **Appendix Figure 3-A.1**): 4 holes at the corner (shown as purple circles), 16 holes at the edge (shown as grey circles), 12 intermediate holes (shown as green circles), and 4 holes at the center (shown as red circles).
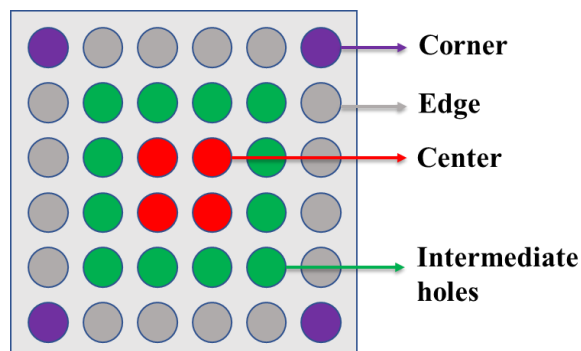
Appendix Figure 3-A.1. Schematic figure for the PMMA sample cell. 36 holes were divided into four categories including 4 holes at the corner (purple), 16 holes at the edge (grey), 12 intermediate holes (green), and 4 holes at the center (red).

The temperatures inside the PMMA sample cell changing with the experimental time were shown in **Appendix Figure 3-A.2** to **Appendix Figure 3-A.4** with the cooling rates of 0.003 K/s, 0.001 K/s and 0.0003 K/s, respectively.
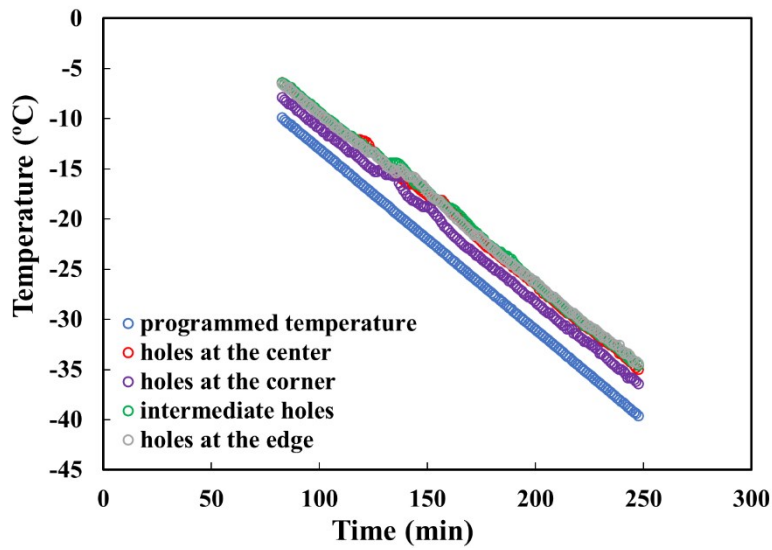
Appendix Figure 3-A.2. The temperatures inside the different holes of PMMA sample cell changing with the experimental time during the linear cooling ramp. The cooling rate was 0.003 K/s.
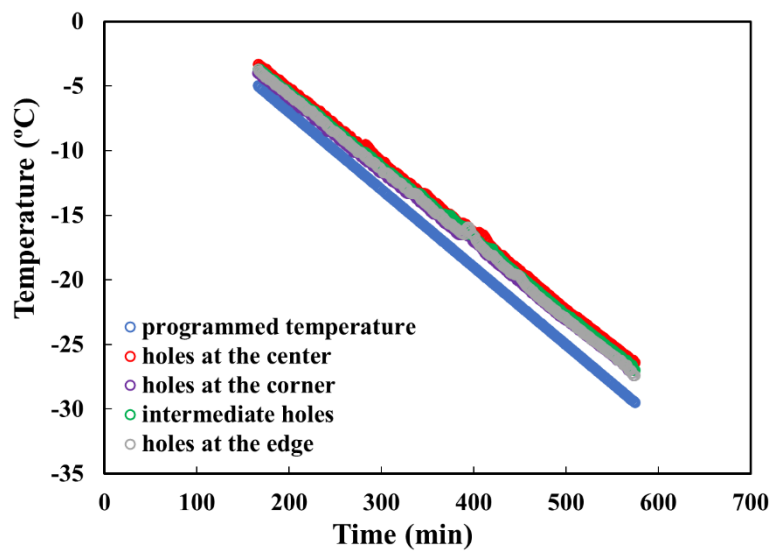
Appendix Figure 3-A.3. The temperatures inside the different holes of PMMA sample cell changing with the experimental time during the linear cooling ramp. The cooling rate was 0.001 K/s.
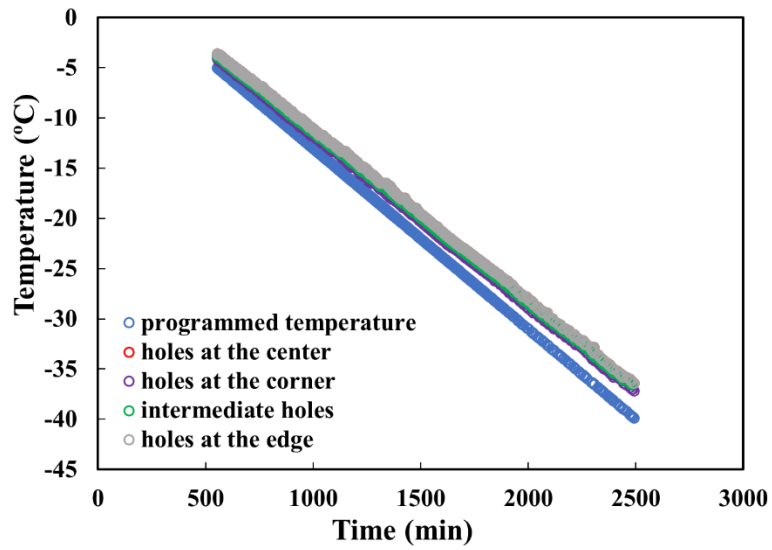
Appendix Figure 3-A.4. The temperatures inside the different holes of PMMA sample cell changing with the experimental time during the linear cooling ramp. The cooling rate was 0.0003 K/s.

Appendix 3-B: Temperature Calibration for Teflon Sample Cell

The procedure of temperature calibration for Teflon sample cell is the same as that for PMMA sample cell. The temperatures inside the Teflon sample cell changing with the experimental time were shown in **Appendix Figure. 3-B.1** to **Appendix Figure. 3-B.3** with the cooling rates of 0.003 K/s, 0.001 K/s and 0.0003 K/s, respectively.
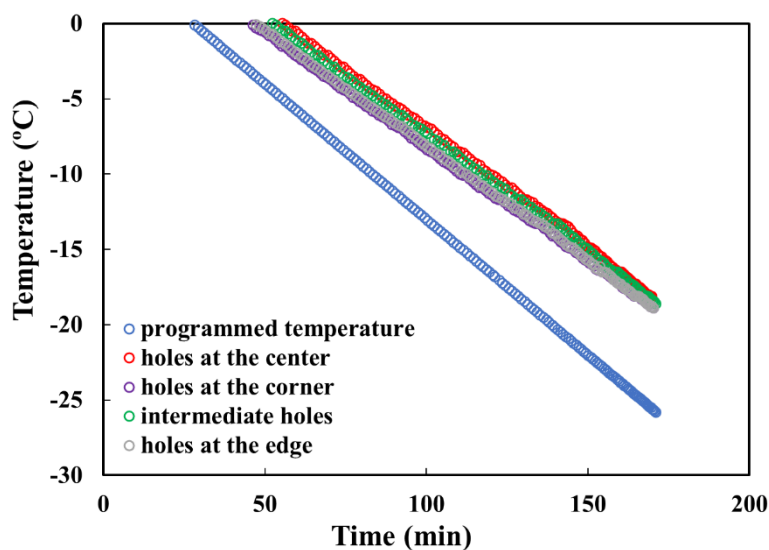
Appendix Figure. 3-B.1. The temperatures inside the different holes of Teflon sample cell changing with the experimental time during the linear cooling ramp. The cooling rate was 0.003 K/s.
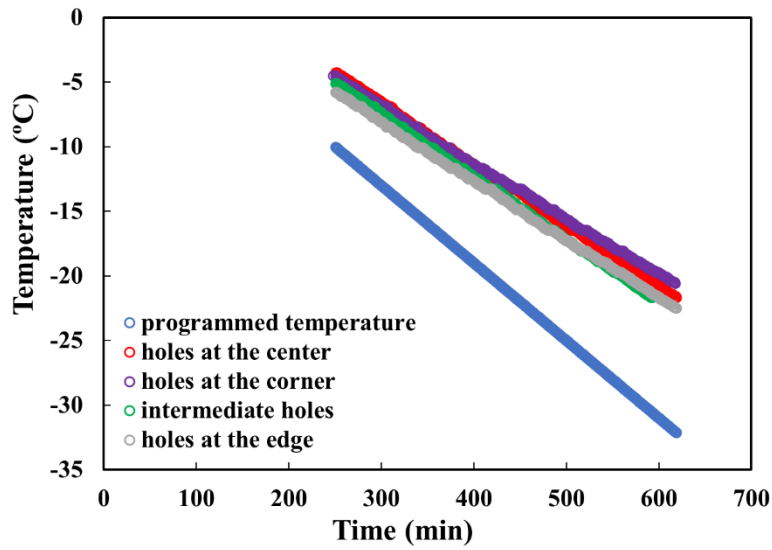
Appendix Figure. 3-B.2. The temperatures inside the different holes of Teflon sample cell changing with the experimental time during the linear cooling ramp. The cooling rate was 0.001 K/s.
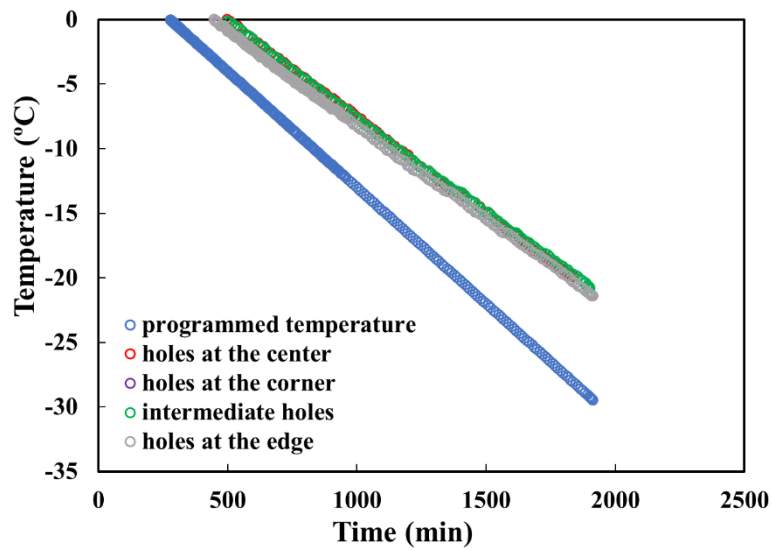
Appendix Figure. 3-B.3. The temperatures inside the different holes of Teflon sample cell changing with the experimental time during the linear cooling ramp. The cooling rate was 0.0003 K/s.

CHAPTER 4 NUCLEATION CURVES OF ICE IN THE PRESENCE OF NUCLEATION PROMOTERS

A version of this chapter has been accepted for publication in *Chemical Engineering Science*.

Abstract

Ice nucleation plays an important role in many fields like global environment, biology, food engineering and so on. It also lays foundation for further studies in the nucleation of clathrate hydrates and other more complex systems. Although the subject of ice nucleation has been studied for decades, several problems remain such as the lack of reliable heterogeneous ice nucleation promoters. For example, both organic and inorganic additives have been reported to be effective ice nucleation promoters but it remains unclear which group is more effective. In this paper, we employed a linear cooling ramp method to determine the nucleation rates of ice in the presence of a range of nucleation promoters, both organic and inorganic, and ranked their efficacy. The additives tested are; silver iodide (AgI), kaolinite, cellulose, cholesterol, steroid and Snomax. We found that the efficacy ranking among the tested additives was; Snomax $\approx$ AgI $\geq$ kaolinite $>$ steroid $>$ cholesterol $\approx$ celluloses $\geq$ Teflon wall.

4.1 Introduction

Nucleation is the initial step of ice formation, which has great impacts on global climate [1] and the supercooled water on aircraft wings [2], bridge cables [3] and many other engineered and structured surfaces. In oil and gas industry, the study of ice nucleation could lay a baseline and help enhance the understanding of nucleation of clathrate hydrates since ice has similar structures and properties as clathrate hydrates [4, 5]. For example, some nucleation promoters of ice were also reported to be effective in promoting the nucleation of clathrate hydrates [6], and the studies on promoters of ice nucleation could help the understanding the mechanisms of nucleation promoters on the formation of hydrate.

The nucleation promoters for ice have been studied for decades due to their application in cloud seeding [7], and many criteria for what make an effective nucleation promoter have been proposed. Pruppacher and Klett proposed several requirements for a particle to be an effective ice nucleus, including insolubility, size, chemical bond requirement, and crystallography [8]. Zachariassen and Kristiansen also pointed out that an ice nucleator has to carry functional groups at a proper position to be effective [9]. However, these criteria were found to be limited [1]. Silver iodide (AgI) was widely used as a nucleation promoter for cloud seeding, and it was studied both theoretically and experimentally for years [10]. However, its promotion mechanism remains unclear to this day [7]. AgI has traditionally been considered to be a good nucleation promoter since it has close lattice matching to ice [11], but ice was found to grow as discrete hexagonal islands instead of a uniform film on the AgI surface [7]. In addition to AgI, some clay minerals (e.g., kaolinite [12] and illite [1]) and soot particles [13] were also studied as potential nucleators. Other than inorganic substances, some insoluble organic molecules such as steroids and cholesterol were reported to be effective nucleation promoters [14], and Sosso et al. tried to elucidate the

physical origins of the nucleating activity of them [15]. Other than water-insoluble particles, Pummer et al. pointed out that even water-soluble macromolecules could also effectively induce ice nucleation when they are in the same size range as the critical ice embryos [16]. They investigated several fungal species (Acremonium implicatum, Isaria farinose, and Mortierella alpina) and proposed that their ice nucleation activity is caused by proteinaceous water-soluble macromolecules. In addition, bacteria [17], pollen [18], and other biological materials were also studied for enhancing the ice nucleation process for years. Hiranuma et al. investigated ice nucleation in the presence of different types of cellulose particles derived from green plants, algae or wood fiber and reported that some cellulose have similar efficacies in nucleating ice as some mineral dust samples [19]. Snomax is a commercial product that has been widely used in ski resorts and is made of proteins derived from a natural microbe, Pseudomonas Syringae. Polen et al. reported a Snomax product could nucleate ice at temperatures up to -2 °C [20].

Although many substances were found to promote ice nucleation, several problems remain. One of the most important problems is that the efficacy of different nucleation promoters has not been quantitatively characterized. For example, people reported several substances such as cholesterols, bacteria and other biological materials as effective ice nucleation promotes but did not report how often such promotion occurred [21, 22]. Consequently, it is not clear which promotors are the most effective. A probabilistic approach based on a large number of measurements is required to deal with these issues for which the nucleation rate (defined as the rate or frequency with which critically sized nuclei form) is the central parameter [7, 23]. Nucleation rate can quantitatively characterize nucleation phenomena and rank the efficacy of a group of nucleation promoters. For example, if 100 out of 100 cooling trials in the presence of an additive result in nucleation of ice at 272 K, then this particular additive is much more effective

than another additive that results in nucleation of only 1 out of 100 cooling trials at the same temperature.

In this study, we first established a new baseline in which water directly contacts a Teflon sample cell and compared the results to the two quasi-free water droplet systems we previously reported (water droplets supported by stable wetting films of squalane and water droplets suspended at an interface between two immiscible liquids) [24]. After the baseline is set, we investigated the efficacy of several types of nucleation promoters of ice using two cooling rates of 0.003 K/s and 0.001 K/s. The key parameter for evaluating the efficacy of the nucleation promoters is the nucleation rate of ice in the presence of each of these additives. For systematic comparisons, we compared the nucleation rate of ice in the presence of different additives at the same driving force (supercooling).

4.2   Materials and Methods

The details of the experimental setup, preparations of quasi-free water droplet samples, experimental ramps and data analysis are described in our earlier publication [24]. Here, we describe additional details below.

4.2.1   The Experimental Setup

The schematic illustration of the experimental setup is shown in **Figure 4.1**. Briefly, it consisted of a custom-made cuboid sample cell, a refrigerated circulator (FPW50-HE, Julabo Company, capable of cooling down to 223K if required), an aluminum lab jack (Fisher Scientific Company), two cameras (Model C922 and C270, Logitech), and a computer (DELL).
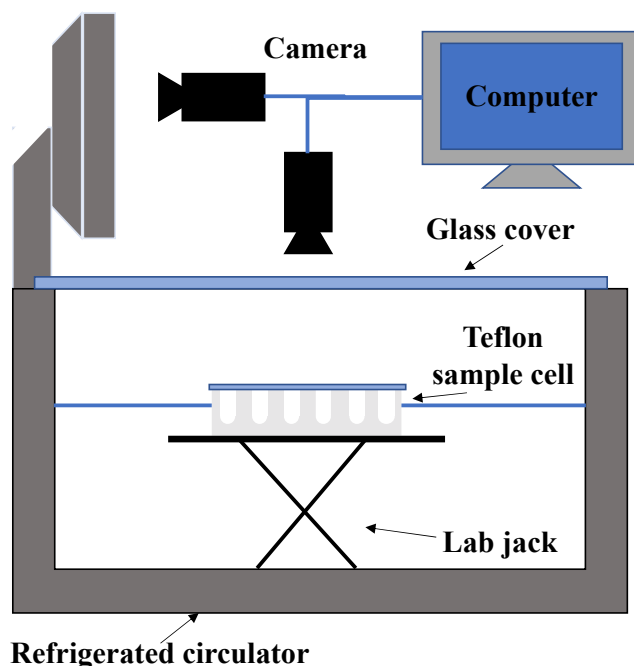
Figure 4.1. Schematic illustration of experimental setup with Teflon sample cell. After the sample preparation, the sample cell was sealed and directly placed on the lab jack, contacted with the coolant, ethanol.

The sample cell was made of Polytetrafluoroethylene (Teflon), and it was placed on a lab jack which is adjusted to a proper height. After that, a glass cover was placed on the top of the refrigerated circulator to prevent the evaporation of the coolant. The two cameras controlled by software on the computer recorded the images of sample cell and the thermometer reading shown on the panel of the refrigerated circulator every 1 min, respectively. Because there is a differential between the temperature measured by the refrigerated circulator and the real temperature of the sample, the temperature calibrations were carried out first before the experimental ramps [24].

4.2.2   Sample Preparation

The schematic illustration of the system used in this study (water directly in contact with the Teflon sample cell) is shown in **Figure 4.2** (a) and its comparison to that of our earlier system (a water droplet suspended between two immiscible liquids) [24] is shown in **Figure 4.2** (b). In

our earlier study, a water droplet was suspended between two immiscible liquids, perfluoromethyldecalin and squalane, and 60 mg of Milli-Q water (ultra-pure water of 18.2 MΩ resistivity from a Millipore unit) were added into each hole of the Teflon sample cell. Since perfluoromethyldecalin is denser than water and squalane is less dense than water, the water droplet was suspended between these two immiscible liquids. In the current study, 120 mg of Milli-Q water alone was placed to each hole of the Teflon sample cell. The Teflon sample cell had 36 holes in total. After the sample was placed to each hole, the sample cell was covered with a glass slide using a vacuum grease (Dow Corning, High vacuum grease) at the rim.
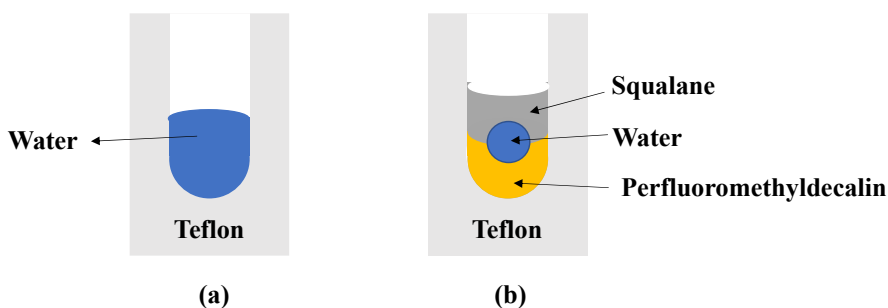
Figure 4.2. Schematic illustration of the new water droplet system ((a), water directly contact with Teflon wall) and the quasi-free water droplet suspended between two immiscible liquids (b).

The seven additives we investigated are; two inorganic additives of AgI (purchased from Sigma-Aldrich and used as received) and kaolinite, and five organic additives of cellulose (2-Hydroxyethyl cellulose, molecular weight of 90000 and 1300000, purchased from Sigma-Aldrich and used as received), cholesterol (99% purity, purchased from Sigma-Aldrich and used as received), Snomax (Snomax International Company) and steroid (progesterone, purchased from Sigma-Aldrich, purity 99%). When measuring the ice nucleation rate in the presence of a nucleation promoter, about 0.003g of the nucleation promoter together with 120 mg of Milli-Q water were placed to each sample hole before the sample cell was closed. For Snomax, 0.01 wt%

Snomax suspension was first prepared as a stock solution (as shown in **Figure 4.3** (left)), then 0.0005 wt% suspension was prepared (as shown in **Figure 4.3** (right)) by diluting the stock solution with Milli-Q water. Finally, 120 mg of the dilute suspension was placed to each sample hole of the sample cell.

Figure 4.3. Photographs of Snomax suspensions (0.01 wt% stock solution (left) and 0.0005 wt% suspension (right)).

4.2.3   Experimental Ramps and Data Analysis

As in our earlier study, we used the linear cooling ramp method for the measurements of ice nucleation rates [24]. Three different cooling rates of 0.003 K/s, 0.001 K/s and 0.0003 K/s were used for ice nucleation rates, while the two faster cooling rates (0.003 K/s and 0.001 K/s) were used for the measurements in the presence of the nucleation promoters to save time. For each experimental cooling ramp, the sample cell was cooled rapidly from room temperature to 5 ºC and held for thermal equilibrium at 5 ºC. After that, the sample cell was cooled linearly with a constant cooling rate from 5 ºC to -40 ºC, until all the droplets froze. We note that the volume expansion

91

due to freezing was chosen to indicate the freezing of the droplet. However, in some poor optical cases, especially in the measurements with nucleation promoters, the moment water became opaque was chosen to be the freezing time. Finally, it was warmed back to room temperature again and all the frozen droplets melted. The freezing temperature (T_f) of each water droplet was obtained after the application of a temperature calibration table that related the temperature of the coolant to the temperature inside the sample cell.

After obtaining all the raw data (T_f of all water droplets), we used the procedure described in [24-26] to deduce a nucleation curve. The procedure involves several steps: (1) Obtain the survival curve of the survival probability, F, as a function of supercooling $\Delta T = 273K - T_f$, where $F(\Delta T)$ was calculated from the number of the surviving droplets (unfrozen droplets) divided by the total number of the droplets at that ΔT; (2) Calculate $\ln F$ as a function of the lag time, t. Lag time is the time a sample has spent in a metastable state prior to the eventual nucleation. Since linear cooling ramps were applied in the experiments, the lag time could be calculated from the calibrated supercooling, T_f, divided by the experimental cooling rate; (3) Obtain the local slope of $\ln F$ at each t by fitting a curve to $\ln F(t)$ and analytically differentiating the fitted curve with respect to t. Here we used an exponential function of the form $A \cdot \exp(Bt) + C$ for the fitting of each $\ln F$ curve; (4) Divide each local slope by a factor of $-\ln 2$, which yields the experimental nucleation rate. The nucleation curve is the nucleation rate as a function of the supercooling. The reported nucleation rate can be either an experimental nucleation rate or a nucleation rate normalized to the system size.

4.3 Results

4.3.1 Nucleation Rates of Ice in Water that is Directly in Contact with the Teflon Sample Cell

In our previous study, we reported the nucleation rates of ice in quasi-free water droplets (water droplets supported by stable wetting films and water droplets suspended between two immiscible liquids) [24]. However, the PMMA sample cell is inconvenient for cleaning after an additive is used. In addition, the density mismatch between an additive and the supporting liquids means that different additives end up at different locations within the sample cell hole for fair comparisons. Since Teflon is inert and has a low specific surface free energy, additives do not stick to the walls and hence easy to wash off after the measurements. Thus, in this study we used water samples that are directly in contact with the Teflon sample cell for our investigation of the effect of additives. We assume that no chemical reaction takes place among Teflon, water and an additive. Since a nucleation promoter is expected to promote the nucleation of ice, more so than a Teflon wall does, the impact of the Teflon walls on ice nucleation is assumed to be insignificant compared to the impact of an additive when one is present.

We first establish the baseline for the new setup by measuring the nucleation rates of ice in water that was in direct contact with the Teflon sample cell, using the linear cooling ramps of three different cooling rates (0.003 K/s, 0.001 K/s and 0.0003 K/s). We show the resulting survival curves in **Figure 4.4**, the corresponding natural logarithm of the survival curves in **Figure 4.5** and the corresponding nucleation curves in **Figure 4.6**. We note that about 500 data points, 360 data points and 240 data points were collected for the cooling rates of 0.003 K/s, 0.001 K/s and 0.0003 K/s, respectively. As mentioned in our previous study, the nucleation curve hardly changes with the accumulation of data after the first few hundred data points, which means 200 or 300 data

93

points are sufficient for a reliable determination of a nucleation curve [24]. It is also noted that in

quasi-free water droplet systems, all water droplets are assumed to have the same spherical shape

with the volume of 60 µL. For water directly in contact with Teflon wall, all water droplets are

assumed to be cylindrical with the volume of 120 µL.
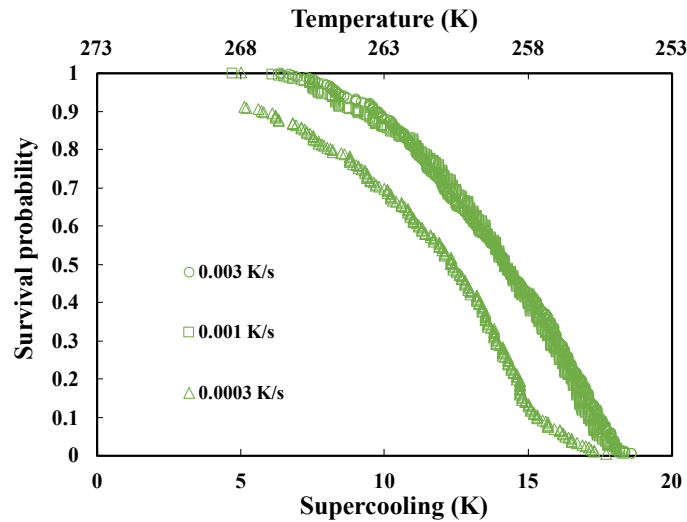
Figure 4.4. Survival curves measured in water directly in contact with Teflon sample cell using three different cooling rates. The circle, square and triangle marker corresponds to data points at cooling rates of 0.003 K/s, 0.001 K/s and 0.0003 K/s, respectively.
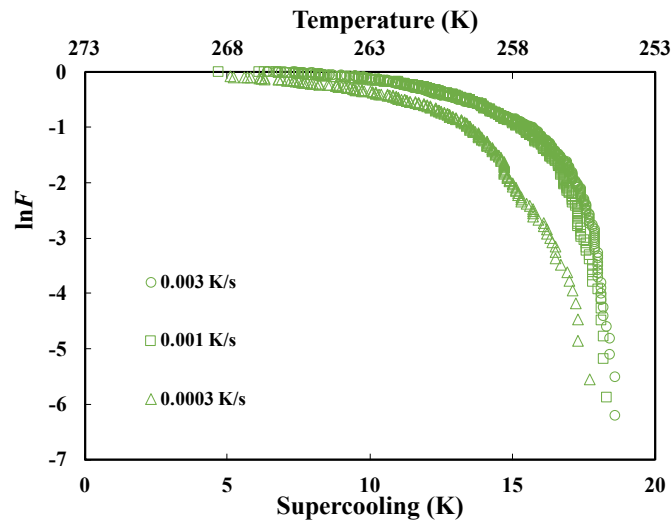
Figure 4.5. Natural logarithm of the survival curves (lnF vs ΔT) of ice formation measured in water directly in contact with Teflon sample cell using three different cooling rates. The circle,
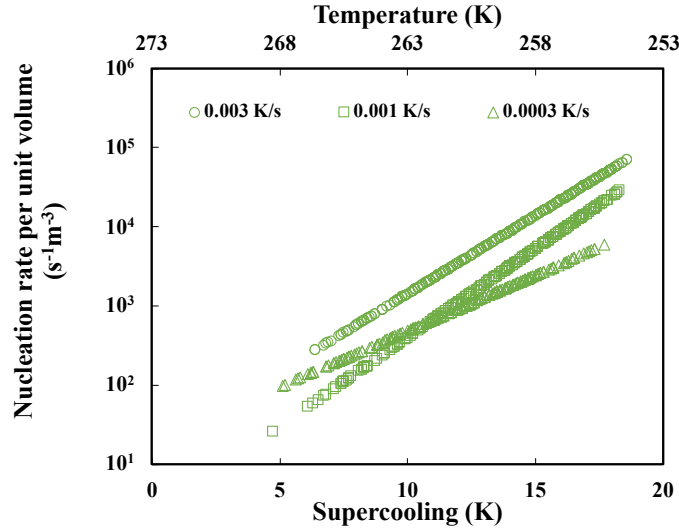
Figure 4.6. Nucleation curves (nucleation rate per unit volume) measured in water directly in contact with Teflon sample cell using three different cooling rates. The circle, square and triangle marker corresponds to data points at cooling rates of 0.003 K/s, 0.001 K/s and 0.0003 K/s, respectively.

As shown in **Figure 4.4**, the survival curves measured in this new water system (water that is directly in contact with Teflon sample cell) were in the supercooling range of 6.4 to 18.6 K, 4.7 to 18.3 K, 5.1 to 17.7 K for the cooling rate of 0.003 K/s, 0.001 K/s and 0.0003 K/s, respectively. The survival curves for the two fast cooling rates were almost overlapping with each other when supercooling was larger than 10 K (temperature lower than 263 K), but the supercooling of the lower end of the survival curve with the cooling rate of 0.001 K/s was lower than that of the cooling rate of 0.003 K/s. Water froze at a lower supercooling (higher temperature) for a slower cooling rate, which is similar to the results in our previous study [24]. **Figure 4.5** showed that the ln$F$ curves measured with two fast cooling rates were close to each other, while the local slope of ln$F$ measured with 0.0003 K/s was less steep than the others at the same supercooling. When the

95

supercooling is larger than 11 K, the nucleation rates became lower as the cooling rate became

slower at the same supercooling, as shown in **Figure 4.6**.

4.3.2   Comparison with Quasi-Free Water Droplet Systems

In this part, the nucleation rates in the new system (water directly in contact with Teflon

sample cell) were compared to the nucleation rates in quasi-free water droplets supported by stable

and thick wetting films of squalane and water droplet suspended between two immiscible liquids

in our earlier study [24]. The survival curves were shown in **Figure 4.7**, the corresponding ln$F$

curves were shown in **Figure 4.8** and the nucleation curves were shown in **Figure 4.9**. The results

shown in **Figure 4.4**-**Figure 4.6** are now shown in green symbols, the results of quasi-free water

droplets supported by stable wetting films of squalene are shown in blue symbols and the results

of quasi-free water droplet suspended between two immiscible liquids are shown in yellow

symbols. For each category, the results of 0.003 K/s, 0.001 K/s and 0.0003 K/s are shown in circles,

squares and triangles, respectively.
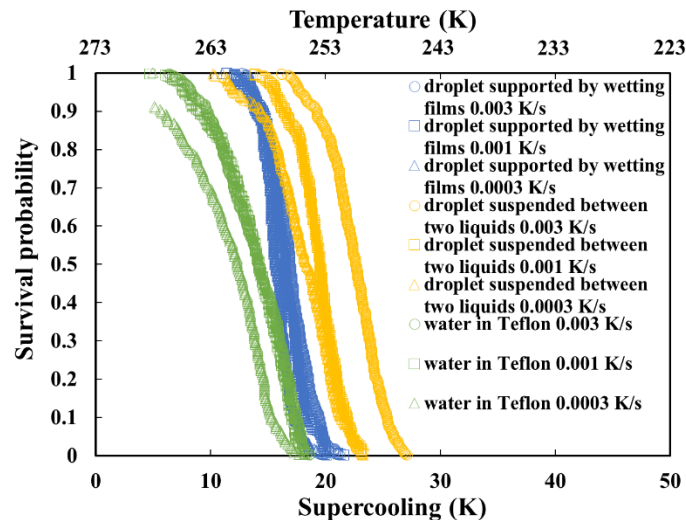
Figure 4.7. Survival curves measured in water directly in contact with Teflon sample cell using
three different cooling rates, compared with that measured in water droplets supported by stable
wetting films of squalane and in water droplets suspended at the interface between two

96

immiscible liquids. The curves measured in droplet supported by stable wetting films of squalane and droplet suspended between two immiscible liquids were the same as those shown in our previous study.
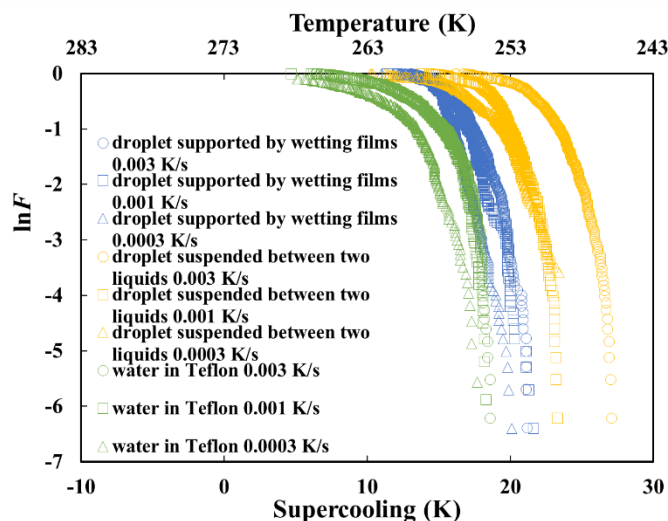
Figure 4.8. Natural logarithm of the survival curves (lnF vs ΔT) of ice formation measured in water directly in contact with Teflon sample cell using three different cooling rates, compared with that measured in water droplets supported by stable wetting films of squalane and in water droplets suspended at the interface between two immiscible liquids. The curves measured in water droplets supported by stable wetting films of squalane and water droplets suspended between two immiscible liquids were the same as those shown in our previous study.
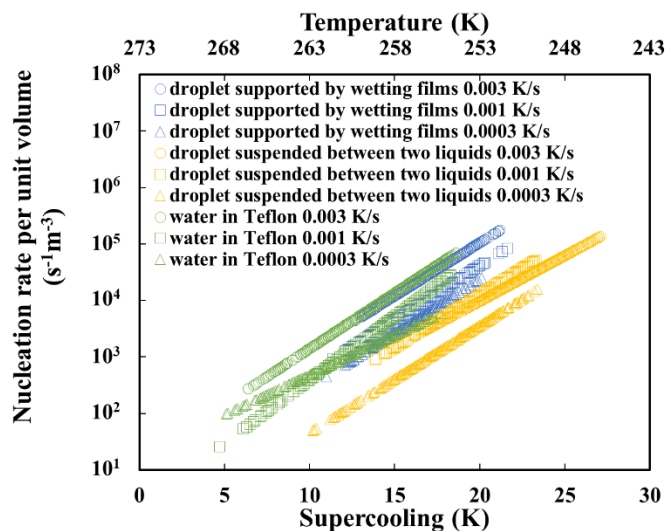
Figure 4.9. Nucleation curves (nucleation rate per unit volume) measured in water directly in contact with Teflon sample cell using three different cooling rates, compared with that measured in water droplets supported by stable wetting films of squalane and water droplets suspended at the interface between two immiscible liquids. The curves measured in water droplets supported

by stable wetting films of squalane and water droplets suspended between two immiscible liquids were the same as those shown in our previous study.

For cooling rate of 0.003 K/s, as shown in **Figure 4.7**, water directly in contact with Teflon sample cell froze at a lower supercooling (higher temperature) than in the quasi-free water droplet systems, as expected. Although Teflon is hydrophobic, it appears that Teflon wall still acted as heterogeneous nucleation sites for ice. For the two quasi-free water droplet systems, the droplets supported by stable wetting films of squalane behaved somewhat in between the water directly in contact with Teflon sample cell and the droplets suspended between two immiscible liquids, also as expected. Even though the van der Waals forces in the stable wetting films of squalane are repulsive, the water droplet was nonetheless within the range of the surface forces of the bottom wall of the sample cell. We note that the difference in the nucleation rates measured in water directly in contact with Teflon cell and those measured in the quasi-free water droplet suspended between two immiscible liquids was less than 1 order of magnitude for a given supercooling.

Between the two cooling rates of 0.001 K/s and 0.0003 K/s, the results were quite similar to each other. Among the three systems, the water directly in contact with Teflon sample cell had the lowest supercooling range (highest temperature range), while the water droplets suspended between two immiscible liquids had the highest supercooling range. As shown in **Figure 4.9**, the nucleation curves of water in direct contact with the Teflon sample cell almost overlapped those of quasi-free water droplets supported by stable wetting films of squalane at the supercooling range of 12 to 18 K, while the nucleation rates were less than 1 order of magnitude higher than that of the quasi-free water droplets suspended between two liquids at the same supercooling.

Overall, the nucleation rates of ice in the water directly in contact with Teflon sample cell were somewhat higher than those in the quasi-free water droplets suspended between two immiscible liquids but the difference was smaller than the gap between the quasi-free water droplets suspended between two immiscible liquids and the quasi-free water droplets supported by the stable wetting films. **Figure 4.9** also shows that ice nucleates at higher temperatures in the water in direct contact with a Teflon wall than in the quasi-free water droplets supported by the stable wetting films and yet their nucleation rates were virtually the same at the same temperature. These results suggest that the increase in the nucleation rate of ice by an inert, hydrophobic solid like Teflon is limited and that any additional increase in the nucleation rate of ice by an additive would be measurable.

4.3.3 The Effect of Nucleation Promoters on the Ice Nucleation Rates

As mentioned in the first subsection of the Results section, using quasi-free water droplets may not be suitable for the study of nucleation curves of ice in the presence of nucleation promoters because we cannot control the density mismatch between the nucleation promoters and the two immiscible liquids, and we have trouble cleaning the sample cell after the use of each additive. Since the difference between the nucleation curves of water directly in contact with Teflon walls and those of quasi-free water droplets was not large at the overlapping supercooling range, we may use the nucleation curves of (pure) water directly in contact with Teflon walls as our baseline in this study. The rationale is that any effective nucleation promoter would increase the nucleation rate of ice by a significant amount that would render the effect of the Teflon walls insignificant.

We tested the efficacy of seven nucleation promoters; celluloses of two different molecular weights of 90000 and 1300000, silver iodide (AgI), kaolinite, cholesterol, Snomax and steroid. We

99

used the linear cooling ramp method with two cooling rates of 0.003 K/s and 0.001 K/s. For the

cooling rate of 0.003 K/s, the survival curves are shown in **Figure 4.10**, the corresponding natural

logarithm of the survival probability are shown in **Figure 4.11**, and the corresponding nucleation

curves (experimental nucleation rate) are shown in **Figure 4.12**. For cooling rate of 0.001 K/s, the

corresponding data are shown in **Figure 4.13** to **Figure 4.15**. We note that about 200 data points

were collected for the determination of each nucleation curve.
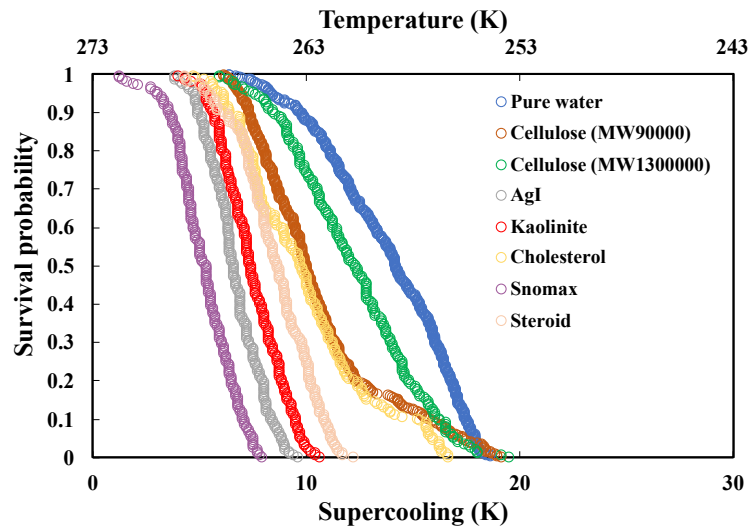
Figure 4.10. Survival curves measured in water directly in contact with Teflon sample in the
presence of different nucleation promoters comparing to the data of pure water, with the cooling
rate of 0.003 K/s. The curve measured with pure water was the same as that in Figure 4.4.
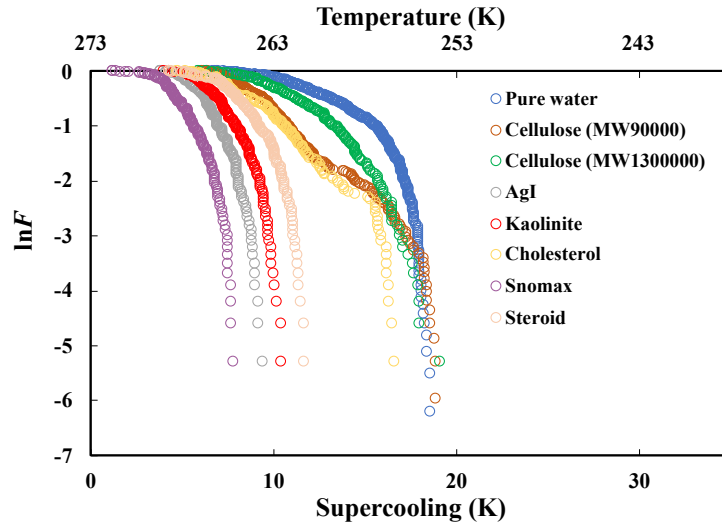
Figure 4.11. Natural logarithm of the survival curves (lnF vs ΔT) of ice formation measured in water directly in contact with Teflon sample in the presence of different nucleation promoters comparing to the data of pure water, with cooling rate of 0.003 K/s. The curve measured with pure water was the same as that in Figure 4.5.
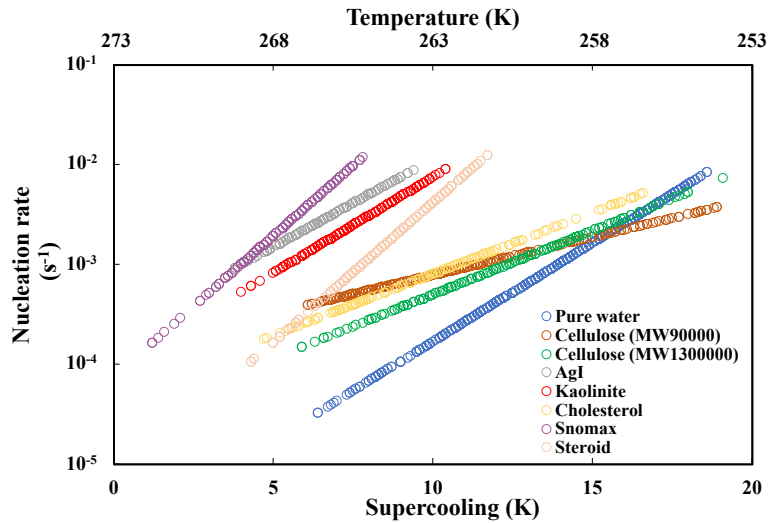
Figure 4.12. Nucleation curves (experimental nucleation rate) measured in water directly in contact with Teflon sample in the presence of different nucleation promoters comparing to the data of pure water, with cooling rate of 0.003 K/s. The curve measured with pure water was the same as that in Figure 4.6.

For the cooling rate of 0.003 K/s, as shown in **Figure 4.10**, the survival curves measured in the presence of the cellulose (molecular weight of 90000 and 1300000) had similar supercooling ranges (6.1 K to 18.9 K and 5.9 K to 19.1 K) as that of pure water (6.4 K to 18.6 K). The survival curve measured in the presence of cholesterol (4.7 K to 16.6 K) had a slightly lower supercooling (higher temperature) range than pure water. For the other nucleation promoters, the survival curves were in the range of 1.2 K to 7.8 K, 3.8 K to 9.4 K, 4 K to 10.4 K and 4.3 K to 11.7 K for Snomax, AgI, kaolinite and steroid, respectively.

The supercooling range in the presence of each of these four additives was narrower and lower (at higher temperature ranges) than that of pure water, which indicated that these four substances increased the nucleation temperature of water. **Figure 4.11** showed that for all nucleation promoters, the ln$F$ had steeper slopes than that of pure water at a comparable supercooling range.

As shown in **Figure 4.12**, the molecular weight of the cellulose did not make a significant difference in the nucleation rate and they were both close to the nucleation rate of pure water. The three nucleation curves crossed over around the supercooling of 15.3 K. Generally, the difference in the nucleation rate in the presence of cellulose and that of pure water was less than 1 order of magnitude at the same supercooling, which indicated that cellulose had little promotion effect, not much more than that of a Teflon wall.

Compared to celluloses, cholesterol appeared to have a slightly better promotion effect, as cholesterol could freeze water at a lower supercooling (higher temperature) range and render the nucleation rate higher than that of pure water at the same supercooling, although the difference was still less than 1 order of magnitude. Steroid had a better promotion effect, both in terms of the higher temperature range and the higher nucleation rate by 1 to 2 orders of magnitude, comparing

to pure water. AgI and kaolinite turned out to be much better nucleation promoters of ice than steroid or cholesterol as the nucleation rates were (about 2 orders of magnitude) higher than that of pure water at the comparable supercooling range (about 6 K to 10 K). Compared to AgI and kaolinite, the lower end of the nucleation curve in the presence of Snomax was only at 1.2 K, which indicated that Snomax could improve the freezing temperature of water even more effectively. As shown in **Figure 4.12**, the nucleation rates measured in the presence of Snomax were more than 2 orders of magnitude higher than that in pure water at a comparable supercooling range (6.4 K to 7.7 K), and the difference would widen at higher supercooling (lower temperature). We would thus conclude that for the cooling rate of 0.003 K/s, the efficacy of nucleation promoters could be ranked as: Snomax $\geq$ AgI $\approx$ kaolinite > steroid > cholesterol $\geq$ celluloses $\approx$ Teflon wall.
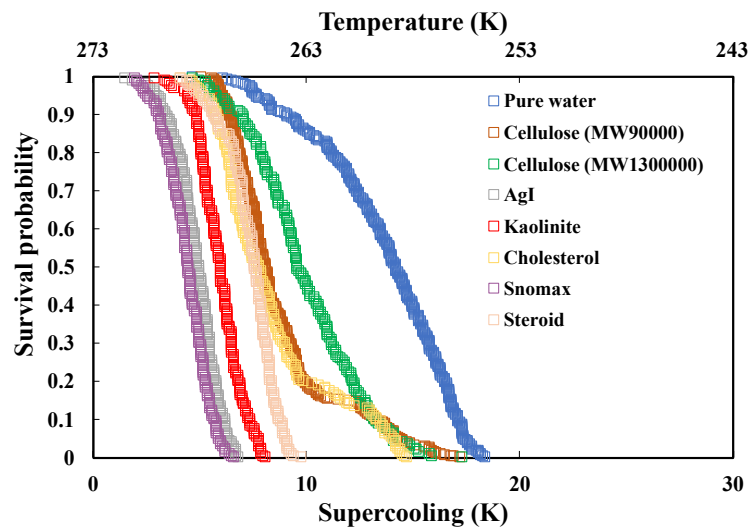
Figure 4.13. Survival curves measured in water directly in contact with Teflon sample in the presence of different nucleation promoters comparing to the data of pure water, with cooling rate of 0.001 K/s. The curve measured with pure water was the same as that in Figure 4.4.
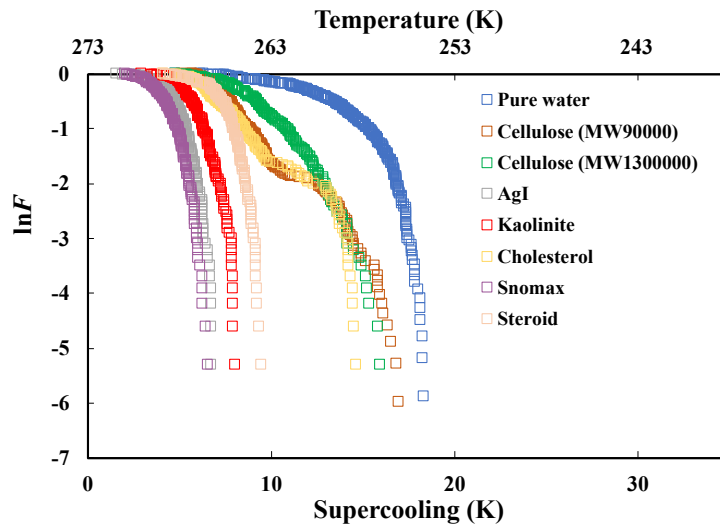
Figure 4.14. Natural logarithm of the survival curves (lnF vs ΔT) of ice formation measured in water directly in contact with Teflon sample in the presence of different nucleation promoters comparing to the data of pure water, with cooling rate of 0.001 K/s. The curve measured with pure water was the same as that in Figure 4.5.
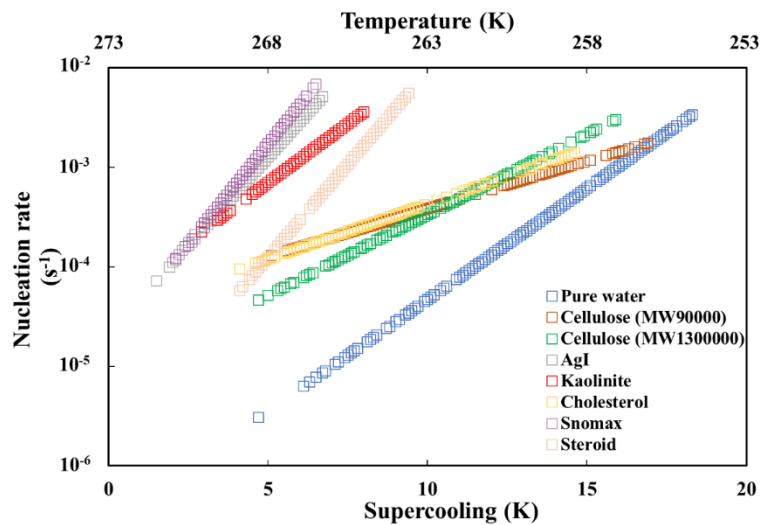
Figure 4.15. Nucleation curves (nucleation rate per unit volume) measured in water directly in contact with Teflon sample in the presence of different nucleation promoters comparing to the data of pure water, with cooling rate of 0.001 K/s. The curve measured with pure water was the same as that in Figure 4.6.

For the cooling rate of 0.001 K/s, as shown in **Figure 4.13**, the survival curves measured in the presence of two celluloses (molecular weight of 90000 and 1300000) and cholesterol had similar supercooling ranges (5.1 K to 16.9 K, 4.7 K to 15.9 K and 4.1 K to 14.6 K), which were slightly narrower and lower than that of pure water (4.7 K to 18.3 K). As for the other four additives, the survival curves were concentrated at the supercooling range of 1.5 K to 6.7 K, 2.9 K to 8 K, 2 K to 6.5 K and 4.1 K to 9.4 K in the presence of AgI, kaolinite, Snomax and steroid, respectively. These four additives could improve the freezing temperature of water, since the supercooling ranges measured with them became much lower and narrower comparing to pure water. And for all additives, as shown in **Figure 4.14**, the ln$F$ curves measured in the presence of additives had steeper local slopes than that of pure water at the same supercooling, which results in higher nucleation rates showing in **Figure 4.15**.

Similar to the results measured with the cooling rate of 0.003 K/s, as shown in **Figure 4.15**, the nucleation curves measured with two celluloses were quite close to each other, which indicated that the molecular weight barely had any influence on the nucleation rate. Cholesterol seemed to have similar promotion effect as the celluloses since the three nucleation curves were close to each other, overlapping at the supercooling of 12 K (temperature 261 K). Overall, the difference between the nucleation rates measured with these three additives and that of pure water was less than 1 order of magnitude between the supercooling range of 9 K to 18 K and less than 2 orders of magnitude when supercooling was less than 9 K, which indicated that they had better promotion effect than a Teflon wall.

Steroid has better promotion effect than the above three additives as it could promote the nucleation rates more (by 1 to 2 orders of magnitude comparing to pure water) and also had narrower supercooling range than them. Kaolinite seemed to be better promoter than steroid

because it could increase the nucleation rate by about 2 orders of magnitude (comparing to pure water) as well as increase the freezing temperature of water. Snomax and AgI appeared to be the most effective promoters. The nucleation curves measured with them were almost overlapping with each other, and the nucleation rates were more than 2 orders of magnitude larger than that measured with pure water at the same comparable supercooling (about 5 K to 6 K), the difference would be even larger if extrapolated the curves with Snomax and AgI to a larger supercooling (lower temperature).

Then we may conclude that for the cooling rate of 0.001 K/s, the efficacy of nucleation promoters could be listed from high to low as follows: Snomax ≈ AgI ≥ kaolinite > steroid > cholesterol ≈ celluloses ≥ Teflon wall. The conclusion is quite similar to that of cooling rate 0.003 K/s, which indicates that the cooling rate doesn't have a big influence on determining the efficacy ranking of nucleation promoters.

4.4 Discussion

4.4.1 Assumptions about the Nucleation Promoters

The promoters are not 100% pure. For example, the purity of cholesterol and steroid are both 99%. We do not know the chemical identity of impurities in each promoter, however, we doubt that the nucleation potency can be greater than that of the main component. If they were, then we should obviously use the impurity as the main ingredient of the promoter. If they are not as effective in promoting ice nucleation as the main component, as they should be, then we may assume that the impact of the impurities is insignificant, especially given that their amounts are much smaller than that of the main component. If we can assume that the main components of the promoters are more effective than any impurities, then the next question is if the promoters are

physically and chemically uniform in their nucleation efficacy. This issue leads to the question as to the concentrations of the potential nucleation sites in a system, or equivalently, the question as to an appropriate measure of normalization of the system size, which is the topic of the next section.

4.4.2   Normalization for the Heterogeneous Nucleation

In order to make meaningful comparison with other literature data, the experimental nucleation rates shown in **Figure 4.12** and **Figure 4.15** need be normalized to an appropriate unit system size. In our earlier study that only involved quasi-free water droplets, either supported by the repulsive van der Waals force of a thick and stable wetting film or suspended at an interface between two mutually immiscible liquids of a higher and a lower density than water, the appropriate measure for normalization was the volume of the water in the system because ice nucleation was assumed to be homogeneous [24]. Of course, this assumption is not necessarily true, because the symmetry still breaks at the surface of a quasi-free water droplet even though it is not in contact with a solid phase. Nevertheless, that is what most in the literature assume for homogeneous nucleation.

In contrast, for heterogeneous nucleation in the presence of promoters in this study, the nucleation rate should be normalized to the unit interfacial area between water and each promoter, if we can assume that the surface of each promoter is physically and chemically homogeneous. Unfortunately, it is difficult to estimate the accurate interfacial areas. For kaolinite for example, about 0.003 g kaolinite was added into each sample compartment. However, they were in the form of fine powder and the shape of each powder could be irregular. Consequently, the total interfacial area between water and the kaolinite particles in each hole is not accurately known.

To gain some rough ideas, we summarized in **Table 4.1** how the interfacial area could vary with the numbers of promoter particles contained in the 0.003 g. Take kaolinite as the example here, the total volume of kaolinite was calculated to be 0.0011 cm^3 since its density is 2.65 g/cm^3 [27]. By assuming that each particle is spherical in shape, we estimated the variation in the total contact area between kaolinite and water in a sample hole in **Table 4.1**. The estimates in **Table 4.1** provides the lower bound because a sphere has the smallest possible surface area for a given volume. An important insight from **Table 4.1** is that the total interfacial area increases by 1 order of magnitude as the number of promoter particles increases by 3 orders of magnitude. The number of kaolinite particles and the total interfacial area in each sample hole would have been somewhat different. Still, we can assume that the total interfacial area between kaolinite and water would have been between 0.1 and 0.5 cm^2 if each particle were spherical.

Table 4.1. The impact of numbers of promoter particles on the interfacial area.

Volume (cm^3)	Number of particles	Volume for each particle (cm^3)	R for each particle (cm)	Total interfacial area (cm^2)
	1	0.0011	0.0640	0.0515
	10	0.00011	0.0297	0.1110
0.0011	100	0.000011	0.0138	0.2392
	1000	0.0000011	0.0064	0.5153
	10000	0.00000011	0.0030	1.1102

After getting the rough idea that how the number of kaolinite particles influence the contact area between kaolinite and water, the next question is how the different shape of promoters could influence the contact area. **Table 4.2** shows the variation of the interfacial area between cubic

kaolinite particles and water for the same volume as **Table 4.1**. Compared to the spherical shape, the cubic shape has a larger interfacial area, as expected, but the difference is only about 30%. Even for a much more irregular shape that exposes 7 times as large surface area as that of a cube, the interfacial area will not be more than 1 order of magnitude larger than that of a sphere.

We know that the number of the kaolinite particles must be between 10 to 1000. Then, **Table 4.1** shows that the minimum in the total interfacial area between kaolinite and water in each sample hole would be 0.1 cm^2, which corresponds to the case that each hole contains the minimum number of kaolinite particles and that all the particles are spherical. The other limiting case would be when each hole contains the maximum number of kaolinite particles and the kaolinite particles have irregular shapes. We assume that such irregular shapes may render the surface area 7 times as large surface area as that of a cube. Then, the maximum total interfacial area would be around 6 cm^2.

Table 4.2. The interfacial area of cubic shape particles.

Volume (cm^3)	Number of particles	Volume for each particle (cm^3)	length for each cubic particle (cm)	Total interfacial area (cm^2)
	1	0.0011	0.1042	0.0651
	10	0.00011	0.0484	0.1404
0.0011	100	0.000011	0.0225	0.3025
	1000	0.0000011	0.0104	0.6517
	10000	0.00000011	0.0048	1.4041

4.4.3 Comparison to the Literature Data

The literature seldom reported the nucleation rates of ice in the presence of nucleation promoters. Much literature only reported the freezing temperature range or the survival curves for ice nucleation with promoters. Here, we only compared our experimental results of AgI and kaolinite using the cooling rate of 0.003 K/s with the literature [12, 28]. The comparison of AgI data with Heneghan et al.'s results is shown in **Figure 4.16** and the comparison of kaolinite data with Murray et al.'s results is shown in **Figure 4.17**.

Heneghan et al. [28] applied the linear cooling ramp with cooling rate of 0.018 K/s to investigate the ice nucleation in the presence of AgI in a borosilicate glass sample cell. Since they obtained the average lag-time, $<t>$, as a function of supercooling (Fig. 3 of [28]) and stated that the nucleation rate is $<t>^{-1}$, we could calculate the nucleation curve for their data. Heneghan et al. did not report the interfacial area between AgI and water in their system, so here we only compare the experimental nucleation rates. As shown in **Figure 4.16**, the two nucleation curves crossed at the supercooling 6 K to 7 K, and the supercooling range of Heneghan et al.'s results is slightly narrower than that of our results. Although there's some difference, the difference of nucleation rate was less than 1 order of magnitude at the comparable supercooling range, which indicated that our results were close to Heneghan et al.'s results in the presence of AgI. This may suggest (1) the nature of the sample cell (glass vs Teflon) may be unimportant in the presence of a potent nucleation promotor like AgI, (2) the amount of AgI or the total interfacial area may not be as important as we thought.
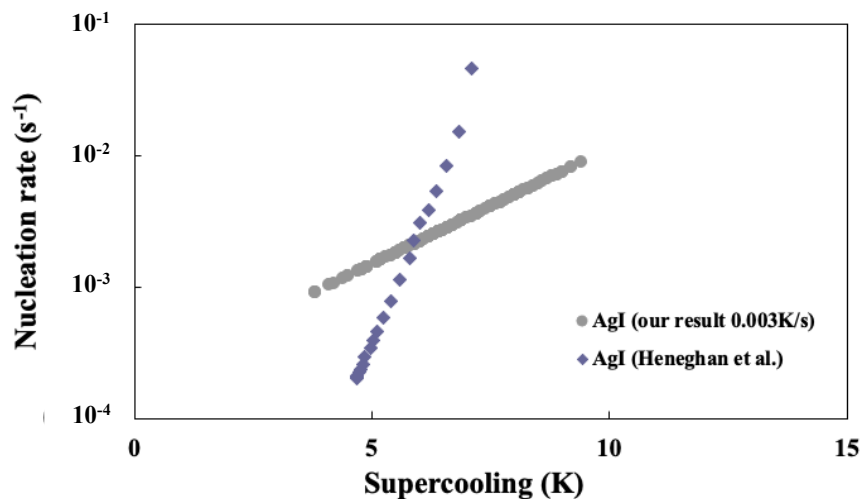
Figure 4.16. Nucleation rates measured with AgI compared to the results of Heneghan et al.'s research. Our results used the data of cooling rate 0.003 K/s, Heneghan et al.'s results used 0.018 K/s as the cooling rate.

Murray et al. reported the experimental results in the Fig. 4 of [12]. However, they only reported the normalized nucleation rates (to unit interfacial area between kaolinite and water) over a broad range of concentrations of kaolinite. Their nucleation rates are shown as the blue square symbols in **Figure 4.17**. As noted above, we assume that the total interfacial area between the kaolinite and water in each sample hole to be between 0.1 and 6 cm^2 and normalized the experimental nucleation rate of our data in **Figure 4.17** by this factor. The above range in the interfacial area results in the red region in **Figure 4.17**.
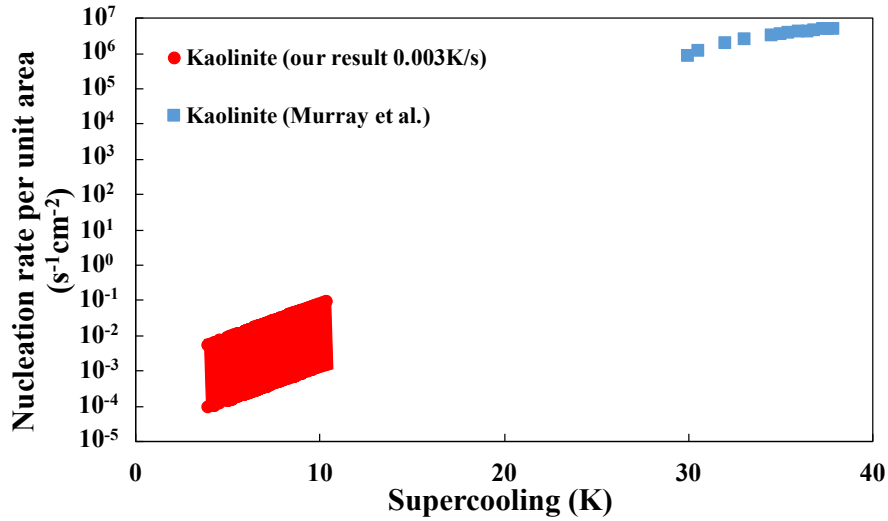
Figure 4.17. Nucleation curves (nucleation rate per unit area) measured with kaolinite compared to the results of Murray et al.'s research. Our results used the data of cooling rate 0.003 K/s, Murray et al.'s results used 0.17 K/s as the cooling rate.

As shown in **Figure 4.17**, the supercooling range of Murray et al.'s results are much higher (lower temperatures) than ours. When extrapolating our nucleation curves to their supercooling range (around 30 K to 40 K), our nucleation rates are about 4 to 5 orders of magnitude lower than their results. We note that the cooling rates used in our experiments (0.001 K/s and 0.003 K/s) were much slower than theirs (0.17 K/s), which would provide enough time for a sample to freeze at higher temperatures. Other than the faster cooling rate, we also noted that Murray et al. used much smaller water droplets (diameter of 10 to 40 μm) than what we used (diameter 4.86 mm), which could also contribute to the much larger supercooling range (smaller temperature range) in their data.

Murray et al. estimated that the surface area for kaolinite would be around 11.8 m^2g^{-1} in Table 1 of [12]. If the surface area of kaolinite in our study had the same ratio, our surface area would be around 354 cm^2 in each sample hole, which would be more than 2 orders of magnitude larger than the range shown in **Table 4.1** and **Table 4.2**.

Our results show that Snomax was the most effective of all the promoters we tested. We suspect that the efficacy of Snomax may be partly aided by its much larger interfacial area than the other promoter samples because Snomax could form a suspension when mixed with water (as shown in **Figure 4.3**). In contrast, we found it difficult to suspend AgI or kaolinite in water. Our results suggest that AgI or kaolinite (or other water-insoluble promoters) might become excellent nucleater of ice if they can be suspended in water.

4.5   Conclusion

We used water samples that were in direct contact with a Teflon sample cell for investigating the efficacy of several ice nucleation promoters. The use of this setting did not increase the nucleation rate of ice in pure water by more than the difference between that of a quasi-free water droplet supported by stable wetting films of squalane and that of a quasi-free water droplet suspended between two immiscible liquids at the same supercooling. This finding suggests that the promotion effect of a Teflon wall is limited and insignificant in the presence of an effective ice nucleation promoter.

The efficacy of several ice nucleation promoters were investigated quantitatively with the linear cooling ramp method, using two cooling rates of 0.003 K/s and 0.001 K/s. We found that the efficacy ranking among the tested additives was; Snomax $\approx$ AgI $\geq$ kaolinite > steroid > cholesterol $\approx$ celluloses $\geq$ Teflon wall.

Steroid/cholesterol was reported to be effective promoters that could nucleate ice at -1 °C in the literature, but it was found in this study that they were not nearly as effective as AgI or kaolinite, which indicated that only systematic comparisons of nucleation rates could rank the efficacy of different promoters quantitatively.

4.6   References

1.   B. Murray, D. O'sullivan, J. Atkinson and M. Webb, *Ice nucleation by particles immersed in supercooled cloud droplets.* Chemical Society Reviews, 2012. **41**(19): p. 6519-6554.

2.   F.T. Lynch and A. Khodadoust, *Effects of ice accretions on aircraft aerodynamics.* Progress in Aerospace Sciences, 2001. **37**(8): p. 669-767.

3.   C. Demartino, H.H. Koss, C.T. Georgakis and F. Ricciardelli, *Effects of ice accretion on the aerodynamics of bridge cables.* Journal of Wind Engineering and Industrial Aerodynamics, 2015. **138**: p. 98-119.

4.   E.D. Sloan Jr and C.A. Koh, *Clathrate hydrates of natural gases*. 2007: CRC press.

5.   G.A. Kimmel, Y. Xu, A. Brumberg, N.G. Petrik, R.S. Smith and B.D. Kay, *Homogeneous ice nucleation rates and crystallization kinetics in transiently-heated, supercooled water films from 188 K to 230 K.* The Journal of Chemical Physics, 2019. **150**(20): p. 204509.

6.   J.-H. Sa and A.K. Sum, *Promoting gas hydrate formation with ice-nucleating additives for hydrate-based applications.* Applied Energy, 2019. **251**: p. 113352.

7.   N. Maeda, *Brief Overview of Ice Nucleation.* Molecules, 2021. **26**(2): p. 392.

8.   H.R. Pruppacher and J.D. Klett, *Microphysics of Clouds and Precipitation*. 1997, Kluwer, Dordrecht.

9.   K.E. Zachariassen and E. Kristiansen, *Ice nucleation and antinucleation in nature.* Cryobiology, 2000. **41**(4): p. 257-279.

10.   C. Marcolli, B. Nagare, A. Welti and U. Lohmann, *Ice nucleation efficiency of AgI: review and new insights.* Atmospheric Chemistry and Physics, 2016. **16**(14): p. 8915-8937.

11. B. Glatz and S. Sarupria, *The surface charge distribution affects the ice nucleating efficiency of silver iodide.* The Journal of Chemical Physics, 2016. **145**(21): p. 211924.

12. B.J. Murray, S. Broadley, T. Wilson, J. Atkinson and R. Wills, *Heterogeneous freezing of water droplets containing kaolinite particles.* Atmospheric Chemistry and Physics, 2011. **11**(9): p. 4191-4207.

13. L. Lupi, A. Hudait and V. Molinero, *Heterogeneous nucleation of ice on carbon surfaces.* Journal of the American Chemical Society, 2014. **136**(8): p. 3156-3164.

14. R.B. Head, *Steroids as ice nucleators.* Nature, 1961. **191**(4793): p. 1058-1059.

15. G.C. Sosso, T.F. Whale, M.A. Holden, P. Pedevilla, B.J. Murray and A. Michaelides, *Unravelling the origins of ice nucleation on organic crystals.* Chemical science, 2018. **9**(42): p. 8077-8088.

16. B. Pummer, C. Budke, S. Augustin-Bauditz, D. Niedermeier, L. Felgitsch, C. Kampf, R. Huber, K. Liedl, T. Loerting and T. Moschen, *Ice nucleation by water-soluble macromolecules.* Atmospheric Chemistry and Physics, 2015. **15**(8): p. 4077-4091.

17. R. Pandey, K. Usui, R.A. Livingstone, S.A. Fischer, J. Pfaendtner, E.H. Backus, Y. Nagata, J. Fröhlich-Nowoisky, L. Schmüser and S. Mauri, *Ice-nucleating bacteria control the order and dynamics of interfacial water.* Science Advances, 2016. **2**(4): p. e1501630.

18. B.G. Pummer, H. Bauer, J. Bernardi, S. Bleicher and H. Grothe, *Suspendable macromolecules are responsible for ice nucleation activity of birch and conifer pollen.* Atmospheric Chemistry and Physics, 2012. **12**(5): p. 2541-2550.

19. N. Hiranuma, K. Adachi, D.M. Bell, F. Belosi, H. Beydoun, B. Bhaduri, H. Bingemer, C. Budke, H.-C. Clemen and F. Conen, *A comprehensive characterization of ice nucleation*

by three different types of cellulose particles immersed in water. Atmospheric Chemistry and Physics, 2019. **19**(7): p. 4823-4849.

20.   M. Polen, E. Lawlis and R.C. Sullivan, *The unstable ice nucleation properties of Snomax® bacterial particles.* Journal of Geophysical Research: Atmospheres, 2016. **121**(19): p. 11,666-11,678.

21.   N. Fukuta and B. Mason, *Epitaxial growth of ice on organic crystals.* Journal of Physics and Chemistry of Solids, 1963. **24**(6): p. 715-718.

22.   P.K. Wolber, *Bacterial ice nucleation.* Advances in microbial physiology, 1993. **34**: p. 203-237.

23.   N. Maeda, *Nucleation of Gas Hydrates*. 2020, Springer: Cham, Switzerland.

24.   X. Zhang, H. Li and N. Maeda, *Nucleation curves of ice in quasi–free water droplets.* Chemical Engineering Science, 2021: p. 116751.

25.   N. Maeda, *Nucleation curves of model natural gas hydrates on a quasi-free water droplet.* AIChE Journal, 2015. **61**(8): p. 2611-2617.

26.   N. Maeda, *Nucleation curves of methane hydrate from constant cooling ramp methods.* Fuel, 2018. **223**: p. 286-293.

27.   *National Center for Biotechnology Information. PubChem Compound Summary for CID 56841936, Kaolin. https://pubchem.ncbi.nlm.nih.gov/compound/Kaolin. Accessed June 23, 2022.*

28.   A. Heneghan, P. Wilson and A. Haymet, *Heterogeneous nucleation of supercooled water, and the effect of an added catalyst.* Proceedings of the National Academy of Sciences, 2002. **99**(15): p. 9631-9634.

CHAPTER 5 ICE NUCLEATION IN THE PRESENCE OF NUCLEATION PROMOTERS DISPERSED IN TETRABUTYLAMMONIUM BROMIDE (TBAB) SOLUTIONS

A version of this chapter has been accepted for publication in *Chemical Engineering Science*.

Abstract

Ice nucleation is the initial step of ice formation that has significant impact on global climate, several engineering and structural surfaces and other systems like clathrate hydrates. The nucleation promoters for ice have been studied for decades but some problems or mechanisms remain unclear. In our earlier study [1], Snomax was found to be the most effective promoter among the common ice nucleation promoters we had tested and it was postulated that the efficacy of Snomax might be aided by its larger interfacial area available for heterogeneous nucleation because it could be easily dispersed in water. Here we attempted to disperse the three ice nucleation promoters which we had previously found to be effective – AgI, kaolinite and cholesterol – into liquid water to increase the interfacial area with water and the heterogeneous nucleation rate of ice. We found dispersion of these promoters into water to be difficult and required addition of Tetrabutylammonium bromide (TBAB) to the aqueous phase before they could be dispersed. We then investigated the nucleation rates of ice in the dispersed nucleation promoter suspensions. We found (1) addition of TBAB alone unexpectedly promoted the nucleation of ice, (2) dispersing AgI into 1 mM TBAB solutions further promoted ice nucleation, (3) dispersing kaolinite or cholesterol in TBAB solutions did not promote ice nucleation more so than the TBAB solutions without kaolinite or cholesterol.

5.1 Introduction

Ice nucleation is the initial step of ice formation which has significant impacts on global climate [2, 3], engineering surfaces such as airfoils [4, 5], food engineering [6, 7], medicine [8, 9], agriculture [10] and other fields [11, 12]. Due to its applications in cloud seeding, artificial snow and so on, ice nucleation promoters have been studied for decades [13-15]. Besides, the studies on ice nucleation promoters could also put insights on finding effective nucleation promoters for the nucleation of clathrate hydrate, which has potential applications on gas storage, carbon capture and sequestration and so on. However, many mechanisms remain unclear especially about the heterogeneous nucleation potency of ice nucleation promoters. In our earlier publication, the efficacy of seven different nucleation promoters (both inorganic and organic) were investigated and ranked as Snomax $\approx$ AgI $\geq$ kaolinite > steroid > cholesterol $\approx$ celluloses $\geq$ Teflon wall [1]. We postulated that the excellent promoting efficacy of Snomax could be due in part to its ability to be dispersed in water with ease, because the resulting much larger interfacial area is expected to increase the heterogeneous nucleation rate of ice. Since other nucleation promoters such as AgI and kaolinite were hardly soluble in water and also difficult to disperse in water, it is reasonable to postulate that the insoluble ice nucleation promoters may have better promoting effects if it could be dispersed in water. Unfortunately, we found that dispersing these ice nucleation promoters in water was not a trivial task.

Tetrabutylammonium bromide (TBAB) has been used as a dispersive agent or stabilizer in many studies, it is also used as one of the main synthetic materials of the deep eutectic solvent (DES) for the liquid-liquid microextraction that acts as a dispersive agent and improves the mass transfer between the phases as a salting-out agent [16, 17]. In the oil and gas industry, TBAB was widely studied as a semi-clathrate promoter, which has potential applications in the fields of

hydrogen storage, carbon dioxide capture, etc. [18-20]. Veluswamy et al. [21] investigated the impact of TBAB, THF and cyclopentane as promoters on hydrogen hydrate formation. After measuring the induction time, formation rate of hydrate, gas consumption and hydrogen storage capacity, etc., it was found that TBAB / hydrogen semi-clathrate hydrates formed fast and easier but had lower hydrogen storage capacity comparing to the results of THF [21]. Ye et al. reported that TBAB could act as a promoter for hydrate formation in the $CO_2 + H_2O + TBAB$ system at low mass fractions (0.05 and 0.10) [22]. In contrast, Nguyen et al. found that TBAB can act as an inhibitor for CO_2 hydrate formation at minuscule concentration [23]. Other than acting as a semi-clathrate promoter, TBAB dissolved in water could also form semi-clathrate [24], which has many applications in air-conditioning system as a refrigerant [25], gas storage and separation [26].

In this study, we investigated the efficacy of TBAB solutions of a range of concentrations to disperse the ice nucleation promoters into liquid water. We then investigated the promotion effects of TBAB over a broad range of concentrations on the nucleation rate of ice. Finally, we investigated the nucleation rates of ice in the dispersed promoter suspensions in the TBAB aqueous solutions.

5.2   Materials and Methods

The nucleation promoters investigated in this study were AgI (99% purity, purchased from Sigma-Adrich), kaolinite and cholesterol (99% purity, purchased from Sigma-Adrich). All nucleation promoters were dispersed in Tetrabutylammonium bromide (TBAB, 99% purity, purchased from Sigma-Adrich and used as received) solutions when investigating the nucleation rates of ice. 1M TBAB solution was prepared first as a stock solution, then the TBAB solutions with specific concentrations (e.g., 0.1 M, 10^{-3} M, 10^{-5} M, etc.) were prepared by diluting the stock

solution with Milli-Q water (ultra-pure water of 18.2 MΩ resistivity from a Millipore unit). Before measuring the nucleation rates of ice in the presence of dispersed promoters, sedimentation experiments were carried out to select a suitable concentration of TBAB in water that resulted in the best stability (longest time) of the suspensions. An ice nucleation promoter was added to a TBAB solution at 2.5 wt%, which is the same the ratio as we had used in our earlier publication [1]. After sonicated in the Ultrasonic device (ELMASONIC E+ series) for 10 min, the suspensions were monitored over time, and the dispersion of the best stability (longest duration) was selected for the subsequent ice nucleation experiments.

After having prepared a suspension, 120 µL of the suspension was added into each hole of the Teflon sample cell (custom-made with 36 holes in total), followed by covering a glass lid at the top of the sample cell with the vacuum grease (Dow Corning, High Vacuum grease). Then the Teflon sample cell was placed into the experimental setup shown in **Figure 5.1**. The details of the experimental setup are described in our earlier publications [1, 27]. During each experimental cooling ramp, 0.003 K/s was used as the cooling rate, and the images of the sample cell were recorded by a webcam every 1 min. After each experimental ramp, the freezing temperature of each sample was recorded with an application of the calibration table that related the nominal experimental temperatures to the real sample temperatures. Finally, the survival curve and the nucleation curve were derived from the recorded data using the procedure described in refs [27-29]. It is noted that the freshly dispersed suspensions were required for each experimental cooling ramp since the stability of some promoter suspensions was not long enough for repeated experimental ramps.
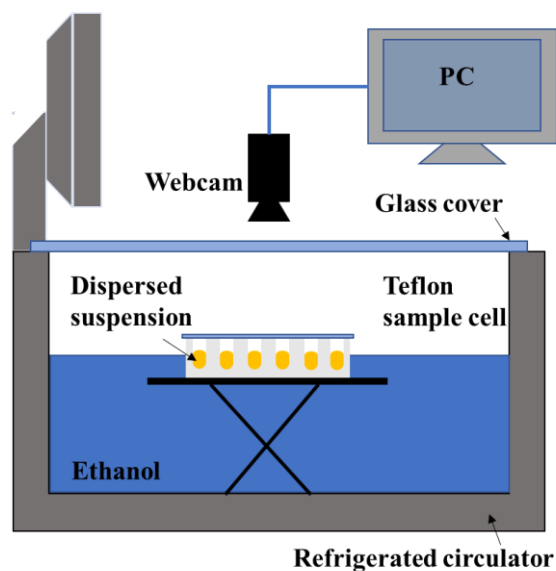
Figure 5.1. Schematic illustration of the experimental setup. After adding the dispersed suspension of promoter into each hole, the Teflon sample cell was sealed by a small glass slide and placed on the lab jack.

5.3 Results

5.3.1 Nucleation Rate of Ice in TBAB Solutions

The nucleation rates of ice formation in TBAB solutions of different concentrations (10^{-5} M to 1 M) were first investigated as control experiments. We show the survival curves in **Figure 5.2**, the corresponding ln*F* curves in **Figure 5.3** and the corresponding nucleation curves in **Figure 5.4**. It is noted that at least 200 data points were collected for the derivation of each curve.
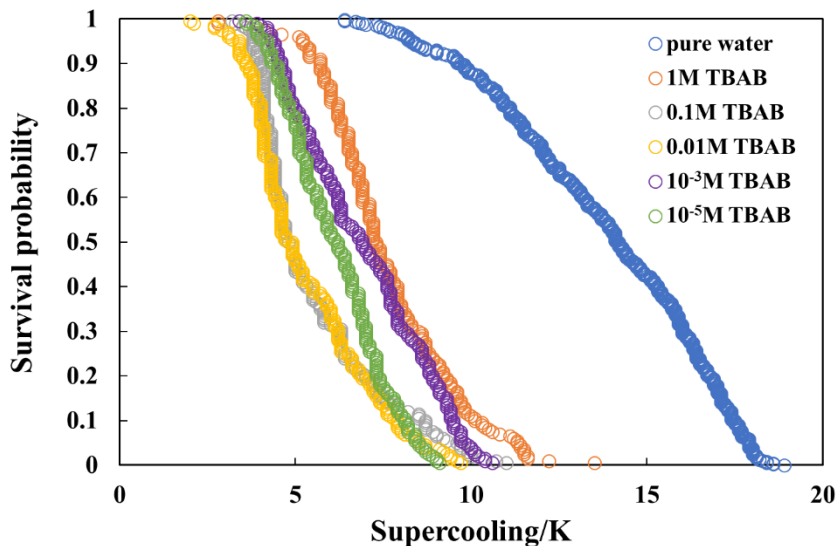
Figure 5.2. Survival curves of ice formation measured in TBAB solutions with different concentrations. 0.003 K/s was used as the cooling rate.

As shown in **Figure 5.2**, the survival curves of TBAB solutions were concentrated to the ranges of 2.8 K to 14 K, 3.2 K to 11 K, 2 K to 10.5 K, 3.4 K to 10.7 K and 3.6 K to 9.3 K for the concentrations of 1 M, 0.1 M, 0.01 M, 10^{-3} M and 10^{-5} M, respectively. Unexpectedly, ice formed at lower supercoolings (higher temperatures) in the TBAB solutions than in pure water (6.4 K to 18.9 K) despite the expected lowering of the activity of water and the concomitant freezing point depression by TBAB, indicating that the observed unexpected result was a kinetic (nucleation kinetics), as opposed to a shift in the thermodynamic phase boundary.

Figure 5.3 shows that the ln$F$ curves measured in the TBAB solutions had steeper slopes than that of pure water at a comparable range of supercooling (around 6.7 K to 12 K). As shown in **Figure 5.4**, the nucleation rates measured in the TBAB solutions with different concentrations were similar to each other, which were all larger than that measured in pure water by 1 to 2 orders of magnitude. The results showed that TBAB acted as a nucleation promoter of ice from the reduced supercooling required for nucleation and the increased nucleation rate at a given

temperature. The nucleation rates of ice in the TBAB solutions of different concentrations over the range of 10^{-5} M to 1 M did not show any systematic trend with the increasing concentrations and were broadly similar to each other at a given supercooling.
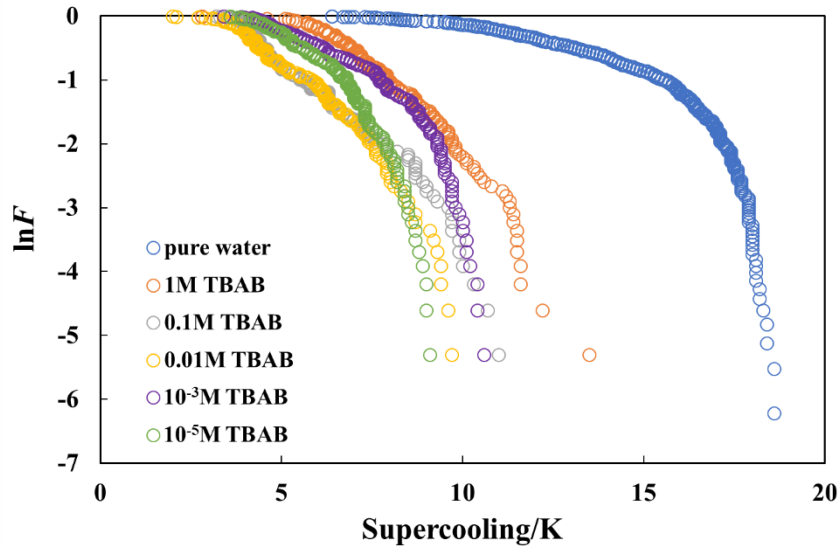
Figure 5.3. Natural logarithm of the survival curves of ice formation measured in TBAB solutions with different concentrations. 0.003 K/s was used as the cooling rate.
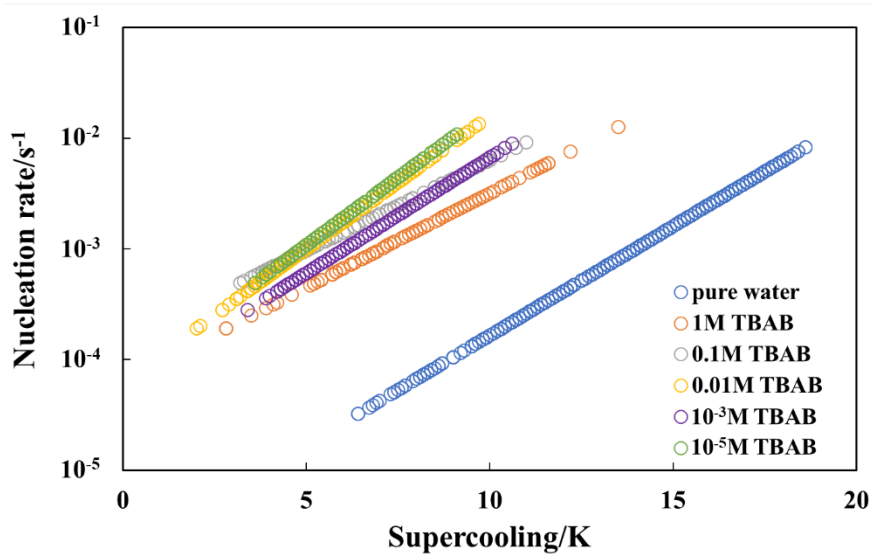
Figure 5.4. Nucleation curves of ice formation measured in TBAB solutions with different concentrations. 0.003 K/s was used as the cooling rate.

5.3.2 Ice Nucleation in Dispersed AgI Suspensions

Figure 5.5 shows the results of the sedimentation experiments for AgI. AgI dispersed in the TBAB solutions and formed suspensions after sonicating, although there was a small amount of sediment at the bottom of the vials. AgI suspended in the TBAB solutions of the concentrations of 1 M, 0.1 M, 10^{-4} M and 10^{-5} M completely phase-separated after 5 minutes. AgI suspended in 0.01 M and 10^{-3} M TBAB solutions completely phase-separated after 2 hours. AgI suspended in 10^{-3} M TBAB solution had the best kinetic stability among the five concentrations we investigated. Therefore, AgI suspended in a 10^{-3} M TBAB solution was selected for the cooling ramp experiments.

The survival curves of ice formation measured in AgI suspensions dispersed in 10^{-3} M TBAB solutions are shown in **Figure 5.6**, the corresponding ln$F$ curves in **Figure 5.7** and the corresponding nucleation curves in **Figure 5.8**. The experimental results are compared to those of our previous results of Snomax and undispersed AgI.
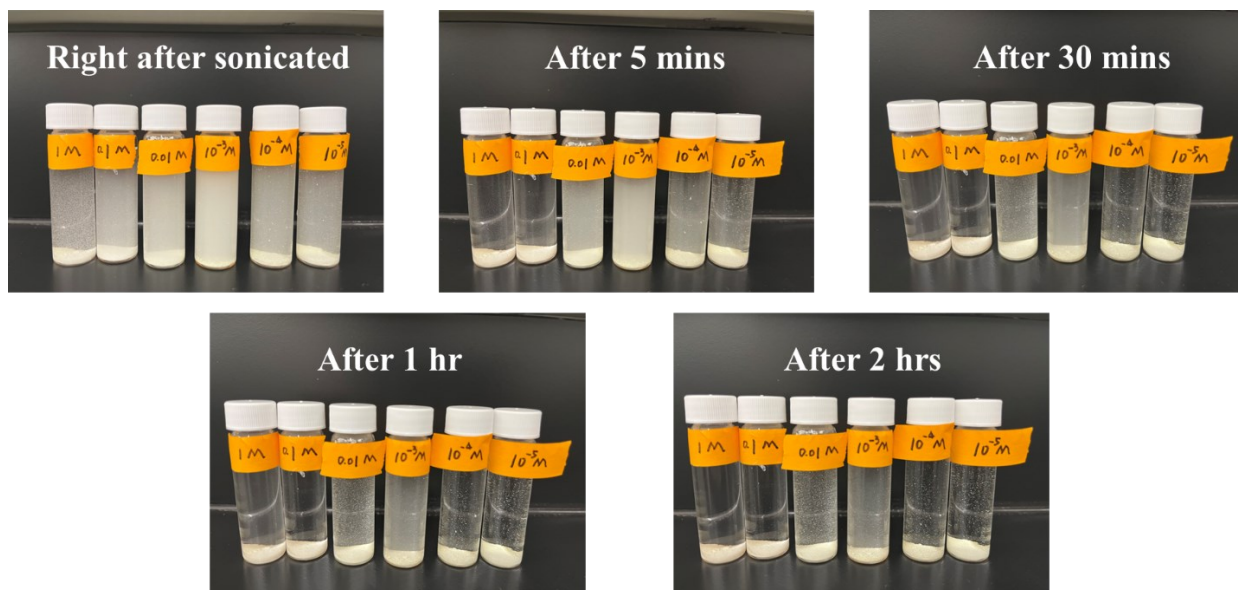
Figure 5.5. Dispersion of AgI in TBAB solutions with different concentrations.
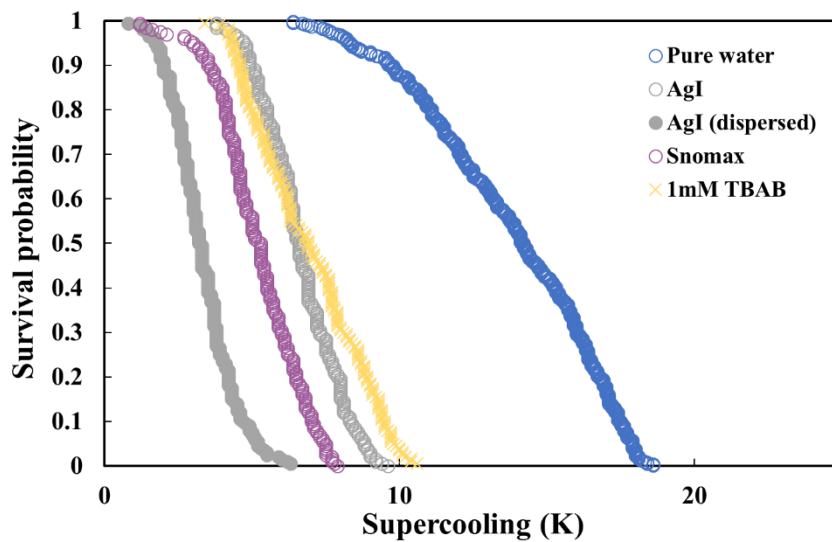
Figure 5.6. Survival curve of ice formation measured in dispersed AgI suspension, comparing with the results of pure water, undispersed AgI, Snomax and 1 mM TBAB solution. The results of pure water, undispersed AgI and Snomax were the same as that in our previous study [1]. The survival curve of 1 mM TBAB solution was the same as that in Figure 5.2.
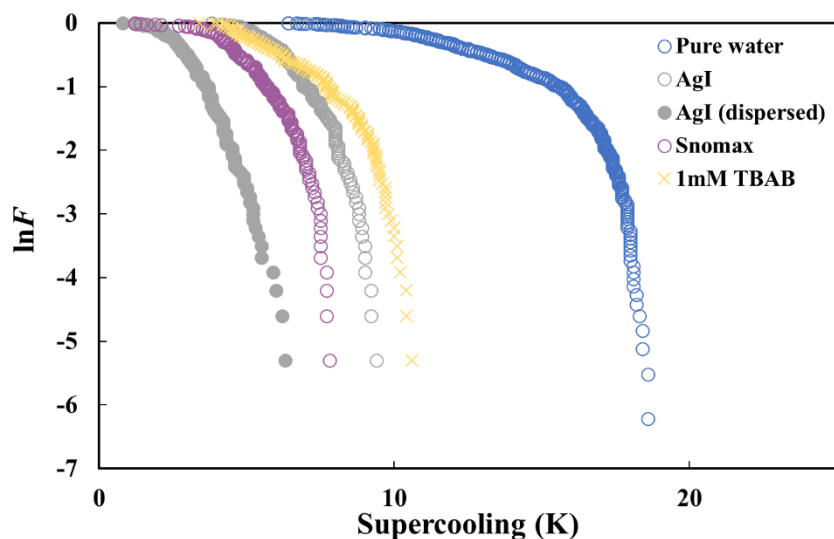
Figure 5.7. Natural logarithm of survival curve measured in dispersed AgI suspension, comparing with the results of pure water, undispersed AgI, Snomax and 1 mM TBAB solution. The results of pure water, undispersed AgI and Snomax were the same as that in our previous study [1]. The curve of 1 mM TBAB solution was the same as that in Figure 5.3.
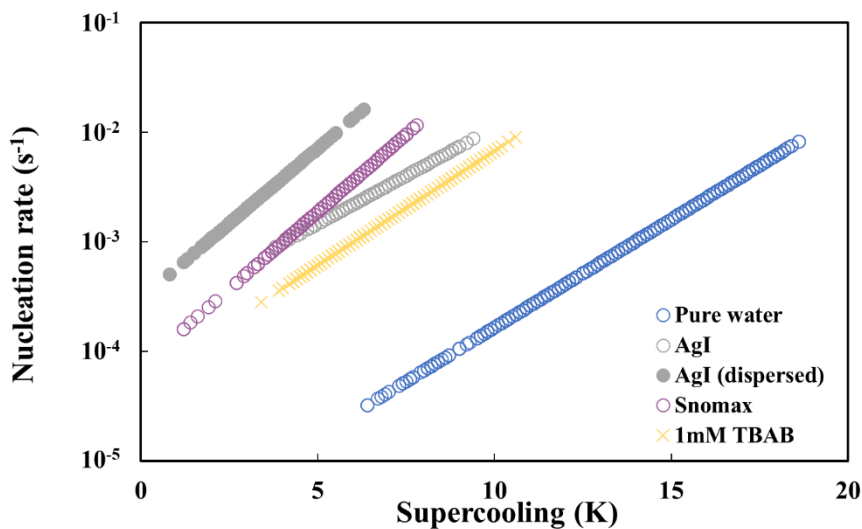
Figure 5.8. Nucleation curve of ice formation measured in dispersed AgI suspension, comparing with the results of pure water, undispersed AgI, Snomax and 1 mM TBAB solution. The results of pure water, undispersed AgI and Snomax were the same as that in our previous study [1]. The nucleation curve of 1 mM TBAB solution was the same as that in Figure 5.4.

127

As shown in **Figure 5.6**, water froze at a largely similar albeit slightly shallower supercooling range (0.8 K to 6.3 K) in dispersed AgI than in Snomax (1.2 K to 7.9 K). The survival curves measured in 10^{-3} M TBAB solution and in undispersed AgI we reported previously are similar to each other. We note that the duration of each cooling ramp was less than 1.5 hrs since the largest supercooling observed was 6.3 K. We thus assume that the dispersed AgI suspension remained stable during each experimental cooling ramp.

Figure 5.7 shows that the ln$F$ curve of the dispersed AgI suspension had steeper slopes than that of Snomax, the undispersed AgI or the 10^{-3} M TBAB solution at a comparable supercooling. **Figure 5.7** also shows that the ln$F$ curve of the dispersed AgI suspension had much steeper slopes than that of pure water, which suggests its nucleation rates would be much higher than that of pure water. As shown in **Figure 5.8**, the nucleation rates in the dispersed AgI suspension were around one order of magnitude greater than that of the undispersed AgI or the 10^{-3} M TBAB solution over the supercooling range of 3 K to 6 K, which indicates that the promoting efficacy of AgI could be improved after dispersion in the TBAB solution. It is surprising that the efficacy of the dispersed AgI was even slightly better than that of Snomax.

5.3.3 Ice Nucleation in Dispersed Kaolinite Suspensions

Similar to AgI, sedimentation experiments for kaolinite were carried out before measuring the nucleation rates. As shown in **Figure 5.9**, kaolinite dispersed in the TBAB solutions and formed suspensions after sonicating. Kaolinite suspended in the TBAB solutions of the concentrations of 1 M, 0.1 M and 0.01 M completely phase-separated after 30 minutes. Kaolinite suspended in 10^{-3} M TBAB solution completely phase-separated after 3 hours. It seems that kaolinite suspended in 10^{-4} M TBAB solution had the best kinetic stability over a period of three

hours. Therefore, 10^{-4} M TBAB solution was selected for the cooling ramp experiments. The survival curves of ice formation measured in kaolinite suspensions dispersed in 10^{-4} M TBAB solution are shown in **Figure 5.10**, the corresponding ln$F$ curves in **Figure 5.11** and the corresponding nucleation curves in **Figure 5.12**. The experimental results are also compared to those of our previous results of undispersed kaolinite. The results for the 10^{-5} M TBAB solution, without kaolinite, are also shown for comparison. As concluded in the former section, the nucleation rate of TBAB solution was independent at the concentration range of 10^{-5} M to 1 M, therefore the results of 10^{-4} M TBAB solution should be quite similar to 10^{-5} M TBAB solution.
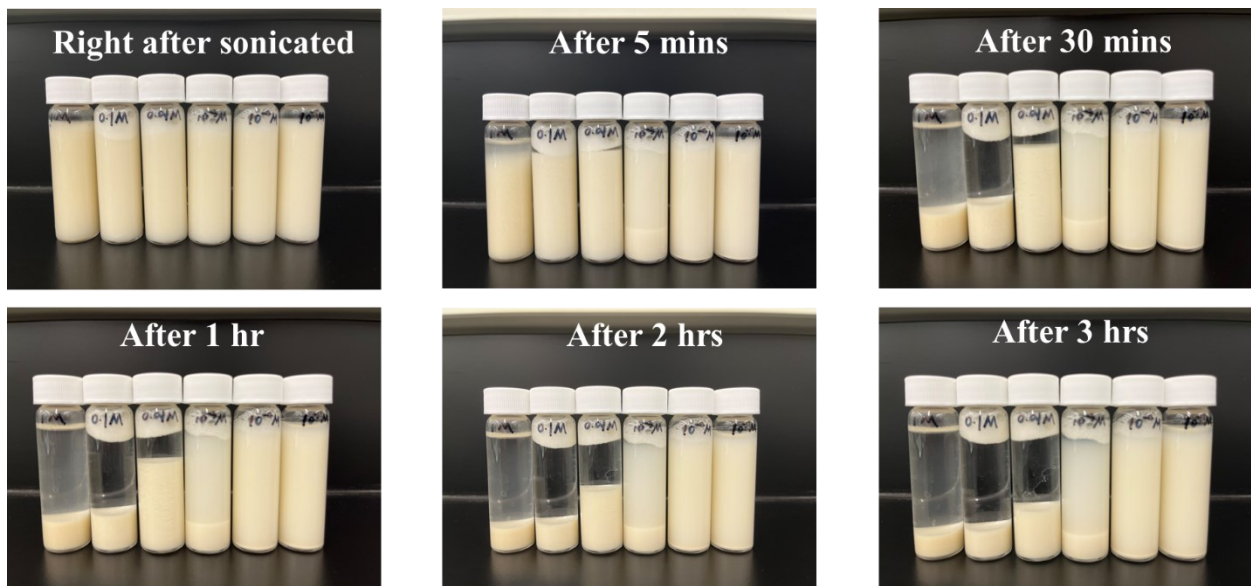
Figure 5.9. Dispersion of kaolinite in TBAB solutions with different concentrations.
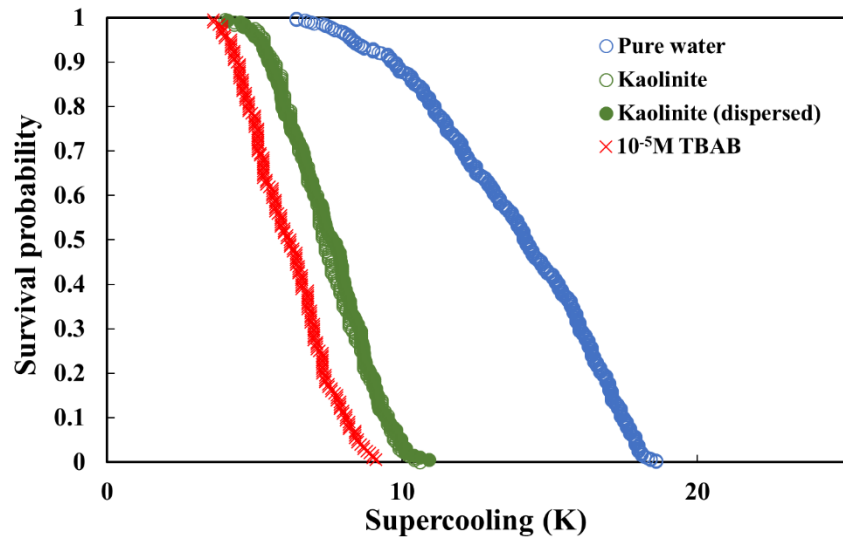
Figure 5.10. Survival curve of ice formation measured in dispersed kaolinite suspension, comparing with the results of pure water, undispersed kaolinite and 10^{-5} M TBAB solution. The results of pure water and undispersed kaolinite were the same as that in our previous study [1]. The survival curve of 10^{-5} M TBAB solution was the same as that in Figure 5.2. The curve measured in dispersed kaolinite suspension was overlapping with that of undispersed kaolinite.
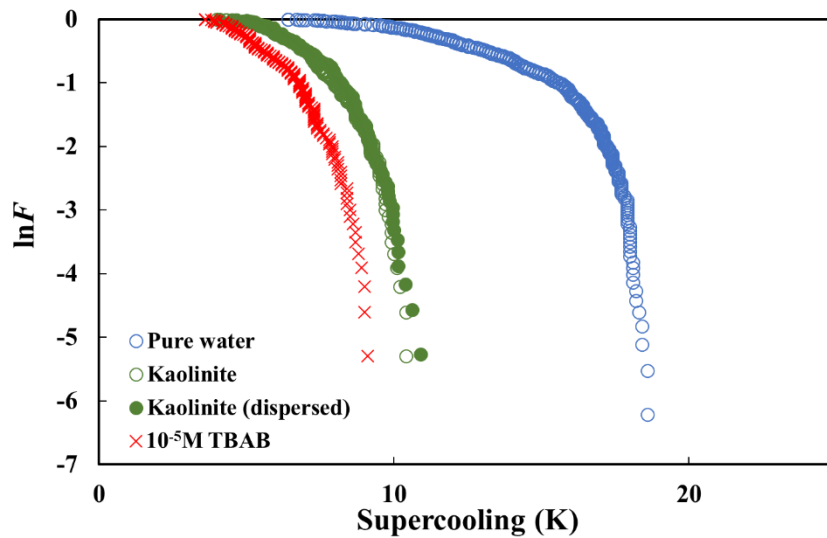
Figure 5.11. Natural logarithm of survival curve measured in dispersed kaolinite suspension, comparing with the results of pure water, undispersed kaolinite and 10^{-5} M TBAB solution. The results of pure water and undispersed kaolinite were the same as that in our previous study [1]. The survival curve of 10^{-5} M TBAB solution was the same as that in Figure 5.3. The curve measured in dispersed kaolinite suspension was overlapping with that of undispersed kaolinite.

130
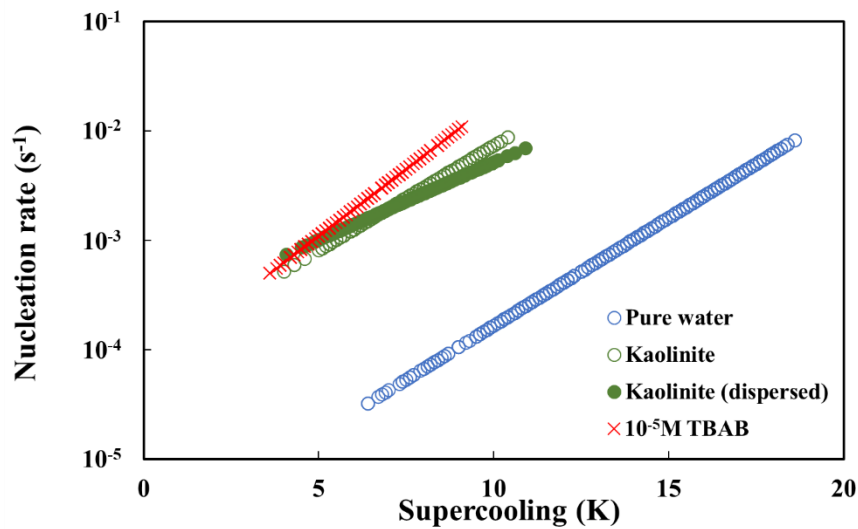
Figure 5.12. Nucleation curve of ice formation measured in dispersed kaolinite suspension, comparing with the results of pure water, undispersed kaolinite and 10^{-5} M TBAB solution. The results of pure water and undispersed kaolinite were the same as that in our previous study [1]. The survival curve of 10^{-5} M TBAB solution was the same as that in Figure 5.4. The curve measured in dispersed kaolinite suspension was almost overlapping with that of undispersed kaolinite.

As shown in **Figure 5.10**, the survival curve of ice formation in the dispersed kaolinite suspension was concentrated to the supercooling range of 4.1 K to 10.9 K, which is similar to that of the undispersed kaolinite (4 K to 10.6 K) and slightly higher than that measured in the 10^{-5} M TBAB solution (3.6 K to 9.1 K). **Figure 5.11** shows that the ln$F$ curve measured in the dispersed kaolinite suspension was almost overlapping with that measured in water with the undispersed kaolinite, and its slope was slightly steeper than that of the 10^{-5} M TBAB solution at the same supercooling.

Figure 5.12 shows that the nucleation curves measured in the dispersed kaolinite suspension, the undispersed kaolinite in water and the 10^{-5} M TBAB solution were close to each other, which were around two orders of magnitude higher than that of pure water. We may thus

conclude that dispersing kaolinite in 10^{-4} M TBAB solution didn't promote ice nucleation more so than the 10^{-4} M TBAB solution alone (without kaolinite) did.

5.3.4 Ice Nucleation in Dispersed Cholesterol Suspensions

Figure 5.13 shows the results of the sedimentation experiments for cholesterol. Cholesterol could be dispersed in the TBAB solutions of all concentrations except for 0.1 M and formed suspensions after sonicating. The kaolinite suspended in the TBAB of all concentrations except for 0.1 M had similar kinetic stability that phase-separated after 3 hours. We selected 10^{-5} M TBAB solution for the cooling ramp experiments of the dispersed cholesterol. The survival curves are shown in **Figure 5.14**, the corresponding ln*F* curves in **Figure 5.15** and the corresponding nucleation curves in **Figure 5.16**.

As shown in **Figure 5.14**, water froze at a much lower supercooling range (higher temperature range) in the dispersed cholesterol suspension (3.4 K to 8.9 K) than the water containing undispersed cholesterol (4.7 K to 16.6 K) or in pure water (6.4 K to 18.6 K). The survival curve measured in dispersed cholesterol suspension was almost overlapping with that measured in the 10^{-5} M TBAB solution without cholesterol, which resulted in the two corresponding ln*F* curves (shown in **Figure 5.15**) overlapping with each other. The slopes of these two ln*F* curves were much steeper than that measured in the presence of undispersed cholesterol or in pure water at a comparable supercooling range (around 6 K to 9 K).

Figure 5.16 shows that the nucleation rates of ice in the dispersed cholesterol suspension were one to two orders of magnitude larger than that measured in the undispersed cholesterol or in pure water. However, similar to the survival curve and ln*F* curve, the nucleation curves of ice in the dispersed cholesterol suspension and in the 10^{-5} M TBAB solution were overlapping with

each other, which indicated that dispersing cholesterol in the 10^{-5} M TBAB solution didn't promote ice nucleation more so than the 10^{-5} M TBAB solution without cholesterol did.
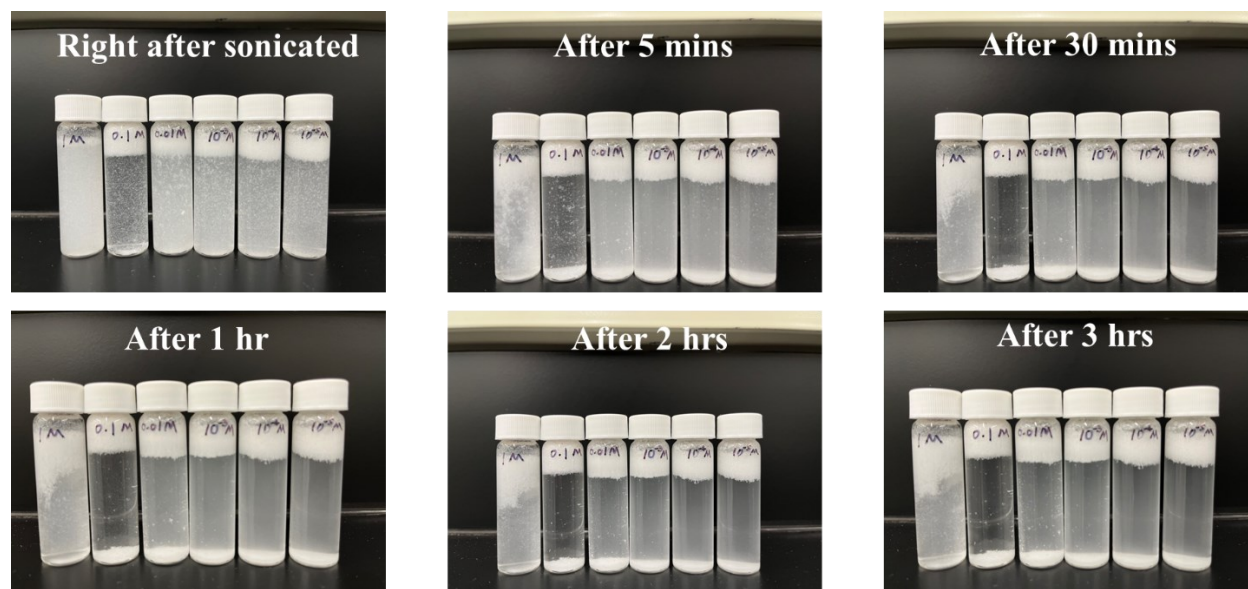
Figure 5.13. Dispersion of cholesterol in TBAB solutions with different concentrations.
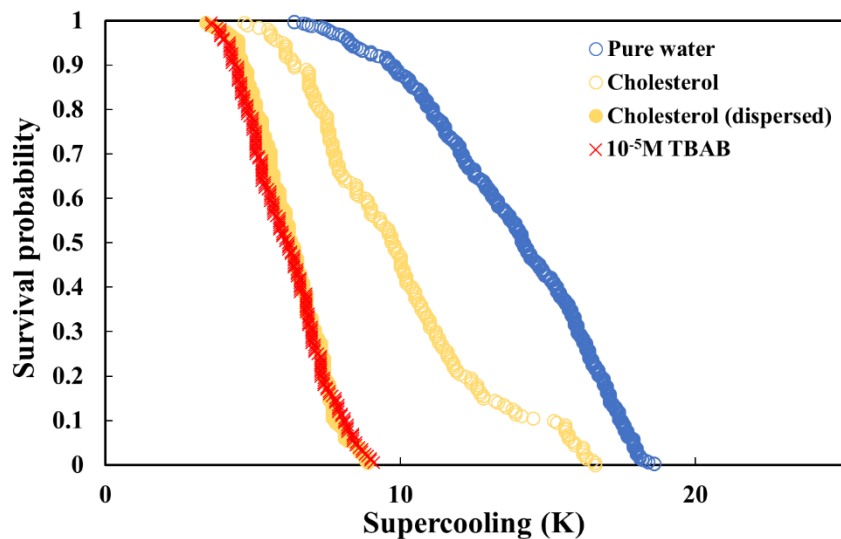
Figure 5.14. Survival curve of ice formation measured in dispersed cholesterol suspension, comparing with the results of pure water, undispersed cholesterol and 10^{-5} M TBAB solution. The results of pure water and undispersed cholesterol were the same as that in our previous study [1]. The survival curve of 10^{-5} M TBAB solution was the same as that in Figure 5.2. The curve

measured in dispersed cholesterol suspension was almost overlapping with that measured in 10⁻⁵M TBAB solution.
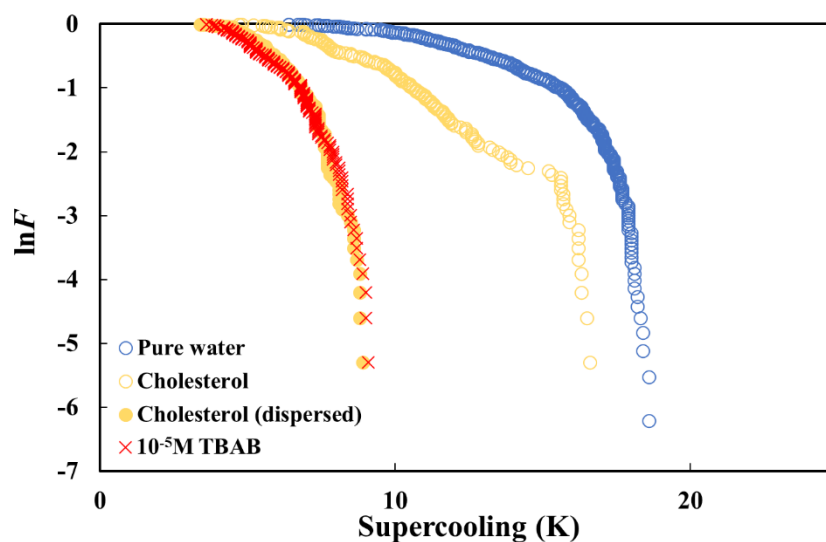
Figure 5.15. Natural logarithm of survival curve measured in dispersed cholesterol suspension, comparing with the results of pure water, undispersed cholesterol and 10^{-5} M TBAB solution. The results of pure water and undispersed cholesterol were the same as that in our previous study [1]. The survival curve of 10^{-5} M TBAB solution was the same as that in Figure 5.3. The curve measured in dispersed cholesterol suspension was almost overlapping with that measured in 10⁻⁵M TBAB solution.
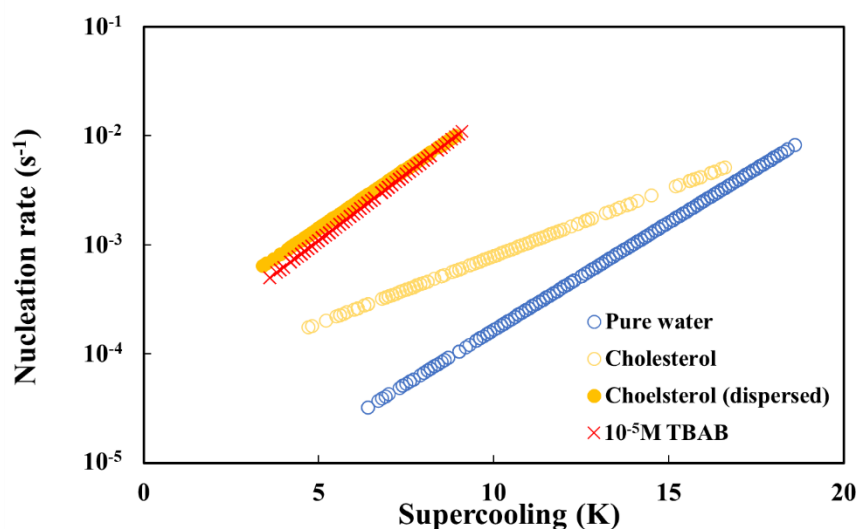
Figure 5.16. Nucleation curve of ice formation measured in dispersed cholesterol suspension, comparing with the results of pure water, undispersed cholesterol and 10^{-5} M TBAB solution. The results of pure water and undispersed cholesterol were the same as that in our previous study [1]. The survival curve of 10^{-5} M TBAB solution was the same as that in Figure 5.4. The curve measured in dispersed cholesterol suspension was almost overlapping with that measured in 10^{-5}M TBAB solution.

5.4   Discussion

5.4.1   Dispersing Effect of TBAB

We found it impossible to disperse AgI, kaolinite or cholesterol into liquid water without any additives, even with rigorous sonication or heating. It has been reported that the catalytic activity of modified nanoparticles could remain unchanged for a three-month period with the addition of TBAB although the exact role of TBAB in this system was unclear [30]. Zheng et al. reported that TBAB could help form oil-in-water emulsions with improved stability for 7 days when its concentration was larger than 1 mM [31]. We thus used TBAB as an additive to help disperse AgI, kaolinite and cholesterol in water.

Our results showed that TBAB indeed helped disperse AgI, kaolinite and cholesterol in water. However, we found that the dispersion of AgI, kaolinite and cholesterol, aided by TBAB,

135

had different impacts on the heterogeneous nucleation rates of ice. The nucleation rates of ice in dispersed AgI suspensions were about one order of magnitude higher than that in water that contained undispersed AgI or in the 1 mM TBAB solutions without AgI. For kaolinite and cholesterol, in contrast, dispersing kaolinite or cholesterol in TBAB solution did not promote ice nucleation more so than the TBAB solution without kaolinite or cholesterol. In other words, the dispersing action of kaolinite or cholesterol hardly impacted the nucleation rate of ice.

5.4.2 Promoting Effect of TBAB on Ice Nucleation

The TBAB solutions increased the nucleation rate of ice over the concentration range of 10^{-5} M to 1 M. Here, we compare the promoting effect of TBAB alone on ice nucleation to the other 7 nucleation promoters we had tested previously [1]. Since the nucleation rates measured in TBAB solutions were independent of the concentration over the range of 10^{-5} M to 1 M, we only used the concentration of 10^{-5} M TBAB solution for this comparison. We note that all 7 nucleation promoters tested in our previous study were undispersed.

The resulting nucleation curves are shown in **Figure 5.17**. The nucleation curve of the TBAB solution was almost overlapping with that of undispersed AgI and close to that of undispersed kaolinite. The nucleation rates measured in these undispersed nucleation promoters were all about two orders of magnitude higher than that of pure water at a comparable supercooling. Therefore, the efficacy of these eight nucleation promoters can be ranked as: Snomax $\geq$ undispersed AgI $\approx$ TBAB $\approx$ undispersed kaolinite > undispersed steroid > undispersed cholesterol $\geq$ undispersed celluloses $\approx$ Teflon wall.
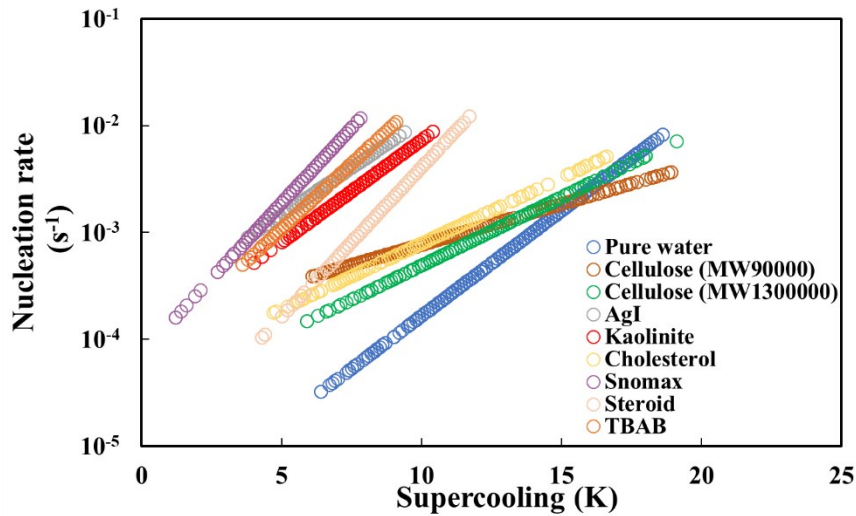
Figure 5.17. Nucleation curve of ice formation measured in 10^{-5} M TBAB solution, compared with other 7 nucleation promoters tested in our previous study [1]. The curve measured in TBAB solution was almost overlapping with that measured in the presence of AgI. The experimental cooling rate was 0.003 K/s for the measurements of all nucleation promoters.

It is surprising that TBAB solutions had similar efficacy to undispersed AgI or kaolinite that tested in our previous study [1]. According to the classical nucleation theory, the nucleation rate of ice, J, could be expressed by the Arrhenius form,

$$J = AN_0 \exp(-\Delta g / kT)$$
<div align="right">Eq. 5.1</div>

Where A is the kinetic constant that includes the attachment frequency of a water molecule in the liquid phase to a growing crystallite, N_0 is the concentration of potential nucleation sites, Δg is the height of activation barrier or the thermodynamic work that is required to form a critically sized nucleus, k is the Boltzmann constant and T is the absolute temperature [13].

The framework of classical nucleation theory basically consists of a so-called kinetic parameter and a so-called thermodynamic parameter, where the kinetic parameter depends on the type of nucleation and accounts for the frequency of attachment of hydrate building units to the

nucleus and the concentration of potential nucleation sites, and the thermodynamic parameter accounts for the probability that a system that can surmount the activation barrier as prescribed by the Boltzmann distribution. Such a probability exponentially diminishes with the size of the activation barrier [32].

With the addition of TBAB, N_0 is expected to increase with the concentration. However, this increase is not significant for small concentrations. We thus assume that the increase in the nucleation rate of ice in TBAB solutions was due to a lowered activation barrier, Δg. In other words, TBAB was speculated to lower the activation barrier (i.e., lower the so-called thermodynamic factor within the framework of classical nucleation theory).

Although TBAB was barely studied as a promoter for ice nucleation in the literature, it was widely used as a promoter for gas hydrate formation, and the underlying mechanisms of TBAB on promoting hydrate nucleation could shed some light into the understanding of its promotion of ice nucleation. Similar to THF (tetrahydrofuran) and cyclopentane, TBAB was thought to act as a thermodynamic promoter because it can serve as a guest or co-guest of semi-clathrate [33-35]. Nguyen et al. [23] applied both experimental and computational simulation methods to study the effect of TBAB on CO_2 hydrate formation. At high TBAB concentrations, they found the water structure would be perturbed by its surrounding TBA^+ cations and become more energetic, resulting in the tendency to transform into a more ordered conformation. However, TBAB could inhibit the nucleation of gas hydrate at low concentrations (e.g., 0.125 wt.% in ref. [23]), and Nguyen et al. speculated that the water alignment at the water – gas interface might be the reason for this unexpected phenomenon. Since ice and clathrate hydrates have similar crystal structures [11], it is reasonable to speculate that similar perturbations of the water structure by TBA^+ cations might occur in ice. Such local alignment/re-orientations of the water molecules by TBA^+ cations

138

could make it easier for the water molecules to form ice-like structures and lower the activation barrier to ice nucleation.

Our results showed that TBAB facilitated the nucleation of ice over a broad range of concentrations. This finding may be in contrast to its inhibitive effect on the nucleation of clathrate hydrates reported by Nguyen et al. In gas hydrates, the water molecules need to rearrange themselves to accommodate the (generally hydrophobic) guest gas molecules during the process of nucleation. In contrast, formation of ice is a single component system and such hydrophobic hydration is not required during the process of ice nucleation. Nguyen et al. reported strong hydrogen-bonded (ice-like) OH peaks in the SFG spectra of the TBAB solutions within the concentration range of 0.075 wt.% to 3 wt.% (Fig. 4 in ref. [23]), which could facilitate the formation of ice-like structures. The differing impacts of TBAB on the nucleation of ice and on that of clathrate hydrate could shed light to the relative importance of hydrophobic hydration in these systems.

5.4.3   Impact of Dispersing Ice Nucleation Promoters

It is interesting to find that dispersing AgI in TBAB solutions is more effective in promoting the nucleation of ice than dispersing kaolinite or cholesterol. This finding suggests that the increased interfacial areas between water and AgI, kaolinite or cholesterol, and the concomitant increase in the heterogeneous nucleation rates, may not be the primary factor. One possible reason could be that TBAB may have synergistic effects in ice nucleation with AgI but not with kaolinite or cholesterol. Another possibility is that TBAB may have negative synergistic effects with kaolinite or cholesterol that cancelled the impact of the increased interfacial areas and the expected increase in the heterogeneous nucleation rates. AgI has been found to have small lattice parameter

mismatch with hexagonal ice surface [36, 37], while kaolinite is a mineral clay that has a complex layered structure [38] and cholesterol is an organic lipid-like molecule that has no affinity to water or ice [39]. The adsorption of TBAB from a given concentration of TBAB aqueous solution onto AgI, kaolinite or cholesterol could be different and consequently differently impacted the interactions between the surfaces of these materials and the water molecules, which may have resulted in more less active sites for the heterogeneous nucleation of ice.

5.5   Conclusions

In this study, we investigated the heterogeneous nucleation rates of ice in the dispersions of AgI, kaolinite and cholesterol dispersed in TBAB aqueous solutions. Several key findings are as follows:

(1) TBAB can act as a nucleation promoter of ice, and the nucleation rate measured in TBAB solutions was largely independent of its concentration over the range of 10^{-5} M to 1 M.

(2) The sedimentation experiments suggested that the suspensions prepared from AgI dispersed in 10^{-3} M TBAB solution, kaolinite dispersed in 10^{-4} M TBAB solution and cholesterol dispersed in 10^{-5} M TBAB solution had the best kinetic stability.

(3) Dispersing AgI in 10^{-3} M TBAB solution further promoted ice nucleation whereas dispersing kaolinite or cholesterol in TBAB solutions did not promote ice nucleation more so than TBAB solutions without kaolinite or cholesterol.

5.6   References

1.   X. Zhang and N. Maeda, *Nucleation curves of ice in the presence of nucleation promoters.* Chemical Engineering Science, 2022. **262**: p. 118017.

2. P.J. Demott, A.J. Prenni, X. Liu, S.M. Kreidenweis, M.D. Petters, C.H. Twohy, M. Richardson, T. Eidhammer and D. Rogers, *Predicting global atmospheric ice nuclei distributions and their impacts on climate.* Proceedings of the National Academy of Sciences, 2010. **107**(25): p. 11217-11222.

3. D.A. Knopf and P.A. Alpert, *Atmospheric ice nucleation.* Nature Reviews Physics, 2023. **5**(4): p. 203-217.

4. S. Alamri, V. Vercillo, A.I. Aguilar‑Morales, F. Schell, M. Wetterwald, A.F. Lasagni, E. Bonaccurso and T. Kunze, *Self‑Limited Ice Formation and Efficient De‑Icing on Superhydrophobic Micro‑Structured Airfoils through Direct Laser Interference Patterning.* Advanced Materials Interfaces, 2020. **7**(22): p. 2001231.

5. S. Özgen and M. Canıbek, *Ice accretion simulation on multi-element airfoils using extended Messinger model.* Heat and Mass Transfer, 2009. **45**(3): p. 305.

6. Y. You, T. Kang and S. Jun, *Control of ice nucleation for subzero food preservation.* Food Engineering Reviews, 2021. **13**: p. 15-35.

7. M. Dalvi-Isfahan, N. Hamdami, E. Xanthakis and A. Le-Bail, *Review on the control of ice nucleation by ultrasound waves, electric and magnetic fields.* Journal of Food Engineering, 2017. **195**: p. 222-234.

8. G.J. Morris and E. Acton, *Controlled ice nucleation in cryopreservation–a review.* Cryobiology, 2013. **66**(2): p. 85-92.

9. N. William, S. Mangan, R.N. Ben and J.P. Acker, *Engineered Compounds to Control Ice Nucleation and Recrystallization.* Annual Review of Biomedical Engineering, 2023. **25**.

10. S. Lindow, *The role of bacterial ice nucleation in frost injury to plants.* Annual review of phytopathology, 1983. **21**(1): p. 363-384.

11.   E.D. Sloan Jr and C.A. Koh, *Clathrate hydrates of natural gases*. 2007: CRC press.

12.   J.-H. Sa and A.K. Sum, *Promoting gas hydrate formation with ice-nucleating additives for hydrate-based applications.* Applied Energy, 2019. **251**: p. 113352.

13.   N. Maeda, *Brief Overview of Ice Nucleation.* molecules, 2021. **26**(392).

14.   B. Murray, D. O'sullivan, J. Atkinson and M. Webb, *Ice nucleation by particles immersed in supercooled cloud droplets.* Chemical Society Reviews, 2012. **41**(19): p. 6519-6554.

15.   B.J. Murray, S. Broadley, T. Wilson, J. Atkinson and R. Wills, *Heterogeneous freezing of water droplets containing kaolinite particles.* Atmospheric Chemistry and Physics, 2011. **11**(9): p. 4191-4207.

16.   A. Shishov, R. Chromá, C. Vakh, J. Kuchár, A. Simon, V. Andruch and A. Bulatov, *In situ decomposition of deep eutectic solvent as a novel approach in liquid-liquid microextraction.* Analytica chimica acta, 2019. **1065**: p. 49-55.

17.   A. Shishov, N. Volodina, D. Nechaeva, S. Gagarinova and A. Bulatov, *Deep eutectic solvents as a new kind of dispersive solvent for dispersive liquid–liquid microextraction.* RSC advances, 2018. **8**(67): p. 38146-38149.

18.   X. Lang, S. Fan and Y. Wang, *Intensification of methane and hydrogen storage in clathrate hydrate and future prospect.* Journal of Natural Gas Chemistry, 2010. **19**(3): p. 203-209.

19.   P. Babu, W.I. Chin, R. Kumar and P. Linga, *Systematic evaluation of tetra-n-butyl ammonium bromide (TBAB) for carbon dioxide capture employing the clathrate process.* Industrial & Engineering Chemistry Research, 2014. **53**(12): p. 4878-4887.

20.   Y. Wang, A. Niu, S. Liu, J. Chen, X. Zhang and J. Zhan, *Effects of Composite Accelerators on the Formation of Carbon Dioxide Hydrates.* ACS omega, 2022. **7**(18): p. 15359-15368.

21.   H.P. Veluswamy, W.I. Chin and P. Linga, *Clathrate hydrates for hydrogen storage: the impact of tetrahydrofuran, tetra-n-butylammonium bromide and cyclopentane as promoters on the macroscopic kinetics.* International journal of hydrogen energy, 2014. **39**(28): p. 16234-16243.

22.   N. Ye, P. Zhang and Q. Liu, *Kinetics of hydrate formation in the CO2+ TBAB+ H2O system at low mass fractions.* Industrial & Engineering Chemistry Research, 2014. **53**(24): p. 10249-10255.

23.   N.N. Nguyen, A.V. Nguyen, K.T. Nguyen, L. Rintoul and L.X. Dang, *Unexpected inhibition of CO2 gas hydrate formation in dilute TBAB solutions and the critical role of interfacial water structure.* Fuel, 2016. **185**: p. 517-523.

24.   M.-Y. Li, M. Gao, Q.-R. Zuo, Y.-G. Zhao and L.-X. Zhang, *Experimental and theoretical investigation on hydrate nucleation in TBAB droplets.* Fuel, 2022. **308**: p. 121994.

25.   A. Rasoolzadeh, J. Javanmardi and A.H. Mohammadi, *An experimental study of the synergistic effects of BMIM-BF 4, BMIM-DCA and TEACl aqueous solutions on methane hydrate formation.* Petroleum Science, 2019. **16**: p. 409-416.

26.   Y. Kamata, Y. Yamakoshi, T. Ebinuma, H. Oyama, W. Shimada and H. Narita, *Hydrogen sulfide separation using tetra-n-butyl ammonium bromide semi-clathrate (TBAB) hydrate.* Energy & Fuels, 2005. **19**(4): p. 1717-1722.

27.   X. Zhang, H. Li and N. Maeda, *Nucleation curves of ice in quasi–free water droplets.* Chemical Engineering Science, 2021: p. 116751.

28.   N. Maeda, *Nucleation curves of model natural gas hydrates on a quasi -free water droplet.* AIChE Journal, 2015. **61**(8): p. 2611-2617.

29.   N. Maeda, *Nucleation curves of methane hydrate from constant cooling ramp methods.* Fuel, 2018. **223**: p. 286-293.

30.   M.M. Coulter, J.A. Dinglasan, J.B. Goh, S. Nair, D.J. Anderson and V.M. Dong, *Preparing water-dispersed palladium nanoparticles via polyelectrolyte nanoreactors.* Chemical Science, 2010. **1**(6): p. 772-775.

31.   R. Zheng, J. Tian, B.P. Binks, Z. Cui, W. Xia and J. Jiang, *Oil-in-Water emulsions stabilized by alumina nanoparticles with organic electrolytes: Fate of particles.* Journal of Colloid and Interface Science, 2022. **627**: p. 749-760.

32.   N. Maeda, *Nucleation of Gas Hydrates.* 2020, Springer: Cham, Switzerland.

33.   Y. Wang, A. Niu, W. Jiao, J. Chen, P. Zhang and J. Li, *Effects of the Presence of Promoters Sodium Dodecyl Sulfate, Nanographite, and Tetra-n-butylammonium Bromide on the Formation of CO2 Hydrates.* Energy & Fuels, 2022. **36**(17): p. 10269-10277.

34.   L. Wang, M. Dou, Y. Wang, Y. Xu, Y. Li, Y. Chen and L. Li, *A Review of the Effect of Porous Media on Gas Hydrate Formation.* ACS omega, 2022. **7**(38): p. 33666-33679.

35.   Z.-M. Xia, Z.-Y. Chen, X.-S. Li, Y. Zhang, K.-F. Yan, Q.-N. Lv, C.-G. Xu and J. Cai, *Thermodynamic equilibrium conditions for simulated landfill gas hydrate formation in aqueous solutions of additives.* Journal of Chemical & Engineering Data, 2012. **57**(11): p. 3290-3295.

36.   B. Vonnegut, *The nucleation of ice formation by silver iodide.* Journal of applied physics, 1947. **18**(7): p. 593-595.

37.   S.A. Zielke, A.K. Bertram and G.N. Patey, *A molecular mechanism of ice nucleation on model AgI surfaces.* The Journal of Physical Chemistry B, 2015. **119**(29): p. 9049-9055.

38.   P.A. O'day, G.A. Parks and G.E. Brown, *Molecular structure and binding sites of cobalt (II) surface complexes on kaolinite from X-ray absorption spectroscopy.* Clays and Clay Minerals, 1994. **42**: p. 337-355.

39.   O.G. Mouritsen and M.J. Zuckermann, *What's so special about cholesterol?* Lipids, 2004. **39**(11): p. 1101-1113.

CHAPTER 6 NUCLEATION CURVES OF ICE IN DILUTE SALT SOLUTIONS

A version of this chapter has been accepted for publication in *Energy & Fuels*.

Abstract

Electrolytes have been used as thermodynamic ice inhibitors since they can depress the melting point of ice by lowering the activity of water. However, the kinetic aspects of electrolytes on ice nucleation have been unclear. Here we report an experimental study of the nucleation rate of ice in quasi-free droplets of eight dilute monovalent salt solutions suspended at an interface between two immiscible liquids of perfluoromethyldecalin and squalane. The studied salts were sodium chloride (NaCl), potassium chloride (KCl), lithium chloride (LiCl), sodium bromide (NaBr), potassium bromide (KBr), lithium bromide (LiBr), sodium iodide (NaI) and potassium iodide (KI). The results showed that some monovalent salts increased the nucleation rate of ice at low supercoolings (high temperatures) and this increase was largely independent of the salt concentrations up to 100 mM. This finding is in marked contrast to the previous finding that the same combinations of the monovalent salts promoted the nucleation of methane – propane mixed gas hydrates, suggesting that fundamental difference may exist between the nucleation mechanisms of ice and clathrate hydrates.

6.1 Introduction

The nucleation of ice is the initial step of the ice formation, which has great impacts on the properties of clouds [1, 2] and the supercooled water on engineered and structured surfaces like aircraft wings [3, 4], bridge cables [5, 6] and wind turbines [7, 8]. In addition, the study of ice nucleation also has potential applications in mineralogy [9], petroleum engineering [10] and other fields [11]. In the oil and gas industry, studying of ice nucleation would be helpful for understanding the nucleation mechanism of gas hydrates [10]. For cloud seeding and other cases where ice formation is desired, we wish to be able to promote the nucleation of ice [12] while for the supercooled water on aircraft wings and airfoils [13] and cryopreservation of food or biological samples [14], we wish to be able to prevent the nucleation of ice.

Salts depress the melting point of ice by decreasing the activity of water and hence are thermodynamic inhibitors of ice [15], and the impacts of different types of salts on ice nucleation have been studied by both modelling and experimental methods for years [16-18]. For example, Espinosa et al. reported the nucleation rate of ice in NaCl solutions with a concentration of 1.85 M by simulation method. They found that salt could decelerate ice nucleation by increasing the liquid-ice interfacial free energy [19]. Soria et al. reported that their computational model captured the trend that the nucleation rate at a given supercooling decreased in the presence of salt [20]. Experimentally, Kanno and Angell investigated ice nucleation in emulsified solutions of alkali halides and reported that these salts could inhibit ice formation by depressing the melting point of ice [21]. Miyata et al. measured the ice nucleation temperatures of emulsified alkali halide solutions as a function of salt concentration and concluded that the nucleation temperature decreased with increasing ionic radius of the cations while it increased with increasing ionic radius of the anions [22]. Demott and Rogers applied a cloud chamber to observe the liquid cloud formation on soluble

cloud condensation nuclei (ammonium sulfate, ammonium bisulfate and sodium chloride) and reported the experimental nucleation rates [23]. Bauerecker et al. investigated the freezing process of salty water droplets freely suspended in an acoustic levitator and reported the kinetic antifreeze effect of the added salts in terms of delayed ice nucleation and also slow-down of the early stages of freezing, combining the results of both experimental and computational methods [16].

The experimental studies of ice nucleation in salt solutions have so far mainly concerned about high concentrations (1 M and higher) and only few studies reported the impact of dilute salt solutions (100 mM and lower) on ice nucleation. In addition, the studies on the nucleation rates in dilute salt solutions are even rarer. Purity of the salts is especially important in dilute salt solutions. Sowa et al. reported a systematic study of hydrate formation and ice formation in monovalent salt solutions in a glass sample cell over a broad range of concentrations (10^{-5} to 3 M) [24]. They found that most of the monovalent ions only had a weak promotion effect on ice formation for all concentrations they tested. However, they only reported the nucleation temperatures and not the nucleation rates. Whale et al. [25] investigated the effect of dilute salt solutions (0.015 M) on ice nucleation with different nucleators and reported that several ammonium salts could cause suspended nucleator particles (feldspars and quartz) to nucleate ice up to 3 °C warmer than they did in pure water. However, they didn't report the effect of dilute salt solutions on ice nucleation of pure water in the absence of any nucleators [25].

In this paper, we focused the study on monovalent salts since they have applications in climate engineering [26], biology [27], clay science [28], food science [29] and other fields. The nucleation rate of ice was investigated in quasi-free droplets of eight dilute monovalent salt solutions suspended at an interface between two immiscible liquids of perfluoromethyldecalin and squalane. The studied monovalent salts were sodium chloride (NaCl), potassium chloride (KCl), lithium

chloride (LiCl), sodium bromide (NaBr), potassium bromide (KBr), lithium bromide (LiBr), sodium iodide (NaI) and potassium iodide (KI).

6.2 Materials and Methods

6.2.1 Sample Preparation

The Milli-Q water (ultra-pure water of 18.2 MΩ resistivity from a Millipore unit) was used for the sample preparation. Sodium chloride (NaCl, 99.5% purity), sodium bromide (NaBr, 99% purity), sodium iodide (NaI, 99.5% purity), potassium chloride (KCl, 99% purity), potassium bromide (KBr, 99% purity), potassium iodide (KI, 99.5% purity), lithium chloride (LiCl, 99% purity) and lithium bromide (LiBr, 99% purity) were purchased from Sigma-Aldrich and purified by recrystallization of the salts from respective solutions prepared with Milli-Q water. In this study, the salt concentrations were less than 100 mM. The solutions of low concentrations were prepared by first preparing a stock solution of 1 M, then diluting the stock solution of 1 M to prepare a stock solution of 100 mM, which in turn was used to prepare another stock solution of 10 mM, etc.

Quasi-free droplets of salt solutions suspended between two immiscible liquids (shown in **Figure 6.1**) were used as the samples. About 50 µL of perfluoromethyldecalin, 50 µL of squalane and 60 mg of Milli-Q water or prepared solutions was added into each sample cell hole. Since perfluoromethyldecalin is denser than water and squalane is lighter than water, a droplet of dilute salt solution suspended between these two immiscible liquids. Salts are hardly soluble in squalane or perfluoromethyldecalin and we ignore their solubility in these supporting liquids. After the sample was placed to each hole, the sample cell was sealed by a glass slide using a vacuum grease (Dow Corning, High vacuum grease) at the rim.

6.2.2 Experimental Setup and Experimental Ramps

The details of the experimental methods and analytical methods were described in our earlier publications [30, 31]. The schematic illustration of the experimental setup is shown in **Figure 6.1**. Briefly, it consisted of a refrigerated circulator (FPW50-HE, Julabo Company, capable of cooling down to 223 K if required), a custom-made cuboid Teflon (polytetrafluoroethylene) sample cell, a webcam (Model C922, Logitech) and a PC (DELL). After the preparation of the samples, the sample cell was placed on a lab jack which was adjusted to the height that half of the cell was submerged in the coolant. Then a glass cover was placed on the top of the refrigerated circulator to prevent the evaporation of the coolant.

Similar to our earlier studies [30, 31], the linear cooling ramp method was used for the measurements of the nucleation rates of ice in salt solutions. For each cooling ramp, the sample cell was cooled rapidly from room temperature to 278 K (5 °C) and held for thermal equilibrium at 278 K for 15 minutes. After that, it was cooled linearly with a constant rate from 278 K (5 °C) to 228 K (-45 °C), until all the droplets were frozen. It is noted that 228 K was selected as the minimum temperature which is sufficiently low to ensure all the water droplets nucleate at the end of each cooling ramp. In order to compare with the results in our previous studies [30, 31], the same cooling rate of 0.003 K/s should be selected as the constant cooling rate in this study. Finally, the sample cell was warmed back to room temperature (around 293 K) within 10 min and held for 2 h to ensure all the water droplets melted. During the experimental ramps, a webcam controlled by software on a PC recorded the images of the sample cell every 1 min. Since there is always a difference between the real temperature in the sample cell and the temperature measured by the refrigerated circulator, the temperature calibrations were carried out beforehand. For the temperature calibration process, two thermometers (BIOS, Model#119) were inserted into

different positions of the Teflon sample cell. The temperatures of the various parts of the sample cell and those of the refrigerated circulator were recorded every 1 min. Similar to the experimental cooling ramp, the refrigerated circulator was programmed to cool from 278 K (5 °C) to 228 K (-45 °C) with a constant cooling rate of 0.003 K/s. A calibration table that related the temperatures in the Teflon sample cell to the temperatures of the coolant measured by the refrigerated circulator over the range of 278 K to 228 K was obtained. It is noted that the measurement accuracy of the refrigerated circulator and thermometer was 0.01 K and 0.1 K, respectively.
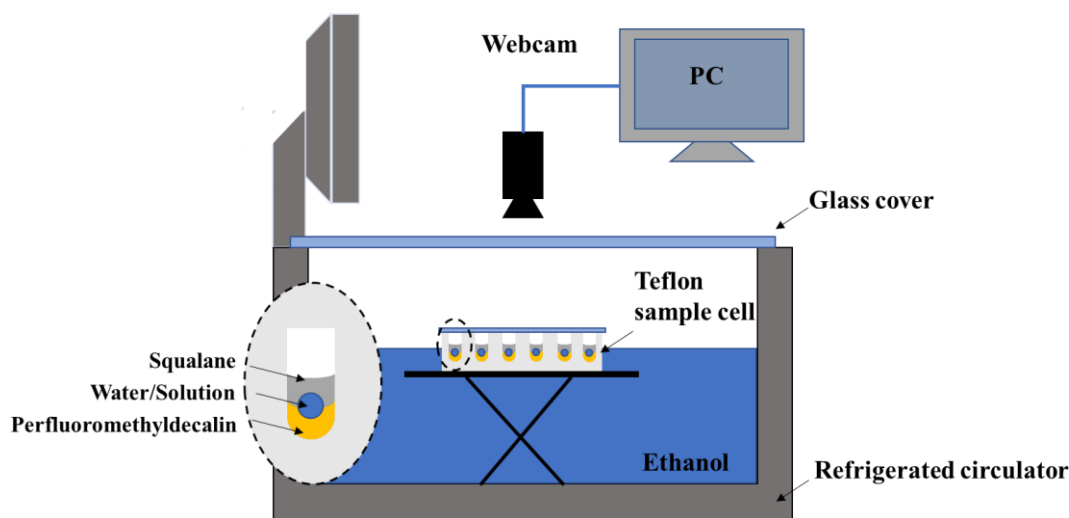
Figure 6.1. Schematic illustration of the experimental setup and the Teflon sample cell. Quasi-free water or salt solution droplets were suspended between two immiscible liquids of squalane and perfluoromethyldecalin in each sample cell hole. After that, the sample cell was sealed and directly placed on a lab jack, contacted with the coolant, ethanol.

6.2.3 Data Analysis

Sudden volume expansions due to freezing were used as the signal that ice nucleation had taken place. The freezing temperature (T_f) of each droplet was then obtained by applying the calibration table. Then we derived a nucleation curve by using the analytical method described in references [30, 32, 33] and the procedure was described briefly as below: (1) Constructing a survival

curve (survival probability, F, as a function of supercooling, ΔT), where $\Delta T = 273$ K - T_f and F was calculated from the number of unfrozen droplets divided by the total number of droplets at a given time. (2) Calculating ln$F$ with respect to lag time, t, where t was calculated from ΔT divided by the experimental cooling rate, 0.003 K/s. (3) Obtaining the slope of ln$F$ at each t by fitting an exponential function curve of the form $A \cdot \exp(Bt) + C$ to ln$F(t)$ and analytically differentiating the fitted curve. (4) Deriving the nucleation curve (nucleation rate as a function of supercooling, ΔT), where the nucleation rate was obtained by correcting each slope by a factor of -ln2.

6.3   Results

6.3.1   Nucleation Rates of Ice in Salt Solutions

For NaCl, the survival curve is shown in **Figure 6.3** (a), the corresponding natural logarithm of the survival probability is shown in **Figure 6.3** (b), and the corresponding nucleation curve is shown in **Figure 6.3** (c). For KCl, the result is shown in **Figure 6.4**. Similarly, the results of LiCl, NaBr, KBr, LiBr, NaI and KI are shown in **Figure 6.5**-**Figure 6.10**, respectively. The three fitting parameters of the exponential functions of the form $A \cdot \exp(Bt) + C$ are summarized in **Table 6.1**.

Table 6.1. Fitting parameters of the exponential function.

	A	B	C
NaCl	0.00087	0.00104	0.03186
KCl	0.00012	0.00117	0.29598
LiCl	0.00048	0.00099	0.07864
NaBr	0.00038	0.00103	0.26252
KBr	0.00002	0.00153	0.03005

LiBr	0.00106	0.00101	0.26514
NaI	0.00003	0.00145	0.17107
KI	0.00018	0.00117	0.13975

It is noted that the values of the fitting parameters reported in **Table 6.1** could be verified by simply plotting the experimental $\ln F(t)$ curve and the analytical $\ln F(t)$ curve and checking if the latter curve fit the former curve well. Take the results of LiCl as an example, the fitting parameters of the exponential function are reported as A=0.00048, B=0.00099 and C=0.07864. And the two $\ln F(t)$ curves are plotted in **Figure 6.2**. As shown in **Figure 6.2**, the analytical $\ln F(t)$ curve fitted perfectly with the experimental $\ln F(t)$ curve, which suggests that the values of the fitting parameters are reasonable.
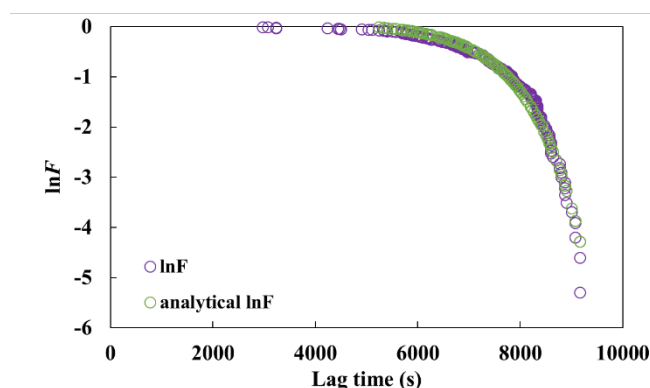
Figure 6.2. The experimental lnF(t) curve and analytical lnF(t) curve measured in quasi-free droplets of 1 mM LiCl solution. The lag time, t, was calculated from supercooling, ΔT, divided by the experimental cooling rate, 0.003 K/s. The analytical lnF(t) was in the form of A·exp(Bt) + C.

We also note that 200 data points were measured for each salt at a given concentration. As mentioned in our earlier publication, the nucleation curve hardly changed with the accumulation of additional data after the first few hundred data points [30].

154
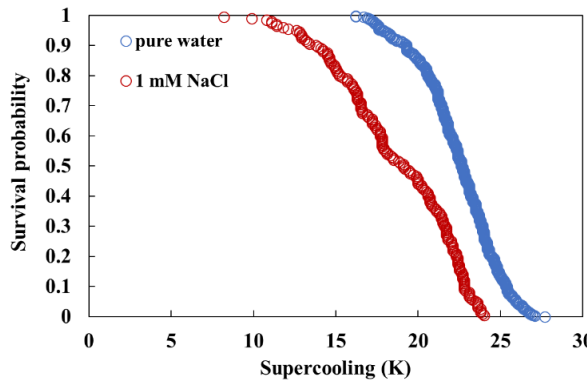
(a)
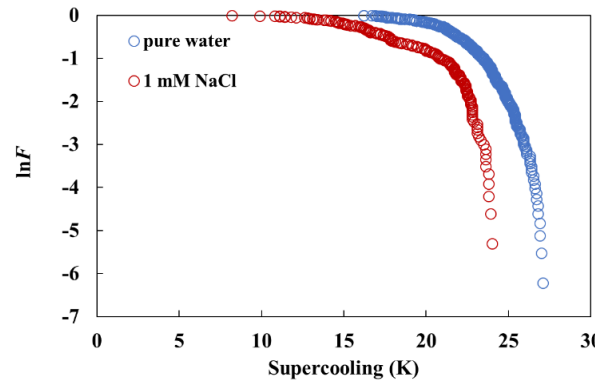
(b)
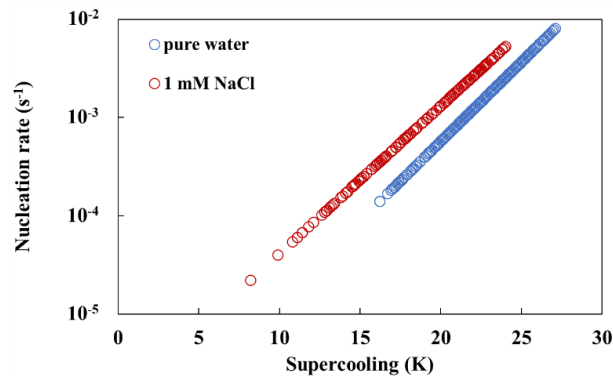
(c)

Figure 6.3. Survival curve (a), corresponding natural logarithm of the survival curve (b) and nucleation curve (c) measured in quasi-free droplets of NaCl solution suspended between two immiscible liquids of squalane and perfluoromethyldecalin. Cooling rate was 0.003 K/s. The concentration of the salt was 1 mM.
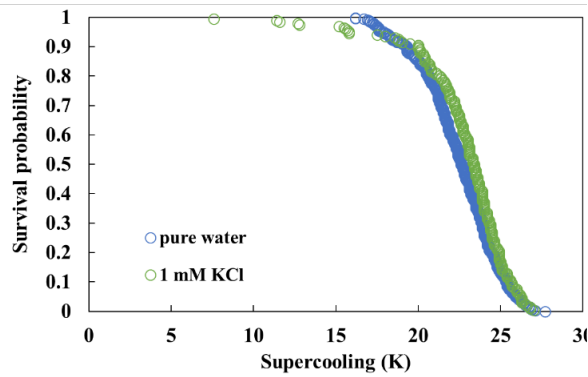
(a)
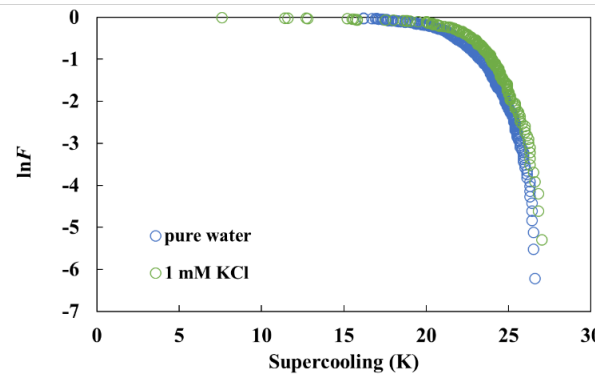
(b)
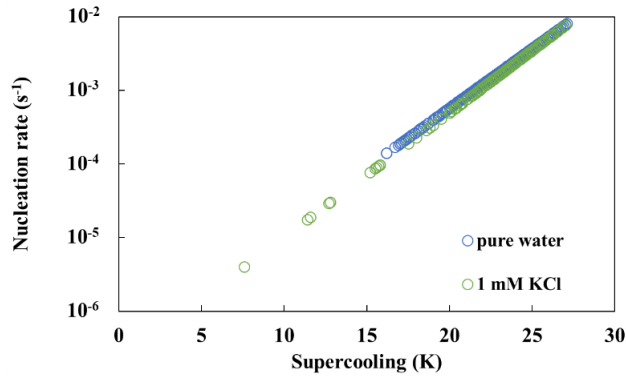
(c)

Figure 6.4. Survival curve (a), corresponding natural logarithm of the survival curve (b) and nucleation curve (c) measured in quasi-free droplets of KCl solution suspended between two immiscible liquids of squalane and perfluoromethyldecalin. Cooling rate was 0.003 K/s. The concentration of the salt was 1 mM.
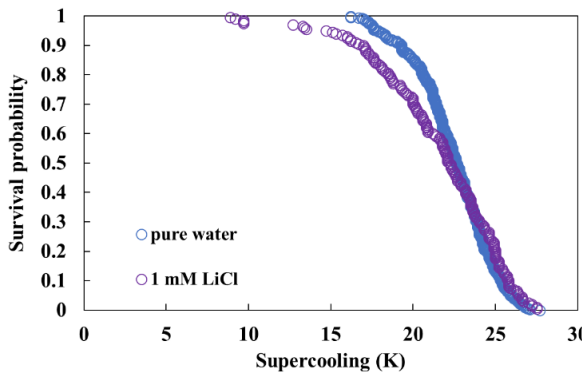
(a)
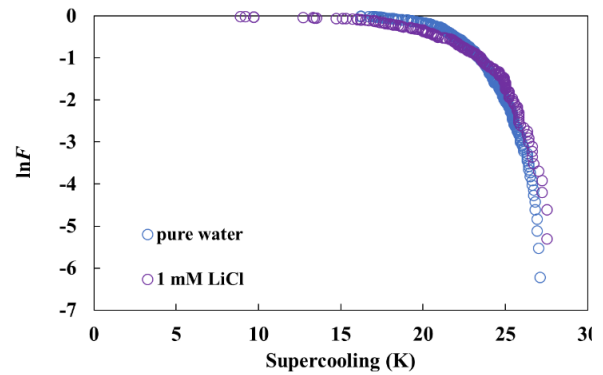
(b)
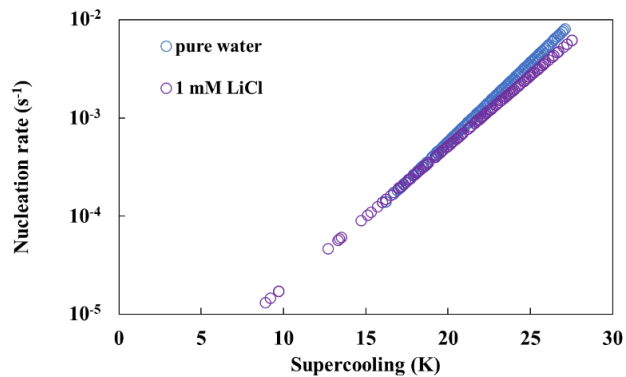
(c)

Figure 6.5. Survival curve (a), corresponding natural logarithm of the survival curve (b) and nucleation curve (c) measured in quasi-free droplets of LiCl solution suspended between two

immiscible liquids of squalane and perfluoromethyldecalin. Cooling rate was 0.003 K/s. The concentration of the salt was 1 mM.

(a)

(b)

(c)
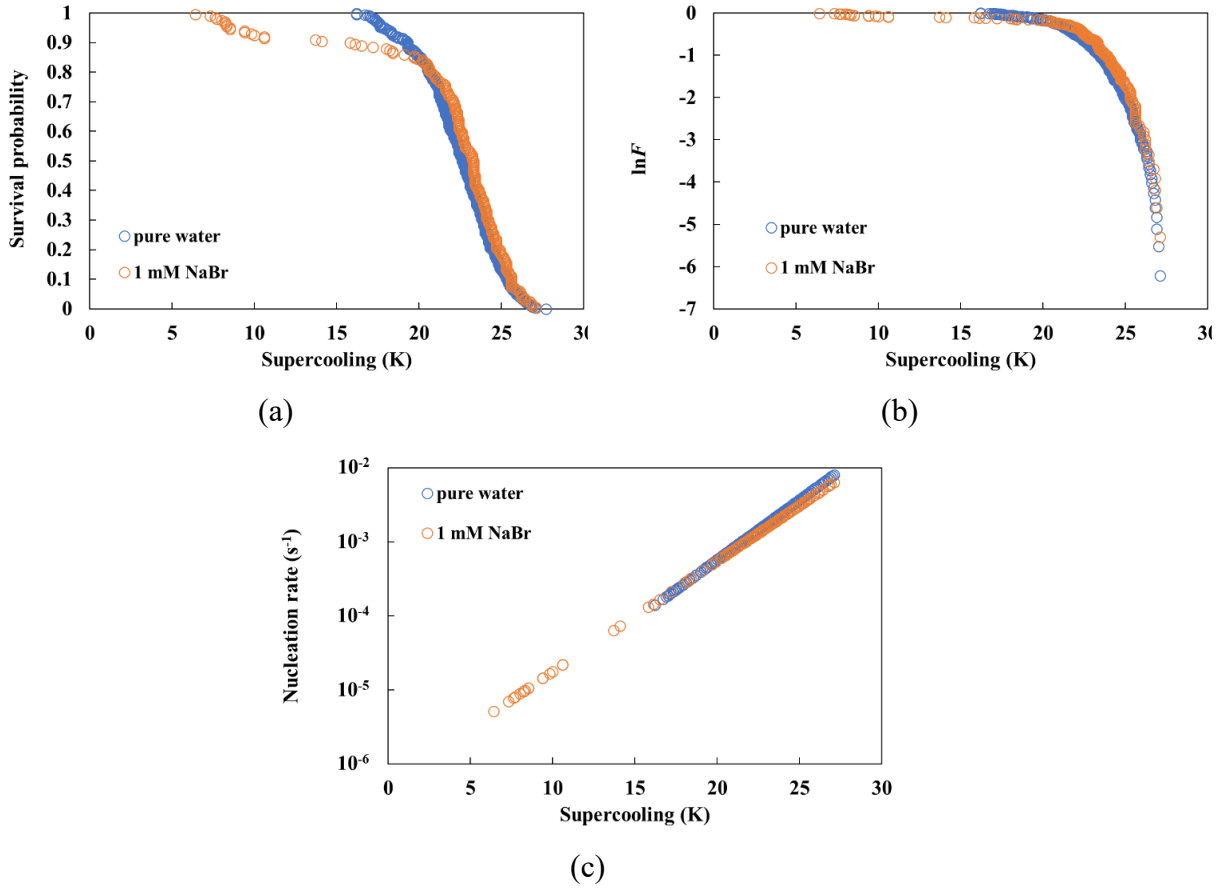
Figure 6.6. Survival curve (a), corresponding natural logarithm of the survival curve (b) and nucleation curve (c) measured in quasi-free droplets of NaBr solution suspended between two immiscible liquids of squalane and perfluoromethyldecalin. Cooling rate was 0.003 K/s. The concentration of the salt was 1 mM.
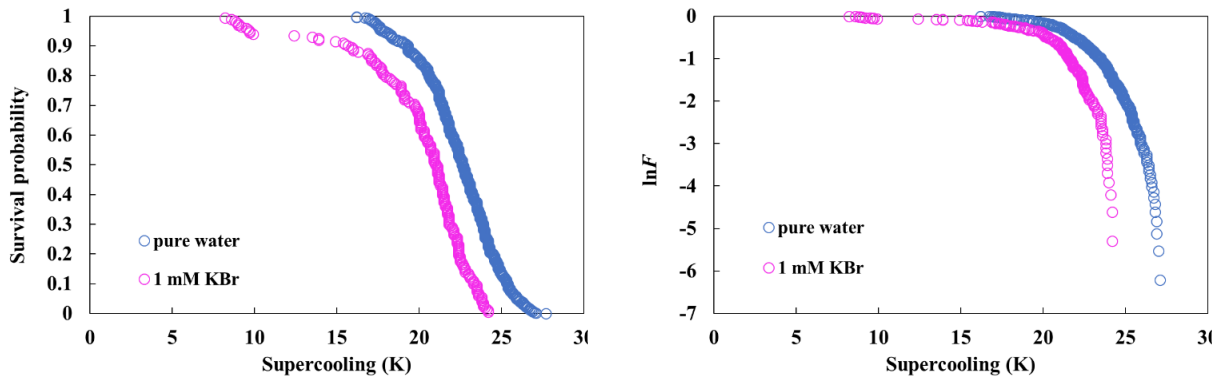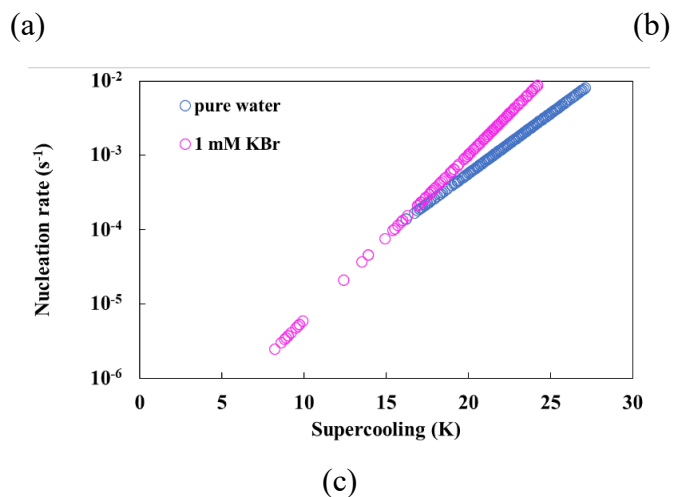
Figure 6.7. Survival curve (a), corresponding natural logarithm of the survival curve (b) and nucleation curve (c) measured in quasi-free droplets of KBr solution suspended between two immiscible liquids of squalane and perfluoromethyldecalin. Cooling rate was 0.003 K/s. The concentration of the salt was 1 mM.

(a)   (b)
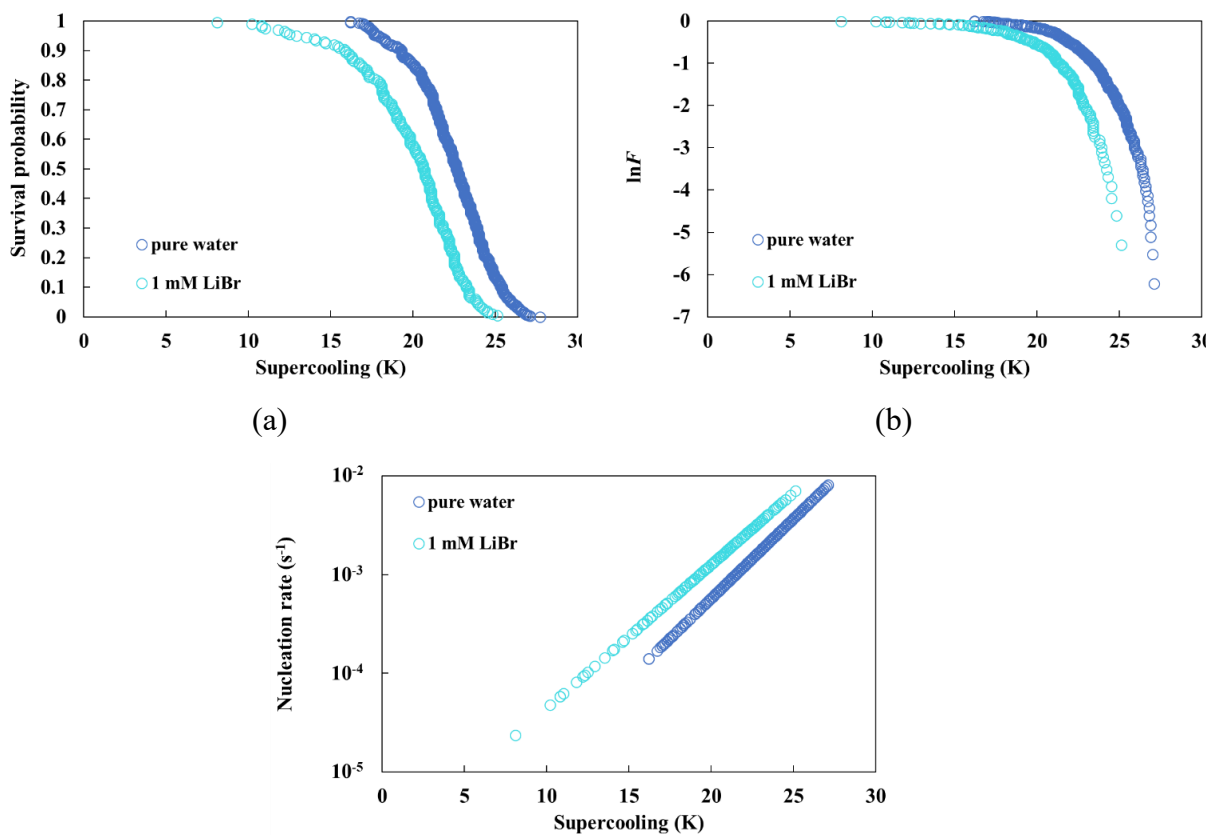
(c)

Figure 6.8. Survival curve (a), corresponding natural logarithm of the survival curve (b) and nucleation curve (c) measured in quasi-free droplets of LiBr solution suspended between two immiscible liquids of squalane and perfluoromethyldecalin. Cooling rate was 0.003 K/s. The concentration of the salt was 1 mM.
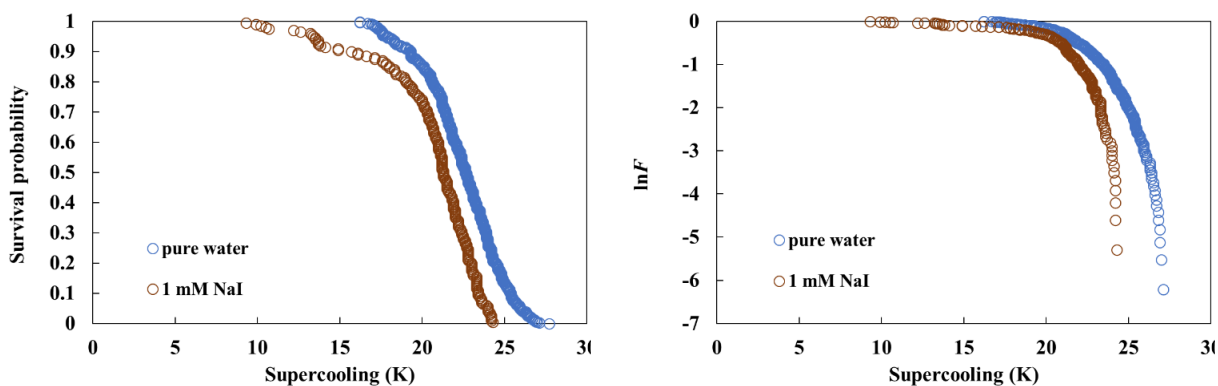
(a)

(b)
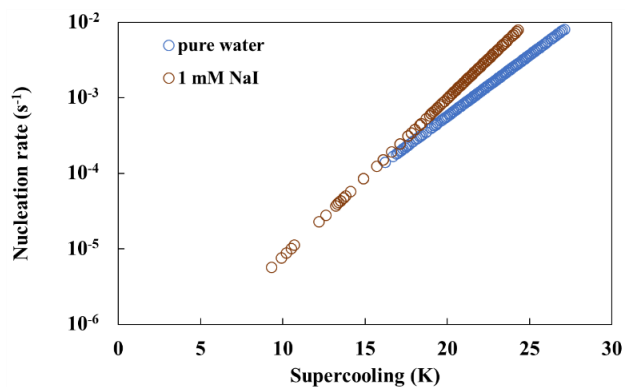
(c)

Figure 6.9. Survival curve (a), corresponding natural logarithm of the survival curve (b) and nucleation curve (c) measured in quasi-free droplets of NaI solution suspended between two immiscible liquids of squalane and perfluoromethyldecalin. Cooling rate was 0.003 K/s. The concentration of the salt was 1 mM.
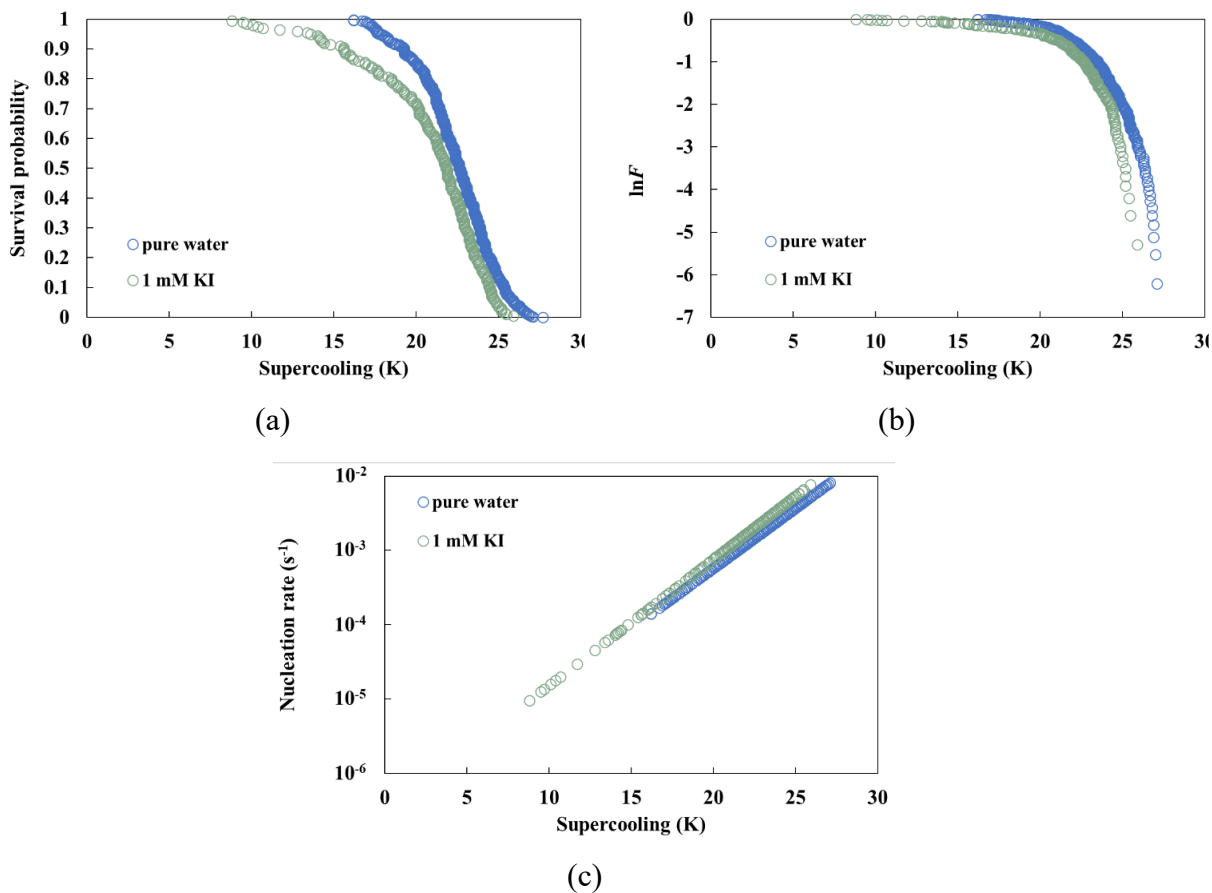
Figure 6.10. Survival curve (a), corresponding natural logarithm of the survival curve (b) and nucleation curve (c) measured in quasi-free droplets of KI solution suspended between two immiscible liquids of squalane and perfluoromethyldecalin. Cooling rate was 0.003 K/s. The concentration of the salt was 1 mM.

For NaCl, as shown in **Figure 6.3** (a), the survival curve was in the range of 8.2 to 24.2 K, which was lower than that of pure water (16.2 to 27.7 K). **Figure 6.3** (b) showed that the ln$F$ curve had slightly steeper slopes than that of pure water at a comparable supercooling range. As shown in **Figure 6.3** (c), the nucleation rate of ice in the presence of NaCl was slightly greater than that of pure water at a comparable supercooling (16 to 24 K), although the nucleation curve with NaCl somewhat reached the lower supercooling range. Similar to NaCl, the survival curve in the presence of salt LiBr was concentrated at the range of 8.1 to 25.2 K (shown in **Figure 6.8** (a)). **Figure 6.8** (b) showed that the ln$F$ curve with dilute LiBr solution also had slightly steeper slopes

than that of pure water at a comparable supercooling range (16 to 25 K). Despite the nucleation curve with LiBr solution (shown in **Figure 6.8** (c)) reached lower supercooling range, the nucleation rates were much less than one order of magnitude higher than that of pure water. It appeared that salts NaCl and LiBr had very weak to no promotion of nucleation of ice.

Figure 6.7 (a) and **Figure 6.9** (a) showed that the supercooling ranges of these two survival curves were 8.2 to 24.2 K for KBr and 9.3 to 24.8 K for NaI. The survival curves were concentrated at somewhat lower supercoolings (higher temperatures) than that of pure water. **Figure 6.7** (b) and **Figure 6.9** (b) showed that the ln$F$ curves of these two salts were overlapping with those of pure water at the supercooling range of 16 to 20 K and had steeper slopes when supercooling was larger than 20 K. **Figure 6.7** (c) and **Figure 6.9** (c) showed that the nucleation curves in the presence of KBr and NaI crossed the nucleation curve of pure water at the point of 20 K, and the nucleation rates of these two salts were slightly greater than those of pure water when the supercooling was greater than 20 K. Since the gap in nucleation rates between these two salts and pure water was much less than 1 order of magnitude, KBr and NaI hardly made any difference to the nucleation rates of ice.

As shown in **Figure 6.4** (a), **Figure 6.5** (a), **Figure 6.6** (a) and **Figure 6.10** (a), the survival curves of KCl, LiCl, NaBr and KI were in the range of 7.6 to 27.1 K, 8.9 to 29.7 K, 6.4 to 27.2 K and 8.8 to 25.9 K, respectively. The lower ends of the survival curves of all four salts were at smaller supercoolings than those of pure water, whereas the higher ends were similar to those of pure water. **Figure 6.4** (b), **Figure 6.5** (b), **Figure 6.6** (b) and **Figure 6.10** (b) showed that the ln$F$ curves of these four salts were similar to those of pure water. The nucleation curves of ice in the presence of these four salts shown in **Figure 6.4** (c), **Figure 6.5** (c), **Figure 6.6** (c) and **Figure 6.10** (c) were almost overlapping with those of pure water at a comparable supercooling range.

These results showed that the salts KCl, LiCl, NaBr and KI could somehow induce freezing of ice at higher temperatures (lower supercoolings) but barely influence the nucleation rate of ice.

All in all, none of the eight salts investigated inhibited the nucleation of ice at 1 mM. All diluted salt solutions seemed to promote ice formation at a lower supercooling range, and some salts slightly increased the nucleation rate of ice at low supercoolings. This finding is in marked contrast to the previous finding that the same combinations of the monovalent salts promoted the nucleation of methane – propane mixed gas hydrates, suggesting that fundamental difference may exist between the nucleation mechanisms of ice and clathrate hydrates.

6.3.2 Concentration Dependence

Our results showed that all eight salts we investigated hardly influence the nucleation of ice at 1 mM. Then one of the related questions is whether increasing the salt concentrations will eventually thermodynamically inhibit ice nucleation. Sowa et al. [24] investigated the matter up to salt concentrations of 3 M and found, perhaps as expected, that these salts indeed strongly inhibited nucleation of ice when concentrations were larger than 1 M, except for LiBr. We note that Sowa et al. [24] used a glass sample cell (without suspending a water droplet), unlike in the current study. We expect qualitatively similar results that the salts will strongly inhibit ice nucleation in suspended droplets when the concentrations of the salt solutions are larger than 1 M; however, given the generally deeper supercoolings required for ice nucleation in suspended droplets compared to that in water contained in a glass sample cell, we expect the required supercoolings to approach the cooling power of our instrument.

To examine the ice formation in dilute salt solutions (concentration smaller than 1 M), we investigated the nucleation rate of ice in chloride salt solutions of two different concentrations (100

162

mM and 1 mM). The results are shown in **Figure 6.11**-**Figure 6.13**. We again collected 200 data points for the determination of each nucleation curve.

(a)

(b)

(c)
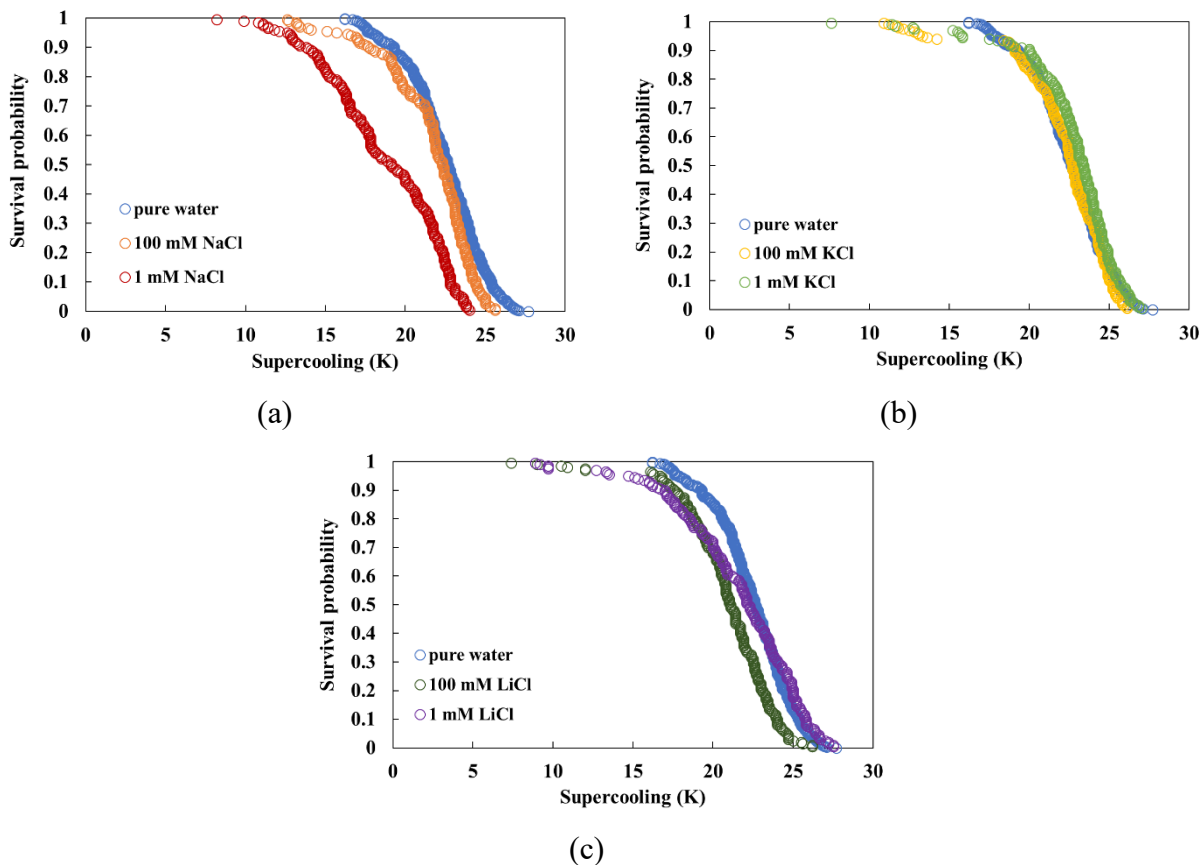
Figure 6.11. Survival curves measured in quasi-free droplets of chloride salt solutions (NaCl (a), KCl (b) and LiCl (c)) of different concentrations suspended between two immiscible liquids of squalane and perfluoromethyldecalin. Cooling rate was 0.003 K/s.

(c)
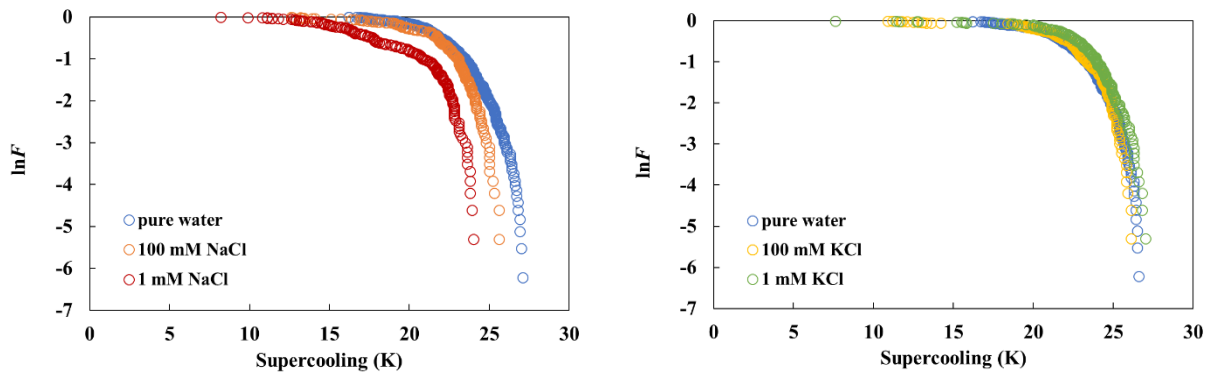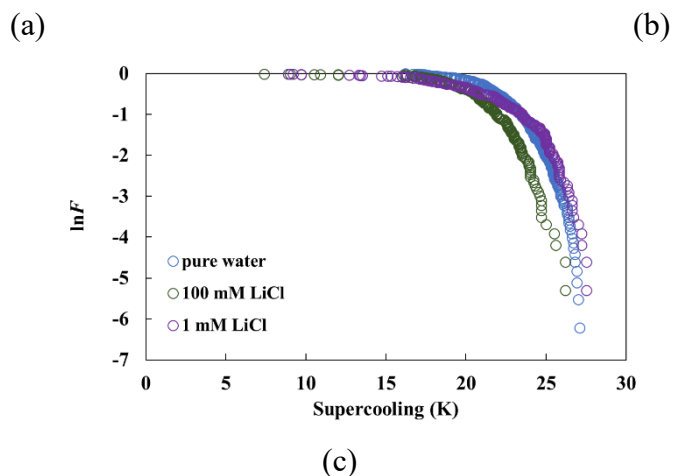
Figure 6.12. Natural logarithms of the survival curves (lnF vs ΔT) of ice measured in quasi-free droplets of chloride salt solutions (NaCl (a), KCl (b) and LiCl (c)) of different concentrations suspended between two immiscible liquids of squalane and perfluoromethyldecalin. Cooling rate was 0.003 K/s.

(a)   (b)
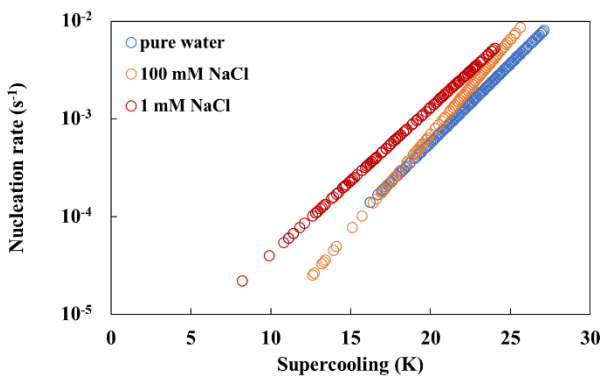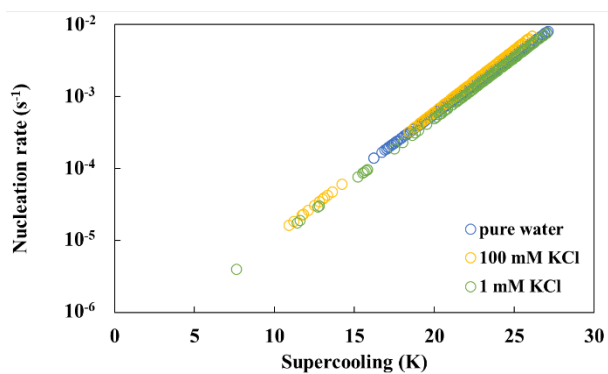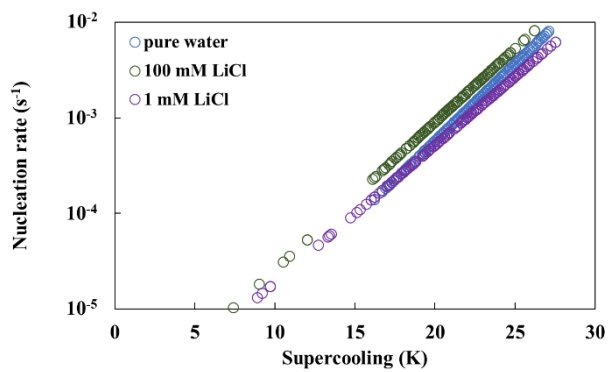
Figure 6.13. Nucleation curves of ice in quasi-free droplets of chloride salt solutions (NaCl (a), KCl (b) and LiCl (c)) of different concentrations suspended between two immiscible liquids of squalane and perfluoromethyldecalin. Cooling rate was 0.003 K/s.

For NaCl, as shown in **Figure 6.11** (a), the survival curve measured in 100 mM solution was concentrated over the range of 12.6 to 25.9 K, which was somewhat lower than that of pure water (16.2 to 27.7 K) but higher than that of 1 mM solution (8.2 to 24.2 K). The survival curves measured in pure water and in 100 mM solution were almost overlapping with each other. **Figure 6.12** (a) shows that the ln$F$ curve measured in a 100 mM solution was close to that measured in pure water at a comparable supercooling range but had slightly less steep slopes than that of a 1 mM solution. The nucleation curves (shown in **Figure 6.13** (a)) measured in dilute NaCl solutions with two different concentrations were similar with those of the pure water since the difference of the nucleation rates was much less than 1 order of magnitude at the same supercooling although the nucleation curves measured in the presence of NaCl reached lower supercooling ranges.

For KCl, **Figure 6.11** (b) showed that the survival curves measured in dilute solutions were in the supercooling ranges of 10.9 to 26.7 K and 8.9 to 29.7 K for 100 mM and 1 mM, respectively. The lower ends of the survival curves of KCl solutions were at smaller supercoolings than those of pure water, whereas the higher ends were similar to those of pure water. And the three survival curves were almost overlapping with each other in a comparable supercooling range (around 16 to 27 K). **Figure 6.12** (b) shows that the ln$F$ curves measured in KCl solutions with two different concentrations were similar to that of the pure water. And the nucleation curves (shown in **Figure 6.13** (b)) measured in KCl solutions and in pure water were almost overlapping with each other, which indicated that the dilute KCl solutions (less than 100 mM) had no effect on the nucleation of ice.

Similar to KCl, the survival curves (shown in **Figure 6.11** (c)) measured in LiCl solutions with two different concentrations were close to those of the pure water. **Figure 6.12** (c) and **Figure 6.13** (c) show that the ln$F$ curves and nucleation curves of dilute LiCl solutions were almost overlapping with the curves measured in pure water.

To be concluded, the nucleation rate of ice was independent of the salt concentration when the concentrations were 100 mM or lower. These three salts hardly had an influence on the nucleation rate of ice when the concentration of the solution was less than 100 mM.

6.4   Discussion

6.4.1   Effect of Monovalent Ions on Ice Nucleation

Since some of the monovalent salts share some similarities and differences (e.g., NaCl, NaBr and NaI have the same cation Na^+ but with different anions), it is interesting to compare and discuss the effect of monovalent ions on ice nucleation. To discuss the effect of cations, we compared the survival curves and nucleation curves measured in NaCl, KCl and LiCl solutions. And the results are shown in **Figure 6.14**. Similarly, we compared the survival curves and nucleation curves measured in NaCl, NaBr and NaI solutions (shown in **Figure 6.15**) to discuss the effect of anions on ice nucleation.
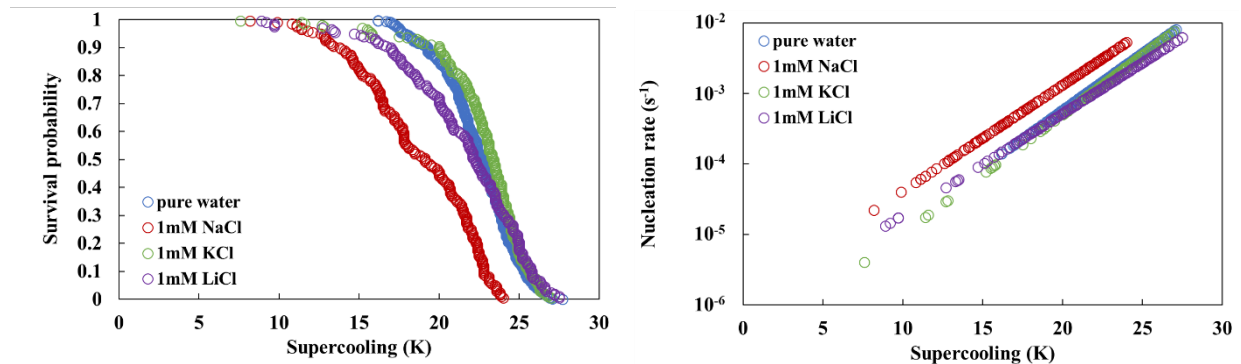
Figure 6.14. Survival curves (a) and nucleation curves (b) measured in three different chloride salt solutions. The cooling rate is 0.003 K/s and salt concentration is 1mM.

(a)

(b)
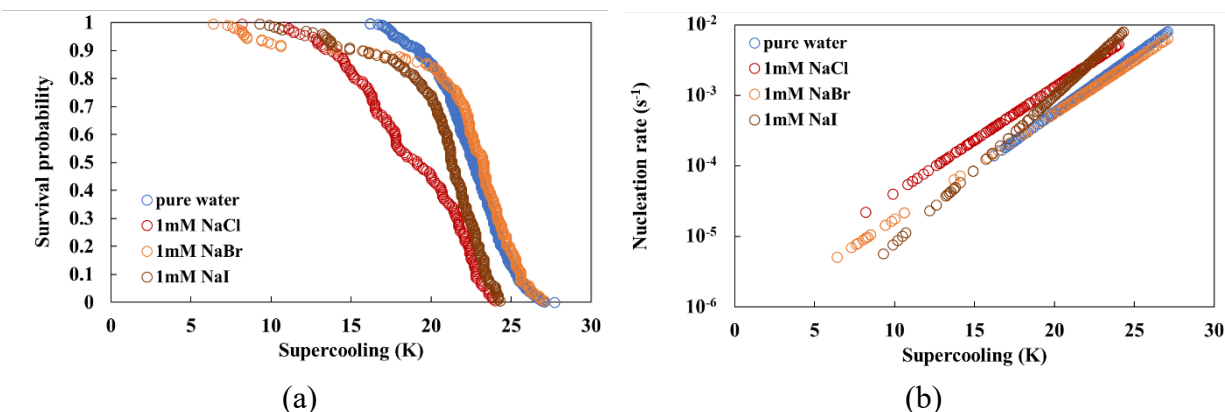
Figure 6.15. Survival curves (a) and nucleation curves (b) measured in three different sodium salt solutions. The cooling rate is 0.003 K/s and salt concentration is 1mM.

As for the impact of cations, as shown in **Figure 6.14** (a), the survival curve measured in NaCl solution was concentrated at the lowest supercooling range (highest temperature range) among these three chloride salts, while the supercooling range measured in LiCl solution was slightly lower than that of pure water. And the survival curve measured in KCl solution was almost overlapping with that of pure water. **Figure 6.14** (b) shows the nucleation curves of KCl and LiCl were almost overlapping with those of pure water, while the nucleation rate measured in NaCl solution was slightly higher than that of pure water at the same supercooling. Therefore, we could conclude that although these three chloride salts hardly influence the nucleation rates of ice, they could somewhat promote ice to nucleate at a lower supercooling range (higher temperature range). And the impact of cations could be ranked as $Na^+ > Li^+ > K^+$.

As for the impact of anions, **Figure 6.15** (a) shows that the survival curves were concentrated from low to high supercooling ranges in the sequence of NaCl, NaI and NaBr. As

shown in **Figure 6.15** (b), the nucleation curve measured in NaBr solution was almost overlapping with that of pure water. And the nucleation rates measured in NaCl and NaI solutions were slightly higher than those of pure water at a comparable supercooling range (16 to 23 K). Similar to the comparison of cations, the impact of anions on supercooling degree of ice nucleation could be ranked as $Cl^- > I^- > Br^-$.

6.4.2 Comparison with the Literature Data

Few people reported the nucleation rate of ice in diluted salt solutions. Sowa et al. measured the survival curves with respect to ice formation in monovalent salt solutions and reported the most probable supercooling over a broad range of concentrations [24]. Since Sowa et al. did not report the nucleation rates, we here only compare the most probable supercooling of different salt solutions at a concentration of 1 mM, and the results are summarized in **Table 6.2**. The most probable supercooling in our study was chosen as the supercooling that corresponded to the survival probability of 50%, and Sowa et al.'s results were obtained from the Figure 5 in ref. [24].

Table 6.2. Comparison of the most probable supercooling values with Sowa et al.'s results.

	Sowa et al.'s results	Our results
Pure water	14 K	22.6 K
NaCl	6 K	19.1 K
KCl	12 K	23.4 K
LiCl	13 K	22.2 K
NaBr	8 K	23.3 K
KBr	14 K	21.0 K

LiBr	14 K	20.6 K
NaI	14.5 K	21.3 K
KI	14.5 K	21.8 K

Sowa et al. [24] used 200 µL of a salt solution in a glass tube, whereas we used 60 µL of quasi-free droplets. It is thus expected that the supercooling values in Sowa et al. results would be smaller than ours because both a larger volume and the presence of a solid wall would increase the nucleation rate of ice. According to the probability distribution and the most probable supercooling, Sowa et al. qualitatively concluded from their results that the dilute monovalent salt solutions had a very weak to no promotion of ice nucleation. Since our results showed that all dilute monovalent salt solutions had negligible effects on ice nucleation when concentrations were less than 100 mM, either from the most probable supercoolings shown in **Table 6.2** or from the nucleation rates quantified in the RESULTS part, it appeared that our results were in agreement with Sowa et al.'s results. It is noted that Sowa used a much faster cooling rate (0.05 K/s) than that of our experiments (0.003 K/s). They reported the width of the probability were around 3 to 4 K for KI and LiI salt solutions and 1 to 2 K for other salt solutions when concentration was 1 mM, which was much narrower than our results (around 20 K for KCl, LiCl and NaBr salt solutions and 15.5 to 17 K for other salt solutions at the same concentration of 1 mM). However, it is unclear as to whether this finding was a result of the use of a fast cooling rate that compressed the survival curves or not.

Miyata et al. [22] investigated the ice nucleation temperatures of aqueous alkali halide solutions as a function of salt concentration (0.5 - 5 mol/kg). They reported that the cationic effect on nucleation temperature increased with the decreasing ionic radius, while the anionic effect increased with the increasing ionic radius [22]. Since they did not report the nucleation rates and their

study was entirely over the high concentration range (0.5-5 mol/kg), their nucleation data would not be directly comparable to our results. Qualitatively, we found that all salt solutions made little difference to the nucleation rate of ice at a concentration of 1 mM, then neither the type of cations nor anions impact the nucleation rate. The results are in agreement with Sowa et al.'s results and are different from Miyata et al.'s results. We may consider there are two causes for the differences: (1) Miyata et al. [22] did not derive the nucleation rates and the ionic effects could be different if the nucleation rates were used as the measure of comparisons; and (2) according to Fig. 1 and Fig. 3 in reference [22], the difference in the nucleation temperatures among the different cations or anions decreased with the concentration. At the concentration of 1 mol/kg, the nucleation temperatures of different cations or anions were quite similar. Then it is reasonable to speculate that the cationic effect or the anionic effect would become insignificant as there were diluted to the low concentrations of our range (1 mM or lower) because the effect of the electrostatic forces caused by the cations, the viscosity effect and the disruptive action of the halide ions on the water structure, which were considered to be the leading mechanisms behind the ionic effects in the reference [22], would be weak at such low concentrations.

6.4.3 Nucleation Mechanisms of Ice and Clathrate Hydrates in Salt Solutions

It is interesting that Sowa et al. [24] reported that all dilute monovalent salt solutions had almost no effect on the nucleation of ice, which is in agreement with our findings, but some of the monovalent salts acted as kinetic promoters for the nucleation of methane-propane mixed (C1/C3) gas hydrates formation at similarly low concentrations, which suggested that a fundamental difference may exist between the nucleation mechanisms of ice and clathrate hydrates.

One potential reason might be that the nucleation of ice could be either surface nucleation or bulk nucleation [12], whereas the nucleation of hydrates occurs at the water – guest gas interface. Due to the low solubility of non-polar gases (e.g., methane, propane, etc.) in water and the mass transfer limitation, the nucleation of hydrates occurs at the gas-water interface, which has the highest concentrations of the guest gases [34, 35]. The solubility of such non-polar gases would be reduced in the presence of salts due to the salting-out effect [24]. It has been known that different types of salts or ions distribute at different distances from a gas – aqueous interface since they have different affinity to the interface, which is known as ion specificity or ion surface propensity [36]. Such local reductions of the guest gas solubility in the aqueous phase would in turn impact the nucleation rate of clathrate hydrates. Simply put, the salt or ion that has a high affinity to the gas – aqueous interface (that positively adsorb in accordance with the Gibbs adsorption isotherm) would reduce the local solubility of the guest gas where the nucleation of clathrate hydrate takes place, whereas the salt or ion that has a poor affinity to the gas – aqueous interface (that negatively adsorb in accordance with the Gibbs adsorption isotherm) would not impact the local solubility of the guest gas where the nucleation of clathrate hydrate takes place (the nucleation rate of the clathrate hydrate would remain similar to that of pure water).

Sowa et al. reported that dilute iodide salt solutions could promote the nucleation of C1/C3 hydrates by about 2 to 4 K compared to that of pure water [24]. One possible reason is that the ions might help re-orientating the water molecules around them, and if such orientations of the water molecules happen to resemble the structure of the clathrate hydrates, then the presence of such ions may promote the nucleation of clathrate hydrates (despite being thermodynamically inhibitive). It is noted that Sowa et al. only reported the most probable supercoolings of the

nucleation of either ice or clathrate hydrates and did not go so far as to quantify the nucleation rates of clathrate hydrates in these dilute monovalent salt solutions.

6.5   Conclusions

We used the quasi-free droplet system for investigating the impact of diluted salt solutions (100 mM or lower) on ice nucleation. The results showed that the dilute monovalent salts had negligible influence on the nucleation rates of ice. And the nucleation rate of ice was independent of the concentration when the concentrations were 100 mM or lower. Our results are in agreement with Sowa et al.'s results, reporting a very weak to no promotion of _ice_ nucleation in dilute monovalent salt solutions, and are in marked contrast to the previous finding that the same combinations of the monovalent salts promoted the nucleation of methane – propane mixed gas hydrates, suggesting that fundamental difference may exist between the nucleation mechanisms of ice and clathrate hydrates.

6.6   References

1.   Murray, B.; O'sullivan, D.; Atkinson, J.; Webb, M., Ice nucleation by particles immersed in supercooled cloud droplets. *Chemical Society Reviews* **2012,** *41* (19), 6519-6554.

2.   Hoose, C.; Möhler, O., Heterogeneous ice nucleation on atmospheric aerosols: a review of results from laboratory experiments. *Atmospheric Chemistry and Physics* **2012,** *12* (20), 9817-9854.

3.   Lynch, F. T.; Khodadoust, A., Effects of ice accretions on aircraft aerodynamics. *Progress in Aerospace Sciences* **2001,** *37* (8), 669-767.

4.	Schrod, J.; Weber, D.; Drücke, J.; Keleshis, C.; Pikridas, M.; Ebert, M.; Cvetković, B.; Nickovic, S.; Marinou, E.; Baars, H., Ice nucleating particles over the Eastern Mediterranean measured by unmanned aircraft systems. *Atmospheric Chemistry and Physics* **2017,** *17* (7), 4817-4835.

5.	Demartino, C.; Koss, H. H.; Georgakis, C. T.; Ricciardelli, F., Effects of ice accretion on the aerodynamics of bridge cables. *Journal of Wind Engineering and Industrial Aerodynamics* **2015,** *138*, 98-119.

6.	Brassard, J.-D.; Blackburn, C.; Toth, M.; Momen, G., Ice accretion, shedding, and melting on cable-stayed bridges: A laboratory performance assessment. *Cold Regions Science and Technology* **2022,** *204*, 103672.

7.	Saleh, S.; Ahshan, R.; Moloney, C., Wavelet-based signal processing method for detecting ice accretion on wind turbines. *IEEE Transactions on Sustainable Energy* **2012,** *3* (3), 585-597.

8.	Dalili, N.; Edrisy, A.; Carriveau, R., A review of surface engineering issues critical to wind turbine performance. *Renewable and Sustainable energy reviews* **2009,** *13* (2), 428-438.

9.	Tollefsen, E.; Stockmann, G.; Skelton, A.; Mörth, C.-M.; Dupraz, C.; Sturkell, E., Chemical controls on ikaite formationELIN TOLLEFSEN ET AL. CHEMICAL CONTROLS ON IKAITE FORMATION. *Mineralogical Magazine* **2018,** *82* (5), 1119-1129.

10.	Liang, S.; Hall, K. W.; Laaksonen, A.; Zhang, Z.; Kusalik, P. G., Characterizing key features in the formation of ice and gas hydrate systems. *Philosophical Transactions of the Royal Society A* **2019,** *377* (2146), 20180167.

11. Kelton, K.; Greer, A. L., *Nucleation in condensed matter: applications in materials and biology*. Elsevier: 2010.

12. Maeda, N., Brief Overview of Ice Nucleation. *molecules* **2021,** *26* (392).

13. Özgen, S.; Canıbek, M., Ice accretion simulation on multi-element airfoils using extended Messinger model. *Heat and Mass Transfer* **2009,** *45* (3), 305.

14. Morris, G. J.; Acton, E., Controlled ice nucleation in cryopreservation–a review. *Cryobiology* **2013,** *66* (2), 85-92.

15. Koop, T.; Luo, B.; Tsias, A.; Peter, T., Water activity as the determinant for homogeneous ice nucleation in aqueous solutions. *Nature* **2000,** *406* (6796), 611-614.

16. Bauerecker, S.; Ulbig, P.; Buch, V.; Vrbka, L.; Jungwirth, P., Monitoring ice nucleation in pure and salty water via high-speed imaging and computer simulations. *The Journal of Physical Chemistry C* **2008,** *112* (20), 7631-7636.

17. Diehl, K.; Wurzler, S., Heterogeneous drop freezing in the immersion mode: Model calculations considering soluble and insoluble particles in the drops. *Journal of the atmospheric sciences* **2004,** *61* (16), 2063-2072.

18. Chelf, J. H.; Martin, S. T., Homogeneous ice nucleation in aqueous ammonium sulfate aerosol particles. *Journal of Geophysical Research: Atmospheres* **2001,** *106* (D1), 1215-1226.

19. Espinosa, J. R.; Soria, G. D.; Ramirez, J.; Valeriani, C.; Vega, C.; Sanz, E., Role of salt, pressure, and water activity on homogeneous ice nucleation. *The Journal of Physical Chemistry Letters* **2017,** *8* (18), 4486-4491.

20.   Soria, G. D.; Espinosa, J. R.; Ramirez, J.; Valeriani, C.; Vega, C.; Sanz, E., A simulation study of homogeneous ice nucleation in supercooled salty water. *The Journal of chemical physics* **2018,** *148* (22), 222811.

21.   Kanno, H.; Angell, C., Homogeneous nucleation and glass formation in aqueous alkali halide solutions at high pressures. *The Journal of Physical Chemistry* **1977,** *81* (26), 2639-2643.

22.   Miyata, K.; Kanno, H.; Niino, T.; Tomizawa, K., Cationic and anionic effects on the homogeneous nucleation of ice in aqueous alkali halide solutions. *Chemical physics letters* **2002,** *354* (1-2), 51-55.

23.   DeMott, P. J.; Rogers, D. C., Freezing nucleation rates of dilute solution droplets measured between− 30 and− 40 C in laboratory simulations of natural clouds. *Journal of the atmospheric sciences* **1990,** *47* (9), 1056-1064.

24.   Sowa, B.; Zhang, X. H.; Hartley, P. G.; Dunstan, D. E.; Kozielski, K. A.; Maeda, N., Formation of ice, tetrahydrofuran hydrate, and methane/propane mixed gas hydrates in strong monovalent salt solutions. *Energy & fuels* **2014,** *28* (11), 6877-6888.

25.   Whale, T. F.; Holden, M. A.; Wilson, T. W.; O'Sullivan, D.; Murray, B. J., The enhancement and suppression of immersion mode heterogeneous ice-nucleation by solutes. *Chemical science* **2018,** *9* (17), 4142-4151.

26.   Olson, S.; Jansen, M. F.; Abbot, D. S.; Halevy, I.; Goldblatt, C., The effect of ocean salinity on climate and its implications for Earth's habitability. *Geophysical research letters* **2022,** *49* (10), e2021GL095748.

27. Ahmed, M. Z.; Parveen, F.; Gulzar, S.; Gul, B.; Khan, M. A., Effects of chloride and sulfate salts on seed germination of halophytes from dry alpine climate. *Journal of Plant Nutrition* **2020,** *43* (15), 2299-2310.

28. Ismail, A.; El-Shamy, A., Engineering behaviour of soil materials on the corrosion of mild steel. *Applied clay science* **2009,** *42* (3-4), 356-362.

29. Albarracín, W.; Sánchez, I. C.; Grau, R.; Barat, J. M., Salt in food processing; usage and reduction: a review. *International Journal of Food Science & Technology* **2011,** *46* (7), 1329-1336.

30. Zhang, X.; Li, H.; Maeda, N., Nucleation curves of ice in quasi–free water droplets. *Chemical Engineering Science* **2021**, 116751.

31. Zhang, X.; Maeda, N., Nucleation curves of ice in the presence of nucleation promoters. *Chemical Engineering Science* **2022,** *262*, 118017.

32. Maeda, N., Nucleation curves of model natural gas hydrates on a quasi-free water droplet. *AIChE Journal* **2015,** *61* (8), 2611-2617.

33. Maeda, N., Nucleation curves of methane hydrate from constant cooling ramp methods. *Fuel* **2018,** *223*, 286-293.

34. Maeda, N.; Wells, D.; Hartley, P. G.; Kozielski, K. A., Statistical analysis of supercooling in fuel gas hydrate systems. *Energy & fuels* **2012,** *26* (3), 1820-1827.

35. Sloan Jr, E. D.; Koh, C. A., *Clathrate hydrates of natural gases*. CRC press: 2007.

36. Craig, V. S.; Henry, C. L., Specific ion effects at the air–water interface: Experimental studies. In *Specific Ion Effects*, World Scientific: 2010; pp 191-214.

CHAPTER 7 NUCLEATION OF CO₂ HYDRATE IN QUASI – FREE DROPLETS OF DILUTE ELECTROLYTES

A version of this chapter has been submitted to *Energy & Fuels* and currently under peer-review.

Abstract

Salts are known to be thermodynamic inhibitors for gas hydrates at high concentrations by lowering the activity of water and shifting the phase boundary of gas hydrates to lower temperatures and higher pressures. However, some salts have been reported to kinetically promote the formation of gas hydrate at low concentrations. Studies on kinetic promotions of clathrate hydrate formation in dilute salt solutions are rare and the mechanisms are poorly understood. The impact of solid walls on heterogeneous nucleation of gas hydrates is complex and depends on the nature of the solid walls and it is difficult to decouple the impact of solid walls from that of dilute electrolytes when they are present. In particular, a solid wall often becomes charged when in contact with an aqueous phase and the binding of the counter ions to the solid wall in an aqueous phase further complicates the investigations of heterogeneous nucleation of gas hydrates. Here we investigated the nucleation rates of CO_2 hydrate in quasi-free droplets of sodium chloride (NaCl) and potassium iodide (KI) at low concentrations (≤ 10 mM). The results showed that NaCl solution had no inhibition effect while KI solution had a weak promotion effect at low concentrations and the nucleation rates were largely independent of the salt concentrations up to 10 mM. The impacts of dilute NaCl and KI solutions on the nucleation of CO_2 hydrate in this study were broadly similar to the previous findings of the methane – propane mixed gas hydrates in Sowa et al.'s study [1].

7.1 Introduction

Clathrate hydrate is a multi-component system in which the "guest" gas molecules are trapped in the cages of "host" water molecules[2, 3]. It looks similar to ice but clathrate hydrate could form at the temperatures above the "ice-point", depending on the pressure and the type of the guest gases[4]. Some typical guest gases for clathrate hydrate include methane (CH_4), ethane (C_2H_6), propane (C_3H_8), carbon dioxide (CO_2), cyclopentane, Tetrahydrofuran (THF), etc.[5, 6]. The crystal structures of clathrate hydrates are mainly sI, sII and sH but other uncommon crystal structures like structure III – VII and T have also been reported to form for some guests under certain conditions[2, 7].

Clathrate hydrate has potential applications in energy storage[8, 9], gas separation[10, 11], CO_2 capture and sequestration[12, 13], water desalination[14, 15] and others. On the other hand, in the oil and gas industry, the formation of natural gas hydrates could cause flow assurance problems in flowlines and destroy the structural integrity of the pipelines or surface facilities if it is not controlled properly [16]. We wish to be able to promote the nucleation of clathrate hydrate for gas storage applications and other instances where hydrate formation is desired, while we wish to be able to inhibit the nucleation of clathrate hydrate in other cases where hydrate formation is to be avoided.

Salts have been known to be thermodynamic inhibitors for clathrate hydrate formation and they have been studied for years by both computational and experimental methods[17]. Hsieh et al. presented a computational method ("PRSV + MHV1 + COSMOSAC + vdW-P method") for modelling the phase behavior of gas hydrates in the presence of different saline inhibitors[18]. Bai et al. demonstrated that the NaCl solutions with a concentration of 3.5 wt.% had a clear inhibition effect on both the nucleation and the growth stages of the CH_4 hydrate formation by a molecular

dynamics simulation method[19]. Liu at el. simulated the formation of CO_2 hydrate from NaCl solutions (concentration range from 0 to 20 wt.%) at a molecular level[20] and reported that the formation rate of CO_2 hydrate decreased with the increasing concentration of salt solutions, and the salt ions could not enter or absorb on the water molecule cages during the formation process. Maekawa experimentally determined the equilibrium conditions for methane-ethane mixed gas hydrate in 3.0 wt.% NaCl solution and reported that the addition of the salt solution shifted the equilibrium conditions of the methane-ethane mixed gas hydrate to a lower temperature at a constant pressure[21].

Although salts have been well known as thermodynamic inhibitors, some salts have been reported to act as kinetic promoters of clathrate hydrates at low concentrations. Farhang et al. determined the impact of sodium halides (NaF, NaCl, NaBr and NaI) on the formation of CO_2 hydrate and concluded that the effect of sodium halide solutions on CO_2 hydrate kinetics transited from inhibition to promotion when the concentration was lower than 50 mM[22]. Sowa et al. investigated the formation of methane – propane mixed gas hydrate in various salt solutions over a broad range of concentrations (10^{-5} to 3 M) and reported that some salt solutions (e.g., LiBr, NaI, $CaCl_2$, NH_4I, etc.) promoted gas hydrate formation at concentrations below 100 mM[1, 23]. Asadi et al. reported that the alkali metal chlorides and sodium halides at low concentrations decreased the induction time and kinetically promoted the formation methane hydrate[24]. They proposed that the ion-specific effects and the increased mass transfer due to the formation of small gas bubbles might be the mechanisms[24]. However, none of the above experimental studies reported the nucleation rate of clathrate hydrates in dilute salt solutions free of solid contacts.

The impact of solid walls on heterogeneous nucleation of gas hydrates is complex and depends on the nature of the solid walls and it is difficult to decouple the impact of sold walls from

that of dilute electrolytes when they are present. In particular, a solid wall often becomes charged when in contact with an aqueous phase and the binding of the counter ions to the solid wall in an aqueous phase further complicates the investigations of heterogeneous nucleation of gas hydrates. To this end, here we investigate and report the nucleation rate of CO_2 hydrate in dilute electrolytes in the absence of a solid wall.

Nucleation of gas hydrate in dilute salt solutions is relevant to oil & gas industry as there is always some amount of salts in offshore pipelines that may impact the formation of hydrates[24]. In addition, the kinetic studies on CO_2 hydrate formation, especially the nucleation rates, have been rare [22]. To this end, we investigated the nucleation rates of CO_2 hydrate formation in quasi-free droplets of dilute salt solutions in this study. The studied salts were sodium chloride (NaCl), sodium iodide (NaI), and potassium iodide (KI).

7.2   Materials and Methods

7.2.1   Sample Preparation

Milli-Q water (ultra-pure water of 18.2 MΩ resistivity from a Millipore unit) was used for the sample preparation. Sodium chloride (NaCl, 99.5% purity), sodium iodide (NaI, 99.5% purity) and potassium iodide (KI, 99.5% purity) were purchased from Sigma-Aldrich and purified by recrystallization of the salts from respective solutions prepared with Milli-Q water. In this paper, the salt concentrations were 10^{-5} M to 10 mM. The dilute salt solutions were prepared by first preparing a stock solution of 1 M, then diluting the stock solution of 1 M to prepare a stock solution of 100 mM, which in turn was used to prepare another stock solution of 10 mM, etc.
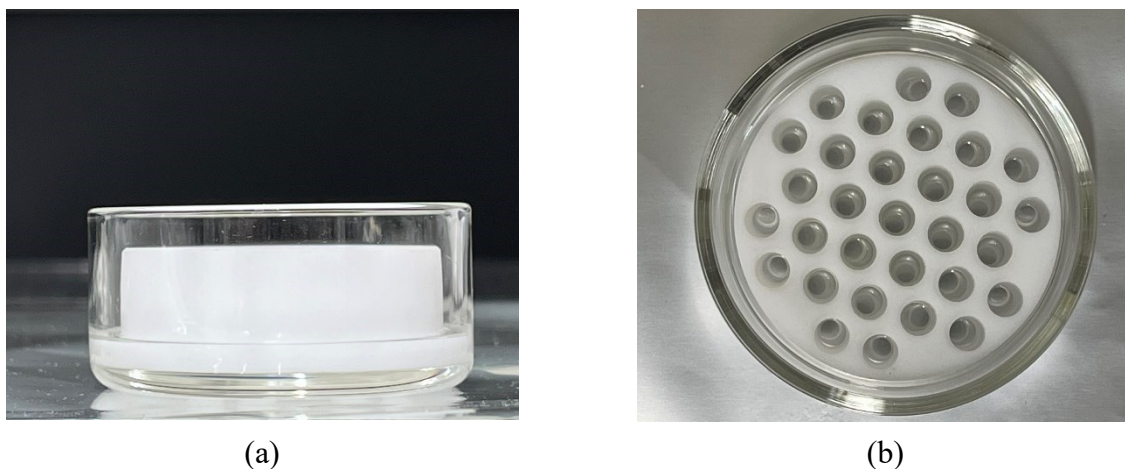
Figure 7.1. Photos of the sample cell (side view (a) and top view (b)). After the cleaning procedure, a thin layer of perfluoromethyldecalin was placed to the bottom of a glass Petri dish as the supporting liquid. 20 µL of salt solution was added to each hole and the droplet sat on top of the denser perfluoromethyldecalin layer.

The sample cell is consisted of a custom-made cylindrical Teflon (polytetrafluoroethylene) block with 31 circular through-holes and a Pyrex glass Petri dish (dimensions: 50 mm in diameter, 20 mm in height). **Figure 7.1** shows the photos of the sample cell (both side view (a) and top view (b)). The dimensions of the Teflon block are 45 mm in diameter and 15 mm in height, while each vertical through-hole is 5 mm in the inner diameter. After cleaning both the glass dish and Teflon block with sodium hydroxide (NaOH, 97% purity, purchased from Fisher Chemical and used as received) solution, a thin layer of perfluoromethyldecalin (technical grade, 80% purity) was applied to the bottom of the glass Petri dish as the supporting liquid. Around 20 µL of prepared salt solution was added into each vertical hole of the Teflon block by applying the Eppendorf pipette (Eppendorf Research, 2-20 µL). Since perfluoromethyldecalin is denser than water, the droplet of salt solution would float at the surface of the perfluoromethyldecalin layer. It is noted that the solubility of salts in perfluoromethyldecalin is negligible. After preparing the sample cell, the glass Petri dish with the Teflon block was placed at the center of the pressure chamber, and then the lid of the pressure chamber was closed and sealed.

7.2.2 Experimental Setup

The details of the experimental high-pressure setup were described in the reference [25]. Briefly, the high-pressure setup (shown in **Figure 7.2**) consisted of a CO_2 gas cylinder (99.5% purity for CO_2 gas, supplied by Linde Welding and Supplies), a 2-stage vacuum pump (model: VP10D, CPS Products Inc.), a pressure transducer (model: PM, Heise), a gas piston (model: ZR-3), an ISCO syringe pump (model: 260X, Syrixus) and a high-pressure chamber with the sample cell placed in it. And the function of each part of the high-pressure setup is listed in **Table 7.1**.

Table 7.1. The function of each part of the high-pressure setup

Equipment	Function
CO_2 gas cylinder	The CO_2 gas source for the experiments
Vacuum pump	Remove the air in gas lines, gas piston and the high-pressure chamber at the beginning of the experiments
Pressure transducer	Monitor the pressure inside the high-pressure chamber
Gas piston	Applied for the CO_2 replenishment into the high-
ISCO syringe pump	Pressurize and maintain the constant pressure during the experiments
High-pressure chamber	The reactor for CO_2 hydrate formation

A schematic illustration which describes the details of the high-pressure chamber is shown in **Figure 7.3**. The high-pressure chamber was supported by two lab jacks in a programmed refrigerated circulator (model: FPW50-HE, Julabo Company), submerging in the coolant of ethanol. During the experimental cooling ramps, the images of the sample cell could be recorded through the two windows located above and below the high-pressure chamber, aiding by the light guides (model: CL 4500, ZEISS) and the mirror reflection.
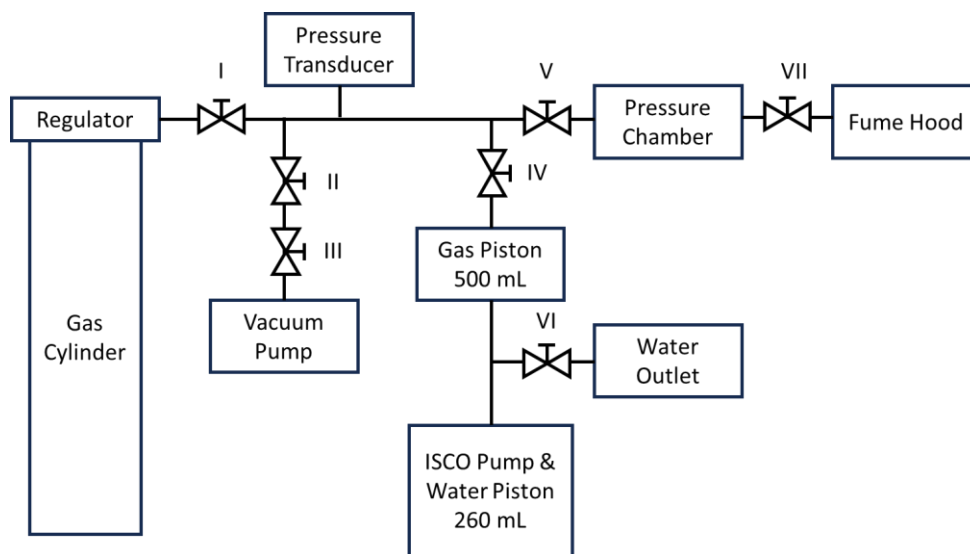
Figure 7.2. Schematic illustration of the high-pressure setup. It mainly consisted of a gas cylinder, a vacuum pump, a pressure transducer, a gas piston, an ISCO pump and a high-pressure chamber.
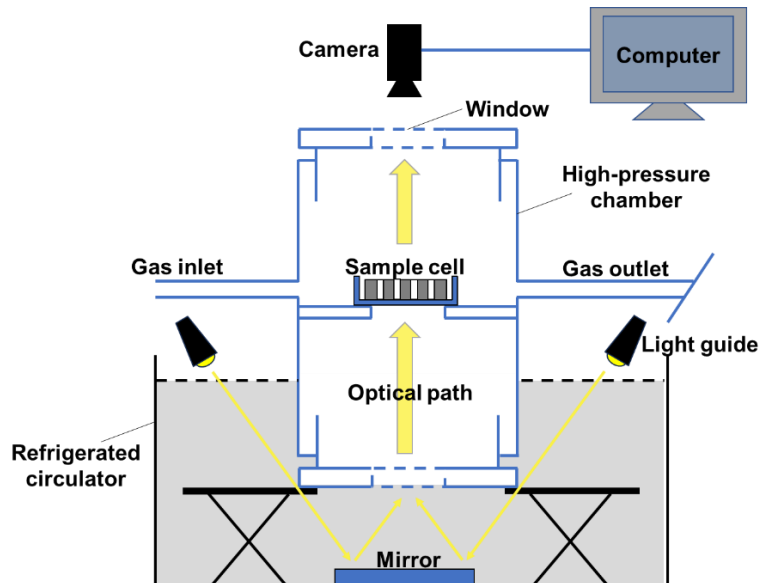
Figure 7.3. Schematic illustration of the high-pressure chamber. It was supported by two lab jacks in the refrigerated circulator, partially submerged in the coolant of ethanol. After the sample preparation, the sample cell was placed at the center of the high-pressure chamber, the lid was closed and sealed. The images of the sample cell were recorded by a camera through the top window during the experimental cooling ramps.

7.2.3 Experimental Procedures

After preparing the sample cell, it was placed into the high-pressure chamber, after which the lid of the chamber was closed and sealed. At this time, only valves IV and V (shown in **Figure 7.2**) were open. To diminish the impact of air, the vacuum pump was applied to remove all the air inside the gas lines, the gas piston and the high-pressure chamber with the valves II and III open. And the vacuum pump was disconnected from the main gas lines when the pressure value shown on the panel of the pressure transducer reached -5 psi. After that, the gas cylinder was connected to the main gas lines by opening valve I. When pressurized to 25 psi, valve VII was opened for 1-2 min to allow the CO_2 gas flush the gas lines, the gas piston and the high-pressure chamber. A leak check was performed when the reading of the pressure transducer reached 120 psi, and the CO_2 pressure inside the high-pressure chamber was gradually increased to 435 psi (3 MPa) after confirming the absence of gas leaking. Once the high-pressure chamber was pressurized to 435 psi, the gas cylinder was disconnected with the main gas lines by closing valve I. And the ISCO syringe pump was applied to maintain the constant pressure during the cooling ramp. The refrigerated circulator was programmed to cool at a constant rate of 0.4 K/h, and the camera was set to record the images of the sample cell at a time interval of 1 min. It is noted that only valves IV and V were open during the experimental cooling ramps.

7.2.4 Data Analysis

Typical photos of the top view of the sample cell at different stages of the cooling ramp are shown in **Figure 7.4**. All the droplets were transparent at the beginning of each experimental cooling ramp (**Figure 7.4**a). With cooling, CO_2 hydrate formed on some droplets and the droplets

became opaque (shown in **Figure 7.4**b). Eventually, all the sample droplets became opaque, indicating CO_2 hydrate formed on all sample droplets by the end of the experimental cooling ramp (shown in **Figure 7.4**c). It is noted that there was no volume expansion observed during the experiments, which indicated that CO_2 hydrate formed instead of ice. By combining the linear cooling program set on the refrigerated circulator and the images showing the moment that CO_2 hydrate formed for each droplet, the hydrate nucleating temperature shown on the panel of the refrigerated circulator of each droplet was obtained after each experimental cooling ramp. Since there's always a difference between the real temperature of the droplets and the temperature that shown on the panel of the refrigerated circulator, a temperature calibration was carried out first. After calibration, the "real" nucleation temperature (T_f) of each droplet was obtained as the raw data for the experiments.

(a)   (b)

(c)

Figure 7.4. Photos of CO_2 hydrate formed on droplets of dilute salt solutions. During each experimental cooling ramp, all the droplets were transparent and liquid at the beginning (a). With cooling, CO_2 hydrate formed on some droplets (b). Eventually, all the droplets nucleated and became opaque at the end of the cooling ramp (c).

After obtaining the raw data, the survival curve and nucleation curve were derived by using the analytical method described in the earlier publications[25-28]. The procedure could be concluded as below: (1) obtaining the supercooling (ΔT) of each droplet, where $\Delta T = T_{equilibrium} - T_f$. (2) constructing the survival curve that survival probability, F, as a function of ΔT, where F was calculated from the number of unnucleated droplets divided by the total number of droplets at a given time. (3) Calculating $\ln F$ with respect to the lag time (t), where t was calculated from ΔT divided by the real sample cooling rate (derived from the calibration table). (4) fitting an exponential function curve with the form of $A \cdot \exp(Bt) + C$ to the curve $\ln F(t)$ and obtaining the slope of $\ln F$ at each t by analytically differentiating the fitted curve. (5) deriving the nucleation rate as a function of ΔT, where the nucleation rate was calculated from correcting each slope by a factor of $-\ln 2$.

7.3 Results

7.3.1 Nucleation Rates of CO_2 Hydrate in Dilute Salt Solutions

For NaCl, the survival curve is shown in **Figure 7.5**, the corresponding natural logarithm of the survival probability and the nucleation curve are shown in **Figure 7.6** and **Figure 7.7**, respectively. Similarly, the results for KI are shown in **Figure 7.8**-**Figure 7.10**. It is noted that the experimental results measured in pure water were the same as those in reference [25]. We also noted that the concentration of these two salts was 1 mM, and around 120 data points were collected for deriving the nucleation curve for each salt.

For NaCl, **Figure 7.5** shows that the required supercooling for nucleation of CO_2 hydrate was 4.5 to 14.5 K, which was similar to that of pure water (4.3 to 15.3 K). The supercooling width of the survival curve of the 1 mM NaCl solution (10 K) was slightly narrower than that of pure water (11 K). **Figure 7.6** shows that the ln$F$ curve of the 1 mM NaCl solution had steeper slopes than that of pure water at the supercooling range of 12 to 14.5 K. **Figure 7.7** shows that the nucleation rate of CO_2 hydrate in the presence of NaCl was similar to that of pure water. We conclude that 1 mM NaCl had negligible impact on the nucleation of CO_2 hydrate.
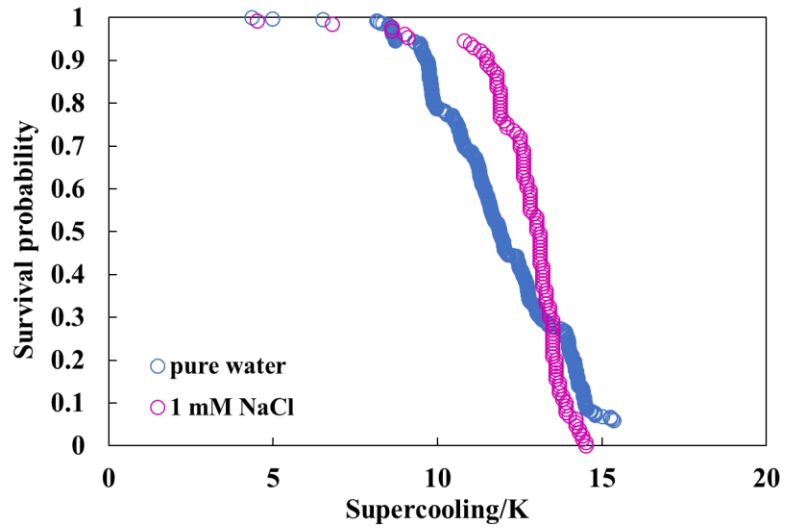
Figure 7.5. Survival curves of CO_2 hydrate measured in quasi-free droplets of pure water and 1 mM NaCl solution. The linear cooling rate was 0.4 K/h.
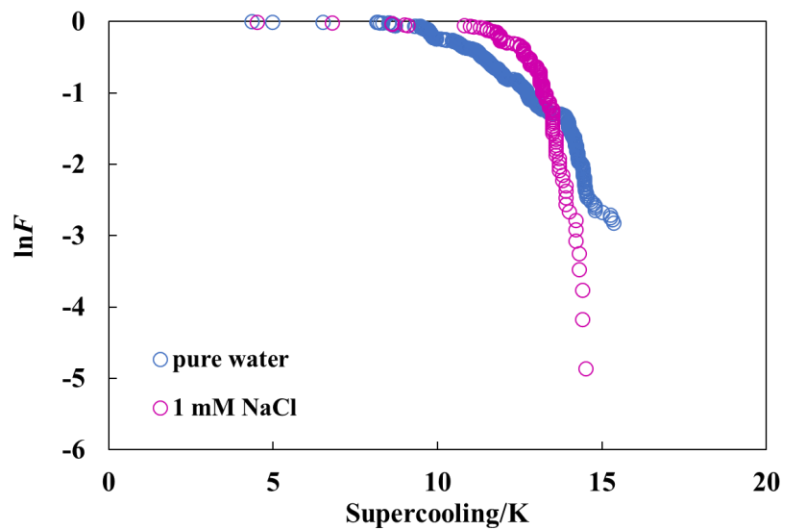
Figure 7.6. Natural logarithm of the survival curves of CO_2 hydrate in quasi-free droplets of pure water and 1 mM NaCl solution.
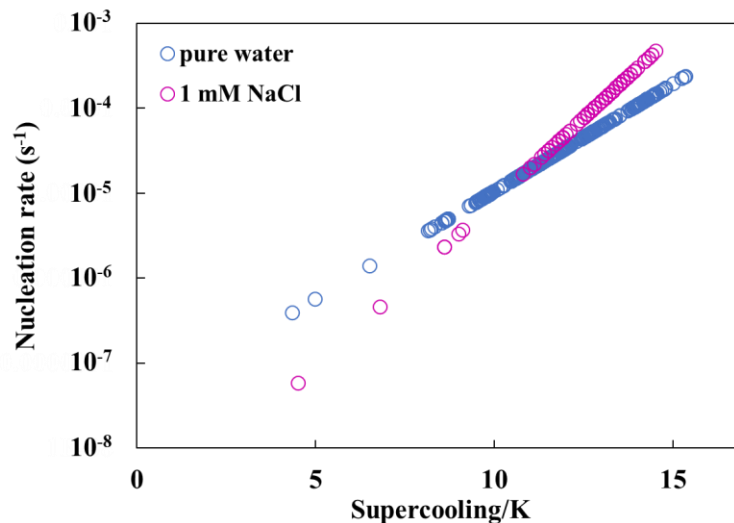
Figure 7.7. Nucleation curves of CO_2 hydrate measured in quasi-free droplets of pure water and 1 mM NaCl solution.

For KI, as shown in **Figure 7.8**, the supercooling range of the survival curve was 7.3 to 14.7 K. The survival curve of the 1 mM KI solution was very close to that of pure water but had a narrower supercooling width. **Figure 7.9** shows that the $\ln F$ curve of the KI solution was almost overlapping with that of pure water at the supercooling range of 7 to 13 K and had steeper slopes than that of pure water over the supercooling range of 13 to 15 K. As shown in **Figure 7.10**, the nucleation rate of the 1 mM KI solution somewhat greater than that of pure water at a comparable supercooling range but the difference was no greater than 1 order of magnitude. The results showed that 1 mM KI solution had a weak promotion effect on the formation of CO_2 hydrate.

Figure 7.8. Survival curve of CO_2 hydrate in quasi-free droplets of pure water and 1 mM KI solution. The cooling rate used was 0.4 K/h.

Figure 7.9. Natural logarithm of the survival curves of CO_2 hydrate in quasi-free droplets of pure water and 1 mM KI solution.

Figure 7.10. Nucleation curves of CO_2 hydrate in quasi-free droplets of pure water and 1 mM KI solution.

7.3.2   The Concentration Dependence

Neither NaCl nor KI inhibited the formation of CO_2 hydrate at 1 mM. However, we expect all salts to thermodynamically inhibit formation of clathrate hydrates at sufficiently high concentrations. We thus investigated the nucleation rate of CO_2 hydrate in NaCl and KI solutions of three different concentrations (10 mM, 1 mM and 10^{-5} M). The results for NaCl solutions are shown in **Figure 7.11-Figure 7.13**, and the results for KI solutions are shown in **Figure 7.14-Figure 7.16**. We again collected 120 data points for the determination of each nucleation curve.

Figure 7.11 shows that the survival curves of CO_2 hydrate in dilute NaCl solutions shifted toward slightly greater supercoolings with the increasing concentration up to 10 mM. However, the ln$F$ curves shown in **Figure 7.12** and the nucleation curves shown in **Figure 7.13** were both similar to each other over the concentration range investigated. We thus conclude that the nucleation rate of CO_2 hydrate in NaCl solutions was largely independent of the salt concentration up to 10 mM.

192
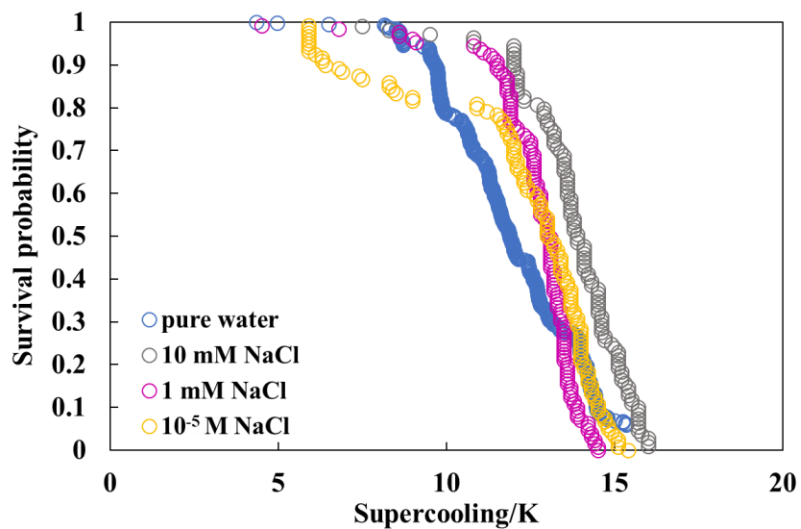
Figure 7.11. Survival curve of CO_2 hydrate in quasi-free droplets of pure water and dilute NaCl solutions of different concentrations (from 10^{-5} to 10^{-2} M). The cooling rate used was 0.4 K/h.
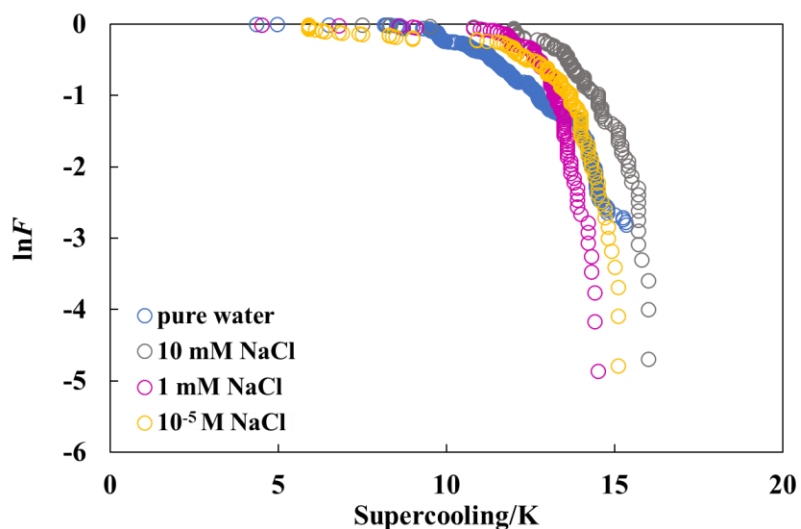
Figure 7.12. Natural logarithm of the survival curve of CO_2 hydrate in quasi-free droplets of pure water and dilute NaCl solutions of different concentrations (from 10^{-5} to 10^{-2} M).

193
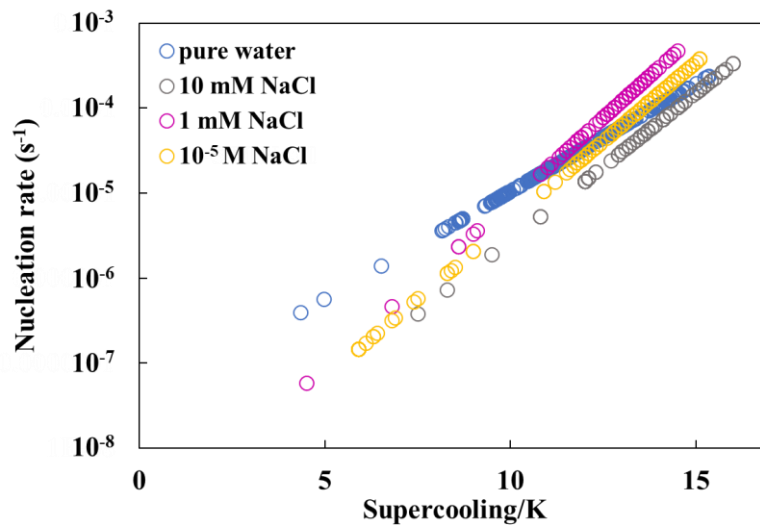
Figure 7.13. Nucleation curve of the survival curve of CO_2 hydrate in quasi-free droplets of pure water and dilute NaCl solutions of different concentrations (from 10^{-5} to 10^{-2} M).

For KI, **Figure 7.14** and **Figure 7.15** show that the survival curves and the ln$F$ curves of CO_2 hydrate in dilute KI solutions were similar to that of pure water up to 10 mM. The nucleation curves in **Figure 7.16** show that KI weakly promoted the formation of CO_2 hydrate over the concentration range investigated and that this promotion effect was largely independent of the concentration of KI up to 10 mM.
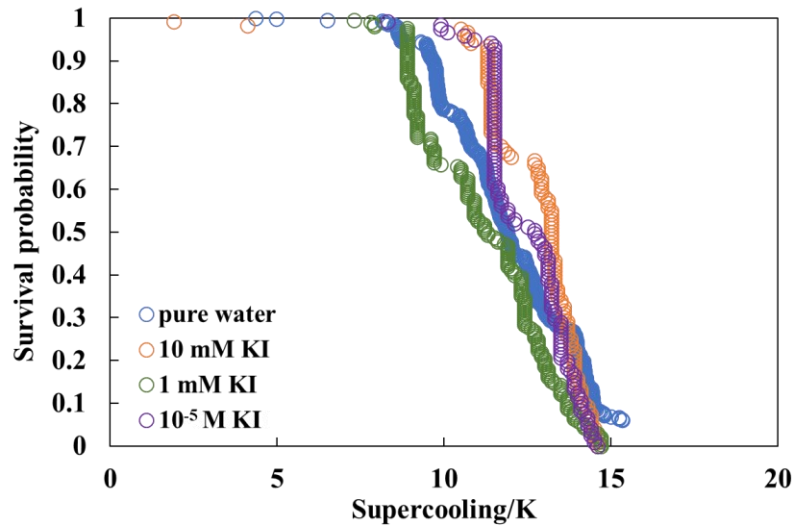
Figure 7.14. Survival curves of CO_2 hydrate in quasi-free droplets of pure water and dilute KI solutions of different concentrations (from 10^{-5} to 10^{-2} M). The cooling rate used was 0.4 K/h.
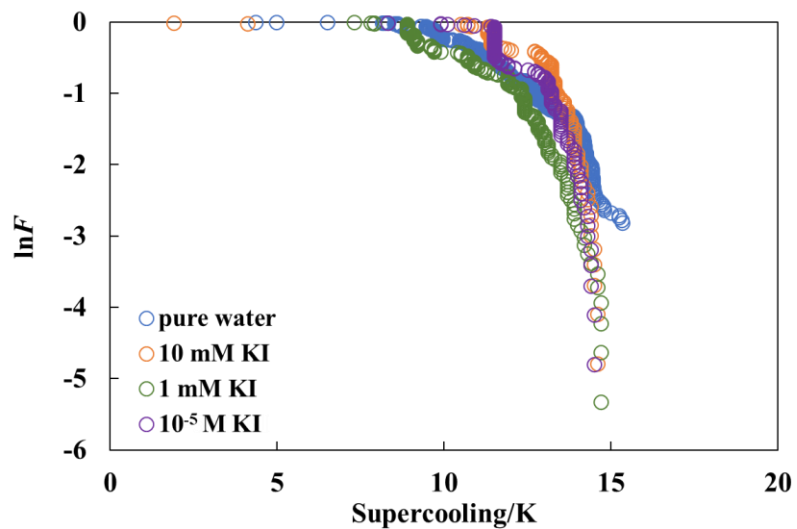
Figure 7.15. Natural logarithm of the survival curves of CO_2 hydrate in quasi-free droplets of pure water and dilute KI solutions of different concentrations (from 10^{-5} to 10^{-2} M).
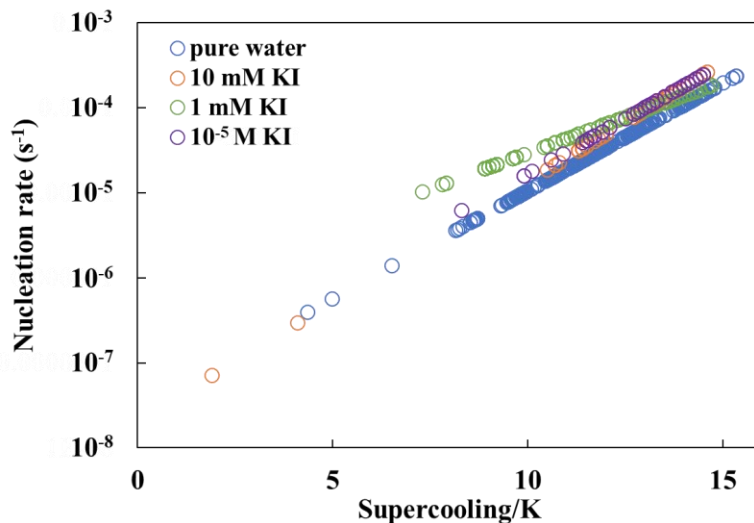
Figure 7.16. Nucleation curves of CO_2 hydrate in quasi-free droplets of pure water and dilute KI solutions of different concentrations (from 10^{-5} to 10^{-2} M).

7.4 Discussion

In our earlier study on ice, the survival curve of ice in quasi-free droplet of 1 mM NaCl solution was over the supercooling range of 8.2 to 24.2 K (the temperature range of -8.2 to -24.2 °C)[29]. Thus, it is clear that CO_2 hydrate formed on the quasi-free droplets of 1 mM NaCl solution in the current study was in the absence of ice because the range of the survival curve was 4.5 to 14.5 K, which corresponded to the temperature range of 2.5 to -7.5 °C. Additionally, no volume expansion that is characteristic of freezing of water was observed in the current study.

Our results showed that neither NaCl nor KI inhibited the nucleation of CO_2 hydrate at the concentration of 1 mM. And the nucleation rates measured in these two salt solutions were largely independent of salt concentrations when the concentrations were 10 mM or lower. However, increasing the salt concentrations should thermodynamically inhibit the nucleation of CO_2 hydrate. To this end, we investigated the nucleation of CO_2 hydrate in 100 mM KI solution and the survival curve is showed in **Figure 7.17**. It is noted that only 19 out of the first 62 samples nucleated before

196

the end of the experimental ramps. The lowest temperature of the experimental cooling ramps was set to -8.5 °C because in our earlier study we found that the survival curve of ice in quasi-free droplet of 1 mM KI solution was over the supercooling range of 8.8 to 25.9 K (the temperature range of -8.8 to -25.9 °C)[29]. Though the survival curve was incomplete, it appears clear that the survival curve of 100 mM KI solution shifted to much deeper supercoolings than that of pure water, which suggests that the 100 mM was already a high enough concentration that thermodynamically inhibited the nucleation of CO_2 hydrate.
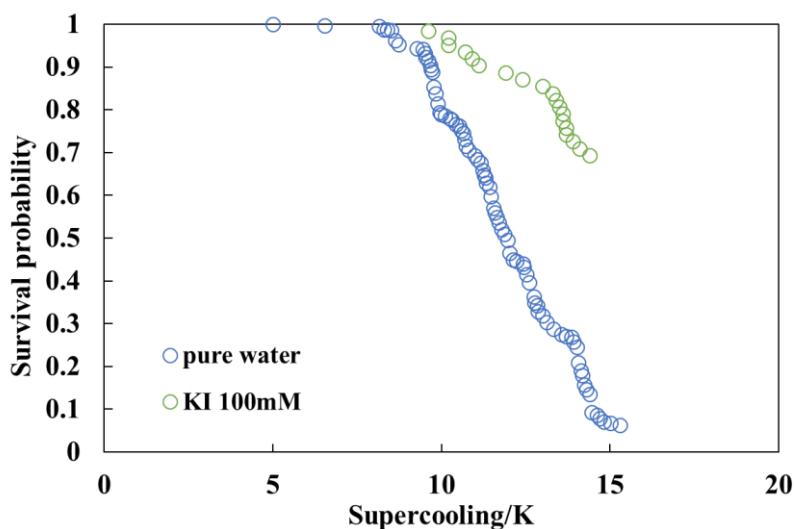
Figure 7.17. The survival curve measured in quasi-free droplets of 100 mM KI solution. To avoid the presence of ice, the lowest temperature of each experimental ramp was set to be around -8.5 °C for the droplet samples. Since only 19 out of 62 droplets were nucleated at the end of the experimental ramps, the survival curve of 100 mM KI solution was an incomplete curve.

7.4.1 Effect of Individual Monovalent Ions on the Nucleation of CO_2 Hydrate

To compare the impact of NaCl and KI on the nucleation rate of CO_2 hydrate, we also investigated the nucleation rate of CO_2 hydrate in NaI solution at the concentration of 1 mM. We first compare the experimental results of dilute NaI and KI solutions in **Figure 7.18**-**Figure 7.20** to discuss the impact of monovalent cations on the nucleation of CO_2 hydrate. We then compare

the experimental results of dilute NaI and NaCl solutions in **Figure 7.21**-**Figure 7.23** to discuss the impact of monovalent anions on the nucleation of CO_2 hydrate.

Figure 7.18-**Figure 7.20** show that the highest supercooling of the survival curve and nucleation curve measured in 1 mM NaI solution was similar to that in 1 mM KI solution but the width of the survival curve of the 1 mM NaI solution was somewhat narrower. The nucleation rates of CO_2 hydrate in the 1 mM KI solution and in the 1 mM NaI solution were both slightly greater (no more than 1 order of magnitude) than that in pure water, which indicated that both KI and NaI weakly promoted the nucleation of CO_2 hydrate. However, the impact of the monovalent cations on the nucleation of CO_2 hydrate seemed to be unclear.
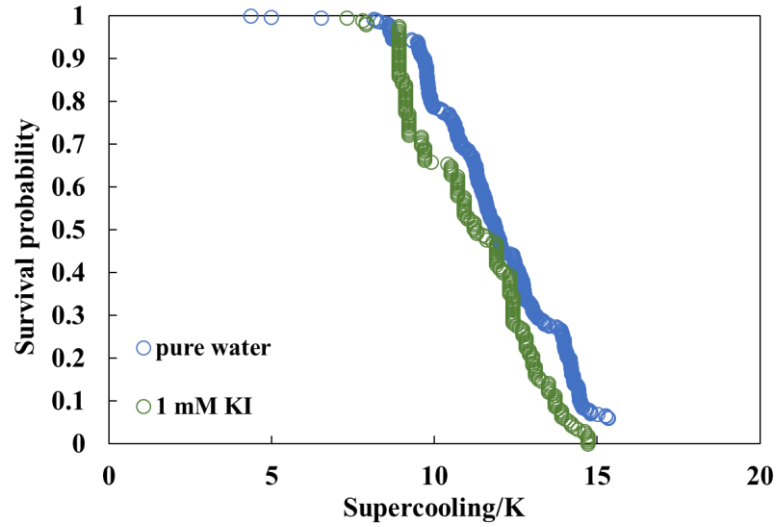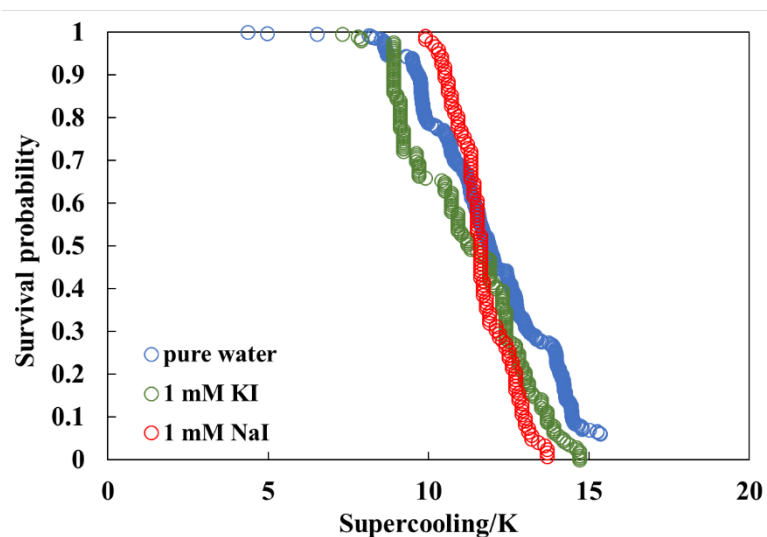

Figure 7.18. Survival curves of CO_2 hydrate in quasi-free droplets of 1 mM KI and NaI solutions. The cooling rate used was 0.4 K/h.
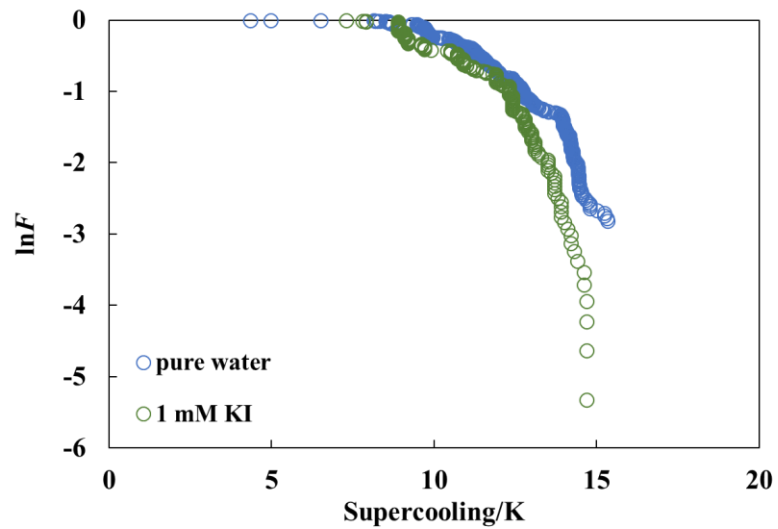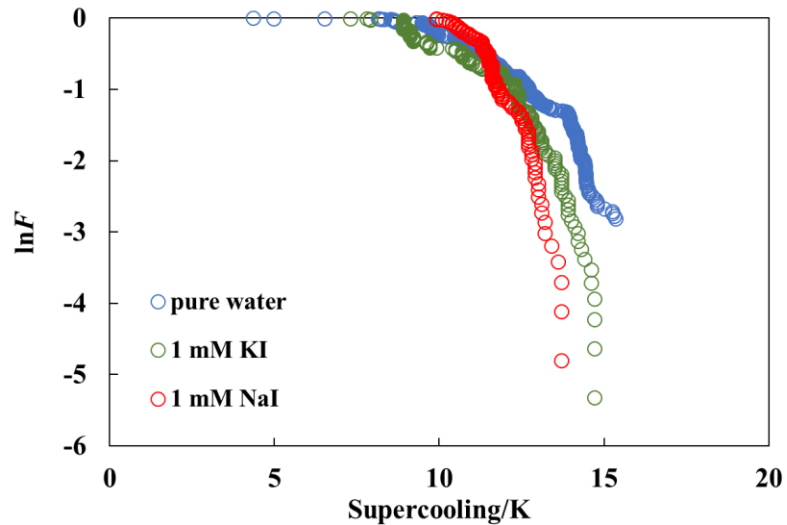
Figure 7.19. Natural logarithm of the survival curves of CO_2 hydrate in quasi-free droplets of 1 mM KI and NaI solutions.
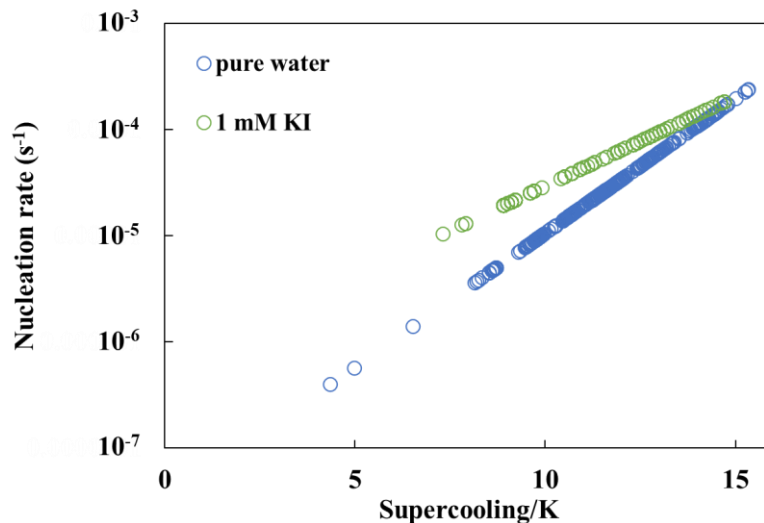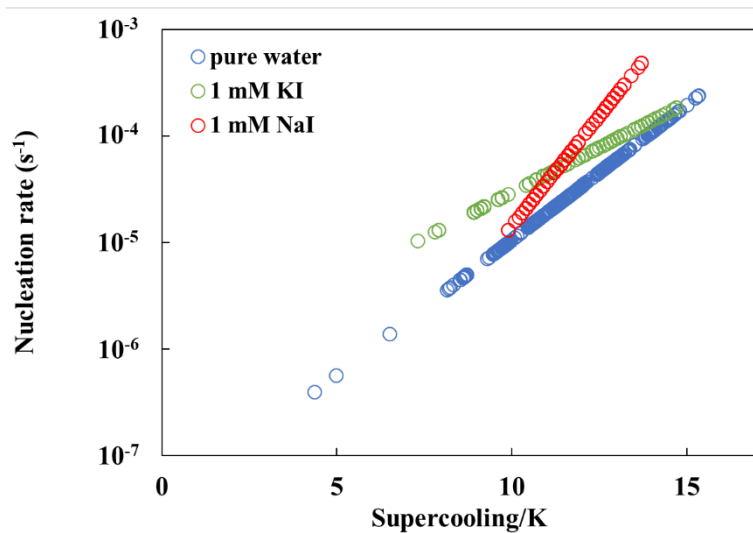

Figure 7.20. Nucleation curves of CO_2 hydrate in quasi-free droplets of 1 mM KI and NaI solutions.

Figure 7.21-**Figure 7.23** show that the survival curve measured in 1 mM NaI solution had a similar average supercooling but narrower width than that measured in pure water, resulting in higher nucleation rates. CO_2 hydrate seemed to require somewhat greater supercoolings in 1 mM

NaCl solution than in 1 mM NaI solution or pure water. 1 mM NaI weakly promoted the nucleation

of CO_2 hydrate while the impact of 1 mM NaCl was negligible. Therefore, I^- is somewhat more

promoting than Cl^-. It appears that the larger anions are more conducive to the nucleation of CO_2
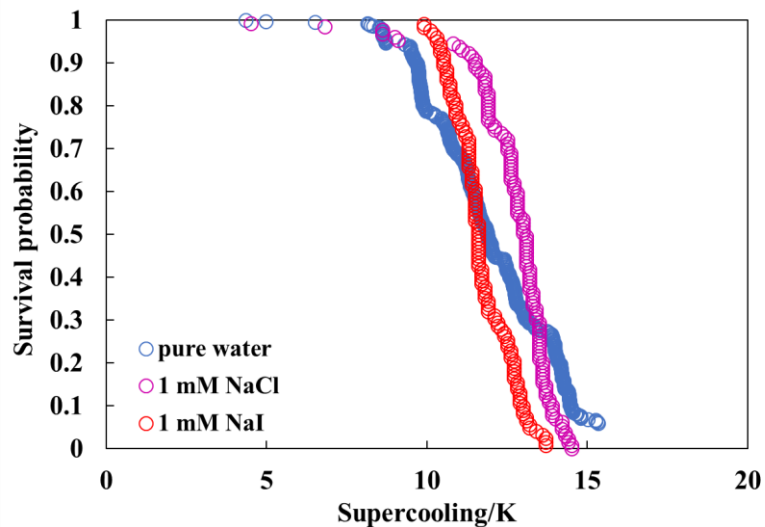
hydrate.

Figure 7.21. Survival curves of the formation of CO_2 hydrate measured in quasi-free droplets of dilute NaCl and NaI solutions at the concentration of 1 mM. 0.4 K/h was used as the cooling rate.
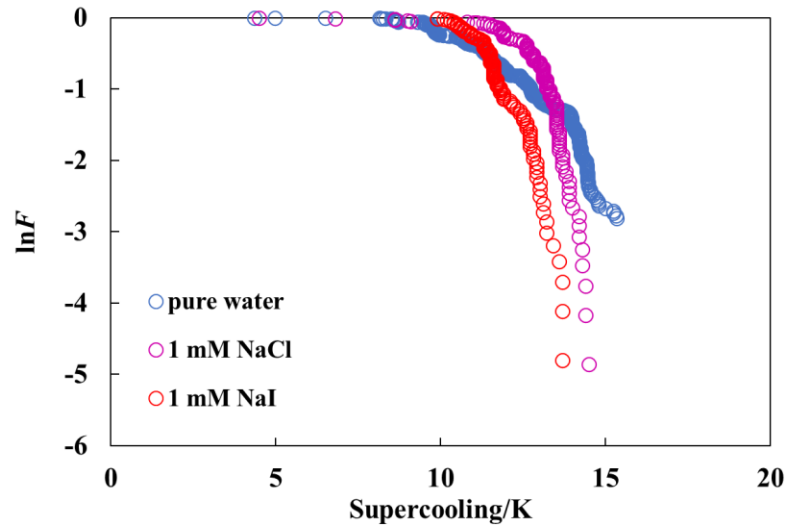
Figure 7.22. Natural logarithm of the survival curve of the formation of CO_2 hydrate measured in quasi-free droplets of dilute NaCl and NaI solutions at the concentration of 1 mM. 0.4 K/h was used as the cooling rate.
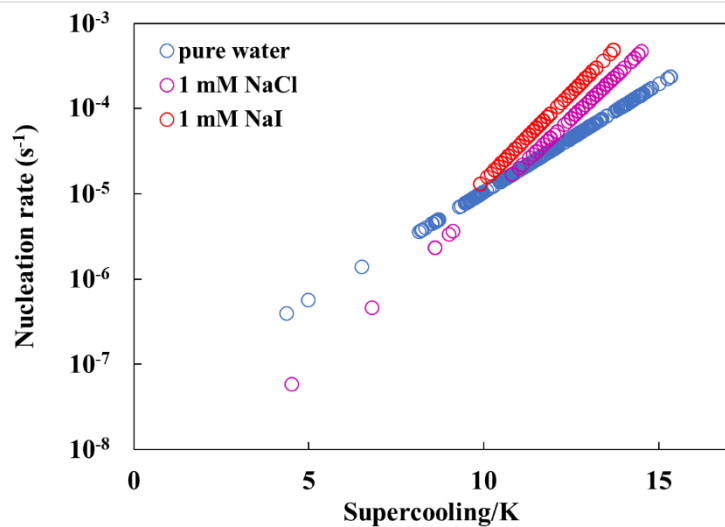
Figure 7.23. Nucleation curves of the formation of CO_2 hydrate measured in quasi-free droplets of dilute KI and NaI solutions at the concentration of 1 mM. 0.4 K/h was used as the cooling rate.

Lu et al. reported that the thermodynamic stability conditions (the phase boundaries) of gas hydrates (CO_2 hydrate, methane hydrate and propane hydrate) in concentrated (> 200 mM) salt

solutions were mainly determined by the type of anions [30]. Farhang et al. presented the experimental studies on the formation of CO_2 hydrate in sodium halides from the kinetic point of view [22] and they observed that the gas uptake rate after 24 h and the maximum growth rate of CO_2 hydrate were higher in concentrated (25 to 500 mM) salt solutions of larger anions ($I^- > Br^- > Cl^- > F^-$). Although the concentration ranges of the salt solutions investigated were vastly different from ours, it is interesting that Farhang et al. also found that the larger anions were more conducive to the formation of CO_2 hydrate [22].

7.4.2   Comparison Between Ice, C1/C3 Mixed Gas Hydrate and CO_2 Hydrate Formation

To obtain further insight into the nucleation of CO_2 hydrate in dilute salt solutions, we compared the experimental results in this study to our earlier study on the nucleation of ice in dilute salt solutions [29] and to Sowa et al.'s study on the formation of 90 mol% methane – 10 mol% propane (C1/C3) mixed gas hydrate [1].

Our earlier study on ice showed that the 1 mM NaCl solution had a weak to no promotion effect on ice nucleation while the 1 mM KI solution could lower the required supercoolings (higher temperatures) for freezing with negligible change in the nucleation rate of ice. These earlier findings on ice are similar to the results of the current study that 1 mM NaCl solution had negligible effect on the nucleation of CO_2 hydrate while 1 mM KI solution had a weak promotion effect.

Sowa et al. investigated the C1/C3 hydrate formation in different monovalent salt solutions over a concentration range of 10^{-5} to 3 M [1]. Since they did not report the nucleation rates, we here only compare the supercooling range of the survival curves and the median values in NaCl and KI solutions at a concentration range of 10^{-5} to 10^{-2} M. The results are summarized in **Table 7.2**. It is noted that Sowa et al.'s results were obtained from the Figure 3 in ref [1]. Sowa et al used a much

faster cooling rate of 0.025 K/sec than ours so quantitative comparisons are not possible. Below, we only make qualitative comparisons.

Table 7.2. Comparison of the results for the nucleation of CO_2 hydrate in this study with C1/C3 hydrate in Sowa et al.'s study[1].

	Concentration (M)	Supercooling range of the survival curve (K)		Supercooling width of the survival curve (K)		Median supercooling (K)	
		C1/C3 hydrate	CO_2 hydrate	C1/C3 hydrate	CO_2 hydrate	C1/C3 hydrate	CO_2 hydrate
Pure water	-	10 – 37	4.3 – 15.3	27	11	17	11.9
NaCl	10^{-2}	15 – 26	7.5 – 16	11	8.5	21	13.9
	10^{-3}	23 – 34	4.5 – 14.5	11	10	26	13.0
	10^{-5}	10 – 24	5.9 – 15.4	14	9.5	17	13.0
KI	10^{-2}	11 – 17	1.9 – 14.6	6	12.7	14	13.2
	10^{-3}	10 – 22	7.3 – 14.7	12	7.4	13	11.2
	10^{-5}	-	8.3 – 14.6	-	6.3	-	12.7

As shown in **Table 7.2**, the survival curves of C1/C3 hydrate measured in NaCl solutions had narrower supercooling range and greater median supercoolings than in pure water, which is consistent with our current results for CO_2 hydrate in NaCl solutions. As for KI solutions, the survival curves of C1/C3 hydrate had slightly smaller median supercoolings and narrower supercooling range than that of pure water whereas the survival curves of CO_2 hydrate in KI solutions had similar or slightly greater median supercoolings and narrower supercooling widths than that of pure water. Qualitatively similar conclusions can be drawn that KI solutions had a weak promotion effect on the nucleation of both C1/C3 hydrate and CO_2 hydrate. Therefore, it could be concluded that the impacts of dilute NaCl and KI solutions on the nucleation of CO_2 hydrate in the current results were broadly similar to those of C1/C3 hydrate in Sowa et al.'s results.

7.5 Conclusions

In this study, the quasi-free droplets supported by a layer of perfluoromethyldecalin were applied to investigate the impacts of dilute salt solutions (10 mM or lower) on the nucleation of CO_2 hydrate. The results showed that 1 mM NaCl solution had no effect on the nucleation of CO_2 hydrate whereas the 1 mM KI solution had a weak promotion effect on the nucleation of CO_2 hydrate. The nucleation rates of CO_2 hydrate measured in these two salt solutions was largely independent of the salt concentration when the concentrations were 10 mM or less than 10 mM. By comparing with the nucleation rates measured in dilute NaI solution, it seemed that the larger anions are more conducive to the nucleation of CO_2 hydrate while the impact of monovalent cations was unclear. The effects of dilute NaCl and KI solutions on the nucleation of CO_2 hydrate were broadly similar to those of ice nucleation in our previous studies and the formation of C1/C3 mixed gas hydrates in Sowa et al.'s results [1].

7.6 References

(1)   Sowa, B.; Zhang, X. H.; Hartley, P. G.; Dunstan, D. E.; Kozielski, K. A.; Maeda, N. Formation of ice, tetrahydrofuran hydrate, and methane/propane mixed gas hydrates in strong monovalent salt solutions. *Energy & fuels* **2014**, *28* (11), 6877-6888.

(2)   Maeda, N.; Maeda, N. *Nucleation of gas hydrates*; Springer, 2020.

(3)   Ripmeester, J. A.; Alavi, S. Some current challenges in clathrate hydrate science: Nucleation, decomposition and the memory effect. *Current Opinion in Solid State and Materials Science* **2016**, *20* (6), 344-351.

(4)   Warrier, P.; Khan, M. N.; Srivastava, V.; Maupin, C. M.; Koh, C. A. Overview: Nucleation of clathrate hydrates. *The Journal of chemical physics* **2016**, *145* (21).

(5)   Koh, C.; Westacott, R. E.; Zhang, W.; Hirachand, K.; Creek, J.; Soper, A. Mechanisms of gas hydrate formation and inhibition. *Fluid Phase Equilibria* **2002**, *194*, 143-151.

(6)   Sloan Jr, E. D. Fundamental principles and applications of natural gas hydrates. *Nature* **2003**, *426* (6964), 353-359.

(7)   Sloan Jr, E. D.; Koh, C. A. *Clathrate hydrates of natural gases*; CRC press, 2007.

(8)   Castellani, B.; Morini, E.; Filipponi, M.; Nicolini, A.; Palombo, M.; Cotana, F.; Rossi, F. Clathrate hydrates for thermal energy storage in buildings: overview of proper hydrate-forming compounds. *Sustainability* **2014**, *6* (10), 6815-6829.

(9)   Kumar, A.; Kushwaha, O. S.; Rangsunvigit, P.; Linga, P.; Kumar, R. Effect of additives on formation and decomposition kinetics of methane clathrate hydrates: Application in energy storage and transportation. *The Canadian Journal of Chemical Engineering* **2016**, *94* (11), 2160-2167.

(10)   Prasad, P. S.; Sai Kiran, B. Clathrate hydrates of greenhouse gases in the presence of natural amino acids: storage, transportation and separation applications. *Scientific reports* **2018**, *8* (1), 8560.

(11)   Ahmadloo, F.; Mali, G. A.; Chapoy, A. Gas separation and storage using semi-clathrate hydrates. In *6th International Conference on Gas Hydrates 2008*, 2008.

(12)   Hirai, S.; Tabe, Y.; Kuwano, K.; Ogawa, K.; Okazaki, K. MRI measurement of hydrate growth and an application to advanced CO2 sequestration technology. *Annals of the New York Academy of Sciences* **2000**, *912* (1), 246-253.

(13)   Kim, K.; Truong-Lam, H. S.; Lee, J. D.; Sa, J.-H. Facilitating clathrate hydrates with extremely rapid and high gas uptake for chemical-free carbon capture and methane storage. *Energy* **2023**, *270*, 126902.

(14)   Babu, P.; Nambiar, A.; Chong, Z. R.; Daraboina, N.; Albeirutty, M.; Bamaga, O. A.; Linga, P. Hydrate-based desalination (HyDesal) process employing a novel prototype design. *Chemical Engineering Science* **2020**, *218*, 115563.

(15)   Babu, P.; Bollineni, C.; Daraboina, N. Energy analysis of methane-hydrate-based produced water desalination. *Energy & Fuels* **2021**, *35* (3), 2514-2519.

(16)   Khurana, M.; Yin, Z.; Linga, P. A review of clathrate hydrate nucleation. *ACS Sustainable Chemistry & Engineering* **2017**, *5* (12), 11176-11203.

(17)   Dalmazzone, D.; Clausse, D.; Dalmazzone, C.; Herzhaft, B. The stability of methane hydrates in highly concentrated electrolyte solutions by differential scanning calorimetry and theoretical computation. *American Mineralogist* **2004**, *89* (8-9), 1183-1191.

(18)   Hsieh, M.-K.; Yeh, Y.-T.; Chen, Y.-P.; Chen, P.-C.; Lin, S.-T.; Chen, L.-J. Predictive method for the change in equilibrium conditions of gas hydrates with addition of inhibitors and electrolytes. *Industrial & engineering chemistry research* **2012**, *51* (5), 2456-2469.

(19)   Bai, D.; Wu, Z.; Lin, C.; Zhou, D. The effect of aqueous NaCl solution on methane hydrate nucleation and growth. *Fluid Phase Equilibria* **2019**, *487*, 76-82.

(20)   Liu, C.; Zhou, X.; Liang, D. Molecular insight into carbon dioxide hydrate formation from saline solution. *RSC advances* **2021**, *11* (50), 31583-31589.

(21)   Maekawa, T. Equilibrium conditions for gas hydrates of methane and ethane mixtures in pure water and sodium chloride solution. *Geochemical Journal* **2001**, *35* (1), 59-66.

(22)   Farhang, F.; Nguyen, A. V.; Hampton, M. A. Influence of sodium halides on the kinetics of CO2 hydrate formation. *Energy & fuels* **2014**, *28* (2), 1220-1229.

(23) Sowa, B.; Zhang, X. H.; Kozielski, K. A.; Hartley, P. G.; Dunstan, D. E.; Maeda, N. Nucleation probability distributions of methane–propane mixed gas hydrates in salt solutions and urea. *Energy & Fuels* **2015**, *29* (10), 6259-6270.

(24) Asadi, F.; Ejtemaei, M.; Birkett, G.; Searles, D. J.; Nguyen, A. V. The link between the kinetics of gas hydrate formation and surface ion distribution in the low salt concentration regime. *Fuel* **2019**, *240*, 309-316.

(25) Wei, Y.; Nobuo, M. Nucleation Curves of Carbon Dioxide Hydrate in the Absence of a Solid Wall. *Energy & Fuels* **2023**, *37* (5), 3760-3774.

(26) Zhang, X.; Maeda, N. Nucleation curves of ice in the presence of nucleation promoters. *Chemical Engineering Science* **2022**, *262*, 118017.

(27) Zhang, X.; Li, H.; Maeda, N. Nucleation curves of ice in quasi–free water droplets. *Chemical Engineering Science* **2021**, *242*, 116751.

(28) Maeda, N. Nucleation curves of model natural gas hydrates on a quasi-free water droplet. *AIChE Journal* **2015**, *61* (8), 2611-2617.

(29) Zhang, X.; Li, H.; Maeda, N. Nucleation curves of ice in dilute salt solutions. *Energy & Fuels* **2023**, *37* (18), 13937-13948.

(30) Lu, H.; Matsumoto, R.; Tsuji, Y.; Oda, H. Anion plays a more important role than cation in affecting gas hydrate stability in electrolyte solution?—a recognition from experimental results. *Fluid phase equilibria* **2001**, *178* (1-2), 225-232.

CHAPTER 8 CONCLUSIONS, GENERAL DISCUSSIONS, AND RECOMMENDATIONS

8.1 Conclusions and General Discussions

In this dissertation, in order to enhance the understanding of the mechanisms of both clathrate hydrate nucleation and ice nucleation, we aimed to take a dual approach, studying the nucleation of ice and clathrate hydrates and using the findings in one of them to help understanding of the other. Since ice is structurally similar but less complex than clathrate hydrates, we started from the study of ice nucleation. We investigated the nucleation of ice and CO_2 hydrate in the presence of different types of additives (promoters/inhibitors) and determined the nucleation rates which could quantitatively describe the efficacy (either promotion or inhibition) of the additives. The main conclusions of this thesis are summarized as follows:

Firstly, a new experimental setup was established, calibrated, and assessed for the measurement of ice nucleation rate that uses linear cooling ramps. The nucleation of ice was investigated in three microliter-sized water systems, including 1) quasi-free water droplets supported by a stable wetting film of squalane; 2) quasi-free water droplets suspended between two immiscible liquids (perfluoromethyldecalin and squalane); and 3) water directly in contact with a hydrophobic Teflon wall. The nucleation rates of ice measured in these three water systems were determined from the procedure that was previously developed by N. Maeda [1] for clathrate hydrates. The effect of the number of the data points and the experimental cooling rates was also investigated in detail. The results showed that: 1) the nucleation curve of a given system remained largely unchanged with the addition of data after the first 100 data points; 2) the nucleation curve shifted downward with a slower cooling rate; 3) the nucleation rates measured in the two quasi-

free water droplet systems were broadly similar to each other and our results showed broad agreements with literature data when the differences in the scales were accounted for, which indicated that the experimental method using quasi-free water droplet systems was reliable and could provide a basis for future work; 4) the nucleation rates of ice in water directly in contact with a Teflon wall were somewhat higher than those in quasi-free droplet systems but the difference was smaller than the gap between two quasi-free droplet systems.

After the baseline was set up, the nucleation rates of ice in the presence of seven different nucleation promoters (AgI, kaolinite, Snomax, cholesterol, steroid and two types of celluloses) were investigated by the linear cooling ramp method. Due to the density mismatch and the cleaning problem, water directly in contact with a Teflon wall was selected to study the impact of nucleation promoters on ice nucleation. Since the difference between the nucleation rates measured in water directly in contact with a Teflon wall and those in quasi-free water droplet systems was not big, we assumed that the increase in the nucleation rate of ice by a hydrophobic Teflon wall is limited and that any additional increase in the nucleation rate of ice by a promoter would be measurable. The results showed that the efficacy ranking among these seven nucleation promoters was Snomax $\approx$ AgI $\geqslant$ kaolinite > steroid > cholesterol $\approx$ celluloses $\geqslant$ Teflon wall. The impact of the cooling rates was also discussed, and the results suggested that the cooling rate did not have a big influence on determining the efficacy ranking of nucleation promoters.

It is noticed that Snomax could form a suspension when mixed with water, while the other water-insoluble promoters (e.g., AgI, kaolinite, etc.) could not. We therefore suspected that the efficacy of Snomax may partly be aided by its much larger interfacial area than the other promoters, and these other water-insoluble promoters might become excellent nucleators of ice if they could be suspended in water. we thus attempted to disperse the three nucleation promoters which had

been found to be effective earlier (AgI, kaolinite and cholesterol) into water to increase the interfacial area with water and the heterogeneous nucleation rate of ice. Since TBAB (Tetrabutylammonium bromide) was reported to act as a dispersive agent or stabilizer in a few studies [2, 3], it was applied to aid the dispersion of the nucleation promoters into water in this study. The sedimentation experiments were carried out firstly to select the most suitable concentration of TBAB in water that resulted in the best stability of the promoter suspensions. The results suggested that the suspensions prepared from AgI dispersed in 10^{-3} M TBAB solution, kaolinite dispersed in 10^{-4} M TBAB solution and cholesterol dispersed in 10^{-5} M TBAB solution had the best kinetic stability. We accidentally discovered that TBAB itself could act as a nucleation promoter of ice, and its efficacy was found to be similar to that of undispersed AgI and undispersed kaolinite showed in our previous results. The nucleation rate measured in TBAB solutions was largely independent of its concentration over the range of 10^{-5} M to 1 M. After determining the nucleation rates in promoter suspensions, it was found that dispersing AgI in 10^{-3} M TBAB solution further promoted ice nucleation whereas dispersing kaolinite or cholesterol in TBAB solutions did not promote ice nucleation more so than TBAB solutions without kaolinite or cholesterol.

Salts are known as thermodynamic inhibitors for both ice and clathrate hydrates [4-6]. The nucleation rates of both ice and CO_2 hydrate were investigated in quasi-free droplets of dilute monovalent salt solutions. For the nucleation of ice, the concentration of salt solutions is 1 mM to 100 mM. It was found that none of the eight salts tested (NaCl, NaBr, NaI, KCl, KBr, KI, LiCl and LiBr) inhibited the ice nucleation at concentration of 1 mM. All dilute salt solutions could induce the formation of ice at a lower supercooling range, and some monovalent salts increased the nucleation rate of ice at low supercoolings. The nucleation rates of ice were largely independent of the salt concentration when the concentrations were 100 mM or lower. Our results were found

to be in agreement with Sowa et al.'s results on ice nucleation, reporting a weak to no promotion of ice nucleation in dilute monovalent salt solutions [7].

As for the nucleation of CO_2 hydrate, the nucleation rates were investigated in quasi-free droplets supported by a layer of perfluoromethyldecalin of dilute NaCl and KI solutions (with a concentration range of 10^{-5} M to 10 mM). The results showed that NaCl solution had no effect on the nucleation of CO_2 hydrate whereas KI solution had a weak promotion effect on the nucleation of CO_2 hydrate at a concentration of 1 mM. The nucleation rate of CO_2 hydrate measured in these two salt solutions was found to be largely independent of the concentration when the concentrations were 10 mM or lower. The impact of cations and anions was also discussed by comparing with the nucleation rates that measured in 1 mM NaI solution, and it seemed that larger anions were more conducive to the nucleation of CO_2 hydrate whereas the impact of cations remained unclear. The impact of dilute NaCl and KI solution on the nucleation rates of CO_2 hydrate were found to be similar to those of ice nucleation in our previous results and those of methane-propane mixed gas hydrate in Sowa et al.'s study [7].

8.2 Limitations and Suggested Future Work

In the work of CHAPTER 3, we applied microliter-sized water samples for the investigation of the nucleation rate of ice. When comparing to the literature data, we found that our results concentrated at a much smaller supercooling range than other literature data except Bigg's [8], and Bigg's data appeared to bridge the gas between our data and the other literature data that were obtained at deep supercoolings using smaller droplets [9, 10]. Therefore, the future work could be conducted by using smaller water droplets for the investigations of ice nucleation rates. In this case, the apparatus used in the work of CHAPTER 3 will need to be modified so that it will

suit for the investigations of smaller droplets by updating the sample cell, improving the accuracy of observation, etc.

In the work of CHAPTER 4, we investigated the nucleation rates of ice in the presence of seven promoters, including commercial product (Snomax), inorganic material (AgI), mineral clay (kaolinite), organic molecules (cholesterol and steroid) and celluloses. However, there are also other substances that have been reported to be effective nucleation promoters for ice, such as soot particles, water insoluble macromolecules (e.g., some fungal species) and some biological materials (e.g., bacteria, pollen, etc.) [11-13]. Then the future work can be investigating the nucleation rates of ice in the presence of other types of nucleation promoters. Secondly, we found that some promoters such as cholesterol and steroid that had been reported to be very effective were not as other promoters such as AgI. Therefore, the future studies could focus on the effective promoters we found to explore the major factors that impact the efficacy of promoters. Besides, one of the effective promoters reported in this study, kaolinite, has different facets with different wetting properties. Then it would be interesting to come up with the experimental studies that investigating the nucleation rates on different facets of kaolinite. This may also put insights into the promoting mechanism of kaolinite on ice nucleation.

In the work of CHAPTER 6, we measured the nucleation rates of ice in dilute monovalent salt solutions. In the future, the impact of other salts (e.g., sulfide salts, ammonium salts, etc.) or mixed salt solutions on the nucleation rates of ice can be studied. Other than salts that were known as the thermodynamic inhibitors for ice and clathrate hydrates, some inhibitors such as PVP, PVCap that used for inhibiting the formation of clathrate hydrates could be investigated for the nucleation of ice. And the impact of some types of anti-freeze proteins could also be tested for the nucleation of clathrate hydrate.

In the work of CHAPTER 7, the high-pressure chamber which used as the reactor of the nucleation of CO_2 hydrate has a thick wall and large volume, resulting in the slow heat transfer to the surrounding coolant and hence a large thermal lag. This large thermal lag limited the choice of faster experimental cooling rates, making the experiments time-consuming and lowering the efficiency of data collection. Therefore, the existing apparatus could be improved to reduce the thermal lag between the sample in the chamber and its surrounding coolant and increasing the experimental efficiency. Secondly, we investigated the nucleation rate of CO_2 hydrate. Future work could be conducted by using different guest gases such as methane. Thirdly, the nucleation rates were measured in quasi-free droplet with a volume of 20 µL in this study. Future work could be scaling up to larger sizes that could put more insights on the oil and gas industry. In addition, this study mainly concentrated on dilute salt solutions. In the future, nucleation rates of clathrate hydrates in salt solutions with higher concentrations (e.g., similar as the brine concentration of sea water) could be studied.

In this thesis, a large number of experimental measurements were carried out to derive the nucleation curves of both ice and CO_2 hydrate, in the presence/absence of different types of additives. We thus go further to analyze the experimental data using the Classical Nucleation Theory to derive the thermodynamic factor and kinetic factor [14, 15]. The nucleation rate, J, could be derived according to the Classical Nucleation Theory and expressed as [14, 15]:

$$\ln J - \Delta S_{eq}\Delta T / kT = \ln A - B' / T\Delta T^2 \qquad \text{Eq. 8.1}$$

where J is the nucleation rate, $\Delta S_{eq} = \Delta h_{eq}/T_{eq}$, Δh_{eq} is the latent heat of melting/dissociating a building unit of ice/hydrate crystal into liquid water/guest gas and liquid water at the thermodynamic melting point/dissociation temperature, T_{eq}, ΔT is the supercooling, k is the Boltzmann constant, T is the absolute temperature, A is the so-called kinetic factor which depends

on the type of nucleation and accounts for the frequency of attachment of ice/hydrate building units to the nucleus and the concentration of potential nucleation sites, and B' is the so-called thermodynamic factor that accounts for the probability that a system that can surmount the activation barrier as prescribed by the Boltzmann distribution.

Therefore, one can plot $(\ln J - \Delta S_{eq}\Delta T / kT)$ versus $(1/T\Delta T^2)$ and fit the curve with a straight line. Then the thermodynamic factor, B', could be obtained from the slope of the fitted straight line and the natural logarithm of the kinetic factor, $\ln A$, could be obtained from the offset [14, 15]. During our analyzing process, the slope of the fitted straight line (i.e., the thermodynamic factor) was found to be very sensitive to the number of the molecules that forming the building unit (which needed to set as an input for calculating the Δh_{eq}). For example, at least 30, 60 or more water molecules were needed for constructing a single-layer or multiple-layer hexagonal ice unit cell [14], it is difficult at this stage to get meaningful values for the thermodynamic factor and kinetic factor unless we could find a way to ensure the numbers of water molecules that constructing the building unit of the hexagonal ice. Future work could be finding reliable methods to ensure such numbers of molecules that form the building unit of ice/hydrate and hence put more insights into the Classical Nucleation Theory by deriving the size of the activation barrier, etc.

8.3   References

(1)   Maeda, N. Nucleation curves of model natural gas hydrates on a quasi-free water droplet. AIChE Journal 2015, 61 (8), 2611-2617.

(2)   Coulter, M. M.; Dinglasan, J. A.; Goh, J. B.; Nair, S.; Anderson, D. J.; Dong, V. M. Preparing water-dispersed palladium nanoparticles via polyelectrolyte nanoreactors. *Chemical Science* **2010**, *1* (6), 772-775.

(3)   Zheng, R.; Tian, J.; Binks, B. P.; Cui, Z.; Xia, W.; Jiang, J. Oil-in-Water emulsions stabilized by alumina nanoparticles with organic electrolytes: fate of particles. *Journal of Colloid and Interface Science* **2022**, *627*, 749-760.

(4)   Nasir, Q.; Suleman, H.; Elsheikh, Y. A. A review on the role and impact of various additives as promoters/inhibitors for gas hydrate formation. *Journal of Natural Gas Science and Engineering* **2020**, *76*, 103211.

(5)   Koop, T.; Luo, B.; Tsias, A.; Peter, T. Water activity as the determinant for homogeneous ice nucleation in aqueous solutions. *Nature* **2000**, *406* (6796), 611-614.

(6)   Espinosa, J. R.; Soria, G. D.; Ramirez, J.; Valeriani, C.; Vega, C.; Sanz, E. Role of salt, pressure, and water activity on homogeneous ice nucleation. *The Journal of Physical Chemistry Letters* **2017**, *8* (18), 4486-4491.

(7)   Sowa, B.; Zhang, X. H.; Hartley, P. G.; Dunstan, D. E.; Kozielski, K. A.; Maeda, N. Formation of ice, tetrahydrofuran hydrate, and methane/propane mixed gas hydrates in strong monovalent salt solutions. *Energy & fuels* **2014**, *28* (11), 6877-6888.

(8)   Bigg, E. K. The supercooling of water. *Proceedings of the Physical Society. Section B* **1953**, *66* (8), 688.

(9)   Stöckel, P.; Weidinger, I. M.; Baumgärtel, H.; Leisner, T. Rates of homogeneous ice nucleation in levitated H2O and D2O droplets. *The Journal of Physical Chemistry A* **2005**, *109* (11), 2540-2546.

(10)   Murray, B.; O'sullivan, D.; Atkinson, J.; Webb, M. Ice nucleation by particles immersed in supercooled cloud droplets. *Chemical Society Reviews* **2012**, *41* (19), 6519-6554.

(11)   Pummer, B.; Budke, C.; Augustin-Bauditz, S.; Niedermeier, D.; Felgitsch, L.; Kampf, C.; Huber, R.; Liedl, K.; Loerting, T.; Moschen, T. Ice nucleation by water-soluble macromolecules. *Atmospheric Chemistry and Physics* **2015**, *15* (8), 4077-4091.

(12)   Pandey, R.; Usui, K.; Livingstone, R. A.; Fischer, S. A.; Pfaendtner, J.; Backus, E. H.; Nagata, Y.; Fröhlich-Nowoisky, J.; Schmüser, L.; Mauri, S. Ice-nucleating bacteria control the order and dynamics of interfacial water. *Science advances* **2016**, *2* (4), e1501630.

(13)   Pummer, B. G.; Bauer, H.; Bernardi, J.; Bleicher, S.; Grothe, H. Suspendable macromolecules are responsible for ice nucleation activity of birch and conifer pollen. *Atmospheric Chemistry and Physics* **2012**, *12* (5), 2541-2550.

(14)   Maeda, N. *Nucleation of gas hydrates*; Springer, 2020.

(15)   Kashchiev, D.; Firoozabadi, A. Nucleation of gas hydrates. *Journal of crystal growth* **2002**, *243* (3-4), 476-489.

BIBLIOGRAPHY

Adamsom, A. and A. Gast (1997). Physical Chemistry of surfaces, Wiley, New York.

Ahmadloo, F., et al. (2008). "Gas separation and storage using semi-clathrate hydrates."

Ahmed, M. Z., et al. (2020). "Effects of chloride and sulfate salts on seed germination of halophytes from dry alpine climate." Journal of Plant Nutrition **43**(15): 2299-2310.

Alamri, S., et al. (2020). "Self - Limited Ice Formation and Efficient De - Icing on Superhydrophobic Micro - Structured Airfoils through Direct Laser Interference Patterning." Advanced Materials Interfaces **7**(22): 2001231.

Albarracín, W., et al. (2011). "Salt in food processing; usage and reduction: a review." International Journal of Food Science & Technology **46**(7): 1329-1336.

Asadi, F., et al. (2019). "The link between the kinetics of gas hydrate formation and surface ion distribution in the low salt concentration regime." Fuel **240**: 309-316.

Babu, P., et al. (2021). "Energy analysis of methane-hydrate-based produced water desalination." Energy & Fuels **35**(3): 2514-2519.

Babu, P., et al. (2014). "Systematic evaluation of tetra-n-butyl ammonium bromide (TBAB) for carbon dioxide capture employing the clathrate process." Industrial & Engineering Chemistry Research **53**(12): 4878-4887.

Babu, P., et al. (2020). "Hydrate-based desalination (HyDesal) process employing a novel prototype design." Chemical Engineering Science **218**: 115563.

Bai, D., et al. (2019). "The effect of aqueous NaCl solution on methane hydrate nucleation and growth." Fluid Phase Equilibria **487**: 76-82.

Barlow, T. W. and A. Haymet (1995). "ALTA: An automated lag-time apparatus for studying the nucleation of supercooled liquids." Review of scientific instruments **66**(4): 2996-3007.

Bartels-Rausch, T., et al. (2012). "Ice structures, patterns, and processes: A view across the icefields." Reviews of Modern Physics **84**(2): 885.

Barwood, M. T., et al. (2022). "Extracting nucleation rates from ramped temperature measurements of gas hydrate formation." Chemical Engineering Journal **450**: 137895.

Bauerecker, S., et al. (2008). "Monitoring ice nucleation in pure and salty water via high-speed imaging and computer simulations." The Journal of Physical Chemistry C **112**(20): 7631-7636.

Benz, S., et al. (2005). "T-dependent rate measurements of homogeneous ice nucleation in cloud droplets using a large atmospheric simulation chamber." Journal of Photochemistry and Photobiology A: Chemistry **176**(1-3): 208-217.

Bigg, E. K. (1953). "The supercooling of water." Proceedings of the Physical Society. Section B **66**(8): 688.

Brassard, J.-D., et al. (2022). "Ice accretion, shedding, and melting on cable-stayed bridges: A laboratory performance assessment." Cold Regions Science and Technology **204**: 103672.

Broni-Bediako, E., et al. (2017). "Gas hydrate formation phase boundary behaviour of synthetic natural gas system of the keta basin of Ghana." The Open Petroleum Engineering Journal **10**(1).

Brus, D., et al. (2005). "Homogeneous nucleation rate measurements of 1-butanol in helium: A comparative study of a thermal diffusion cloud chamber and a laminar flow diffusion chamber." The Journal of chemical physics **122**(21): 214506.

Cao, Y., et al. (2012). "Numerical simulation of ice accretions on an aircraft wing." Aerospace Science and Technology **23**(1): 296-304.

Castellani, B., et al. (2014). "Clathrate hydrates for thermal energy storage in buildings: overview of proper hydrate-forming compounds." Sustainability **6**(10): 6815-6829.

Cebeci, T. and F. Kafyeke (2003). "Aircraft icing." Annual review of fluid mechanics **35**(1): 11-21.

Chelf, J. H. and S. T. Martin (2001). "Homogeneous ice nucleation in aqueous ammonium sulfate aerosol particles." Journal of Geophysical Research: Atmospheres **106**(D1): 1215-1226.

Congdon, T., et al. (2015). "Probing the biomimetic ice nucleation inhibition activity of poly (vinyl alcohol) and comparison to synthetic and biological polymers." Biomacromolecules **16**(9): 2820-2826.

Conrad, P., et al. (2005). "Ice nucleation on BaF2 (111)." The Journal of chemical physics **122**(6).

Coulter, M. M., et al. (2010). "Preparing water-dispersed palladium nanoparticles via polyelectrolyte nanoreactors." Chemical Science **1**(6): 772-775.

Craig, V. S. and C. L. Henry (2010). Specific ion effects at the air–water interface: Experimental studies. Specific Ion Effects, World Scientific**:** 191-214.

Dalili, N., et al. (2009). "A review of surface engineering issues critical to wind turbine performance." Renewable and Sustainable energy reviews **13**(2): 428-438.

Dalmazzone, D., et al. (2004). "The stability of methane hydrates in highly concentrated electrolyte solutions by differential scanning calorimetry and theoretical computation." American Mineralogist **89**(8-9): 1183-1191.

Dalvi-Isfahan, M., et al. (2017). "Review on the control of ice nucleation by ultrasound waves, electric and magnetic fields." Journal of Food Engineering **195**: 222-234.

Debenedetti, P. G. (2003). "Supercooled and glassy water." Journal of Physics: Condensed Matter **15**(45): R1669.

Demartino, C., et al. (2015). "Effects of ice accretion on the aerodynamics of bridge cables." Journal of Wind Engineering and Industrial Aerodynamics **138**: 98-119.

DeMott, P. J., et al. (2010). "Predicting global atmospheric ice nuclei distributions and their impacts on climate." Proceedings of the National Academy of Sciences **107**(25): 11217-11222.

DeMott, P. J. and D. C. Rogers (1990). "Freezing nucleation rates of dilute solution droplets measured between− 30 and− 40 C in laboratory simulations of natural clouds." Journal of the atmospheric sciences **47**(9): 1056-1064.

Diehl, K., et al. (2014). "Particle surface area dependence of mineral dust in immersion freezing mode: investigations with freely suspended drops in an acoustic levitator and a vertical wind tunnel." Atmospheric Chemistry and Physics **14**(22): 12343-12355.

Diehl, K. and S. Wurzler (2004). "Heterogeneous drop freezing in the immersion mode: Model calculations considering soluble and insoluble particles in the drops." Journal of the atmospheric sciences **61**(16): 2063-2072.

Djikaev, Y. and E. Ruckenstein (2008). "Thermodynamics of heterogeneous crystal nucleation in contact and immersion modes." The Journal of Physical Chemistry A **112**(46): 11677-11687.

Du, N., et al. (2003). "Ice nucleation inhibition: mechanism of antifreeze by antifreeze protein." Journal of Biological Chemistry **278**(38): 36000-36004.

Duft, D. and T. Leisner (2004). "Laboratory evidence for volume-dominated nucleation of ice in supercooled water microdroplets."

Eickhoff, L., et al. (2019). "Contrasting behavior of antifreeze proteins: Ice growth inhibitors and ice nucleation promoters." The journal of physical chemistry letters **10**(5): 966-972.

Espinosa, J. R., et al. (2017). "Role of salt, pressure, and water activity on homogeneous ice nucleation." The Journal of Physical Chemistry Letters **8**(18): 4486-4491.

Falenty, A., et al. (2014). "Formation and properties of ice XVI obtained by emptying a type sII clathrate hydrate." Nature **516**(7530): 231-233.

Farhang, F., et al. (2014). "Influence of sodium halides on the kinetics of CO2 hydrate formation." Energy & Fuels **28**(2): 1220-1229.

Fazlali, A., et al. (2013). "Impact of different surfactants and their mixtures on methane‑hydrate formation." Energy Technology **1**(8): 471-477.

Fukuta, N. and B. Mason (1963). "Epitaxial growth of ice on organic crystals." Journal of Physics and Chemistry of Solids **24**(6): 715-718.

Glatz, B. and S. Sarupria (2016). "The surface charge distribution affects the ice nucleating efficiency of silver iodide." The Journal of chemical physics **145**(21): 211924.

Gorbunov, B., et al. (2001). "Ice nucleation on soot particles." Journal of Aerosol Science **32**(2): 199-215.

Gurganus, C., et al. (2014). "Nucleation at the contact line observed on nanotextured surfaces." Physical review letters **113**(23): 235701.

Haji-Akbari, A. and P. G. Debenedetti (2015). "Direct calculation of ice homogeneous nucleation rate for a molecular model of water." Proceedings of the National Academy of Sciences **112**(34): 10582-10588.

Head, R. B. (1961). "Steroids as ice nucleators." Nature **191**(4793): 1058-1059.

Heneghan, A., et al. (2002). "Heterogeneous nucleation of supercooled water, and the effect of an added catalyst." Proceedings of the National Academy of Sciences **99**(15): 9631-9634.

Hirai, S., et al. (2000). "MRI measurement of hydrate growth and an application to advanced CO2 sequestration technology." Annals of the New York Academy of Sciences **912**(1): 246-253.

Hiranuma, N., et al. (2019). "A comprehensive characterization of ice nucleation by three different types of cellulose particles immersed in water." Atmospheric Chemistry and Physics **19**(7): 4823-4849.

Holt, C. (2003). "Substances which inhibit ice nucleation: a review." CryoLetters **24**(5): 269-274.

Hoose, C. and O. Möhler (2012). "Heterogeneous ice nucleation on atmospheric aerosols: a review of results from laboratory experiments." Atmospheric Chemistry and Physics **12**(20): 9817-9854.

Hsieh, M.-K., et al. (2012). "Predictive method for the change in equilibrium conditions of gas hydrates with addition of inhibitors and electrolytes." Industrial & engineering chemistry research **51**(5): 2456-2469.

Ickes, L., et al. (2015). "Classical nucleation theory of homogeneous freezing of water: thermodynamic and kinetic parameters." Physical Chemistry Chemical Physics **17**(8): 5514-5537.

Igboanusi, U. and A. Opara (2011). "The advancement from thermodynamic inhibitors to kinetic inhibitors and anti-agglomerants in natural gas flow assurance." International Journal of Chemical and Environmental Engineering **2**(2).

Ismail, A. and A. El-Shamy (2009). "Engineering behaviour of soil materials on the corrosion of mild steel." Applied clay science **42**(3-4): 356-362.

Israelachvili, J. N. (2011). Intermolecular and surface forces, Academic press.

Ivall, J., et al. (2015). "Profiling the concentration of the kinetic inhibitor polyvinylpyrrolidone throughout the methane hydrate formation process." Energy & Fuels **29**(4): 2329-2335.

Jeong, K., et al. (2019). "Hydrate nucleation and growth on water droplets acoustically-levitated in high-pressure natural gas." Physical Chemistry Chemical Physics **21**(39): 21685-21688.

Jeong, K., et al. (2022). "Gas hydrate nucleation in acoustically levitated water droplets." Chemical Engineering Journal **433**: 133494.

Jing, F., et al. (2019). "Supercooling and heterogeneous nucleation in acoustically levitated deionized water and graphene oxide nanofluids droplets." Experimental Thermal and Fluid Science **103**: 143-148.

Jung, S., et al. (2012). "Mechanism of supercooled droplet freezing on surfaces." Nature Communications **3**(1): 615.

Kamata, Y., et al. (2005). "Hydrogen sulfide separation using tetra-n-butyl ammonium bromide semi-clathrate (TBAB) hydrate." Energy & Fuels **19**(4): 1717-1722.

Kanno, H. and C. Angell (1977). "Homogeneous nucleation and glass formation in aqueous alkali halide solutions at high pressures." The Journal of Physical Chemistry **81**(26): 2639-2643.

Karaaslan, U. and M. Parlaktuna (2000). "Surfactants as hydrate promoters?" Energy & Fuels **14**(5): 1103-1107.

Kashchiev, D. (2000). Nucleation. Oxford, UK, Elsevier.

Ke, W. and M. A. Kelland (2016). "Kinetic hydrate inhibitor studies for gas hydrate systems: a review of experimental equipment and test methods." Energy & Fuels **30**(12): 10015-10028.

Kelton, K. and A. L. Greer (2010). Nucleation in condensed matter: applications in materials and biology, Elsevier.

Khurana, M., et al. (2017). "A review of clathrate hydrate nucleation." ACS Sustainable Chemistry & Engineering **5**(12): 11176-11203.

Kim, K., et al. (2023). "Facilitating clathrate hydrates with extremely rapid and high gas uptake for chemical-free carbon capture and methane storage." Energy **270**: 126902.

Kimmel, G. A., et al. (2019). "Homogeneous ice nucleation rates and crystallization kinetics in transiently-heated, supercooled water films from 188 K to 230 K." The Journal of chemical physics **150**(20).

Knopf, D. A. and P. A. Alpert (2023). "Atmospheric ice nucleation." Nature Reviews Physics **5**(4): 203-217.

Koh, C., et al. (2002). "Mechanisms of gas hydrate formation and inhibition." Fluid Phase Equilibria **194**: 143-151.

Koop, T., et al. (2000). "Water activity as the determinant for homogeneous ice nucleation in aqueous solutions." Nature **406**(6796): 611-614.

Krämer, B., et al. (1999). "Homogeneous nucleation rates of supercooled water measured in single levitated microdroplets." The Journal of chemical physics **111**(14): 6521-6527.

Kumar, A., et al. (2015). "Role of surfactants in promoting gas hydrate formation." Industrial & Engineering Chemistry Research **54**(49): 12217-12232.

Kumar, A., et al. (2016). "Effect of additives on formation and decomposition kinetics of methane clathrate hydrates: Application in energy storage and transportation." The Canadian Journal of Chemical Engineering **94**(11): 2160-2167.

Kutschan, B., et al. (2014). "Dynamical mechanism of antifreeze proteins to prevent ice growth." Physical Review E **90**(2): 022711.

Lang, X., et al. (2010). "Intensification of methane and hydrogen storage in clathrate hydrate and future prospect." Journal of Natural Gas Chemistry **19**(3): 203-209.

Li, M.-y., et al. (2022). "Experimental and theoretical investigation on hydrate nucleation in TBAB droplets." Fuel **308**: 121994.

Liang, S., et al. (2019). "Characterizing key features in the formation of ice and gas hydrate systems." Philosophical Transactions of the Royal Society A **377**(2146): 20180167.

Lihavainen, H. and Y. Viisanen (2001). "A laminar flow diffusion chamber for homogeneous nucleation studies." The Journal of Physical Chemistry B **105**(47): 11619-11629.

Lindow, S. (1983). "The role of bacterial ice nucleation in frost injury to plants." Annual review of phytopathology **21**(1): 363-384.

Liu, C., et al. (2021). "Molecular insight into carbon dioxide hydrate formation from saline solution." RSC advances **11**(50): 31583-31589.

Lu, H., et al. (2001). "Anion plays a more important role than cation in affecting gas hydrate stability in electrolyte solution?—a recognition from experimental results." Fluid Phase Equilibria **178**(1-2): 225-232.

Lü, Y., et al. (2005). "Observation of ice nucleation in acoustically levitated water drops." Applied Physics Letters **87**(18).

Lupi, L., et al. (2014). "Heterogeneous nucleation of ice on carbon surfaces." Journal of the American Chemical Society **136**(8): 3156-3164.

Lynch, F. T. and A. Khodadoust (2001). "Effects of ice accretions on aircraft aerodynamics." Progress in Aerospace Sciences **37**(8): 669-767.

Maeda, N. (2015). "Fuel gas hydrate formation probability distributions on quasi-free water droplets." Energy & Fuels **29**(1): 137-142.

Maeda, N. (2015). "Nucleation curves of model natural gas hydrates on a quasi‑free water droplet." AIChE Journal **61**(8): 2611-2617.

Maeda, N. (2016). "Nucleation curves of methane–propane mixed gas hydrates in hydrocarbon oil." Chemical Engineering Science **155**: 1-9.

Maeda, N. (2018). "Nucleation curves of methane hydrate from constant cooling ramp methods." Fuel **223**: 286-293.

Maeda, N. (2019). "Nucleation Curve of Carbon Dioxide Hydrate from a Linear Cooling Ramp Method." The Journal of Physical Chemistry A **123**(37): 7911-7919.

Maeda, N. (2020). Nucleation of Gas Hydrates. Cham, Switzerland, Springer.

Maeda, N. (2021). "Brief Overview of Ice Nucleation." molecules **26**(2): 392.

Maeda, N., et al. (2011). "Development of a high pressure automated lag time apparatus for experimental studies and statistical analyses of nucleation and growth of gas hydrates." Review of Scientific Instruments **82**(6): 065109.

Maeda, N., et al. (2012). "Statistical analysis of supercooling in fuel gas hydrate systems." Energy & Fuels **26**(3): 1820-1827.

Maekawa, T. (2001). "Equilibrium conditions for gas hydrates of methane and ethane mixtures in pure water and sodium chloride solution." Geochemical Journal **35**(1): 59-66.

Mahanty, J. and B. W. Ninham (1976). Dispersion forces, Academic Press.

Mahrt, F., et al. (2018). "Ice nucleation abilities of soot particles determined with the Horizontal Ice Nucleation Chamber." Atmospheric Chemistry and Physics **18**(18): 13363-13392.

Marcolli, C., et al. (2016). "Ice nucleation efficiency of AgI: review and new insights." Atmospheric Chemistry and Physics **16**(14): 8915-8937.

May, E. F., et al. (2014). "Quantitative kinetic inhibitor comparisons and memory effect measurements from hydrate formation probability distributions." Chemical Engineering Science **107**: 1-12.

Metaxas, P. J., et al. (2019). "Gas hydrate formation probability distributions: Induction times, rates of nucleation and growth." Fuel **252**: 448-457.

Millot, M., et al. (2019). "Nanosecond X-ray diffraction of shock-compressed superionic water ice." Nature **569**(7755): 251-255.

Miyata, K., et al. (2002). "Cationic and anionic effects on the homogeneous nucleation of ice in aqueous alkali halide solutions." Chemical physics letters **354**(1-2): 51-55.

Morris, G. J. and E. Acton (2013). "Controlled ice nucleation in cryopreservation–a review." Cryobiology **66**(2): 85-92.

Mouritsen, O. G. and M. J. Zuckermann (2004). "What's so special about cholesterol?" Lipids **39**(11): 1101-1113.

Murray, B., et al. (2010). "Kinetics of the homogeneous freezing of water." Physical Chemistry Chemical Physics **12**(35): 10380-10387.

Murray, B., et al. (2012). "Ice nucleation by particles immersed in supercooled cloud droplets." Chemical Society Reviews **41**(19): 6519-6554.

Murray, B. J., et al. (2011). "Heterogeneous freezing of water droplets containing kaolinite particles." Atmospheric Chemistry and Physics **11**(9): 4191-4207.

Nasir, Q., et al. (2020). "A review on the role and impact of various additives as promoters/inhibitors for gas hydrate formation." Journal of Natural Gas Science and Engineering **76**: 103211.

Nguyen, N. N., et al. (2016). "Unexpected inhibition of CO2 gas hydrate formation in dilute TBAB solutions and the critical role of interfacial water structure." Fuel **185**: 517-523.

Ning, D. and X. Liu (2002). "Controlled ice nucleation in microsized water droplet." Applied physics letters **81**(3): 445-447.

O'Day, P. A., et al. (1994). "Molecular structure and binding sites of cobalt (II) surface complexes on kaolinite from X-ray absorption spectroscopy." Clays and Clay Minerals **42**: 337-355.

Olson, S., et al. (2022). "The effect of ocean salinity on climate and its implications for Earth's habitability." Geophysical research letters **49**(10): e2021GL095748.

Özgen, S. and M. Canıbek (2009). "Ice accretion simulation on multi-element airfoils using extended Messinger model." Heat and Mass Transfer **45**(3): 305.

Pandey, J. S., et al. (2019). "Insights into kinetics of methane hydrate formation in the presence of surfactants." Processes **7**(9): 598.

Pandey, R., et al. (2016). "Ice-nucleating bacteria control the order and dynamics of interfacial water." Science advances **2**(4): e1501630.

Pinti, V., et al. (2012). "Ice nucleation efficiency of clay minerals in the immersion mode." Atmospheric Chemistry and Physics **12**(13): 5859-5878.

Polen, M., et al. (2016). "The unstable ice nucleation properties of Snomax® bacterial particles." Journal of Geophysical Research: Atmospheres **121**(19): 11,666-611,678.

Prasad, P. S. and B. Sai Kiran (2018). "Clathrate hydrates of greenhouse gases in the presence of natural amino acids: storage, transportation and separation applications." Scientific reports **8**(1): 8560.

Pruppacher, H. R. and J. D. Klett (1997). Microphysics of Clouds and Precipitation. Kluwer, Dordrecht.

Pummer, B., et al. (2015). "Ice nucleation by water-soluble macromolecules." Atmospheric Chemistry and Physics **15**(8): 4077-4091.

Pummer, B. G., et al. (2012). "Suspendable macromolecules are responsible for ice nucleation activity of birch and conifer pollen." Atmospheric Chemistry and Physics **12**(5): 2541-2550.

Rasoolzadeh, A., et al. (2019). "An experimental study of the synergistic effects of BMIM-BF 4, BMIM-DCA and TEACl aqueous solutions on methane hydrate formation." Petroleum Science **16**: 409-416.

Ricaurte, M., et al. (2013). "CO2 removal from a CO2–CH4 gas mixture by clathrate hydrate formation using THF and SDS as water-soluble hydrate promoters." Industrial & engineering chemistry research **52**(2): 899-910.

Ripmeester, J. A. and S. Alavi (2016). "Some current challenges in clathrate hydrate science: Nucleation, decomposition and the memory effect." Current Opinion in Solid State and Materials Science **20**(6): 344-351.

Rogers, D. C. (1988). "Development of a continuous flow thermal gradient diffusion chamber for ice nucleation studies." Atmospheric Research **22**(2): 149-181.

Rogers, D. C. (1994). "Detecting Ice Nuclei with a Continuous—Flow Diffusion Chamber-Some Exploratory Tests of Instrument Response." Journal of Atmospheric and Oceanic Technology **11**(4): 1042-1047.

Rossi, F. and A. M. Gambelli (2021). "Thermodynamic phase equilibrium of single-guest hydrate and formation data of hydrate in presence of chemical additives: A review." Fluid Phase Equilibria **536**: 112958.

Sa, J.-H., et al. (2011). "Amino acids as natural inhibitors for hydrate formation in CO2 sequestration." Environmental science & technology **45**(13): 5885-5891.

Sa, J.-H. and A. K. Sum (2019). "Promoting gas hydrate formation with ice-nucleating additives for hydrate-based applications." Applied Energy **251**: 113352.

Saleh, S., et al. (2012). "Wavelet-based signal processing method for detecting ice accretion on wind turbines." IEEE Transactions on Sustainable Energy **3**(3): 585-597.

Salzmann, C. G., et al. (2021). "Structure and nature of ice XIX." Nature Communications **12**(1): 3162.

Salzmann, C. G., et al. (2011). "The polymorphism of ice: five unresolved questions." Physical Chemistry Chemical Physics **13**(41): 18468-18480.

Schicks, J., et al. (2005). "Raman spectra of gas hydrates—differences and analogies to ice 1h and (gas saturated) water." Spectrochimica acta part A: molecular and biomolecular spectroscopy **61**(10): 2399-2403.

Schrod, J., et al. (2017). "Ice nucleating particles over the Eastern Mediterranean measured by unmanned aircraft systems." Atmospheric Chemistry and Physics **17**(7): 4817-4835.

Shishov, A., et al. (2019). "In situ decomposition of deep eutectic solvent as a novel approach in liquid-liquid microextraction." Analytica chimica acta **1065**: 49-55.

Shishov, A., et al. (2018). "Deep eutectic solvents as a new kind of dispersive solvent for dispersive liquid–liquid microextraction." RSC advances **8**(67): 38146-38149.

Sloan, E. D. (2000). "Clathrate hydrates: the other common solid water phase." Industrial & engineering chemistry research **39**(9): 3123-3129.

Sloan Jr, E. D. (2003). "Fundamental principles and applications of natural gas hydrates." Nature **426**(6964): 353-359.

Sloan Jr, E. D. and C. A. Koh (2007). Clathrate hydrates of natural gases, CRC press.

Soria, G. D., et al. (2018). "A simulation study of homogeneous ice nucleation in supercooled salty water." The Journal of chemical physics **148**(22): 222811.

Sosso, G. C., et al. (2018). "Unravelling the origins of ice nucleation on organic crystals." Chemical science **9**(42): 8077-8088.

Sowa, B., et al. (2014). "Formation of ice, tetrahydrofuran hydrate, and methane/propane mixed gas hydrates in strong monovalent salt solutions." Energy & Fuels **28**(11): 6877-6888.

Sowa, B., et al. (2015). "Nucleation probability distributions of methane–propane mixed gas hydrates in salt solutions and urea." Energy & Fuels **29**(10): 6259-6270.

Stan, C. A., et al. (2009). "A microfluidic apparatus for the study of ice nucleation in supercooled water drops." Lab on a Chip **9**(16): 2293-2305.

Stetzer, O., et al. (2008). "The Zurich Ice Nucleation Chamber (ZINC)-A new instrument to investigate atmospheric ice formation." Aerosol science and technology **42**(1): 64-74.

Stöckel, P., et al. (2005). "Rates of homogeneous ice nucleation in levitated H2O and D2O droplets." The Journal of Physical Chemistry A **109**(11): 2540-2546.

Stopelli, E., et al. (2014). "Freezing nucleation apparatus puts new slant on study of biological ice nucleators in precipitation." Atmospheric measurement techniques **7**: 129-134.

Sum, A. K., et al. (2009). "Clathrate hydrates: from laboratory science to engineering practice." Industrial & engineering chemistry research **48**(16): 7457-7465.

Szakáll, M., et al. (2021). "Comparative study on immersion freezing utilizing single-droplet levitation methods." Atmospheric Chemistry and Physics **21**(5): 3289-3316.

Tabazadeh, A., et al. (2002). "Surface crystallization of supercooled water in clouds." Proceedings of the National Academy of Sciences **99**(25): 15873-15878.

Taborek, P. (1985). "Nucleation in emulsified supercooled water." Physical Review B **32**(9): 5902.

Takeya, S., et al. (2006). "Structure and thermal expansion of natural gas clathrate hydrates." Chemical Engineering Science **61**(8): 2670-2674.

Tanaka, R., et al. (2009). "Crystal growth of clathrate hydrates formed at the interface of liquid water and gaseous methane, ethane, or propane: variations in crystal morphology." Crystal Growth and Design **9**(5): 2529-2536.

Tang, C. and D. Liang (2019). "Inhibitory effects of novel green inhibitors on gas hydrate formation." Chinese Journal of Chemical Engineering **27**(9): 2107-2117.

Tobo, Y. (2016). "An improved approach for measuring immersion freezing in large droplets over a wide temperature range." Scientific reports **6**(1): 1-9.

Tollefsen, E., et al. (2018). "Chemical controls on ikaite formationELIN TOLLEFSEN ET AL. CHEMICAL CONTROLS ON IKAITE FORMATION." Mineralogical Magazine **82**(5): 1119-1129.

Trueba, A. T., et al. (2011). "Phase equilibrium measurements of structure II clathrate hydrates of hydrogen with various promoters." Fluid Phase Equilibria **307**(1): 6-10.

Tse, J. S., et al. (1983). "Molecular dynamics studies of ice Ic and the structure I clathrate hydrate of methane." The Journal of Physical Chemistry **87**(21): 4198-4203.

Udachin, K. A., et al. (2001). "A dense and efficient clathrate hydrate structure with unusual cages." Angewandte Chemie **113**(7): 1343-1345.

Vali, G. (1996). "Ice nucleation—A review." Nucleation and atmospheric aerosols 1996: 271-279.

Veluswamy, H. P., et al. (2014). "Clathrate hydrates for hydrogen storage: the impact of tetrahydrofuran, tetra-n-butylammonium bromide and cyclopentane as promoters on the macroscopic kinetics." International journal of hydrogen energy **39**(28): 16234-16243.

Vonnegut, B. (1947). "The nucleation of ice formation by silver iodide." Journal of applied physics **18**(7): 593-595.

Walker, V. K., et al. (2015). "Antifreeze proteins as gas hydrate inhibitors." Canadian Journal of Chemistry **93**(8): 839-849.

Wang, L., et al. (2022). "A Review of the Effect of Porous Media on Gas Hydrate Formation." ACS omega **7**(38): 33666-33679.

Wang, Y., et al. (2022). "Effects of the Presence of Promoters Sodium Dodecyl Sulfate, Nanographite, and Tetra-n-butylammonium Bromide on the Formation of CO2 Hydrates." Energy & Fuels **36**(17): 10269-10277.

Wang, Y., et al. (2022). "Effects of Composite Accelerators on the Formation of Carbon Dioxide Hydrates." ACS omega **7**(18): 15359-15368.

Warrier, P., et al. (2016). "Overview: Nucleation of clathrate hydrates." The Journal of chemical physics **145**(21).

Wei, Y. and M. Nobuo (2023). "Nucleation Curves of Carbon Dioxide Hydrate in the Absence of a Solid Wall." Energy & Fuels **37**(5): 3760-3774.

Whale, T. F., et al. (2018). "The enhancement and suppression of immersion mode heterogeneous ice-nucleation by solutes." Chemical science **9**(17): 4142-4151.

Whale, T. F., et al. (2015). "A technique for quantifying heterogeneous ice nucleation in microlitre supercooled water droplets." Atmospheric Measurement Techniques Discussions **8**.

William, N., et al. (2023). "Engineered Compounds to Control Ice Nucleation and Recrystallization." Annual Review of Biomedical Engineering **25**.

Wolber, P. K. (1993). "Bacterial ice nucleation." Advances in microbial physiology **34**: 203-237.

Wood, G. and A. Walton (1970). "Homogeneous nucleation kinetics of ice from water." Journal of Applied Physics **41**(7): 3027-3036.

Wu, R., et al. (2013). "Methane–propane mixed gas hydrate film growth on the surface of water and Luvicap EG solutions." Energy & Fuels **27**(5): 2548-2554.

Xia, Z.-M., et al. (2012). "Thermodynamic equilibrium conditions for simulated landfill gas hydrate formation in aqueous solutions of additives." Journal of Chemical & Engineering Data **57**(11): 3290-3295.

Yang, C., et al. (2022). "Concentration effect of kinetic hydrate inhibitor on hydrate formation and inhibition." Fuel **323**: 124448.

Ye, N., et al. (2014). "Kinetics of hydrate formation in the CO2+ TBAB+ H2O system at low mass fractions." Industrial & Engineering Chemistry Research **53**(24): 10249-10255.

You, Y., et al. (2021). "Control of ice nucleation for subzero food preservation." Food Engineering Reviews **13**: 15-35.

Zachariassen, K. E. and E. Kristiansen (2000). "Ice nucleation and antinucleation in nature." Cryobiology **41**(4): 257-279.

Zhang, X., et al. (2021). "Nucleation curves of ice in quasi–free water droplets." Chemical Engineering Science: 116751.

Zhang, X., et al. (2023). "Nucleation Curves of Ice in Dilute Salt Solutions." Energy & Fuels **37**(18): 13937-13948.

Zhang, X., et al. (2018). "Experimental investigation and statistical analysis of icing nucleation characteristics of sessile water droplets." Experimental Thermal and Fluid Science **99**: 26-34.

Zhang, X. and N. Maeda (2022). "Nucleation curves of ice in the presence of nucleation promoters." Chemical Engineering Science **262**: 118017.

Zhang, Z. and X.-Y. Liu (2018). "Control of ice nucleation: freezing and antifreeze strategies." Chemical Society Reviews **47**(18): 7116-7139.

Zheng, R., et al. (2022). "Oil-in-Water emulsions stabilized by alumina nanoparticles with organic electrolytes: fate of particles." Journal of Colloid and Interface Science **627**: 749-760.

Zielke, S. A., et al. (2015). "A molecular mechanism of ice nucleation on model AgI surfaces." The Journal of Physical Chemistry B **119**(29): 9049-9055.